

The Role of Very Long Chain Fatty Acids in *Arabidopsis* Growth and Development

Laura Elizabeth Seamons, BSc.

Thesis submitted to the University of Nottingham for the
degree of Doctor of Philosophy

July 2015

Abstract

Very long chain fatty acids (VLCFAs) are essential to *Arabidopsis* growth and development. VLCFAs are found in sphingolipids, glycerophospholipids, triacylglycerols, suberin and cuticular waxes. VLCFAs are synthesized by the addition of 2 carbons from malonyl-CoA to pre-existing acyl-CoAs to produce chain lengths of greater than 18 carbon atoms. VLCFA synthesis involves four consecutive reactions that are catalysed by the microsomal Fatty Acid Elongase. In *Arabidopsis* the first reaction is catalysed by one of 21 different Keto-CoA Synthases (KCS) with diverse levels of expression and overlapping tissue specificities. The other three enzymes are ubiquitously expressed throughout the plant, and form the core components of the elongase.

Lipidomic profiling has been performed on roots and shoots of plants with reduced levels of VLCFAs. Mutants of the core components of the elongase were analysed along with herbicides that inhibit a number of KCS enzymes, this allowed the whole elongase complex to be analysed. Differences were seen in the lipidomic profiles of the different elongase mutants and between the roots and shoots of the same mutants. This has revealed correlations between phenotypic differences and lipidomic changes giving insight into which lipid classes might be responsible for the various phenotypes.

A forward genetic screen has been conducted in the *Arabidopsis cer10-1* mutant to identify novel genes involved in VLCFA metabolism. *CER10* encodes for the fourth component of the elongase complex. One suppressor mutant that has been identified has flower buds and fertility comparable to wild type plants but still displays the reduced size of the *cer10-1* mutant. The second suppressor mutant identified showed restored size of aerial organs but the flower buds remained fused. Whole genome sequencing allowed localisation of these suppressor mutations on Chromosome 3. Partial biochemical characterisation of these mutants revealed interesting changes in their acyl-CoA and cuticular lipid profiles.

Acknowledgments

I would like to thank my supervisors Dr Frederic Beaudoin, Prof Malcolm Bennett and Prof Johnathan Napier for giving me the opportunity to carry out this research project and your help and guidance for the past 4 years. I would also like to thank BBSRC for funding this studentship.

I would like to thank the whole of Lab115 for the help and support you have given me over the last 4 years. I would especially like to thank Dr Sarah Usher for having limitless patience and time to guide me through various protocols and for making the most amazing cakes. I would also like to thank Dr Louise Michaelson and Dr Richard Haslam for teaching me the various lipidomic techniques used in this project. Thank you to Louise and Freddie for helping proof read various sections of this thesis.

To Fiona and Anthony in the Glasshouses thank you for providing hundreds of pots of soil with very little notice, this has saved me so much time and your attention to detail in looking after me plants have been these experiments possible. Additionally, to Dr Stephen Powers thank you for your help with the statistical analysis, and putting up with my stupid questions. Thank you to Anthony Hall's group at the University of Liverpool Genomic centre, for the analysis of my NGS data.

Thank you to the entire afternoon coffee group for making the last 4 years so enjoyable. Jon, Joanna and Hayley thank you for providing the 'weekly fun activity'. Thank you to Rebekah for providing amazing meals and cakes and being a lovely housemate for the last 4 years and for introducing me to Rob and Sarah who are always around to brighten Wednesday evenings.

To James, thank you for putting up with me for the last 4 years! Thank you for being so understanding that my plants need me every weekend, for reading this entire thesis, and caring about pagination. You have been a constant tower of support and I am tremendously grateful for everything you have done to make sure this thesis was completed on time.

Contents

<i>Abstract</i>	2
<i>Acknowledgments</i>	3
<i>Contents</i>	4
<i>List of Figures</i>	10
<i>Declaration</i>	14
<i>List of Abbreviations</i>	15
Chapter 1. General Introduction	17
1.1. Plant lipids	17
1.2. Arabidopsis as a model for studying plant lipids	17
1.3. Lipid structure and fatty acid nomenclature.....	18
1.4. Fatty acid biosynthesis	18
1.4.1. Acetyl-CoA carboxylase	18
1.4.2. Fatty acid synthase in plants	19
1.4.3. Utilisation of the products of fatty acid synthesis	21
1.5. VLCFA synthesis - a four step reaction	22
1.5.1. VLCFA synthesis in plants.....	22
1.5.2. The discovery of the four enzymes of the elongase complex in yeast.....	24
1.6. The four VLCFA elongation reactions in plants.....	27
1.6.1. Reaction 1:- 3- Keto-acyl- CoA Synthase (KCS).....	27
1.6.2. Reaction 2:- 3- Keto- acyl -CoA Reductase (KCR)	31
1.6.3. Reaction 3 :-3-Hydroxy-acyl-CoA Dehydratase; (<i>HCD-PASTICCINO2</i> (<i>PAS2</i>))	33
1.6.4. Reaction 4:-2-Enoyl -CoA Reductase (<i>ECR/CER10</i>).....	36
1.7. Physiological roles of VLCFAs containing lipids	37
1.8. Sphingolipids.....	38
1.8.1. Sphingolipid structure	39

Contents

1.8.2.	Sphingolipid synthesis	41
1.8.3.	Sphingolipid function	47
1.9.	Membrane glycerolipids: Phospholipids and glycolipids	48
1.9.1.	Biosynthesis of glycerolipids.....	49
1.9.2.	The roles of different phospholipids and glycolipids in plant cells.....	50
1.10.	Cuticular waxes.....	53
1.10.1.	Composition and organisation of cuticle.....	53
1.10.2.	Wax synthesis.....	54
1.11.	The role of VLCFAs in plant development	60
1.11.1.	Delayed cell plate formation in <i>pas</i> mutants.....	60
1.11.2.	Developmental defects in <i>pas</i> mutants	61
1.11.3.	Role of VLCFAs in preventing organ fusion.....	65
1.12.	Aims and objectives	66
Chapter 2.	Materials and Methods.....	69
2.1.	Plant material and growth conditions.....	69
2.1.1.	Seed material	69
2.1.2.	Plant growth media.....	69
2.1.3.	Seed sterilisation	70
2.1.4.	Plant growth conditions.....	70
2.1.5.	Cross pollination of <i>Arabidopsis</i>	70
2.2.	Physiological analysis	71
2.3.	Molecular biology	71
2.3.1.	CTAB DNA extractions	71
2.3.2.	Primers and restriction enzymes	72
2.3.3.	Polymerase chain reaction conditions	72
2.3.4.	Agarose gel electrophoresis.....	73
2.3.5.	Genetic analysis	73

2.4.	Biochemical characterisation	74
2.4.1.	Tandem mass spectrometry	74
2.4.2.	Modes of analysis using tandem mass spectrometry	74
2.4.3.	Use of HPLC/ESI-MS/MS	76
2.5.	Acyl-CoA analysis, materials and methods	76
2.5.1.	Extraction of acyl-CoAs from shoot and root material	76
2.5.2.	HPLC-ESI-MS/MS analysis of acyl-CoAs	77
2.6.	Sphingolipid analysis, materials and methods	80
2.6.1.	Extraction of sphingolipids from shoot and root material	80
2.6.2.	HPLC- ESI- MS/MS analysis of sphingolipids	81
2.7.	Membrane glycerolipid analysis, materials and methods	85
2.7.1.	Extraction of membrane glycerolipid from shoot and root material	85
2.7.2.	ESI-MS/MS analysis of membrane glycerolipids	87
Chapter 3.	Lipidomic profiling of plants with mutations in the core components of the elongase	90
3.1.	Introduction	90
3.1.1.	Lipidomic analysis	90
3.1.2.	Comparative analysis of phenotypic variations between elongase mutants	91
3.2.	Results	93
3.2.1.	Acyl-CoA profiling of wild type plants and elongase mutants	94
3.2.2.	Membrane glycerolipid profiling of wild type plants and elongase mutants	101
3.2.3.	Sphingolipid profiling of wild type plants and elongase mutants	110
3.3.	Discussion	125
3.3.1.	Size of reductions in different lipid pools	126
3.3.2.	Changes in the different sphingolipid pools	127
3.3.3.	Comparison of root and shoot data	128

Contents

Chapter 4. Lipidomic analysis of plants treated with herbicides that affect VLCFA synthesis	134
4.1. Introduction.....	134
4.2. Results.....	136
4.2.1. Application of herbicides to wild type seeds.....	136
4.2.2. Acyl-CoA profiling of plants treated with herbicides.....	139
4.2.3. Membrane Glycerolipid profiling of plants treated with herbicides	143
4.2.4. Sphingolipid profiling of plants treated with herbicides.....	149
4.3. Discussion.....	157
4.3.1. Correlating phenotypes with lipidomic results.....	157
4.3.2. Effect of increasing chain length.....	159
4.3.3. Explaining the fused aerial organ phenotype.....	160
4.3.4. Explaining the root phenotype	161
4.3.5. Role of the herbicides.....	162
Chapter 5. Forward genetic screen to identify novel genes involved in VLCFA metabolism	164
5.1. Introduction.....	164
5.1.1. Genetic background for the forward genetic screen	164
5.1.2. Principles of ethyl methane sulfonate mutagenise	165
5.2. Methods.....	166
5.2.1. Genotyping of TILLING lines.....	166
5.2.2. Mutagenesis.....	167
5.2.3. Analysis of plant cuticle.....	167
5.3. Results.....	172
5.3.1. Designing a suppressor/enhancer genetic screen for VLCFA metabolism	172
5.3.2. Conducting an EMS screen in the <i>cer10-1</i> mutant background.....	182
5.3.3. Screening of <i>cer10-1</i> M ₂ pools for suppressor/enhancer mutations....	184

Contents

5.3.4.	Phenotypic characterisation of <i>cer10-1</i> suppressor lines	186
5.3.5.	Acyl-CoA profiling of <i>cer10-1</i> suppressor lines	188
5.3.6.	Wax analysis of <i>cer10-1</i> suppressor lines.....	191
5.4.	Discussion	200
5.4.1.	Evaluation of <i>cer10-1</i> as a background for the genetic screen.....	200
5.4.2.	Explaining the candidate suppressor mutations	201
Chapter 6.	Identifying the gene responsible for the suppressor phenotype	206
6.1.1.	Map based cloning	206
6.1.2.	Next generation sequencing and SHOREmap.....	208
6.2.	Methods	211
6.2.1.	Generation of an F ₂ population.....	211
6.2.2.	Methods used for map based cloning	211
6.2.3.	Preparation of DNA for NGS.....	213
6.3.	Results.....	217
6.3.1.	Generating a F ₂ population for suppressor 36 and suppressor 80	217
6.3.2.	Molecular mapping of the <i>cer10-1</i> suppressor mutants	219
6.3.3.	Next generation sequencing results	222
6.4.	Discussion	231
6.4.1.	Evaluation of rough mapping.....	231
6.4.2.	Difficulties with the identification of plants within the F ₂ populations	232
6.4.3.	Evaluation of the NGS sequencing data.....	232
6.4.4.	Future work.....	233
Chapter 7.	General discussion.....	235
7.1.	Correlating changes in the lipidome with phenotypic traits	236
7.1.1.	Explaining the different root phenotypes shown in the elongase mutants	237

Contents

7.1.2.	Explaining the fused aerial organs shown in elongase mutants.....	238
7.1.3.	The role of lipid rafts	239
7.2.	The importance of sphingolipids containing VLCFAs.....	240
7.3.	A greater reduction in VLCFA results in more severe phenotypes	244
7.4.	The identification of additional components of VLCFA biosynthesis	246
7.4.1.	Regulation of the chain lengths of VLCFAs that are synthesised.....	247
7.4.2.	Identification of an additional Enoyl-CoA Reductase activity	248
7.5.	Future work	250
7.6.	Conclusions	252
	References.....	254
	<i>Appendix</i>	275
	<i>Appendix I: Materials and methods</i>	275
	<i>Appendix II: Lipidomics of elongase mutants</i>	281
	<i>Appendix III: Lipidomics of herbicide treated plants</i>	288
	<i>Appendix IV: Characterisation of suppressor mutants</i>	293
	<i>Appendix V: Identification of the position of the suppressor mutant</i>	296
	<i>Appendix VI: General Discussion</i>	301

List of Figures

Figure 1.1 Stereospecific numbering of a glycerol molecule.	18
Figure 1.2 The reactions required for fatty acid synthesis in plants.	20
Figure 1.3. The very long chain fatty acid elongation cycle in plants.	23
Figure 1.4 The condensation reaction catalysed by KCS.	28
Figure 1.5 The reduction reaction catalysed by KCR.	31
Figure 1.6 The phenotypic traits of the <i>KCR RNAi</i> lines.	32
Figure 1.7 The dehydratase reaction catalysed by PAS2 (HCR).	34
Figure 1.8 The phenotypic traits of <i>pas2-1</i>	35
Figure 1.9 The reduction reaction catalysed by CER10.	36
Figure 1.10 Phenotypic traits of <i>cer10</i>	37
Figure 1.11 The structure of the most common LCBs and complex sphingolipids.	40
Figure 1.12 Sphingolipid synthesis.	41
Figure 1.13. Reaction catalysed by serine palmitoyltransferase.	43
Figure 1.14. Reaction catalysed by 3- ketosphinganine reductase.	43
Figure 1.15. The basic structure of a membrane glycerolipid.	49
Figure 1.16. Synthesis of PA and how that leads to the synthesis of other lipids.	49
Figure 1.17. The mol % of each of the different glycerolipids in <i>Arabidopsis</i> leaves	50
Figure 1.18. The structure of each of the phospholipids and glycolipids.	52
Figure 1.19 Wax synthesis from VLCFAs.	54
Figure 1.20 Alkane forming pathway in wax synthesis.	56
Figure 1.21 Alcohol forming pathway in wax synthesis.	58
Figure 2.1. The three modes of tandem mass spectrometry.	75
Figure 2.2 The 16:0 acyl-CoA MRM pair.	79
Figure 2.3 Acyl-CoA profile of wild type shoots.	79
Figure 2.4. The MRM pairs used to analyse sphingolipid molecules.	84
Figure 2.5. GlcCer profile of wild type shoots.	84
Figure 2.6. Comparison of methods used to extract glycerolipids.	86
Figure 2.7. Fragments detected in neutral loss scan and precursor ion scan.	87
Figure 2.8 Glycerolipid profile of wild type shoots.	89
Figure 3.1. Phenotype of two week old elongase mutants.	92
Figure 3.2 . The accumulation of intermediates of VLCFA synthesis within the acyl-CoA pool in the elongase mutants compared to wild type plants.	96

List of Figures

Figure 3.3. Acyl-CoA profile of saturated acyl-CoAs and intermediates within the VLC-acyl-CoA elongation pathway.....	97
Figure 3.4. The proportion of VLC -acyl- CoAs in the roots of elongase mutants and wild type plants.....	98
Figure 3.5 The proportion of VLC-acyl-CoAs in the shoots of elongase mutants and wild type plants.....	99
Figure 3.6. The quantity of acyl-CoA detected in the roots and shoots of elongase mutants compared to wild type plants.	101
Figure 3.7. Membrane glycerolipid composition in the shoots of elongase mutants and wild type plants.....	103
Figure 3.8 The proportion of phospholipids that contain a VLCFA in the shoots of elongase mutants and wild type plants.	104
Figure 3.9. The proportion of each acyl chain length in the total amount of PS identified in the shoots in elongase mutants and wild type plants.....	105
Figure 3.10 The proportion of PE containing a VLCFA as a percentage of the total amount of PE in the shoots of elongase mutants and wild type plants.	106
Figure 3.11 Membrane glycerolipid composition in the roots of elongase mutants and wild type plants.....	107
Figure 3.12. The proportion of phospholipids that contain a VLCFA in the roots of elongase mutants and wild type plants.	108
Figure 3.13 The proportion of each acyl chain length in the total amount of PS identified in the roots in the elongase mutants and wild type plants.....	109
Figure 3.14. The proportion of PE containing a VLCFA as a percentage of the total amount of PE in the roots of elongase mutants and wild type plants.....	110
Figure 3.15. Sphingolipid composition in the shoots of elongase mutants and wild type plants.....	112
Figure 3.16. Percentage of different fatty acid chain lengths in the different sphingolipids classes in the shoots of elongase mutants and wild type plants.....	114
Figure 3.17. The quantity of different fatty acid chain lengths in the different sphingolipids classes in the shoots of elongase mutants and wild type plants.....	117
Figure 3.18 Sphingolipid composition in the roots of elongase mutants and wild type plants.....	119
Figure 3.19 Percentage of different fatty acid chain lengths in the different sphingolipids classes in the roots of elongase mutants and wild type plants.	120

List of Figures

Figure 3.20. The quantity of different fatty acid chain lengths in the different sphingolipids classes in the roots of elongase mutants and wild type plants.	123
Figure 3.21. The total amount of free LCBs in the elongase mutants and wild type plants.....	125
Figure 4.1 Phenotypes of plants treated with herbicides that affect VLCFA synthesis.	138
Figure 4.2 Acyl-CoA profiles of the roots and shoots of plants treated with herbicides.	141
Figure 4.3 The percentage of total VLC-acyl-CoAs in herbicide treated plants.....	142
Figure 4.4 The quantity of acyl-CoA in herbicide treated plants.....	143
Figure 4.5 Membrane glycerolipid composition in the shoots of herbicide treated plants.....	144
Figure 4.6 Membrane glycerolipid composition in the roots of herbicide treated plants	145
Figure 4.7 The proportion of phospholipids that contain a VLCFA in the roots of herbicide treated plants.	146
Figure 4.8 The proportion of phospholipids that contain a VLCFAs in the shoots of herbicide treated plants.	148
Figure 4.9 Sphingolipid composition in the shoots and roots of herbicide treated plants.....	150
Figure 4.10 Percentage of different fatty acid chain lengths in the different sphingolipids classes in the shoots and roots of herbicide treated plants.....	153
Figure 4.11 The quantity of different fatty acid chain lengths in the different sphingolipids classes in the shoots and roots of herbicide treated plants.....	156
Figure 5.1 The effect of EMS on the genetic code.	166
Figure 5.2 TLC plate showing the separation of the wax components.	169
Figure 5.3 Wax profiles of flowers and stems obtained by GC-FID analysis.	171
Figure 5.4 Position of the TILLING mutations in the amino acid sequence of KCR1. .	174
Figure 5.5. dCAP primers used to determine the genotype of TILLING lines.	176
Figure 5.6 TILLING lines grown in the presence of herbicides.....	179
Figure 5.7. The steps taken in an EMS screen.	183
Figure 5.8. Phenotype of suppressor 36.....	185
Figure 5.9. Phenotype of suppressor 80.....	186
Figure 5.10 Phenotypic traits of suppressor plants.....	187

List of Figures

Figure 5.11. The proportion of VLC-acyl-CoAs in the suppressor mutants.	189
Figure 5.12. Acyl-CoA profiling of suppressor plants.	191
Figure 5.13 Toluidine blue test performed on the suppressor mutants	193
Figure 5.14. The total amount of wax in the two suppressor stems compared to Ler and <i>cer10-1</i>	194
Figure 5.15. Quantity of stem wax components in suppressor plants compared to <i>cer10-1</i>	196
Figure 5.16. Total amount of alkanes and primary alcohols in the flowers of the suppressor mutants.	198
Figure 5.17. Quantity and percentage of alkanes in the flowers of the suppressor mutants.....	199
Figure 6.1. Generation of a F ₂ population	208
Figure 6.2. Paired end illumina next generation sequencing.....	210
Figure 6.3. The structure of the <i>CER10</i> gene and position of the two <i>cer10</i> mutations.	211
Figure 6.4. 25 evenly distributed INDEL markers used to genotype <i>Arabidopsis</i> plants.	212
Figure 6.5. The position of the primers used to detect the purity of the mutant lines.	214
Figure 6.6. The SHOREmap pipeline to identify the SNPs in the suppressor mutants.	216
Figure 6.7. Genotyping F ₁ plants.....	217
Figure 6.8. Floral phenotype of plants within the F ₂ population of suppressor 36.....	218
Figure 6.9 A suppressor 80 plant selected from the F ₂ population.....	218
Figure 6.10. The genotyping results for suppressor 36	219
Figure 6.11 The position of additional markers used for genotyping suppressor 36.....	220
Figure 6.12 The position of additional markers used for genotyping suppressor 80.....	222
Figure 6.13 SHOREmap plots for suppressor 36.	227
Figure 6.14. SHOREmap plots for suppressor 80.	230

Declaration

I declare that the work in presented in this thesis is based purely on my own research, unless otherwise stated, and has not been submitted for a degree in this or any other university

Signed

Laura Elizabeth Seamons

July 2015

List of Abbreviations

ACCase	Acetyl-CoA carboxylase
ALC	Alcohol
ALK	Alkane
ACP	Acyl Carrier protein
BHT	Butylated hydroxylone
BLAST	Basic local alignment search tools
bp	Base pairs
BSTFA+TMS	bis-N-N-(trimethylsilyl) trifluoroacetamide 1% Trimethylsilyl
C	Carbon
CAPS	Cleaved Amplified Polymorphic sequences
CTP	cytidine triphosphate
CDP	cytidine diphosphate
CoA	Coenzyme A
Col- 0	Columbia-0 accession of <i>Arabidopsis</i>
DAG	Triacylglycerol
dCAPs	derived Cleaved Amplified Polymorphic Sequence
DHPLC	Denaturing high performance liquid chromatography
DNA	Deoxyribonucleic acid
ECR	enoyl-CoA-reductase
EMS	Ethyl methane sulphonate
ER	Endoplasmic reticulum
ESI-MS/MS	Electrospray ionisation tandem mass spectrometry
F1	First filial generation
F2	Second filial generation
FAE1	Fatty acid elongation 1
FAR	Fatty acyl reductase
FAS	Fatty acid synthase
FAT	ACP thioesterase
GC-MS	Gas chromatography- mass spectrometry
GlcCer	glucosylceramides
GIPC	glycosylated inositolphosphorylceramides
GPAT	GP acyltransferase
HCD	3- hydroxy-acyl-CoA dehydratase
HPLC	High performance liquid chromatography
INDEL	Insertion/ deletion sequences
IPC	Inositolphosphorylceramides
KAS	β - ketoacyl ACP synthase
kbp	Kilo base pairs
KCR	3 -keto- acyl-CoA reductase
KCS	3-keto-acyl-CoA synthase
KSR	3-ketosphinganine reductase
LAS	Long chain acyl CoA synthase
<i>Ler</i>	Landsberg <i>erecta</i> accession of <i>Arabidopsis</i>
LCB	Long chain base

List of Abbreviations

LSD	Least significant difference
LPA	lysophosphatidic acid
LPAT	lysophosphatidic acid acyltransferase
MAH	Mid-chain alkane hydroxylase
Mbp	Million base pairs
MRM	Multi reaction monitoring
MS	Mass spectrometer
NAD	nicotinamide adenine dinucleotide
NADP	nicotinamide adenine dinucleotide phosphate
NGS	Next generation sequencing
PA	Phosphatidic acid
PC	Phosphatidylcholine
PCD	Programmed cell death
PCR	Polymerase Chain Reaction
PE	Phosphatidylethanolamine
PI	Phosphatidylinositol
PIP ₂	phosphatidylinositol bisphosphate
PS	Phosphatidylserine
Q1, Q2 and Q3	1 st , 2 nd and 3 rd quadrupole
RNA	Ribonucleic acid
SBH	Sphingoid Base Hydroxylase
SBS	Sequencing by synthesis
SNP	Single nucleotide polymorphisms
SPT	Serine palmitoyltransferase
ssSPT	Small subunit of serine palmitoyltransferase
SUBA	Subcellular location of proteins in Arabidopsis
TAG	Triacylglycerol
TAIR	The <i>Arabidopsis</i> Information resource
TB	Toluidine Blue
TLC	Thin layer chromatography
VLC	Very long chains
VLCFA	Very long chain fatty acids
WS	Wax synthase

Chapter 1. General Introduction

1.1. Plant lipids

The demand for plant lipids is increasing, both for food, as larger populations require more seed oils, and for fuel as a sustainable substitute for petrochemicals. Our understanding of plant lipid biochemistry can be used to modify the biosynthesis of lipids so that greater yields can be achieved and allow for the production of novel lipids for desired applications. The success of any potential modification depends on understanding the complex events of lipid metabolism on both a genetic and biochemical level.

1.2. Arabidopsis as a model for studying plant lipids

Arabidopsis thaliana, is a small annual plant from the Brassicaceae family. *Arabidopsis* is the model dicotyledonous plant that is used in many genetic studies. It is a diploid plant containing 5 chromosomes and approximately 25,000 genes (Arabidopsis Genome, 2000). *Arabidopsis* is used as a model species due to a number of characteristics of the plant. These include a small genome, ease of growing, small structure and a short generation time of 6 weeks to produce thousands of seeds (Meinke *et al.*, 1998). Two other important features are its ability to be easily transformed using *Agrobacterium tumefaciens* (Clough and Bent, 1998) and the fact that the full *Arabidopsis* genome was sequenced and published in 2000 (Arabidopsis Genome, 2000). *Arabidopsis* mutants were first used to identify the role of plant lipids in 1985 (Browse *et al.*, 1985). This led the way to showing how mutants of lipid metabolism can be used to modify the existing lipid profile of leaves (Browse *et al.*, 1989). Since this time most lipid biosynthetic

pathways have been discovered in *Arabidopsis* (Ohlrogge and Browse, 1995, Dunn *et al.*, 2004, Bernard and Joubes, 2013).

1.3. Lipid structure and fatty acid nomenclature

Lipids are hydrophobic molecules that are formed from the condensation of thioesters (e.g. fatty acids) or by the condensation of isoprene units (prenols/sterols) (Fahy *et al.*, 2005). Fatty acids are long chain saturated or unsaturated carboxylic acids. Fatty acids are named using the X:Y nomenclature system, where X is the number of carbon atoms and Y is the number of double bonds. It is also necessary to assign carbon numbers to each of the three carbon atoms of a glycerol molecule. This is done using stereospecific numbering, where the prefix 'sn' is added. The carbon atom that appears at the top of a fisher projection, such that the hydroxyl group of carbon two is to the left, is designed 'sn1', followed by in a vertical line to carbon 2, 'sn2' and finally carbon 3, 'sn3'. This is shown in Figure 1.1.

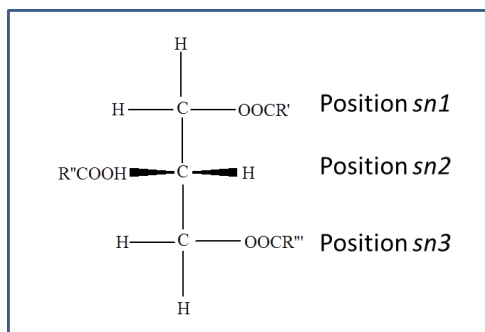


Figure 1.1 Stereospecific numbering of a glycerol molecule.

1.4. Fatty acid biosynthesis

1.4.1. Acetyl-CoA carboxylase

The carbon for fatty acid synthesis is provided by photosynthesis (except for germination where the carbon is provided from storage materials). Fatty acid

synthesis takes place in the plastid. Glycolysis produces acetyl CoA (Coenzyme A) by the action of pyruvate dehydrogenase (Givan, 1983). The first step of fatty acid biosynthesis involves the transfer of a carboxy group to acetyl CoA to produce malonyl CoA. This step requires ATP and bicarbonate, and is catalysed by acetyl CoA carboxylase (ACCase). The function of these enzymes and the steps involved are reviewed by Ohlrogge and Browse, (1995).

1.4.2. Fatty acid synthase in plants

The second step of fatty acid synthesis involves fatty acid synthase (FAS), a multiprotein complex. In plants this is a type II FAS (Overath and Stumpf, 1964, Harwood, 1988). Type II FAS catalyse the reactions of fatty acid synthesis as separate reactions, each catalysed by a specific protein. In contrast, in yeast these reactions are catalysed by a type I FAS, a multidomain protein. Type I FAS proteins have been reviewed by Schweizer and Hofmann, (2004). The following reactions are catalysed by this complex in plants, an acyl transfer reaction, four reactions involved in a 2 carbon addition and a termination reaction as shown in Figure 1.2. An excellent review of each of these reactions has been written by Harwood, (1996). An acyl carrier protein (ACP), (Sikorska and Kacperskapalacz), is used as the acyl carrier for the various reactions (Simoni *et al.*, 1967). The end product of these reactions is a 16-18 carbon chain fatty acid.

The acyl transfer reaction is catalysed by malonyl CoA-ACP transacylase (Figure 1.2a) which is needed to generate malonyl- ACP. The four reactions required for a 2 carbon addition, start with a condensation reaction catalysed by one of three 3 keto-acyl-ACP synthase (KAS) enzymes depending on the chain length of the substrate. The initial reaction between acetyl-CoA and malonyl-ACP is catalysed by KAS III

to produce a 4 carbon product (Figure 1.2b). KAS I elongates the chain from 4 to 16 carbons, (Figure 1.2c), and the final condensation reaction is catalysed by KAS II to generate 18 carbon chains, (Figure 1.2d). A reduction reaction catalysed by 3-ketoacyl-ACP reductase catalyses the second step in the 2 carbon addition (Figure 1.2e), followed by the third reaction which is a catalysed by 3-hydroxyacyl-ACP dehydrase, (Figure 1.2f). The fourth and final reaction, a second reduction reaction is catalysed by enoyl-ACP reductase (Figure 1.2g), (Harwood, 1996). A termination reaction then takes place which determines the fate of the lipid that has been synthesised (Figure 1h).

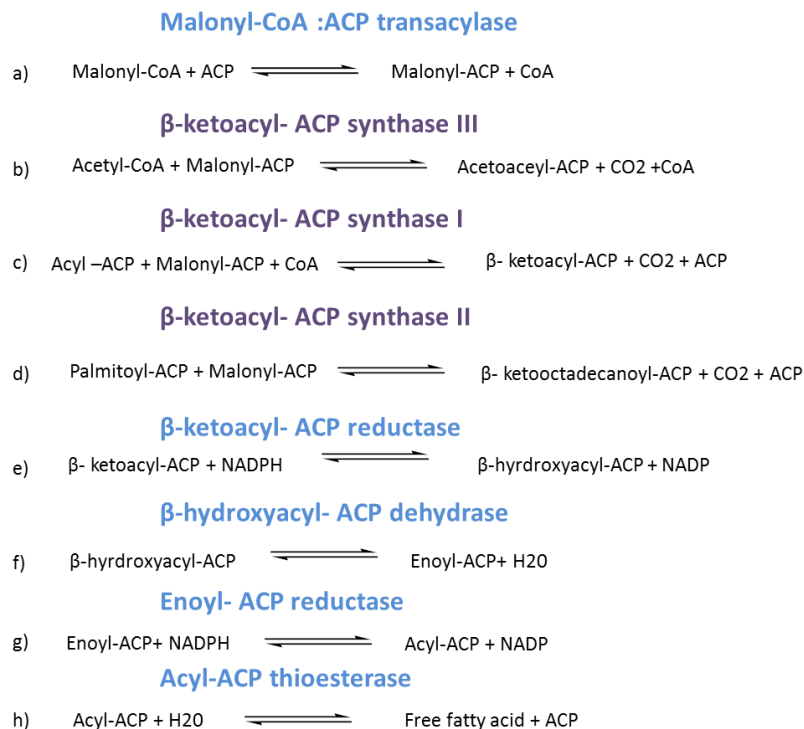


Figure 1.2 The reactions required for fatty acid synthesis in plants. Reaction (a) uses malonyl CoA as the substrate, which is produced in the first committed step of fatty acid synthesis. This reaction is followed by 5 reactions that result in the elongation and release of a free fatty acid of up to 18 carbons in length (b-h). Reactions (b),(c) and (d) are catalysed by three different KAS enzymes (highlighted in purple). Only one of these three reactions takes place in each round of elongation depending on the chain length of the substrate. Reaction (b) elongates from 2 carbon chains to 4 carbon chains, reaction (c) elongates carbon chains from 4 to 16 carbons, and finally reaction (d) elongates 16 carbon to 18 carbon chains (Harwood, 1996).

1.4.3. Utilisation of the products of fatty acid synthesis

The 16 or 18 carbon chain molecules which are produced by the FAS have one of two fates; the eukaryotic pathway or the prokaryotic pathway. In the eukaryotic pathway free fatty acids are released by ACP thioesterases, (Figure 1.2h), which terminates the synthesis and releases free fatty acids. ACP thioesterases determine the amount and type of fatty acids that are exported from the plastid. Two different classes of acyl-ACP thioesterases have been identified in plants, FatA and FatB (Voelker, 1996). The FatA class has the highest level of activity towards 18:1 and much lower activity towards saturated compounds. Whereas FatB has a higher catalytic activity towards saturated acyl groups but can act on unsaturated groups (Salas and Ohlrogge, 2002). Two genes encode FatA and a single gene encodes FatB in *Arabidopsis* (Salas and Ohlrogge, 2002). Once they have been released as free fatty acids they are then reesterified on the chloroplast envelope to acyl-CoAs, from there they can then be exported to the endoplasmic reticulum (ER) (Harwood, 1996). This reaction is catalysed by a long-chain acyl-CoA synthetase (LACS). There are nine LACS genes that have been annotated in the *Arabidopsis* genome to date (Shockey *et al.*, 2002). In the prokaryotic pathway the acyl chains (as acyl ACPs) are utilised within the chloroplast (Frentzen *et al.*, 1983).

There are similar enzymes in both pathways, which carry out comparable reactions. For example, both pathways acylate the *sn1* and *sn2* positions of the glycerol-3-phosphate to produce phosphatidic acid (PA). This is an important precursor for a number of different lipids. The glycerol 3-phosphate is first converted to lysophosphatidic acid (LPA), which is catalysed by glycerol 3-phosphate acyltransferase (GPAT). In which a carbon chain is added to the *sn1* position. This

is subsequently used to produce phosphatidic acid which is catalysed by LPA acyltransferase (LPAT), where a carbon chain is added to the *sn2* position. In the *Arabidopsis* prokaryotic pathway, GPAT activity is encoded for by one gene (Kunst *et al.*, 1988). In contrast within the eukaryotic pathway, this activity is encoded for by a family of GPAT enzymes in *Arabidopsis* (Zheng *et al.*, 2003). The LPAT enzymes of the plastid and cytoplasm show different substrate preferences. This is responsible for the characteristic lipids of the prokaryotic and eukaryotic pathway. The plastid LPAT is encoded for by a single gene. This gene has a higher activity when 16:0 is the substrate (Kim and Huang, 2004). In contrast, in the eukaryotic pathway the LPAT enzymes have a preference for 18:0. The two pathways therefore show characteristic chain lengths in the *sn2* position (Ohlrogge and Browse, 1995, Kim *et al.*, 2005).

1.5. VLCFA synthesis - a four step reaction

Fatty acids produced by the eukaryotic pathway can be elongated further to produce very long chain fatty acids (VLCFAs). VLCFAs contain chain lengths with greater than 18 carbon atoms. VLCFAs contribute only a small proportion of the total fatty acids in plant cells, as most cells contain high amounts of C16 and C18 for the synthesis of phospholipids and glycolipids that make up cellular membranes. However, despite their smaller proportions, VLCFAs are an absolute requirement in *Arabidopsis* (Bach *et al.*, 2008, Beaudoin *et al.*, 2009).

1.5.1. VLCFA synthesis in plants

VLCFAs are synthesized by the elongase complex in the ER. Like fatty acid synthesis, VLCFA synthesis involves four consecutive reactions and results in the

extension of the carbon chain by 2 carbon units. The elongase complex uses a pre-existing 16 or 18 carbon acyl-CoA which reacts with malonyl-CoA, (unlike the FAS which uses malonyl-ACP as the substrate), elongating the chain by 2 carbon units. The sequence of reactions is as follows;

1. *Condensation of malonyl- CoA with acyl CoA, catalysed by 3- Keto-acyl –CoA Synthase (KCS)*
2. *Reduction of the 3-keto-acyl CoA, catalysed by 3 –Keto- acyl-CoA Reductase (KCR)*
3. *Dehydration of the 3-hydroxy-acyl-CoA, catalysed by 3–Hydroxy-acyl-CoA Dehydratase (HCD/PAS2)*
4. *Reduction of the 2-enoyl-CoA to produce an acyl-CoA that is 2 carbon atoms longer catalysed by 2 Enoyl-CoA Reductase (ECR/CER10)*

At this point the carbon chain can either go through the cycle again and be elongated by a further 2 carbon units or it can be channelled into the various lipid pools (Bach and Faure, 2010). The four step reaction is shown in Figure 1.3.

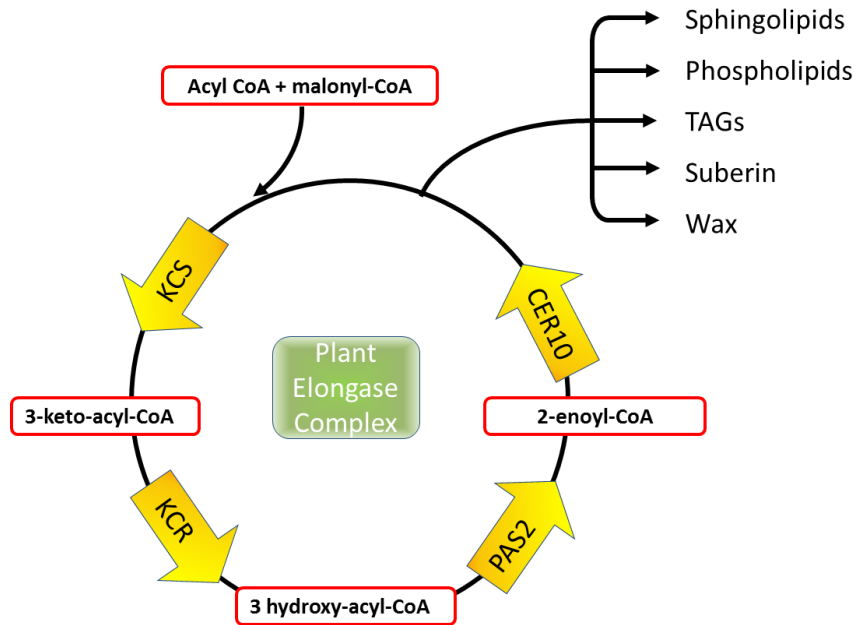


Figure 1.3. The very long chain fatty acid elongation cycle in plants. Long chain acyl- CoAs are elongated by the addition of a 2 carbon unit that requires four enzymatic reactions. Figure modified from (Bach and Faure, 2010).

1.5.2. The discovery of the four enzymes of the elongase complex in yeast

The ECR, HCR and HCD activity of the plant elongase were initially identified in microsomal fatty acid elongation in yeast, which has the same cycle of 4 reactions that are seen in plants. This led to the discovery of these enzymes in *Arabidopsis*.

1.5.2.1. Discovery of Enoyl-CoA Reductase (ECR)

The gene encoding for the Enoyl-CoA Reductase (ECR) (the fourth component of the elongase) was first discovered in yeast in a forward genetic screen for mutants defective in sphingolipid metabolism, and was identified as *TSC13* (Beeler *et al.*, 1998). Proof that *TSC13* encoded for the 2-Enoyl-CoA Reductase came from four lines of evidence. Firstly mutants shared phenotypic traits with the *elo* mutant genes (the genes responsible for the condensing reaction in yeast). It was also shown to interact physically with these condensing enzymes in co-immunoprecipitation experiments. There was also a build-up of the substrate of the ECR reaction, trans-2-enoil-CoA in the mutant. Finally *TSC13* showed homology to steroid 5- α -reductase, an enzyme that also reduces double bonds to a carbonyl group (Kohlwein *et al.*, 2001). The *ECR* gene *AtTSC13* (At3g55360) was discovered in *Arabidopsis*, by homology searches (Gable *et al.*, 2004). It was shown that heterologous expression of the *Arabidopsis TSC13* homologue was able to functionally complement the temperature sensitive phenotype of a yeast *tsc13* mutant and interact physically with the ELO proteins in yeast (Gable *et al.*, 2004). It was later shown that the mutant line *cer10* which was initially identified in a wax mutant screen in *Arabidopsis* by Koornneef *et al.*, (1989), was shown to cause disruptions in the characterised *ECR* gene (At3g55360). The *ECR* gene in *Arabidopsis* is known as *CER10* and will be referred to as *CER10* throughout this thesis.

1.5.2.2. Discovery of 3-Keto-acyl-CoA Reductase

The second component of the elongase to be identified in yeast was *YBR159*, encoding for the 3-Keto-acyl-CoA Reductase (KCR). The gene was identified when the *Saccharomyces cerevisiae* genome was searched for proteins of unknown function which contained domains likely to encode an oxidoreductase activity and that were predicted to be localised in the ER (Beaudoin *et al.*, 2002). Knockout mutations of various candidates were assayed with a condensing enzyme from *Arabidopsis* or from *Caenorhabditis elegans*, which are both capable of elongating unsaturated fatty acids in yeast, to see if these mutants had lost the ability to elongate fatty acids. *YBR159* was the only candidate shown to be essential for the elongation ability (Beaudoin *et al.*, 2002). Biochemical studies were used to confirm that *YBR159* is the major KCR for fatty acid elongation (Han *et al.*, 2002). Mutants were viable and accumulated small amounts of VLCFAs (Han *et al.*, 2002). For this reason it was thought that there must be another reductase that carried out a residual KCR activity. *AYR1* was discovered to carry out residual KCR activity and the double mutants of *Ayr1* and *ybr159* were not viable. However, *YBR159* is the major KCR as *ayr1* mutants showed no apparent deficiency in VLCFAs (Han *et al.*, 2002). The plant ortholog of *YBR159* was identified in *Arabidopsis* and is known as 3- Keto-acyl-CoA Reductase 1 (*KCR1*). The activity of *KCR1* was confirmed by functional complementation of the yeast *ybr159* mutant (Beaudoin *et al.*, 2002).

1.5.2.3. Discovery of 3-Hydroxy-acyl-CoA Dehydratase

The final component of the elongase to be identified in yeast was the 3-Hydroxy-acyl-CoA Dehydratase (HCR), identified as *PHS1* (Denic and Weissman, 2007). It

was shown that PHS1 interacted physically with the other identified components of the elongase; ELO, TSC13 and YBR159. Reduced levels of PHS1 resulted in a build-up of long chain bases, which suggested that VLCFA level had been reduced (Denic and Weissman, 2007). In *Arabidopsis* the *PAS2* gene was shown to encode for a protein which had 33% similarity with the protein sequence of PHS1 and was identified as the single functional orthologue of PHS1 in *Arabidopsis*. It was also shown to restore the function of the dehydratase in yeast containing dysfunctional PHS1 (Bach *et al.*, 2008).

1.5.2.4. Discovery of 3-Keto-acyl-CoA Synthase

The first step in the elongation of VLCFA involves a condensation reaction catalysed by a 3-Keto-acyl-CoA Synthase (KCS) producing a 3-keto-acyl-CoA intermediate. The condensing enzyme is encoded for by three *ELO* genes in yeast. The first to be identified was *ELO1*, which was shown to be involved in the elongation of 14 carbon fatty acids to 16 carbon fatty acids. This was elucidated from four pieces of evidence; 1) *elo1* cells could not grow on fatty acids shorter than 16:0, 2) mutant cells which were fed with C14:0 showed no further chain length extension, 3) the expression of *ELO1* increased when higher levels of 14:0 were added and 4) due to an NADPH binding domain found in its structure (Toke and Martin, 1996). This led to the identification of ELO2 and ELO3 as additional condensing enzymes due to similarities in their amino acid sequences with ELO1. ELO2 was shown to catalyse the elongation of fatty acids up to 24 carbons in length whereas ELO3 was shown to be essential for the conversion of C24 to C26 (Oh *et al.*, 1997). The simultaneous disruption of *ELO2* and *ELO3* was lethal (Revardel *et al.*, 1995, Silve *et al.*, 1996).

Unlike the other components of the elongase complex where the enzymes in plant were similar to yeast, the condensation reaction is catalysed by an unrelated family of proteins in plants called the *FAEI-like* genes. While unrelated, the *FAEI-like* genes of plants can rescue the lethality of the temperature sensitive *elo2elo3* mutant in yeast and are able to interact with the other elongase components in yeast (Paul *et al.*, 2006). In addition, there are 4 *ELO-LIKE* genes in *Arabidopsis* which show a large amount of homology to the *ELO* genes in yeast. These genes are largely uncharacterized in *Arabidopsis* (Dunn *et al.*, 2004).

1.6. The four VLCFA elongation reactions in plants

1.6.1. Reaction 1:- 3- Keto-acyl- CoA Synthase (KCS)

1.6.1.1. Structure and mechanism of KCS enzymes

The first component of the elongase complex and the first KCS enzyme to be identified in plants was fatty acid elongation 1 (FAE1), and the reaction which it catalyses is shown in Figure 1.4. This reaction was suggested to be the rate limiting step in VLCFA synthesis and determines the product length of the elongase complex (Millar and Kunst, 1997). *FAEI* was identified in three independent mutant screens for seed VLCFA deficiencies in *Arabidopsis* (James and Dooner, 1990, Lemieux *et al.*, 1990, Kunst, 1992). The discovery of *FAEI* led to the discovery of other KCS enzymes which are known as *FAEI-like* genes, of which, 21 have been found in *Arabidopsis* (Costaglioli *et al.*, 2005). There are also 4 *ELO-like* genes in *Arabidopsis*, the enzymes known to catalyse this step in yeast, but their function in *Arabidopsis* remains largely unknown (Dunn *et al.*, 2004). One *ELO* gene has been characterised in plants, *HOS3* At4g36830, which was identified

in a screen for enhanced response to abscisic acid. It was shown that *hos3* mutants had increased amounts of C22 and C24 and a reduction in the amount of C26. This implied that HOS3 is involved in the elongation of VLCFA to 26 carbons in length. It was suggested that HOS3 could play a role in producing VLCFA for the synthesis of sphingolipids (Quist *et al.*, 2009).

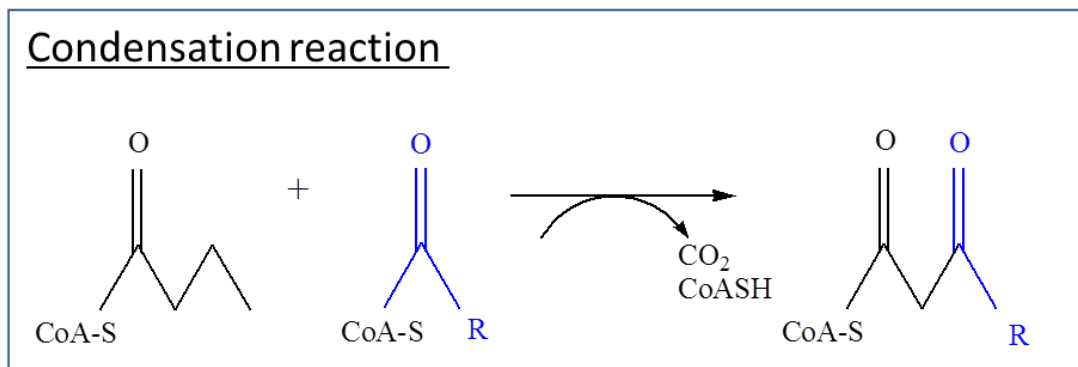


Figure 1.4 The condensation reaction catalysed by KCS showing both the substrate, the acyl CoA and the product, 3-keto-acyl-CoA.

Homology modelling carried out by Joubes *et al.*, (2008), was used to determine the 3D structure of KCS enzymes. This was carried out initially for KCS1 which was then used to infer the structure of the rest of the KCS family. These studies showed that all KCS enzymes contain a similar four-layered α_a - β_b - α_c - α_d fold structure. The α_a of most KCS enzymes was shown to be in the optimal position to act as a membrane anchor and is composed of one or two alpha helices so that the KCS enzymes are correctly positioned in the ER. In seven of the KCS enzymes a membrane anchor did not appear to be present. It is likely that through interaction with other components of the elongase complex these KCS enzymes reach the correct localization and positioning at the ER membrane (Joubes *et al.*, 2008). The remaining components of the KCS enzyme β_b - α_c - α_d make up the cytosolic domain of the enzyme. All of the catalytic residues were found to be on the α_c fold (Joubes

et al., 2008) and were superimposed on top of one another in a protein model. This made it possible to compare the size and shape of the substrate binding pockets for the different KCS enzymes. From this modelling work, it was possible to correlate the size of the binding pocket and the length of the acyl substrate of the KCS enzyme (Joubes *et al.*, 2008). However a crystal structure would be necessary to confirm these findings.

1.6.1.2. Role of KCS enzymes

In contrast to the enzymes catalysing the 3 subsequent reactions in the pathway, which are ubiquitously expressed throughout the plant, KCS enzymes show tissue specific expression. The KCS enzymes characterised so far have different, but overlapping substrate chain length specificities and show some degree of tissue specific expression (Joubes *et al.*, 2008). It is the expression of a particular KCS that determines which VLCFAs are produced (Millar and Kunst, 1997). For example *FAEI* encodes a condensing enzyme involved in the elongation of C18 and C20 fatty acids in seeds, the products of which are stored in triacylglycerols (Kunst, 1992). Whereas, KCS1 (Todd *et al.*, 1999) and KCS6 (Millar *et al.*, 1999) have been shown to play a role in the synthesis of VLCFA precursors for wax production in the shoots epidermis. Table 1.1 shows all of the known KCS enzymes and their function where it is known.

Table 1.1. The 21 different KCS enzymes, their expression patterns and biological function. Table modified from (Haslam and Kunst, 2013). Expression patterns determined by (Joubes *et al.*, 2008) unless otherwise stated.

Name	Biological function	Expression pattern
KCS1	Cuticular wax accumulation affects alcohols and aldehydes(Todd <i>et al.</i> , 1999)	Expressed in all tissues, levels are the highest in siliques, stems and cauline leaves
KCS2 (DAISY)	Suberin synthesis in the roots and cuticular wax biosynthesis	Expression highest in the roots, siliques and flowers, enhanced expression during osmotic stress (Franke <i>et al.</i> , 2009, Lee <i>et al.</i> , 2009)
KCS3	Unknown	Expressed in all tissues except roots, highest expression in siliques
KCS4	Unknown	Highest expression in siliques, low level of expression in all tissues
KCS5 (CER60)	Role in cuticular lipids (Fiebig <i>et al.</i> , 2000)	Expressed in all tissues highest expression in siliques
KCS6 (CER6)	Cuticular wax (Millar <i>et al.</i> , 1999, Fiebig <i>et al.</i> , 2000)	Epidermis specific expression, expression in all tissues except roots (Hooker <i>et al.</i> , 2002)
KCS7	Unknown	Expressed only in flowers and siliques
KCS8	Unknown	Highest expression in cauline leaves, some expression in stems, rosette leaves, flowers and siliques
KCS9	Elongation of 22 to 24 carbon chain length (Kim <i>et al.</i> , 2013)	Expressed in all tissues highest in epidermis, rosette leaves cauline leaves and siliques
KCS10 (FDH)	Development of epidermis (Pruitt <i>et al.</i> , 2000)	Expression in all tissues except roots highest in stems and siliques
KCS11	Unknown	Low expression in all tissues
KCS12	Unknown	Expressed in all tissues except roots, highest expression in cauline leaves and siliques
KCS13 (HIC)	Involved in stomatal development in response to differing levels of CO ₂ (Gray <i>et al.</i> , 2000)	Expression in all tissues, except roots highest in siliques and flowers
KSC14	Unknown	Expressed in siliques otherwise low levels of expression
KCS15	Unknown	Expressed only in flowers

KCS16	Unknown	Low levels of expression except in siliques
KCS17	Unknown	Low levels of expression except in flowers
KCS18 (FAE1)	VLCFAs production in seed storage triacylglycerols (Kunst, 1992)	Seed specific expression (James <i>et al.</i> , 1995)
KCS19	Unknown	Low levels of expression except in siliques
KCS20	Redundant roles in suberin and cuticular wax biosynthesis (Lee <i>et al.</i> , 2009)	Expressed in all tissues, lower levels of expression in the roots
KCS21	Unknown	Only expressed in flowers

1.6.2. Reaction 2:- 3- Keto- acyl -CoA Reductase (KCR)

The product of the KCS reaction is reduced by KCR producing a 3-hydroxy- acyl-CoA. The reaction that KCR catalyses can be seen in Figure 1.5.

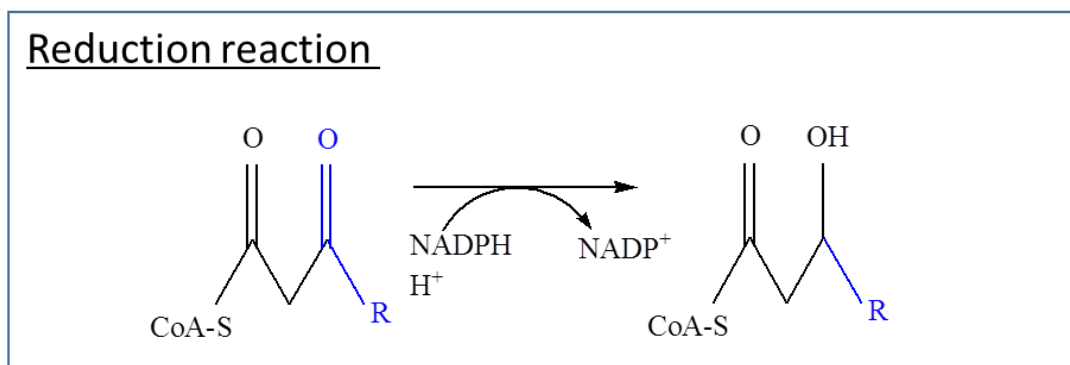


Figure 1.5 The reduction reaction catalysed by KCR showing the substrate for the reaction, 3- keto-acyl CoA and the product of the reaction 3-hydroxy-acyl-CoA.

There are two *KCR*-like genes in *Arabidopsis*, *KCR1* and *KCR2* (Dietrich *et al.*, 2005). *KCR1* has been shown to be embryo lethal when absent, whereas *KCR2* has no effect when absent (Beaudoin *et al.*, 2009). Despite 45% amino acid identity between *KCR1* and *KCR2*, *KCR2* cannot restore the function of *KCR1* when placed behind the *KCR1* promoter. This would suggest that *KCR2* cannot restore the embryo lethal phenotype of *kcr1*. It does however, not rule out the possibility

that KCR2 can carry out KCR activity later in development. In addition *KCR2* cannot complement the *ybr159* mutant in yeast unlike *KCR1* (Beaudoin *et al.*, 2009). *KCR1* and *KCR2* both contain a putative NADH binding motif and an essential SX₁₆YX₃K catalytic motif. However, only *KCR1* contains a C-terminal di-lysine ER retention motif characteristic of other plant reductases involved in VLCFA synthesis. *KCR1* was shown to be ubiquitously expressed in *Arabidopsis* (Beaudoin *et al.*, 2009). RNAi constructs of *KCR1* which specifically down-regulate the expression of only *AtKCR1* produce a variety of phenotypes as shown in Figure 1.6 (Beaudoin *et al.*, 2009). The plants showed a lack of lateral roots, (Figure 1.6 d and e), glossy stems, and fused aerial organs (Figure 1.6a-c) (Beaudoin *et al.*, 2009).

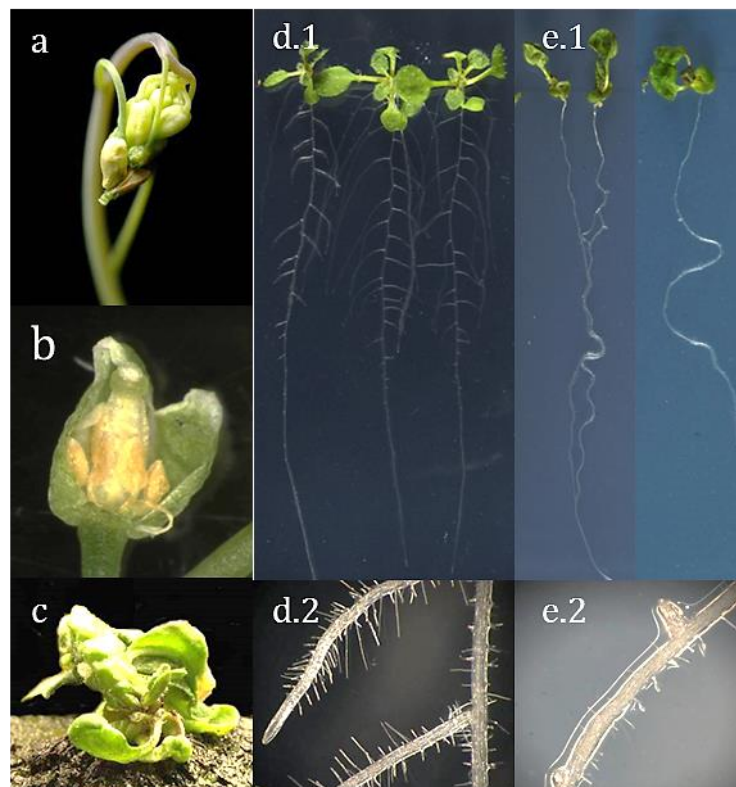


Figure 1.6 The phenotypic traits of the *KCR RNAi* lines. (a) fused flower buds, (b) opened flowers bud, (c) fused rosette leaves, (d) wild type and (e) *KCR RNAi* line roots (Beaudoin *et al.* 2009).

1.6.3. Reaction 3 :-3-Hydroxy-acyl-CoA Dehydratase; (*HCD-PASTICCINO2 (PAS2)*)

The 3-hydroxyl-acyl-CoA product is dehydrated in the third step. This is catalysed by HCD, or PAS2, to produce a 2-enoyl-CoA. The reaction is shown in Figure 1.7. This step was suggested to be a limiting step in VLCFA synthesis because there was an increase in VLCFA levels in the seeds and leaves when the dehydratase expression was increased (Bach *et al.*, 2008). It was previously thought that only the condensation reaction catalysed by KCS was the rate limiting step but the work by Bach *et al.*, (2008) would suggest that the dehydratase reaction catalysed by PAS2 also has an effect on the rate of reaction (Millar and Kunst, 1997). More work is needed to determine which step is the rate limiting step. *PAS2* was originally identified in a screen for uncontrolled growth in the presence of cytokinins, leading to cell proliferation and callus formation (Faure *et al.*, 1998). It was discovered along with the two other characterised *PAS* genes which both have a role in VLCFA synthesis, *PAS1* and *PAS3*. *PAS1* is thought to encode for a scaffold protein for the elongase complex (Roudier *et al.*, 2010). *PAS3* encodes for an acetyl-CoA carboxylase which catalyses the formation of malonyl CoA, the substrate for VLCFA elongation (Baud *et al.*, 2004) (Baud *et al.*, 2003). All three mutants showed similar alterations in development throughout the life of the plant (Faure *et al.*, 1998). *PAS2* was shown to have a role in VLCFA metabolism and identified to encode for the dehydratase through sequence similarity studies with the dehydratase activity in yeast (Bach *et al.*, 2008). The function of the other two *PAS* genes will be discussed in section 1.11.2.

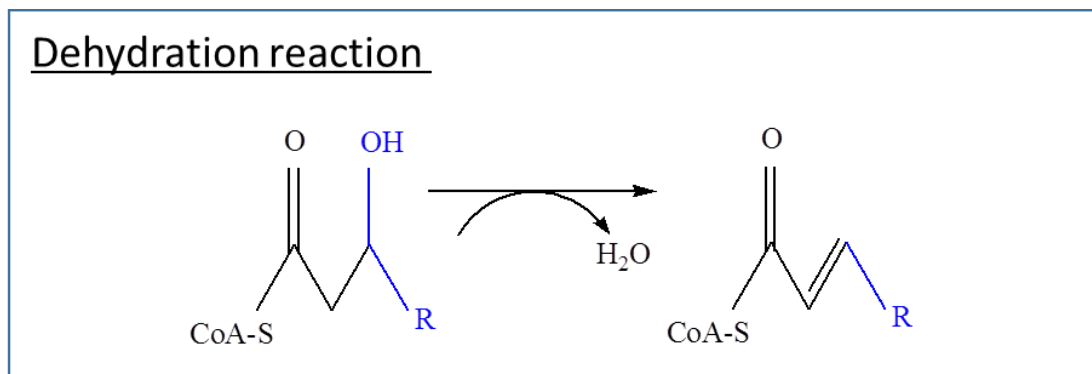


Figure 1.7 The dehydratase reaction catalysed by PAS2 (HCR). The substrate of the reaction is 3-hydroxy-acyl-CoA, the product of the reaction is trans-2-enoyl-CoA.

A leaky mutation of *PAS2*, *pas2-1*, was characterised by a general reduction in the level of VLCFAs in seed storage triacylglycerols, cuticular waxes and sphingolipids, as well as the accumulation of the 3-hydroxy-acyl-CoA intermediate (the substrate for the dehydration reaction) (Bach *et al.*, 2008).

A null mutation of *PAS2* is embryo lethal, showing that the role of VLCFAs in *Arabidopsis* is essential (Bach *et al.*, 2008). The *pas2-1* line was shown to have several developmental alterations. For example; the embryos showed shorter and thicker hypocotyls as well as smaller more rounded cotyledons which lead to dwarf seedlings with shorter, thicker hypocotyls and reduced finger shaped cotyledons (Faure *et al.*, 1998, Bellec *et al.*, 2002). The phenotype of *pas2-1* is shown in Figure 1.8.

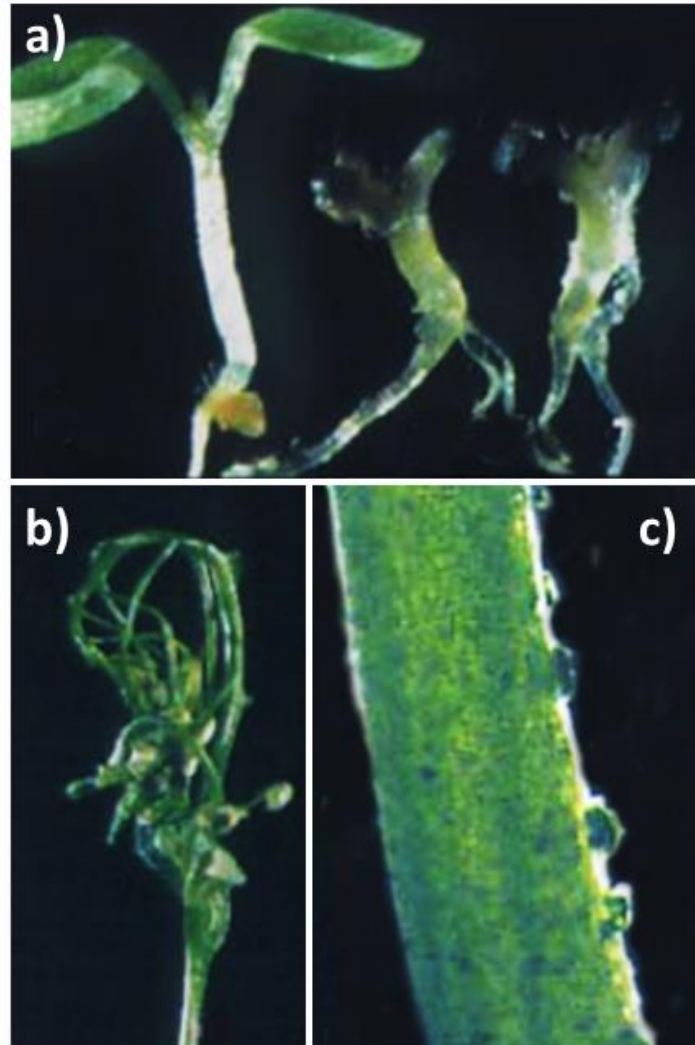


Figure 1.8 The phenotypic traits of *pas2-1*. (a) the phenotype of 10 day old *pas2-1* seedlings compared to WT, (b) fused flower buds of *pas2-1* and (c) localised lumps on *pas2-1* stems (Bellec et al. 2002) .

The *pas2-1* line showed ectopic cell proliferation in tissues which are normally differentiated. The dividing cells developed into larger nodules to form finger like structures, expanding outside the cotyledon. The apical part of the seedling turned into a callus like structure. The mutant meristem gave rise to deformed leaves and stems, and in a few cases, resulted in sterile flowers. *pas2-1* also showed

spontaneous fusion between organs such as leaves, stems, flowers or siliques (Bellec *et al.*, 2002).

1.6.4. Reaction 4:-2-Enoyl -CoA Reductase (ECR/CER10)

During the fourth and final step, the 2-enoyl-CoA intermediate is reduced by ECR (or CER10) to produce an acyl-CoA elongated by two carbon atoms. The reaction is shown in Figure 1.9.

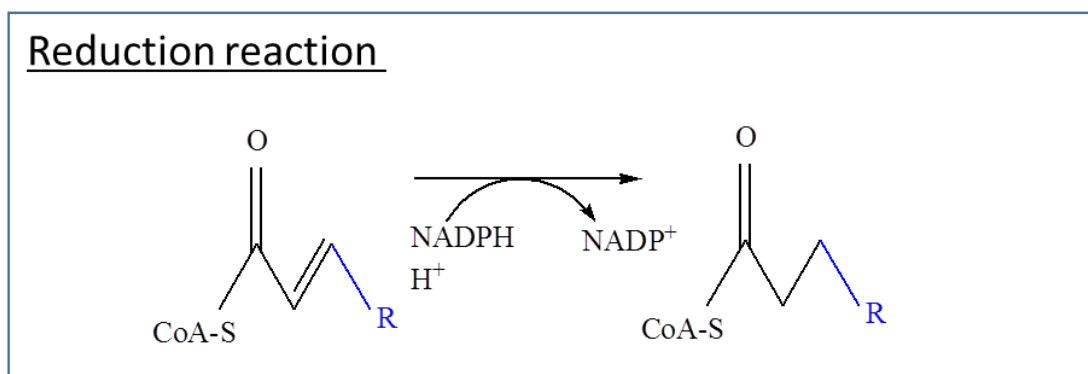


Figure 1.9 The reduction reaction catalysed by CER10. The substrate for the reaction is trans-2-enoyl-CoA and the product is the elongated acyl CoA which has been elongated by 2 carbon atoms. The *cer10* mutant is a null mutation but is not embryo lethal. Since null mutations of the two other core components of the elongase are embryo lethal it suggests that there may be other isoforms of CER10 or, that this redundancy is due to an unrelated gene (Zheng *et al.*, 2005). Nevertheless, the *cer10* mutant displays severe morphological abnormalities, shown in Figure 1.10 (Zheng *et al.*, 2005). The mutant plants have leaves which are smaller and are more crinkled than in wild type plants (Figure 1.10c). The stems of the mutant were shorter than those in wild type plants (Figure 1.10a), and the flower buds were smaller and fused (Figure 1.10b). It was also shown that the *cer10* mutant was male semi-sterile but female fertile. All of the organs in *cer10* were smaller than wild type (Zheng *et al.*, 2005).

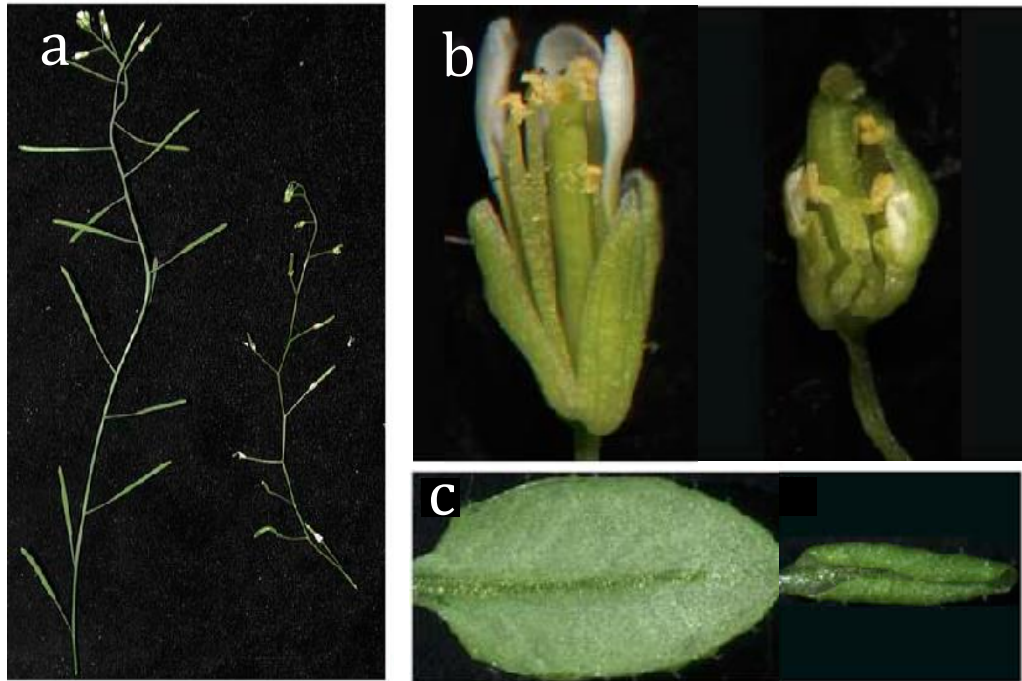


Figure 1.10 Phenotypic traits of *cer10* (a) smaller stems, (b) fused flower buds, (c) smaller crinkled leaves, photographs taken from (Zheng et al. 2005).

1.7. Physiological roles of VLCFAs containing lipids

VLCFAs are found in 5 major lipid pools in *Arabidopsis*; sphingolipids, phospholipids, triacylglycerols, suberin and cuticular waxes. The presence of VLCFAs in these 5 major lipid pools highlights the vital role VLCFAs have in a wide variety of functions in *Arabidopsis*. A brief description of each lipid pool will be given below.

- Triacylglycerols (TAGs) act as a reserve of energy for the germinating seeds and can represent up to half the dry weight of the seed (Aach and Heise, 1998).
- Cuticular waxes are composed primarily of a mixture of different very long chain aliphatic compounds ranging from 26 to 34 carbons in length and are

found on the surface of the plant as part of the cuticle. An excellent review on cuticular waxes has recently been published by Bernard and Joubes, (2013).

- Suberin is deposited on the inner side of the primary cell wall. It's functions include controlling the movement of water and solutes, providing strength to the cell wall and providing a barrier to pathogen movement. Suberin consists of a polymer of polyaliphatic and polyaromatic compounds embedded with waxes with a number of phenolic compounds. Trans esterification of the aliphatic compounds shows that suberin contains ω -hydroxy fatty acids, dicarboxylic acids and alcohols which contain significant amounts of very long chains (VLC) (Kolattukudy, 1980). Suberin is found in the roots and is formed in response to wounding in any organ (Kolattukudy, 1980).
- Sphingolipids have a number of functions including, components of plasma membranes, important signalling molecules, formation of membrane microdomains (lipid rafts), and have a role in programmed cell death. Lipid rafts are thought to have important roles in protein sorting and signal transduction (Michaelson and Napier, 2010).

The lipid classes that will be analysed in this thesis will be discussed in more detail below.

1.8. Sphingolipids

Sphingolipids have been shown to be essential throughout plant development, and play a role in seedling establishment, in young plants and in mature plants (Dietrich

et al., 2008). There is a large diversity of sphingolipid molecules in *Arabidopsis*. Sphingolipids account for 10% of total *Arabidopsis* lipids (Dunn *et al.*, 2004).

1.8.1. Sphingolipid structure

The backbone of any sphingolipid molecule is a ceramide molecule. Ceramides consists of a long chain base (LCB) linked to a fatty acid by an amide link. Figure 1.11c shows the structure of a ceramide molecule. The amide group of the LCB is acylated with a fatty acid of between 16-26 carbon atoms in length to form a ceramide. A polar head group, sugar or phosphate binds to the C1 hydroxy group of the LCB to form a complex sphingolipid. Over 168 sphingolipids have been structurally characterised in *Arabidopsis*, and it is the diversity of the LCB, head group and fatty acid chain that allows for the possibility of such a large group of molecular species (Markham and Jaworski, 2007).

In *Arabidopsis* the predominant fatty acids of sphingolipids are 24:1 and 24:0 which together make up 55% of the total amount of fatty acids in sphingolipids. The fatty acids 16:0, 22:0, 26:0 and 26:1 are also present with approximately 15% of each (Dunn *et al.*, 2004). LCBs contain 18 carbons and up to 3 hydroxy groups. The variation in LCBs is achieved by modifications at C4 of the LCB molecule where desaturation and hydroxylation can occur, and at C8 where desaturation can occur. LCBs are named according to the number of hydroxy groups, t18 would contain three hydroxy groups (Figure 1.11a) and d18 would contain two hydroxy groups (Figure 1.11b). The predominant LCBs in *Arabidopsis* are the cis and trans form of t18:1 comprising 57% and 32% respectively, while d18:1 isomers make up less than 10% (Dunn *et al.*, 2004).

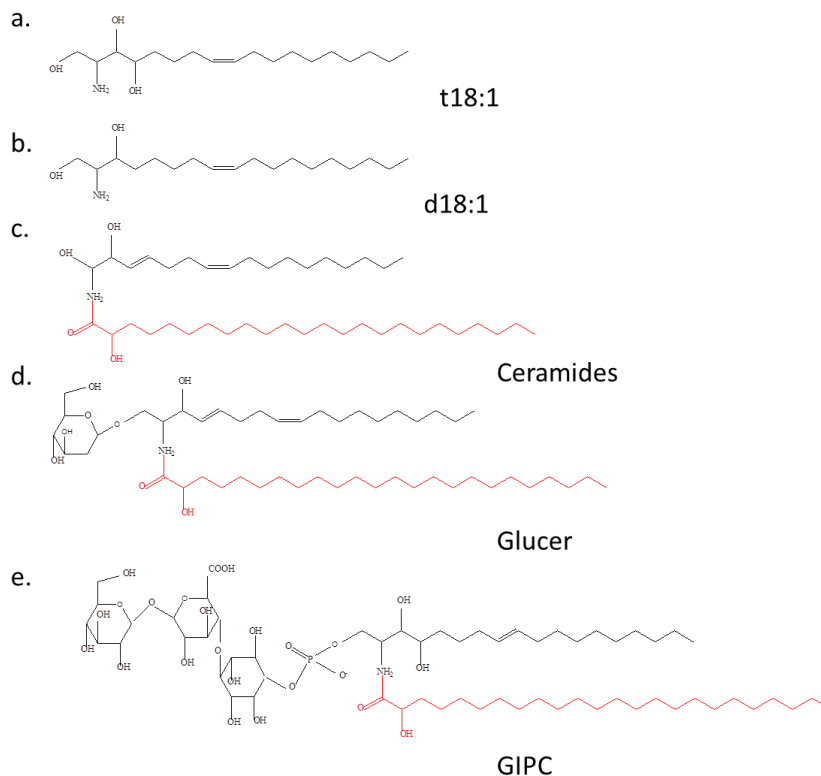


Figure 1.11 The structure of the most common LCBs and complex sphingolipids. The VLCFA is shown in red.

The two most predominant sphingolipids in plants tissue are the glucosylceramides (GlcCer) and glycosylated inositolphosphorylceramides (GIPCs). In *Arabidopsis* leaves GIPCs are the predominant form, making up 60% of total sphingolipids. GIPCs contain glycosylated inositol-1-phosphate linked as a phosphodiester to the head group of the ceramide (Figure 1.11e). GlcCers account for a further 30%. GlcCers have between 1 and 4 glycosyl residues as the head group of the ceramide, (Figure 1.11.d). The remaining 10% of total sphingolipids consist of ceramides (Figure 1.11.c), free LCBs (Figure 1.11a and b), and phosphorylated LCBs (Markham and Jaworski, 2007). Phosphorylated LCBs are formed when free LCBs are phosphorylated.

1.8.2. Sphingolipid synthesis

Sphingolipid synthesis can be divided into a number of stages, LCB synthesis, ceramide synthesis and complex sphingolipid synthesis. An overview of sphingolipid synthesis can be found in Figure 1.12.

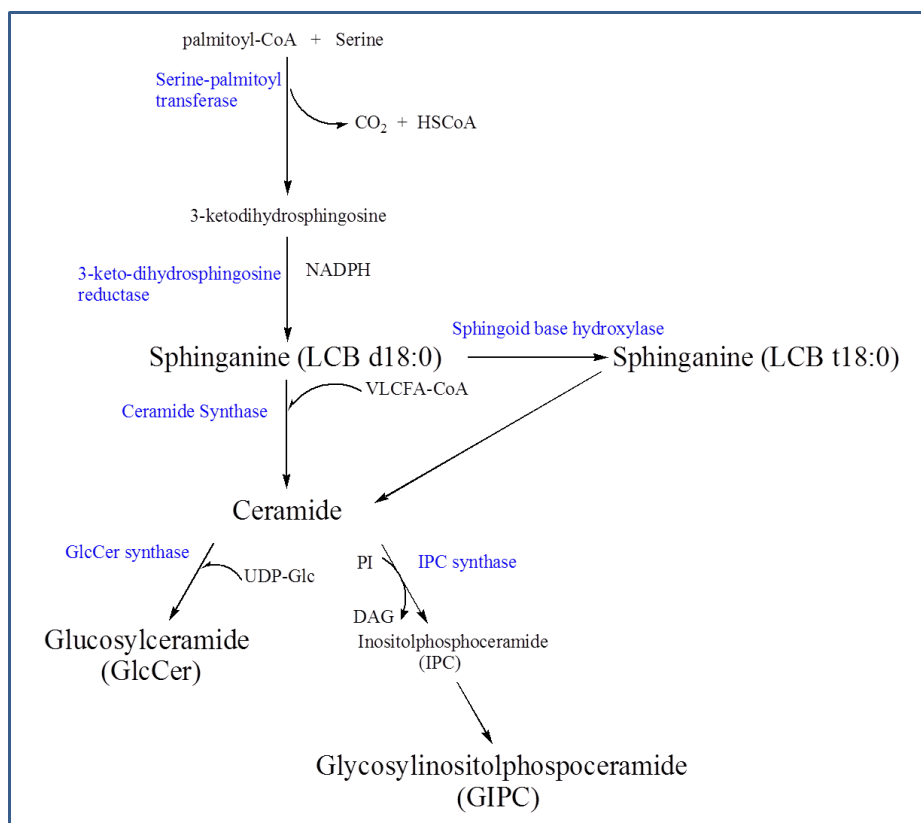


Figure 1.12 Sphingolipid synthesis. The key steps of sphingolipid synthesis, showing the enzymes and intermediates involved.

1.8.2.1. Long chain base synthesis

The first step in sphingolipid synthesis is the formation of the LCB molecule. The acyl-CoA substrate undergoes a condensation reaction with serine to produce 3-ketosphinganine with CO₂ as the by-product. This reaction is catalysed by serine palmitoyltransferase (SPT), a member of a small subfamily of pyridoxal 5'-phosphate (PLP) enzymes. The reaction is shown in Figure 1.13. All enzymes of this family catalyse the condensation of an amino acid and a carboxylic acid CoA

thioester to produce α -oxoamines. Serine palmitoyltransferase is membrane associated and is encoded by two genes, *LCB1* and *LCB2* in all known eukaryotes. A review of current understanding of SPT activity has been written by Hanada, (2003). In yeast, it was shown that *LCB2* contains the catalytic lysine residue that binds the pyridoxal phosphate (the cofactor required for this reaction to occur), whereas *LCB1* is thought to stabilize the *LCB2* subunit and the active site is at the interface of the two subunits (Gable *et al.*, 2002).

An *LCB2* gene was identified in *Arabidopsis*, which was shown to be ER localised and increased the SPT activity in a yeast *lcb2Δ* mutant (Tamura *et al.*, 2001). It was later shown that there are two isoforms of *LCB2* in *Arabidopsis* (*AtLCB2a* and *AtLCB2b*) (Dietrich *et al.*, 2008). The first *LCB2* gene to be characterised (*At5g23670*), was designated *AtLCB2a*. The second *LCB2* gene to be identified (*At3g48780*) was designated *AtLCB2b*. The two genes were shown to be expressed in all organs, with *LCB2a* being present at a higher levels in all organs. It was shown that there was no effect on sphingolipid content or growth in knockout mutants of either of the genes but homozygous double mutants were not recoverable, suggesting the genes are functionally redundant (Dietrich *et al.*, 2008).

The other subunit of SPT, *LCB1*, was shown to be essential (Chen *et al.*, 2006). It was also shown to be localised in the ER like *LCB2*. Coexpression of the gene for *AtLCB1* with the gene for *AtLCB2* yields an active SPT which is able to rescue *lcb1Δ* and *lcb2Δ* single and double knockout mutants in yeast (Chen *et al.*, 2006).

Tsc13p is a small protein, identified in yeast and was shown to stimulate the activity of SPT. It was shown to be essential for high temperature growth (Gable *et al.*,

2000). Two functionally equivalent proteins were then identified in humans and were named small subunits of serine palmitoyltransferase, ssSPTa and ssSPTb (Han *et al.*, 2009). Based on homology to the human ssSPT two similar proteins were identified in *Arabidopsis*. They were shown to physically interact with the *Arabidopsis* LCB1 and LCB2 and showed an increase in SPT activity when expressed in *Saccharomyces cerevisiae* SPT null mutants (Kimberlin *et al.*, 2013).



Figure 1.13. Reaction catalysed by serine palmitoyltransferase to produce 3-ketosphinganine. Diagram modified from (Chen *et al.*, 2008).

The product of this reaction 3-ketosphinganine then undergoes a reduction reaction to form dihydrosphingosine (d18:0). This reaction is shown in Figure 1.14. This is catalysed by 3-ketosphinganine reductase (KSR) via an NADPH dependent reaction. There are two genes which encode a KSR in *Arabidopsis*, *TSC10A* and *TSC10B*; they are functionally redundant and essential. Both genes are expressed throughout the plant and *TSC10A* shows a higher level of expression than *TSC10B* (Chao *et al.*, 2011).

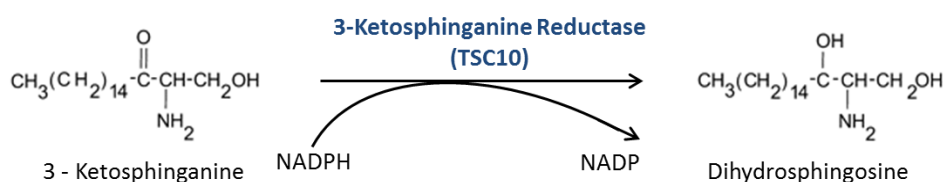


Figure 1.14. Reaction catalysed by 3-ketosphinganine reductase to produce dihydrosphingosine (d18:0). Diagram modified from (Chen *et al.*, 2008).

Dihydrosphingosine is then hydroxylated to produce the dominant form of LCBs, phytosphingosine (t18:0). LCBs can contain up to three hydroxyl groups. The C1

and C3 hydroxy group arise from the precursors, serine and palmitoyl CoA. The C4 hydroxylation occurs once the LCB molecule has been synthesised. This reaction is catalysed by SUR2 in yeast (Grilley *et al.*, 1998). In *Arabidopsis*, two functional SUR2 orthologs have been discovered Sphingoid Base Hydroxylase 1 and 2 (SBH). *SBH1* (At1g69640) and *SBH2* (At1g14290) are able to restore the function of *sur2Δ* mutants in yeast (Sperling *et al.*, 2001). Double mutants show severe growth defects. Plants were reduced in size, showed necrotic lesions and most died before they produced true leaves. C4 hydroxylation is critical for the maintaining the correct sphingolipid and fatty acid composition and for the growth and reproduction of *Arabidopsis* (Chen *et al.*, 2008).

1.8.2.2. Ceramide synthesis

The synthesized LCBs can then react with VLCFAs to form a ceramide, this reaction is catalysed by ceramide synthase and takes place in the ER. The first ceramide synthase gene to be identified in plants was the tomato gene *Asc-1* (Brandwagt *et al.*, 2000, Spassieva *et al.*, 2002). Sequence searches revealed three homologs in *Arabidopsis*, referred to as *LOH1*, *LOH2*, and *LOH3* (Markham *et al.*, 2011). It was shown that *LOH1* and *LOH3* encode for proteins which have redundant activities. The presence of one of these genes is essential for plant growth, whereas *LOH2* mutants had no obvious effect on plant development (Markham *et al.*, 2011). It was shown that *LOH1* and *LOH3* have targeted activities towards VLCFA whereas *LOH2* targets 16:0. This essential nature of *LOH1* and *LOH3* demonstrates that VLCFA containing sphingolipids are essential in *Arabidopsis* (Markham *et al.*, 2011).

Sphingolipids contain monounsaturated fatty acids (Markham and Jaworski, 2007). *ADS2* is a member of the acyl CoA desaturase –like gene family, and mutations in this gene caused reduced amounts of 24:1 and 26:1 in the acyl-CoA pool. Due to this decrease, it is thought that the monounsaturated fatty acids are formed within the acyl-CoA pool before it reacts with a LCB to form a ceramide (Smith *et al.*, 2013).

The sphingolipid fatty acid has a hydroxy group, and in contrast to the desaturation this is thought to occur on the ceramide molecule. This activity was shown to be catalysed by FAH1 in yeast, a cytochrome b₅-fusion enzyme (Mitchell and Martin, 1997). Two functional orthologs have been identified in *Arabidopsis*, *FAH1* and *FAH2*, both sequences lack the cytochrome b₅ domain seen in yeast. Evidence suggests that the FAH enzyme interacts with microsomal cytochrome b₅ which acts as the electron donor in this reaction (Nagano *et al.*, 2009). It is thought that the two enzymes have different substrate specificities. FAH1 has a substrate specificity which favours VLCFA hydroxylation whereas FAH2 acts on 16:0 substrates (Nagano *et al.*, 2012).

1.8.2.3. Synthesis of GIPCs and GlcCers

GIPCs are the predominant species of sphingolipids in *Arabidopsis* (Markham and Jaworski, 2007). Ceramides are synthesized in the ER and are then translocated to the Golgi to produce GIPCs (Hanada *et al.*, 2003, Wang *et al.*, 2008). The first step of GIPC synthesis involves the transfer of inositol phosphate, from the phospholipid phosphatidylinositol (PI), to a ceramide in order to form inositolphosphorylceramides (IPC). This results in the release of diacylglycerol and is catalysed by IPC synthase. In *Arabidopsis* this function is thought to be encoded by *ERH1* (enhancing RPW8-

mediated HR-like cell death 1) in which the mutant showed an increase in the amount of ceramides (Wang *et al.*, 2008). Sugar molecules are then added to the IPC molecule. There appears to be one major species of GIPC in *Arabidopsis*; hexose-hexuronic-inositolphosphoceramide, where the hexose is a glucose and the hexuronic acid is glucuronic acid (Markham *et al.*, 2006, Bure *et al.*, 2011). It was shown that *Arabidopsis* contains 90% monohexosylated GIPCs and 10% dihexosylated GIPCs (Mortimer *et al.*, 2013). In addition to glucose it was also found that mannose, arabinose and galactose are present as the sugar molecules in GIPCs. It has been shown that GONST1 can transport all GDP-sugars into the Golgi for GIPC glycosylation (Mortimer *et al.*, 2013).

GlcCer are the second most abundant form of sphingolipids in *Arabidopsis* (Markham and Jaworski, 2007). GlcCer have sugar head groups attached to the ceramide molecule. The major sugar head groups in plants are the β -D-glucopyranosyl residue and smaller amounts of β -D-mannosyl ceramides (Fujino and Ohnishi, 1982). There can be up to 4 identical mannopyranosyl molecules and each is linked to the previous sugar by a 1-4 linkage. To the end of the sugar chain a terminal 1-4 linked β -D-glucopyranosyl group is added, resulting in glucosyl capped di, tri and tetrahexosyl ceramides (Fujino and Ohnishi, 1982). The biosynthesis of GlcCer is catalysed by glucosylceramide synthase (GCS) which transfers glucose from uridine diphosphate (UDP)-glucose to a ceramide molecule (Basu *et al.*, 1968).

1.8.3. Sphingolipid function

1.8.3.1. *Programmed cell death*

Sphingolipids are thought to play a role in programmed cell death (PCD). Evidence for this comes from the ceramide kinase mutant *accelerated cell death 5 (acd5)*. It is thought that the balance between ceramide and its phosphorylated derivative controls PCD. The *acd5* mutant showed an accumulation of ceramides. This increase in ceramide resulted in apoptotic like cell death and an increased susceptibility to infection (Liang *et al.*, 2003). In contrast ceramide 1- phosphate is able to reduce PCD inducing effects of ceramides. It is thought that the balance of the two plays a role in controlling PCD in plants (Liang *et al.*, 2003). The use of fumonisin, an inhibitor of ceramide synthase, induces PCD in plants, which was thought to be due to the build-up of several LCBs. (Shi *et al.*, 2007). It was shown that increased amounts of the LCBs induced the generation of reactive oxygen species (ROs) followed by cell death. In contrast the phosphorylated forms of these LCBs blocked ROs generation and prevented cell death (Shi *et al.*, 2007).

1.8.3.2. *Presence in membranes*

Sphingolipids have been shown to be present in the plasma membranes and tonoplast membranes (Yoshida and Uemura, 1986). GlcCer have been shown to have a role in chilling and freezing tolerance in plants (Uemura and Steponkus, 1994, Uemura *et al.*, 1995). Sphingolipids however are not thought to be uniformly present in cellular membranes, evidence suggests they form microdomains known as lipid rafts (Borner *et al.*, 2005). These microdomains are characterised by their insolubility at low temperatures and in non-ionic detergents. They are otherwise known as detergent resistant membranes (Brown and Rose, 1992). Lipid rafts are

composed of sphingolipids and sterols which are tightly associated with one another so that they separate from the surrounding phospholipids. The sterols and sphingolipids form a much more organised structure than the phospholipid bilayer and are known as the liquid ordered phase. These structures are thought to coexist with the well-known structure of the phospholipid dominant membrane bilayer, the liquid disorganised phase (Ahmed *et al.*, 1997). The lipid raft hypothesis suggests that these sphingolipid/sterol structures form distinct areas within the membrane but can move freely through the bulk of the membrane (Simons and Ikonen, 1997). A number of GPI anchored proteins, protein kinases and receptor kinases have been identified in these rafts, as well as proteins known to have roles in PCD and cell signalling (Borner *et al.*, 2005, Lefebvre *et al.*, 2007). Current understanding about plant lipid rafts has recently been reviewed by Cacas *et al.*, (2012).

1.9. Membrane glycerolipids: Phospholipids and glycolipids

Phospholipids and glycolipids are the predominant polar lipids in the bilayer of biological membranes and are known as membrane glycerolipids. In addition phospholipids are known to have a number of other signalling roles. Both phospholipids and glycolipids consist of a glycerol molecule with two fatty acids esterified to the *sn1* and *sn2* position and a polar head group at the *sn3* position. Phospholipids contain a phosphate head group whereas glycolipids contain a carbohydrate head group, an example of which is shown in Figure 1.15.

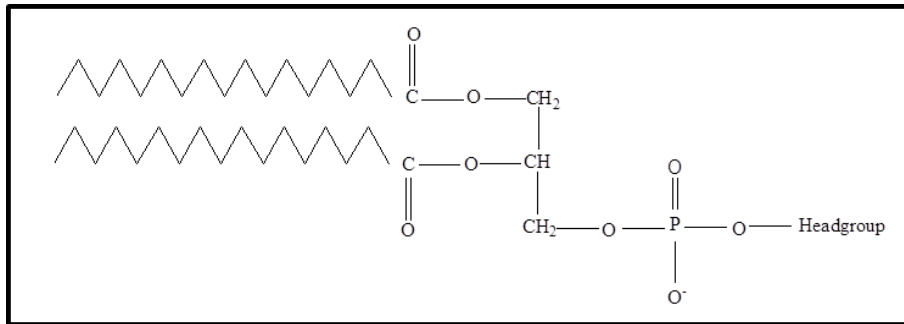


Figure 1.15. The basic structure of a membrane glycerolipid The head group is either a phosphate group for a phospholipid or a carbohydrate group for a glycolipid.

1.9.1. Biosynthesis of glycerolipids

The synthesis of glycerolipids begins with the synthesis of phosphatidic acid (PA). PA is not an abundant lipid in any living organism but its importance comes from the fact that it is the precursor of all membrane glycerolipids and triacylglycerols. The synthesis of PA has been described previously in section 1.4.1.3. A review of the role of PA has been written by Dubots *et al.*, (2012). A diagram of the synthesis of PA and how this leads to the synthesis of membrane lipids and triacylglycerols can be seen in Figure 1.16.

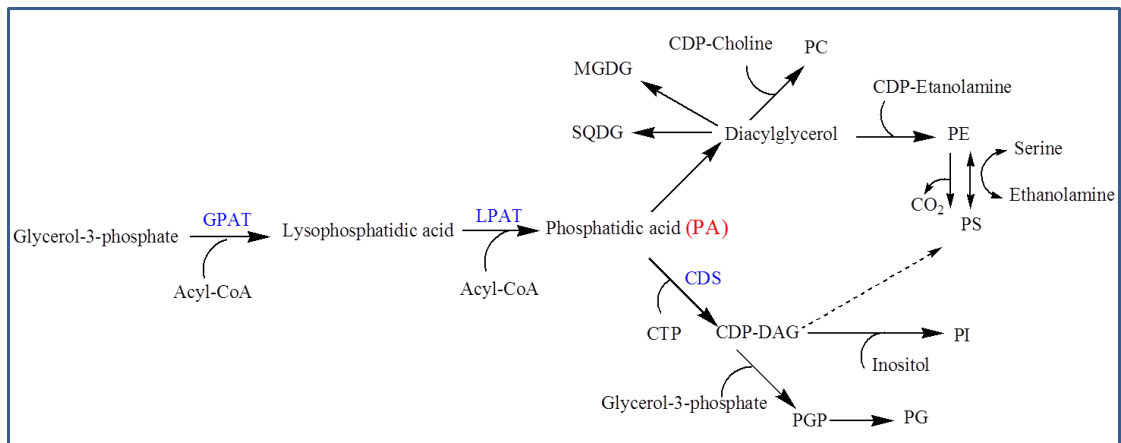


Figure 1.16. Synthesis of PA and how that leads to the synthesis of other lipids.

Lipids are synthesised from PA by two different pathways the ‘diacylglycerol pathway’ or the ‘CDP-diacylglycerol pathway’. The first step in the diacylglycerol pathway is the hydrolyses of PA by phosphatidate phosphatase to produce

diacylglycerol (DAG). An activated head group is then directly bound to the DAG to produce monogalactosyldiacylglycerol (MGDG), sulfoquinovosyldiacylglycerol (SQDG), phosphatidylethanolamine (PE) or phosphatidylcholine (PC). In the CDP-diacylglycerol pathway PA reacts with cytidine triphosphate (CTP) to produce cytidine diphosphate diacylglycerol (CDP) which is catalysed by CDP-diacylglycerol synthase (CDS). CDP diacylglycerol is a precursor for phosphatidylinositol (PI), phosphatidylserine (PS), and phosphatidylglycerol (PG). Both of these pathways have been reviewed by Dormann, (2005).

1.9.2. The roles of different phospholipids and glycolipids in plant cells

The mol % (the number of moles of a substance in a mixture as a percentage of the total number of moles in the mixture) of each of the different glycerolipids in *Arabidopsis* leaves is given in Figure 1.17. Each of the different phospholipids have been shown to have a number of different roles in the plant.

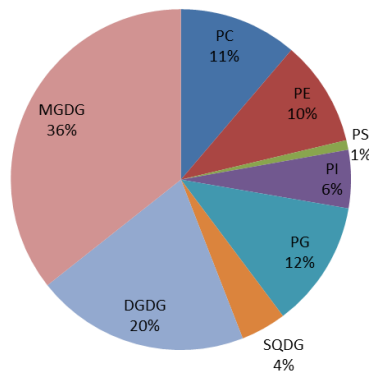


Figure 1.17. The mol % of each of the different glycerolipids in *Arabidopsis* leaves (Bonaventure *et al.*, 2003).

1.9.2.1. PA and PI are important signalling molecules

Besides being an important intermediate in lipid synthesis, PA also has functions as a key second messenger. PI plays a major role in signal transduction as well as

being a minor glycerolipid of plant membranes. PI is phosphorylated twice to form phosphatidylinositol bisphosphate (PIP₂). PIP₂ is cleaved into myo inositol triphosphate and DAG which both act as second messengers triggering different responses in the cell. Both of these second messengers are involved in stress responses such as salt stress, cold stress and oxidative stress as well as infection by pathogens. Both have been shown to play a role in root growth and pollen development. A good review of the function of both PA and PI has been written by Xue *et al.*, (2009). The structure of PA and PI is shown in Figure 1.18.

1.9.2.2. PC and PE are membrane lipids

PC and PE along with PG, are the major phospholipids in eukaryotic cell membranes, and therefore have many structural and functional roles. PC is an important precursor for MGDG, DGDG and SQDG synthesis (Ohlrogge and Browse, 1995). In addition PC is important for the production of second messengers such as PA, lyso PC, DAG and lyso PA (Kent and Carman, 1999). PC is also important in the stress response of plants and has been shown to be involved in freezing tolerance (Sikorska and Kacperskapalacz, 1980, Kinney *et al.*, 1987) and salt stress (Pical *et al.*, 1999). PE is a non- bilayer lipid that is distributed widely in membranes of plant cells except for in the plastids (Mizoi *et al.*, 2003). A non-bilayer lipid is a cone shaped lipid, in which the cross sectional area of the head group is smaller than that of the acyl chains, resulting in an overall conical shape. This preferentially results in the formation of structures with a negative curvature such as the inverted hexagonal phase. In the inverted hexagonal phase the head group is on the inside of the structure with the hydrophobic chains on the outside. Biological membranes are bilayers. However, they contain large amounts of non-

bilayer lipids, which are thought to play a role in; the formation of non-bilayer structures, have an effect on the flexibility and barrier properties of the bilayer, and they could have an effect on the function of membrane proteins (van den Brink-van der Laan *et al.*, 2004). PE plays an important role in cell division and is also the donor of the ethanolamine residue that links the glycosylphosphatidylinositol (GPI) anchor to proteins (Menon and Stevens, 1992, Mileykovskaya *et al.*, 1998).

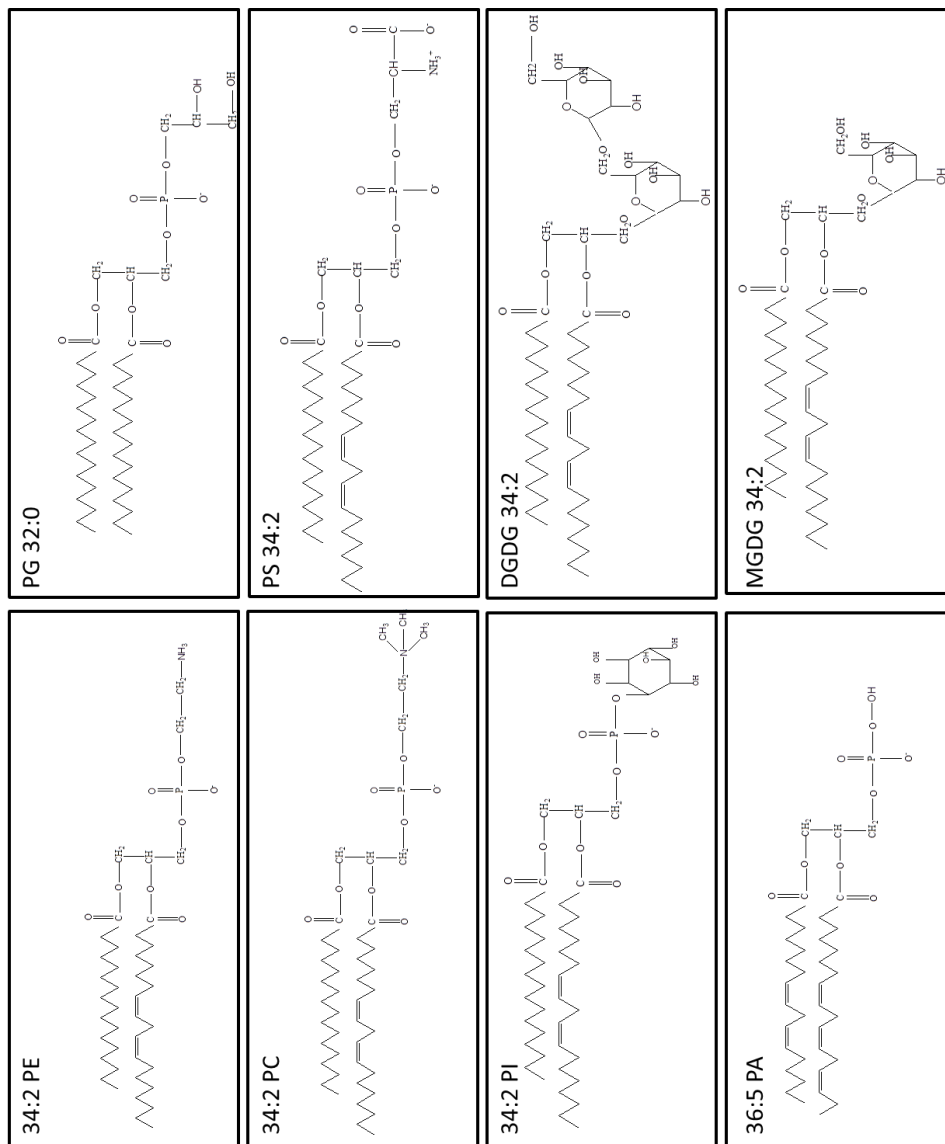


Figure 1.18. The structure of each of the phospholipids and glycolipids. An example of one specific combined acyl chain length is given for each class. Figure modified from (Devaiah *et al.*, 2006).

1.9.2.3. *Galactolipids*

MGDG and DGDG, the galactolipids, are synthesized and localised in the chloroplasts. The galactolipids are required for photosynthesis and they are present in photosystem I and II (Dörmann, 2001).

1.9.2.4. *PS*

PS is a membrane phospholipid. It is also thought to be an important enzyme cofactor and an important precursor for PE synthesis (Vance and Steenbergen, 2005). PS is not present in high amounts but is shown to contain relatively high amount of VLCFAs (Devaiah *et al.*, 2006). PS is enriched in 70- 80 nm diameter ER derived vesicles which are involved in transport to the plasma membrane (Sturbois-Balcerzak *et al.*, 1999).

1.10. Cuticular waxes

The cuticle covers the surface of all aerial organs and plays an essential role in controlling interactions between the plant and its environment. The cuticle has a role in stress response, adaption of the plant to its environment and is also thought to have a role in development.

1.10.1. Composition and organisation of cuticle

The cuticle consists of a matrix composed of intracuticular waxes embedded in a cutin polymer, with a covering of epicuticular waxes. The cutin is composed of a matrix of C16 and C18 ω hydroxy fatty acids and dicarboxylic acids with smaller amounts of phenolics such as ferulate (Kolattukudy, 1980). Cuticular waxes consist of a combination of VLC- aliphatic compounds, triterpenoids and small amounts of sterols and flavonoids. Bernard and Joubes, (2013) recently produced a review on the quantities of each of the wax components in *Arabidopsis*. The cuticle of all

higher plants is thought to be composed of three layers. The first layer, the cuticular layer which overlays the epidermal cell wall, is composed of cutin, intracuticular waxes and polysaccharides. On top of this is the cuticle proper, made up of epicuticular waxes, intracuticular waxes and cutin. The top layer is composed of epicuticular waxes. It has been shown that the composition of epicuticular and intracuticular waxes have different chemical compositions (Jetter and Schaffer, 2001). The epicuticular waxes of *Arabidopsis* assemble as column shaped crystals on the stems, siliques and the stigma of flowers whilst in the leaves they form an amorphous layer (Jenks *et al.*, 1995).

1.10.2. Wax synthesis

There are two distinct pathways leading to wax synthesis: the alcohol forming pathway and the alkane forming pathway. Both pathways can be seen in Figure 1.19.

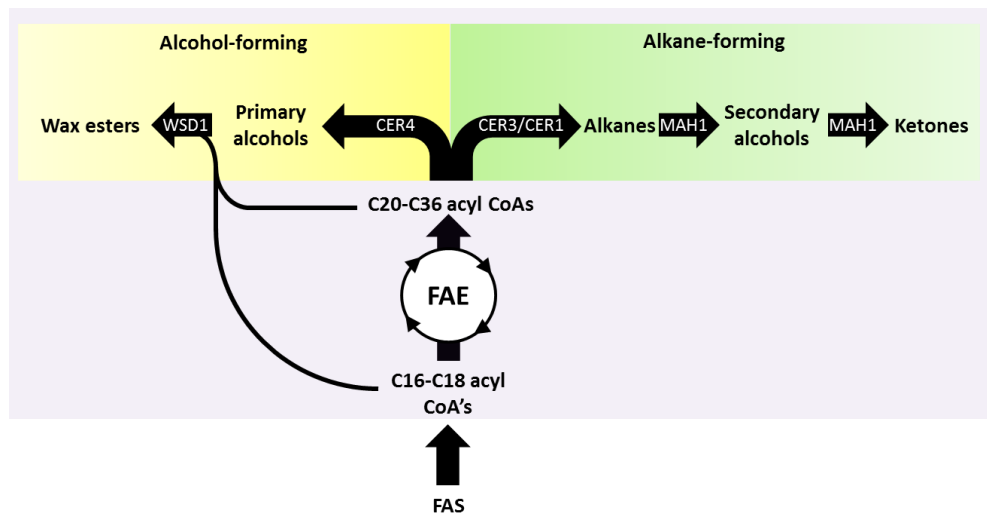


Figure 1.19 Wax synthesis from VLCFAs. Both the alkane and alcohol forming pathway are shown along with the various proteins thought to be involved in the synthesis of the wax components. Figure modified from (Bernard and Joubes 2013).

1.10.2.1. Alkane forming pathway

One branch of the wax biosynthetic pathway is responsible for the formation of odd number carbon chains, of which alkanes are the predominant form. In *Arabidopsis* leaves alkanes are the end product of the pathway. However, in stems these alkanes can then be hydroxylated to form secondary alcohols, which can then be oxidised to ketones. The products of the alkane forming pathway account for 70- 80% of total waxes in *Arabidopsis* (Bernard and Joubes, 2013).

It is hypothesized that the first step in the alkane pathway involves the reduction of acyl-CoA by acyl-CoA reductase to produce an aldehyde (Cheesbrough and Kolattukudy, 1984, Dennis and Kolattukudy, 1991, Vioque and Kolattukudy, 1997). The aldehyde is then decarbonylated to produce alkanes with odd chains, a reaction catalysed by an aldehyde decarbonylase. The alkanes can then be modified further to produce secondary alcohols and ketones. CER1, and CER3 have been showed to have a direct role in alkane synthesis. The *cer3* mutant showed a reduction in aldehydes, alkanes, secondary alcohols and ketones (Jenks *et al.*, 1995, Chen *et al.*, 2003, Rowland *et al.*, 2007). It was therefore suggested that CER3 could be a reductase converting VLCFAs to aldehydes (Chen *et al.*, 2003). The *cer1* mutant also showed a dramatic decrease in alkanes, the mutant contained almost no secondary alcohols and ketones but showed a slight increase in aldehydes. CER1 is thought to potentially encode for the alkane forming enzyme responsible for the decarboxylation of aldehydes to alkanes (Aarts *et al.*, 1995). Plants overexpressing *CER1* resulted in an increase in C27 to C33 alkanes. This is a further indication that *CER1* encodes for an enzyme directly involved in alkane synthesis (Bourdenx *et al.*, 2011). In yeast, these two enzymes were shown to physically interact with one

another and together can result in the production of C27 to C31 alkanes which were not detected when only one of these enzymes was expressed. This evidence suggests that CER1 and CER3 combine to form a complex that is capable of producing VLC alkanes. No aldehyde intermediates were detected in yeast so it is still not understood what role CER3 plays and whether an aldehyde intermediate is involved in alkane synthesis (Bernard *et al.*, 2012).

The cytochrome P450 encoding gene, *CYP96A15*, is thought to be the enzyme responsible for the production of secondary alcohols and ketones from alkanes. It was shown that an insertional mutant in *CYP96A15* resulted in a reduction in these components. Additionally, expression of this gene in leaves resulted in the production of these components, which are otherwise not present in leaves (Greer *et al.*, 2007). The protein is a mid-chain alkane hydroxylase (MAH1) and is capable of catalysing the hydroxylation of the central $-\text{CH}_2$ group, then rebinding the resulting alcohol for the oxidation reaction to produce the ketone (Greer *et al.*, 2007). The various steps in alkane synthesis can be seen in Figure 1.20.

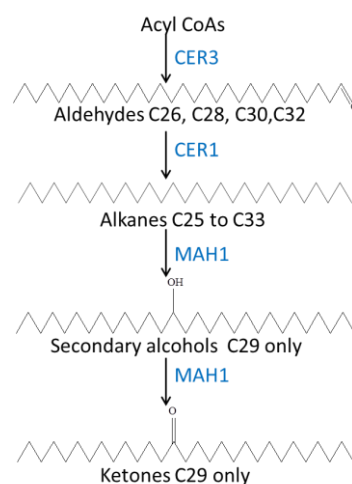


Figure 1.20 Alkane forming pathway in wax synthesis. The enzyme expected to catalyse each reaction and the different chain lengths that have been identified in stems are shown.

1.10.2.2. Alcohol forming pathway

The alcohol forming pathway is involved in the synthesis of primary alcohols and wax esters and accounts for 17-18% of total wax and produces even numbered compounds. The primary alcohols account for approximately 12% of total waxes in *Arabidopsis* stems, whereas wax esters are a minor component of waxes accounting for less than 5% of total wax (Bernard and Joubes, 2013). It has been shown that primary alcohols can be formed by a two-step reaction, in which the VLCFA are first reduced to an aldehyde which is then reduced to a primary alcohol. This system has been shown to be catalysed by a fatty acyl reductase, FAR. FAR enzymes have been shown to be capable of catalysing the synthesis of alcohols from a VLCFA acyl CoAs (Rowland and Domergue, 2012). The *cer4* mutant plants showed a reduction in primary alcohols and wax esters showing a role for CER4 in the alcohol forming pathway in *Arabidopsis* (Rowland *et al.*, 2006). CER4 along with 7 other sequences were found by sequence searches of *Arabidopsis* to potentially encode for the activity of the FAR. It was shown that CER4 was capable of producing VLC- primary alcohols from C24 and C26 carbon chains in yeast, confirming the FAR activity of CER4. However in the mutant there was still a small amount of C30 suggesting that there is more than one protein capable of carrying out the function of FAR in *Arabidopsis* (Rowland *et al.*, 2006).

The primary alcohols can be combined with acyl-CoA substrates to form wax esters. The acyl chain lengths of these wax esters are mostly C16 (Lai *et al.*, 2007). Wax synthase (WS) enzymes were shown to catalyse this reaction in plant seeds (Lardizabal *et al.*, 2000). A second type of protein capable of catalysing this reaction was identified in *Acinetobacter calcoaceticus*. It showed functional activity

as a diacylglycerol acyltransferase (DGAT) and a WS. Eleven similar sequences were identified in *Arabidopsis* (Kalscheuer and Steinbuchel, 2003). From sequence similarity searches of both WS and WS/DGAT, one identified sequence, *WSD1*, was shown to be upregulated in the epidermis in *Arabidopsis*. Loss of function alleles of *WSD1* in *Arabidopsis* showed a complete loss of wax esters. The ability of *WSD1* to catalyse wax ester formation from acyl CoAs and primary alcohols was shown in yeast showing its role as the major WS (Li *et al.*, 2008). The steps involved in the alcohol forming pathway can be seen in Figure 1.21.

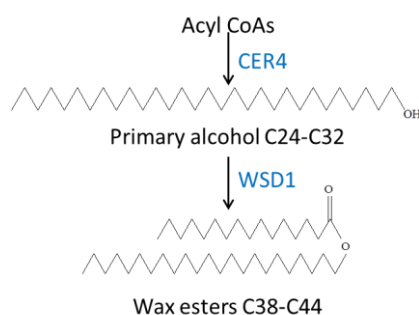


Figure 1.21 Alcohol forming pathway in wax synthesis. The enzyme expected to catalyse each reaction and the different chain lengths that have been identified in stems are shown.

1.10.2.3. Site of wax synthesis

It is believed that wax biosynthesis occurs, at least in part, in the ER. CER4, a component of the alcohol forming pathway, has been shown to be localized in the ER (Rowland *et al.*, 2006). MAH1 which is involved in the alkane forming pathway is also located in the ER (Greer *et al.*, 2007). This suggests that to some degree both sections of the wax pathway occur in the ER. Wax has to be transferred to the outside of the cell from the ER. Two transporters of cuticular wax have been identified, CER5 and WBC11, both of which contain an ATP binding cassette (ABC transporters) (Pighin *et al.*, 2004, Bird *et al.*, 2007). Both transporters were

localised to the plasma membrane of stem epidermal cells (Pighin *et al.*, 2004, Bird *et al.*, 2007). The wax load in plants mutated in *cer5* was decreased by 56% compared to wild type (Pighin *et al.*, 2004) showing that it is likely to play a role in wax transport. Plants with a mutation in *WBC11* showed reduced wax and cutin levels. This suggests that it plays a role in both wax and cutin transport (Bird *et al.*, 2007).

1.10.2.4. Role of the cuticle

The cuticle covers all land plants and the different components of it are responsible for a number of the different functions of the cuticle. VLCFA are components of all wax components. Waxes have a number of functions in the cuticle. These include:-

- Protection of the plant from pollutants, dust and pathogen spores that might be deposited on the plant surface. This is achieved by the so called lotus effect. This occurs through the formation of spherical water droplets on a crystalline surface which does not occur on a smooth surface. This causes water to be repelled from the plant surface (Barthlott and Neinhuis, 1997).
- It is thought that the chemical composition of the wax controls plant/insect and plant/pathogen interactions by acting as chemical attractors in feeding stimulus or by having a repulsive effect (Eigenbrode and Espelie, 1995).
- The cuticle may play a role in systemic acquired resistance (SAR) as several mutants of cutin and wax synthesis showed a reduced ability to induce SAR (Xia *et al.*, 2009).
- Some wax components have been suggested to play a role in pollen grain physiology (Preuss D, 1993, Aarts *et al.*, 1995, Hulskamp *et al.*, 1995).

1.11. The role of VLCFAs in plant development

1.11.1. Delayed cell plate formation in *pas* mutants

It is thought that VLCFAs play a role in cell plate formation which is thought to explain the shorter primary roots seen in some VLCFAs mutants. Cytokinesis in plants is the last step of cell division and requires the formation of a new structure, the cell plate. It is thought that lipid mutants exhibited shorter primary roots due to a delay in cell plate formation (Bach *et al.*, 2011). The *pas2-1* mutant, which has primary roots that are 50% shorter than wild type roots showed a delay in cell plate formation. The roots showed shorter elongation zones and cell division zones than wild type cells but contained similar numbers of cells. The *pas2-1* mutant showed a higher number of dividing cells in total than wild type plants with a higher number of cells in late mitosis which contained delayed, unfinished or abnormal cell walls. This suggested a delay in cell division in particular in cytokinesis. This delay was due to a delay in cell plate formation. A difference could be seen in the mutants at the time when materials were delivered to the site of cell plate formation to form the cell membranes and cell wall via unidirectional vesicle delivery and fusion from the ER and Golgi (Bach *et al.*, 2011).

The same phenotype was shown when the KCS inhibitor flufenacet was applied to wild type plants. Flufenacet is an inhibitor of certain KCS enzymes, suggesting that the delay in cell plate formation is a feature of a decrease in VLCFA levels. It is thought that endocytosis is the cause of the delay in cell plate formation. However the role of endocytosis, and what role VLCFAs, play in in cell plate formation, is not properly understood. The most likely explanation is that sphingolipids and

phospholipids containing VLCFAs which are membrane lipids are necessary for vesicle transport, fusion and or budding (Bach *et al.*, 2011).

1.11.2. Developmental defects in *pas* mutants

The *pas* mutants were identified due to the development of callus like structures when grown in the presence of inhibitory concentrations of cytokinins (Faure *et al.*, 1998). The mutants are composed of three complementation groups, *PAS1*, *PAS2* and *PAS3*. *PAS1* has been shown to have a role in VLCFA synthesis and is thought to behave as a scaffold protein for the elongase complex (Roudier *et al.*, 2010). *PAS2* was shown to encode for the dehydratase activity in VLCFA elongation, described in section 1.6.3. *PAS3* has been shown to be allelic to the *ACC1* gene which encodes for an acetyl-CoA carboxylase which is responsible for catalysing the formation of malonyl CoA from acetyl CoA and bicarbonate. Malonyl CoA is the substrate for VLCFA elongation and *acc1* seeds have been shown to contain no VLCFA (Baud *et al.*, 2003, Baud *et al.*, 2004). All three genes encode for proteins that have a role in VLCFA synthesis.

Differences were first identified in the *pas* mutants at the heart stage of development when the cotyledon primordia are initiated (Faure *et al.*, 1998). During germination the cotyledons and hypocotyl failed to elongate properly and a number of cell division patterns were modified. It was shown that the *pas* mutants showed an increased ability to undergo cell divisions both in the meristematic region and in normally differentiated cells such as cotyledons and hypocotyls, that had retained the ability to divide (Harrar *et al.*, 2003). This is thought to be responsible for the formation of the callus like structures. This was only seen in the apical regions, the roots did not display any of these defects (Faure *et al.*, 1998). The defects seen in

cell division in the three *pas* mutants (all of which encode genes that have a role in VLCFA synthesis) suggest that VLCFAs must have a role in some aspect of cell division.

1.11.2.1. Role of cytokinins in the *pas* phenotype

Cytokinins increased cell proliferation in the three *pas* mutants. For this reason it was investigated whether the role that VLCFA play in cell division was associated with cytokinin biosynthesis or production. The expression of the cytokinin response genes was increased on treatment with cytokinin compared to wild type and expression was maintained for longer in the *pas* mutants (Harrar *et al.*, 2003). It has been shown recently that a decrease in VLCFA results in an increase in cytokinin production (Nobusawa *et al.*, 2013). The mechanism of how this effect occurs is not yet understood.

1.11.2.2. Role of auxin in the *pas* phenotype

1.11.2.2.1. Role of auxin in embryo patterning

Investigations with *pas1* showed that cell identity markers representative of a particular domain overlapped in the embryo. Therefore the fate of the cells in the *pas1* embryo were not clearly defined, which was thought to be caused by defects in auxin mobilization. This was thought to be responsible for the defects seen in cotyledon development and the lack of bilateral symmetry, (Roudier *et al.*, 2010). Auxin response, during embryo development is important for embryo patterning. Two excellent reviews of the role of auxin in embryo patterning have been written by Moller and Weijers, (2009) and Jenik and Barton, (2005). Using the auxin responsive promoter *DR5* it was shown that at the torpedo embryo stage, *pas1* only showed *DR5* expression at the root pole, whereas in wild type cells it is present at

the root poles, the tip of the cotyledons and in the vascular tissues (Friml *et al.*, 2003). In the *pas1* mutant this redistribution does not occur correctly. Auxin distribution in the embryo requires specific influx and efflux carriers (Jenik and Barton, 2005). PIN1 is an auxin efflux carrier, which has been shown to not be targeted correctly in *pas1*. PIN1 was shown to be diffused or aggregated and not tightly localised to the lateral membranes of epidermal cells. Auxin, therefore would not build up and the correct embryo patterning would not occur. The lack of polar localisation of PIN1 was already observable at the globular stage before any changes could be observed in the morphology. This suggests that the changes seen in the embryo were due to defected auxin distribution. This was expected to be due to the trafficking defects as a result of a decrease in the amount of VLCFAs (Roudier *et al.*, 2010).

1.11.2.2.2. Role of auxin in lateral root development

The *pas1* mutant was shown to have a complete absence of lateral roots and, as was shown with the defects in embryo patterning, this was thought to be due to a lack of polar accumulation of auxin. The PIN1 efflux carrier was not sharply localised in the mutant during the periods where a polar build of auxin occurs in the wild type roots such that lateral roots are produced (Roudier *et al.*, 2010). In *pas1* auxin was not detected in outer cortical cells or in the epidermal cells in root formation as was seen in wild type cells (Benkova *et al.*, 2003). This is thought to be responsible for the lack of lateral roots (Roudier *et al.*, 2010). As was the case with the embryo patterning defects this was thought to be due to a decrease in the level of VLCFA, resulting in PIN1 not being trafficked correctly.

Further work has suggested that this mislocalization could be due to the absence of sphingolipids containing VLCFA (Markham *et al.*, 2011). Using the double mutant *loh1 loh3* (mutations in the ceramide synthase gene) and seedling grown in the presence of fumonisin, an inhibitor of the ceramide synthase gene, both had shorter primary roots and a lack of lateral roots (Markham *et al.*, 2011). As all of the *pas* mutants showed a decrease in the amount of VLCFA, a decrease in sphingolipids containing VLCFAs could be responsible for the lack of lateral roots. In plants with altered sphingolipid metabolism AUX1 was also affected in addition to PIN1, which was not the case in *pas1*. AUX1 is a plasma membrane polar auxin transporter and is involved in cellular auxin influx. AUX1, like PIN1, was shown to be aggregated in mutants of *loh1/loh3* cells and was not properly localised. Other auxin proteins were not affected, illustrating that it is a specific effect that occurs for specific proteins. The aggregates which formed were similar to those that form as a result of inhibitors of anterograde transport. The inhibitors of ceramide synthase did not affect recycling of the material, instead it is thought that the aggregation occurred along the secretory pathway (Markham *et al.*, 2011). However, the higher sensitivity of *pas1* to Brefeldin A (BFA) which inhibits anterograde trafficking would suggest that PIN1 recycling was selectively altered (Roudier *et al.*, 2010). It is possible that both pathways were affected.

PIN1 acts with a subset of ATP binding cassette subfamily B (ABCB) transporters to mobilize long distance auxin transport (Titapiwatanakun *et al.*, 2009). ABCB19 is a primary component of auxin transport to the roots and interacts directly with PIN1 at the plasma membrane. It has been isolated in lipid rafts, which sphingolipids form a major component of, and has been shown to be required for

retention of PIN1 in those membranes (Blakeslee *et al.*, 2007, Titapiwatanakun *et al.*, 2009). This provides additional evidence that it is sphingolipids containing VLCFAs which have an effect on PIN1 transport.

1.11.3. Role of VLCFAs in preventing organ fusion

Fused flower buds have been produced in a number of VLCFA mutants including *fdh*, *KCR RNAi*, *pas2-1* and *cer10* (Lolle *et al.*, 1997, Bellec *et al.*, 2002, Zheng *et al.*, 2005, Beaudoin *et al.*, 2009). They are said to display the *fiddlehead (fdh)* phenotype. In wild type *Arabidopsis*, ontogenetic fusion only occurs during the formation of the reproductive system of the plant (Okada *et al.*, 1989). The *fdh* mutant was isolated as it showed organ fusion in other tissues, so that vegetative and floral organs fused postgenitally. This fusion of flower buds resulted in the apical curling of the inflorescences such that it looked like fern fiddleheads (Lolle *et al.*, 1992). The fusion in *fdh* mutants occurs when epidermal cells come into contact along the periclinal walls. The cells then adhere to one another but do not undergo cytoplasmic union (Lolle *et al.*, 1992). The reason for fused organs in VLCFA mutants is largely unknown. It is thought that changes in the cuticle could be responsible, either a decrease in the level of wax or cutin. WBC11 and CER5 are cutin and cuticular wax transporters. The mutation *wbc11* resulted in both organ fusions and increased stem glossiness (characteristic of plants with reduced wax loads) whereas *cer5* only resulted in stem glossiness (Pighin *et al.*, 2004, Bird *et al.*, 2007). As *cer5* only has an effect on the cuticular wax and *wbc11* has an effect on both the wax and cutin load, this suggested that it is defect in the cutin that was responsible for the observed *fdh* phenotype. Transgenic plants expressing the cutinase gene of *Fusarium solani* f.sp displayed impaired cutin synthesis which,

again, resulted in organ fusion, (Sieber *et al.*, 2000). In addition *lacerata*, *lcr*, mutants of *Arabidopsis* also show fused aerial organs. This gene encodes a cytochrome P450 monooxygenase which catalyses ω hydroxylation of fatty acids which are components of the cutin (Wellesen *et al.*, 2001). These additional examples suggested that it is a decrease in cutin that is responsible for these phenotypes. As there are low levels of VLCFA in cutin it does not explain the fused flower buds seen in VLCFA mutants. In addition both *lcr* and *fdh* show an increase in the amount of cutin monomers and wax molecules (Voisin *et al.*, 2009). This suggests that neither a decrease in cutin or wax can be responsible for this phenotype. It is possible that it could both be a decrease in cutin and wax simultaneously that results in organ fusion. Long chain acyl CoA synthases (LACS) are required for the synthesis of long chain acyl CoAs, LACS2 is required for cutin synthesis and LACS1 is required for wax synthesis. While single mutants of both of these genes did not result in organ fusion, double mutants did (Weng *et al.*, 2010). Further evidence that it is a reduction in both components of the cuticle comes from the WBC11 transporter, which transports both wax and cutin and also shows a fused phenotype in the mutant (Bird *et al.*, 2007). Additionally it could be a defect in a particular wax components, or changes in the composition of the cuticle, which would explain why VLCFA mutants result in these fusions.

1.12. Aims and objectives

In this work the role that VLCFAs play in *Arabidopsis* growth and development, has been investigated. Mutations in each of the different components of the core elongase complex result in different phenotypic traits. The reason for this is unknown. It is also suspected that there are a number of interacting partners in

VLCFA synthesis that have not yet been discovered, such as those that are involved in channelling of the products of elongation and the regulation of the elongase activity. It is hoped that by understanding more about function and synthesis of VLCFA that the full potential of these products for biotechnology applications can be realised.

Two main approaches were undertaken in this thesis in order to understand more about how perturbations in VLCFA synthesis affects growth and development :-

1. Lipidomic profiling was performed on mutants of the core elongase complex. The same analysis was performed on plants that had been treated with herbicides which are thought to affect a number of KCS enzymes. By using both chemically treated plants and knockdown/knockout elongase lines, the effect of a reduction in activity on each of the elongase components could be assessed. The aim of the lipidomic analysis was to understand why different phenotypic traits were observed in different mutants of the elongase complex, by trying to correlate changes in the lipidome with a phenotypic trait. For the first time the lipidomic profile was obtained for the roots and shoots separately in order to understand more about the cause of the different phenotypes. The glycerolipids, sphingolipids and acyl-CoAs pools were analysed.
2. A forward genetic screen was performed to identify additional components involved in VLCFA synthesis or regulation. The screen was performed in an already characterised elongase mutants, *cer10*, in order to identify both suppressor and enhancer mutations of *cer10*. Additionally this screen could

identify components that have an indirect effect on VLCFA synthesis. Any candidate mutants identified in this screen, were characterised to understand the effect of this mutation on the lipidome and the position of the gene that had been mutated in the genome.

Chapter 2. Materials and Methods

All reagents listed throughout this thesis were obtained from Sigma-Aldrich unless otherwise stated.

2.1. Plant material and growth conditions

2.1.1. Seed material

Seeds used in this project were obtained from a variety of sources. The *pas2-1* line was obtained from Professor Jean Denis Faure (INRA Versailles, France). The *cer10-1* and *cer10-2* lines were obtained from Professor Ljerka Kunst (The University of British Columbia, Canada). All other seeds were already present in the research group.

2.1.2. Plant growth media

The plant growth media was prepared as follows; for 1 litre of half strength MS media, 2.2g of Murashige and Skoog salts (MS) (Murashige and Skoog, 1962) and 0.5g of 2-(N-Morpholino) ethanesulfonic acid, 4- Morpholineethane sulfonic acid (MES) were added to approximately 900 ml of de ionised water. The media pH was adjusted to 5.8 with potassium hydroxide. 9 g of phytigel (0.9%) was then added to the mixture and the volume was corrected to 1 litre. The media was then autoclaved, and the cooled media was poured into 10cm x 10cm sterilised plates (supplied by Sterilin[®] part of Thermo Fisher Scientific). Plates were stored at 4°C prior to use. For the *pas2-1* line 1% sucrose was added to the media, as it has been shown previously that the mutants could not be grown directly in soil or in a medium free of sucrose (Faure *et al.*, 1998).

2.1.3. Seed sterilisation

All sterile procedures were carried out in a lamina flow hood (Bassaire, UK). *Arabidopsis* seeds were surface sterilised for 1 minute in 100% ethanol followed by 5 minutes in 50% (v/v) bleach, followed by six washes in sterile water. The seeds were left for 48 hours at 4°C to synchronise germination (stratified). The seeds were sown onto plates containing the growth media, using a P20 Gilson pipette and 10-100 µl Ultipette Capillary tips (Barky). One hundred seeds were sown on each plate. Plates were sealed using micropore tape (3M™ Micropore™).

2.1.4. Plant growth conditions

2.1.4.1. *Plants germinated on plates*

Plants were incubated at 23°C in a 16 hour : 8 hour (light : dark) cycle in a Sanyo MLR Growth cabinet. Plant material was harvested 2 weeks after sowing, and separated into roots and shoots using scissors and forceps. Samples were then frozen in liquid nitrogen and stored at -80°C.

2.1.4.2. *Plants grown directly in soil*

Plants grown directly in soil (Levingtons F2's +sand and intercept 5GR 280g/m³) were grown in a controlled environment growth room supplied by Fititron. Plants were grown in long-day conditions at 23°C /16 hours of light and 16°C /8 hours of dark. The light conditions in this growth room were set to 250 µmol at bench level; the humidity was set to 70%. Due to the large number of plants grown the conditions were strictly controlled to reduce the amount of variation between plants grown at different times.

2.1.5. Cross pollination of *Arabidopsis*

Plants were grown under the above conditions until mature flowers were produced (approximately 4-6 weeks). The mature open flowers were removed from the

inflorescence of the plants being used as the female in the cross, along with the smallest unopened buds. The remaining buds were emasculated using forceps under a microscope (Leica CLS 150x). A mature stamen was removed from the flower of the male donor using sterile forceps. The stamen from the male donor was brushed onto the emasculated stigma of the female plant until pollen was visible on the surface of the stigma. A small piece of plastic film was wrapped around the emasculated, pollinated stigma to increase the humidity and prevent any further pollination from unknown donors. Tape was added to the stems to mark which had been cross pollinated. When the siliques had turned yellow they were removed from the plant and allowed to mature in 1.5 ml Eppendorf tubes with a hole in the lid in order to allow excess moisture to evaporate.

2.2. Physiological analysis

Digital photographs of the plants were taken using a standard digital camera (Sony alpha37). All photographs were taken with a ruler within the image to allow for measurements of the plants. Measurements were taken from the digital images using Image J 1.44p image analysis software (National Institutes of Health USA). Microscopic images of seedlings were collected using the Leica Stereomicroscope MZ8.

2.3. Molecular biology

2.3.1. CTAB DNA extractions

For DNA extractions, 0.1g of tissue was weighed, and ground in liquid nitrogen, with a pestle and mortar until the tissue was fully homogenised. The sample was resuspended in 200 µl of 2 x CTAB extraction buffer (0.1 M Tris (pH9.0), 2% CTAB (Hexadecyltrimethylammonium bromide), 1.4 M NaCl, and 20 mM EDTA

(pH8.0) (ethylenediaminetetra Acetic acid Di sodium salt)), with 2 μ l of 10 mg/ml RNase A (Qiagen). Samples were incubated at 65°C for 30 minutes, after which 200 μ l of chloroform was added to the sample, which was mixed vigorously by shaking. The samples were then centrifuged at 14,000 rpm at room temperature for 5 minutes. The supernatant was removed and added to a new tube, 200 μ l of isopropanol was added and the tubes were mixed by shaking. The samples were incubated at room temperature for 5 minutes before being centrifuged at 14,000 rpm for 5 minutes. At this point a pellet formed, and the isopropanol was removed. The pellet was washed by addition of 70% ethanol and incubated for 5 minutes at room temperature. The sample was centrifuged at 14,000 rpm for 2 minutes so that the sample re-pelleted. The ethanol was removed and the samples were air dried to ensure that no traces of ethanol remained. The samples were finally resuspended in 50 μ l of nuclease free H₂O. Murray and Thompson, (1980) first proposed this extraction method, which has subsequently been adapted (Richards *et al.*, 2001).

2.3.2. Primers and restriction enzymes

All primers were ordered from Sigma-Aldrich and restriction enzymes were received from New England Biolabs. All primer sequences are shown in Chapter methods or in the appendices.

2.3.3. Polymerase chain reaction conditions

All polymerase chain reactions (PCR) were carried out in 200 μ l PCR tubes (Star Labs). All reactions, unless otherwise stated, were set up using, 12.5 μ l of 2 X ReddyMix PCR master mix (1.5mM MgCl₂) (Thermo Scientific) and 1 μ l of both forward and reverse primers in a final volume of 25 μ l. Primes were used at a final concentration of 0.5 μ M. PCR reactions were carried out using MJ Research engine

PTC-2000 Peltier thermal cycler. The following standard conditions were modified according to the annealing temperature of the primers (underlined) and extension time (*italics*) depending on the length of the PCR product:-

1. 94°C for 1 minute
2. 94°C for 30 seconds
3. 50°C for 30 seconds
4. *72°C for 30 seconds*
5. Repeat steps 2 to 4, thirty nine times
6. 72°C for 10 minutes

All reactions were stored at -20°C until visualised by agarose gel electrophoresis.

2.3.4. Agarose gel electrophoresis

DNA was separated and visualised by agarose gel electrophoresis. Typically 1% Agarose gels were used, which were prepared as follows: Agarose (1% (w/v)) (molecular grade, supplied by Bionline) in 0.5 x TBE buffer (0.4 M Tris base, 0.4 M boric acid, 10 mM EDTA, pH 8.0) was melted in a microwave oven. The Agarose solution was allowed to cool slightly before ethidium bromide was added (1 µl of a 10 mg/ml stock solution for 100 ml of gel). The gel was poured into a plastic gel tray. Electrophoresis was carried out between 70-100 mV depending on the size of the DNA fragment. The gel was then visualised using the GelDoc-It^{TS2} imager (UVP). A 1KB plus ladder (Invitrogen) was separated alongside the samples on all gels for identification of DNA fragments.

2.3.5. Genetic analysis

Information on gene sequences and protein sequences were obtained from the TAIR 10 sequence (TAIR).

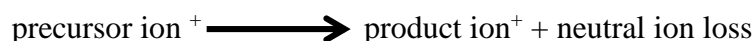
2.4. Biochemical characterisation

2.4.1. Tandem mass spectrometry

Tandem mass spectrometer (MS/MS) (AB4000 QTRAP, ABSCIEX) was utilised for the analysis of a number of different lipid species. The compounds were ionised prior to analysis by MS/MS by passing through an electrospray probe. The MS/MS can be divided into three sections, Q1- 1st quadrupole, Q2- collision cell and Q3 the 2nd quadrupole. In Q1 the ions were filtered according to their mass charge ratio. In Q2, the ions collide with neutral gas molecules. Some of the kinetic energy that is produced from these collisions can be converted into internal energy which can break the chemical bonds in the molecule resulting in fragment ions, this is called collision induced dissociation. In Q3 the fragment ions were analysed according to their mass charge ratio. How MS/MS works can be seen in Figure 2.1.

2.4.2. Modes of analysis using tandem mass spectrometry

In this thesis three different modes of tandem mass spectrometry were used for analysis of different lipid classes, precursor ion scan, neutral ion loss and multiple reaction monitoring (MRM). All of the different modes are dependent on the following reaction occurring in Q2:-



Precursor ion scanning is used to determine which compounds can produce a particular product ion, this mode was used for the analysis of glycerolipids. Q3 transmits only one signal to the detector, and Q1 scans for all the precursor ions that produce this product ion (Figure 2.1a). For neutral loss scanning, again used for the analysis of glycerolipids, both Q1 and Q3 scan for a constant mass difference between the two quadrupoles (Figure 2.1b). The constant mass corresponds to a

particular group that is released as a result of fragmentation in Q2, for example the head group of the glycerolipid molecule. Multiple reaction monitoring (MRM) detects particular ion pairs that are determined by the user which was used for both acyl-CoA and sphingolipid analysis (Figure 2.1c). Both Q1 and Q3 select particular precursor and product ions characteristic of a particular lipid molecule. Q1 only transmits a small population of compounds so it minimizes the chemical background and results in less interference. (Domon and Aebersold, 2006). However, this technique does require prior knowledge of what compounds are in the sample and the structure of them. This means that unexpected compounds would not be identified.

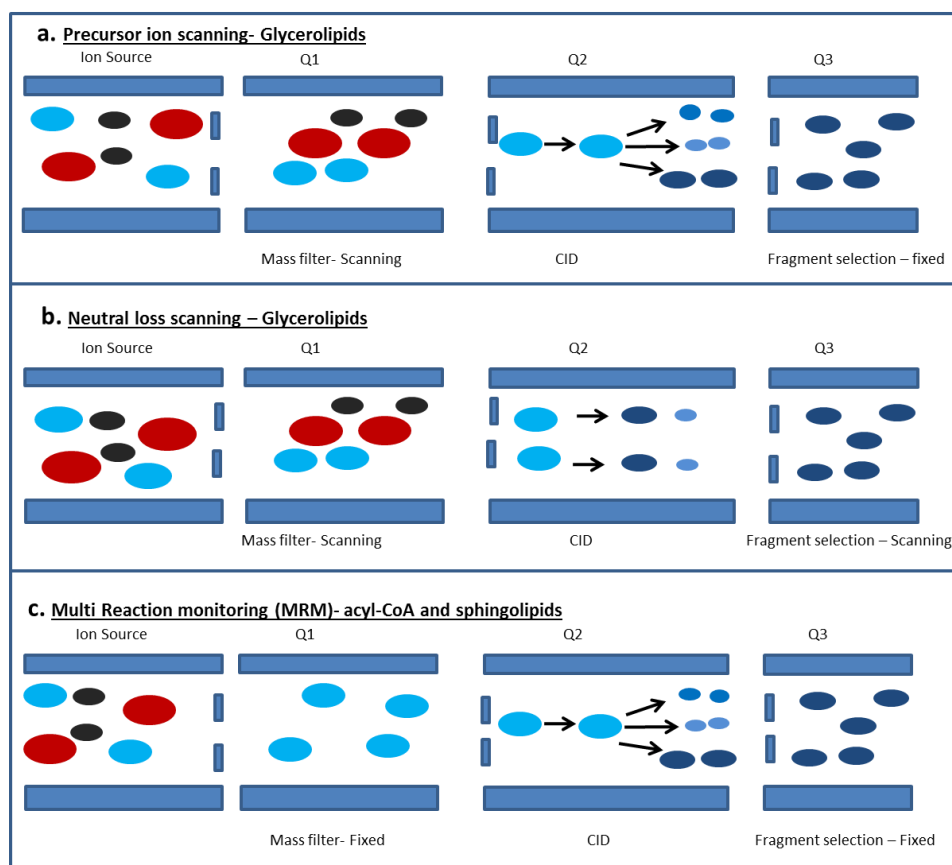


Figure 2.1. The three modes of tandem mass spectrometry. Diagram modified from (Domon and Aebersold, 2006).

2.4.3. Use of HPLC/ESI-MS/MS

High performance liquid chromatography electrospray ionisation tandem mass spectrometry (HPLC/ESI-MS/MS) combines the ability of MS to measure specific compounds within a mixture by monitoring the specific fragmentation pattern of the compounds, with the ability of HPLC to separate compounds with different retention times. This provides double the resolving power and allows for accurate analyte quantification. It also reduces the number of interfering compounds and reduces contamination of the mass spectrometer by compounds in the extract that are non-volatile.

The LC separates compounds by retention time as each of the compounds bind to the column with a different affinity. The compounds are eluted by changing the properties of the mobile phase. The eluent from the HPLC is then passed onto the electrospray probe to be ionised, before passing into the MS. This method is utilised in this study for acyl-CoA and sphingolipid analysis. All solvents for HPLC-ESI/MS/MS were HPLC grade $\geq 99.9\%$, supplied by Sigma-Aldrich.

2.5. Acyl-CoA analysis, materials and methods

The acyl-CoA profile of the samples was analysed using HPLC-ESI-MS/MS in the MRM mode. It monitored precursor and products ions, the MRM pairs, that were specific to a particular acyl-CoA molecule. The MRM pairs of each of the acyl-CoA species can be found in appendix I.

2.5.1. Extraction of acyl-CoAs from shoot and root material

15 mg of shoot or root samples were harvested and frozen in liquid nitrogen and ground with a pestle and mortar. Ice cold extraction buffer was freshly prepared [2 ml 2-propanol, 2 ml pH7.2 mM KH_2PO_4 , 50 μl glacial acetic acid, 80 μl 50 mg/ml

of bovine serum albumin (BSA)] and 200 μ l was added to each sample. The lipids were removed with 3 x 200 μ l washes of petroleum ether saturated with 1:1 (v/v) 2-propanol: water, which is kept at between 40-60 °C. Between washes the samples were centrifuged at 2000 rpm and the upper phase was disposed of. 5 μ l of saturated ammonium sulphate ((NH₄)₂SO₄) was then added to each sample, followed by 600 μ l 2:1 methanol /chloroform (MeOH/CHCl₃). Samples were then incubated for 20 minutes at room temperature before being centrifuged again at 14,000 rpm for 2 minutes. The top phase containing the lipids was removed and transferred to a glass vial. The samples were dried in a speed-vac at 40°C, after which they were resuspended in 40 μ l of acetonitrile. Larson and Graham, (2001) first developed this extraction method.

2.5.2. HPLC-ESI-MS/MS analysis of acyl-CoAs

2.5.2.1. HPLC conditions for acyl-CoA analysis

The LC separation was performed using an Aligent 1200 LC system, with a Gemini C18 Column (2 mm inner diameter, 150 mm with 5 μ m particles). An injection volume of 33 μ l was used at a flow rate of 1 ml/min. The three solvents used were acetonitrile:H₂O, 10:90, v/v and ammonium hydroxide 1% (solvent A), acetonitrile and 1% ammonium hydroxide v/v (solvent B), and H₂O: acetonitrile: formic acid, 30:70:1 v/v (solvent C). The contribution of each solvent to the mobile phase at different times during the analysis can be found in Table 2.1. These gradients was established previously by Han *et al.*, (2010).

Table 2.1. Acyl-CoA solvent table. The percentage each solvent contributes during analysis.

Acyl -CoA						
Step	Total Time (min)	Flow Rate ($\mu\text{l}/\text{min}$)	A (%)	B (%)	C (%)	
0	0	1000	100	0	0	
1	5	1000	75	25	0	
2	11	1000	0	100	0	
3	13	1000	0	100	0	
4	15	1000	0	0	100	
5	18	1000	0	0	100	
6	20	1000	100	0	0	
7	25	1000	100	0	0	

2.5.2.2. Mass spectrometry conditions for acyl -CoA analysis

ESI-MS/MS was performed in the positive ion mode. It has been shown previously that the positive ion mode was on average 3 times more sensitive than the negative ion mode, when comparing the peak areas of C16:0, C18:1 and C24:1-CoA between the two different modes (Haynes *et al.*, 2008). For this reason the positive ion mode was used for analysis. The spray voltage was set to 5 kV, nebulising gas (GS1) at 40p.s.i., focusing gas (GS2) at 40 p.s.i., and curtain gas at 20 p.s.i. The source temperature was held at 750°C.

The MS quantifies the acyl-CoAs by identifying the compounds using their MRM pairs. The values of the MRM pairs correspond to the mass of the singly protonated acyl-CoA in positive ion mode $(M+H)^+$ which was selected in Q1 and the structure specific product ion obtained from the neutral loss of 507.0 Da, so that just the mass of the acyl chain remains, which was selected in Q3. An example of the components of an MRM pair can be seen in Figure 2.2 which shows both the precursor ion and product ion of 16:0 acyl-CoA

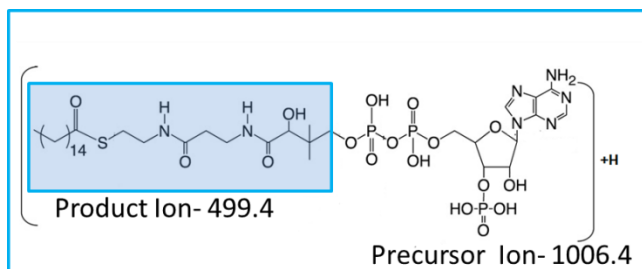


Figure 2.2 The 16:0 acyl-CoA MRM pair. The product ion is selected for in Q3 which is produced as a result of a given collision energy in Q2. The precursor ion detected in Q1 and product ion together result in a unique MRM pair. Figure modified from (Haynes *et al.*, 2008).

Figure 2.3 shows an example of the original output that is produced from the acyl-CoA analysis, showing the retention time against the abundance of the compounds.

Figure 2.3 shows that there is baseline resolution between acyl-CoAs that only differ by one $-\text{CH}_3$ group and/or a single double bond. Each peak was identified using the MRM pairs and the area under each of these peaks was measured, performed using the Analyst software. Any isotopic isomers were added together to give a total amount of each compound. This data was then used to calculate the amount of each compound as a percentage of the total of the MS signal detected.

These values were used in the analysis of the acyl-CoA data.

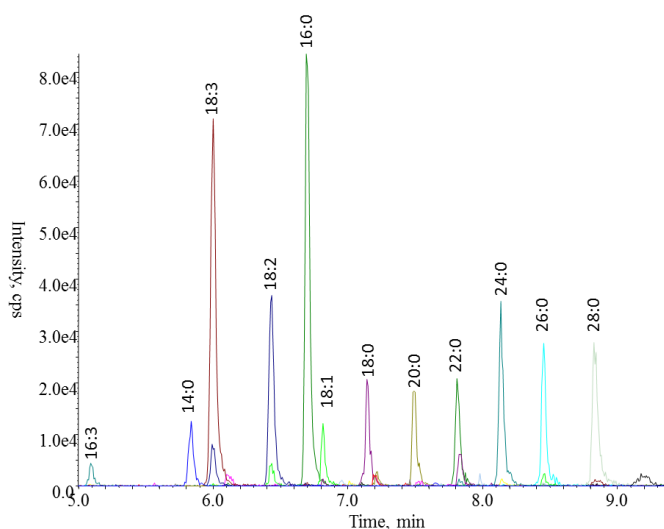


Figure 2.3 Acyl-CoA profile of wild type shoots.

2.6. Sphingolipid analysis, materials and methods

Sphingolipids were analysed using HPLC-ESI-MS/MS in the MRM mode. The MRM pairs that are specific to a particular sphingolipid molecule, can be found in appendix I. Five classes of compounds were analysed using this approach, ceramides, 2-hydroxyceramides (HCer), glucosylceramides (GlcCer), glycosylinositolphosphoceramides (GIPC) and free long chain bases (LCB) and long- chain base phosphates (LCBP).

2.6.1. Extraction of sphingolipids from shoot and root material

Approximately 30 mg of freeze dried tissue was fully ground using a combination of liquid nitrogen, steel balls and vortexing until the tissue was fully homogenised. To this, 3 ml of extraction solvent was added (lower phase of isopropanol/hexane/H₂O 55:20:25 (v/v/v)), and 10 µl internal standard. The internal standard for quantification of sphingolipids consisted of the following quantities: 200 nmol GM1 (ovine), 100 nmol C12-GlcCer, and 10 nmol of C12-Cer, sphingosine (C17 base) and sphingosine-1-phosphate (C17 base). This was prepared according to Markham and Jaworski, (2007). The samples were incubated at 60°C for 15 minutes before being centrifuged at 150 rpm for 5 minutes. The supernatant was transferred to a new tube. The pellet was resuspended in a further 3 ml of extraction solvent. The pellet was then incubated again at 60°C for 15 minutes and centrifuged. The two supernatants are then combined and dried under nitrogen gas. The sample was then de-esterified by dissolving in 2 ml of 33% methylamine solution in ethanol/H₂O (7:3 v/v) and incubating at 50°C for 1 hour. This hydrolyses ester containing lipids such as phospholipids but does not affect sphingolipids. This prevents interference from other lipid compounds during subsequent analysis. The

samples were dried under nitrogen gas and dissolved in 1 ml of tetrahydrofuran (THF)/methanol/H₂O (2:1:2,v/v/v) containing 1% formic acid. This protocol has had minor modifications from that described previously by Markham and Jaworski, (2007).

2.6.2. HPLC- ESI- MS/MS analysis of sphingolipids

2.6.2.1. HPLC conditions for sphingolipid analysis

10 µl of sample was injected onto a 150 x 3mm, 5µm particle size, superCOSIL ABZ+PLUS column which was held at 40°C, at a flow rate of 1 ml/min. Two solvents, A and B, were used to elute the compounds from the column, THF/methanol/ 5 mM ammonium formate (3:2:5 v/v/v) + 0.1% formic acid (solvent A) and THF/methanol/5mM ammonium formate (7:2:1 v/v/v)+ 0.1% formic acid (solvent B). The solvents used for HPLC were monitored previously to produce a suitable gradient resulting in sufficient separation by acyl chain length and the degree of desaturation between the compounds (Markham and Jaworski, 2007). The solvent composition during analysis for each of the different sphingolipid classes is shown in Table 2.2. The sphingolipid classes were always run in the same order on the instrument, GlcCer, Cer, Hcer, GIPC and LCB/LCBP. This was to ensure the composition of solvent at the end of the first sphingolipid class that was analysed was most similar to the composition required for the start of the second class to be analysed.

Table 2.2. Sphingolipid solvent table. The percentage each solvent contributes during the analysis of each of the different sphingolipid classes.

GlcCer				
Step	Total Time (min)	Flow Rate (µl/min)	A (%)	B (%)
0	0	1000	50	50
1	1	1000	50	50
2	9	1000	20	80
3	10	1000	0	100
4	11	1000	0	100
5	11	1000	50	50
6	12	1000	50	50
Cer				
Step	Total Time (min)	Flow Rate (µl/min)	A (%)	B (%)
0	0	1000	60	40
1	1	1000	60	40
2	8	1000	15	85
3	10	1000	0	100
4	11	1000	0	100
5	11.1	1000	60	40
6	12	1000	60	40
HCer				
Step	Total Time (min)	Flow Rate (µl/min)	A (%)	B (%)
0	0	1000	60	40
1	1	1000	60	40
2	9	1000	15	85
3	10	1000	0	100
4	11	1000	0	100
5	11.1	1000	60	40
6	12	1000	60	40
GIPC				
Step	Total Time (min)	Flow Rate (µl/min)	A (%)	B (%)
0	0	1000	75	25
1	1	1000	74	26
2	6	1000	42	58
3	10	1000	0	100
4	11	1000	0	100
5	11.1	1000	75	25
6	12	1000	75	25
LCB/LCBP				
Step	Total Time (min)	Flow Rate (µl/min)	A (%)	B (%)
0	0	1000	90	10
1	2	1000	90	10
2	3.5	1000	80	20
3	8	1000	0	100
4	9	1000	0	100
5	9.1	1000	90	10
6	10	1000	90	10

2.6.2.2. ESI/MS/MS conditions for sphingolipid analysis

ESI/MS/MS was used in the positive ion mode. The temperature was held at 650°C, GS1 was set to 60 p.s.i, GS2 was set to 50 p.s.i., and the curtain gas was set to

20p.s.i..Previously Markham and Jaworski, (2007) used increasing collision energies to produce different possible fragments for each of the different sphingolipid classes. This identified which precursor-product ions (MRM pairs) resulted in the best sensitivity. For ceramide, H₂Cer, GlcCer and LCB/LCBP analysis the product ion was the LCB part of the molecule, shown in Figure 2.4. When the LCB was used as the precursor ion for GIPC analysis it resulted in reduced sensitivity, so the ceramide fragment was used as the precursor ion, shown in Figure 2.4. An example of the spectrum produced after analysis of different sphingolipid classes is shown in Figure 2.5. Each peak was identified based on the MRM pairs and the area under each peak was measured, performed by the Analyst software. This can be used to calculate the amount of each compound as a percentage of the total MS signal. In order to determine the actual amount of each sphingolipid compound, the following formula was used:-

$$\frac{A_{analyte}}{A_{standard}} \times \frac{nmol\ of\ standard \times R}{grams\ of\ tissue} \quad (2.1)$$

Where $A_{analyte}$ and $A_{standard}$ are the peak areas for the analyte and the standard, R is the response factorial which accounts for the different responses on the instrument that sphingolipids with different structures make compared to the standard. The response factorials were assigned from Markham, (2013).

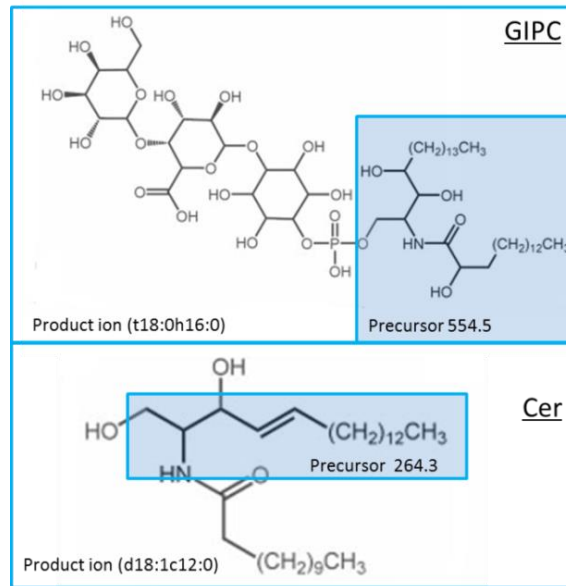


Figure 2.4. The MRM pairs used to analyse sphingolipid molecules. GIPC analysis uses the ceramide as the product ion, whereas, all other sphingolipid classes use the LCB portion of the molecule. Each MRM pair is unique to a particular molecule of which 160 were analysed.

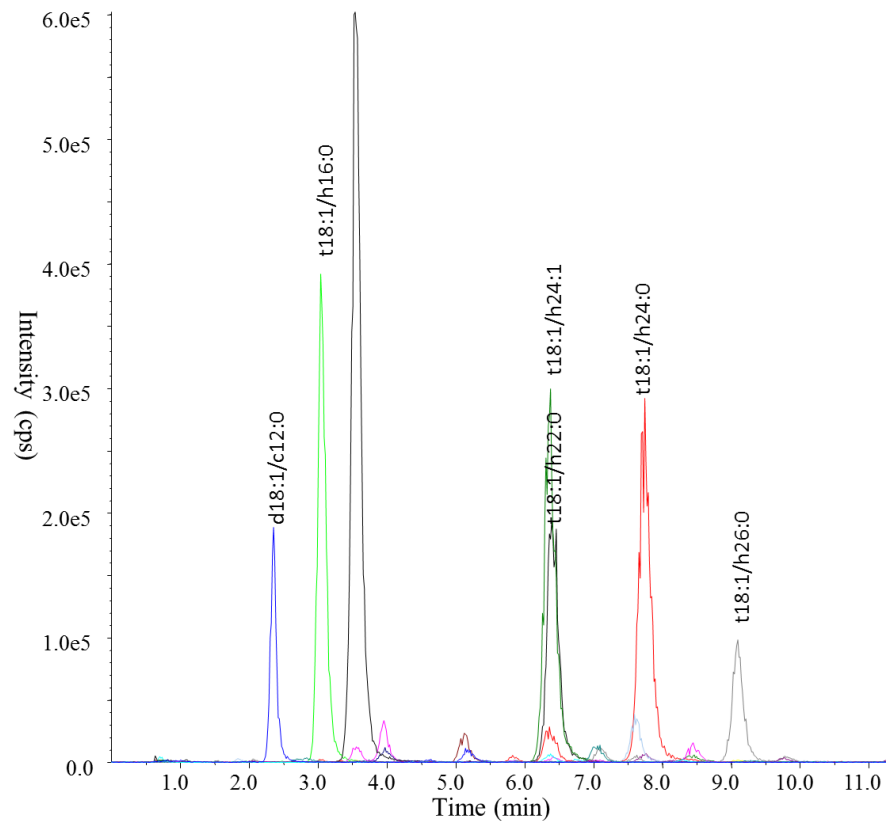


Figure 2.5. GlcCer profile of wild type shoots.

2.7. Membrane glycerolipid analysis, materials and methods

2.7.1. Extraction of membrane glycerolipid from shoot and root material

2.7.1.1. *Developing a 96 well plate method*

Membrane glycerolipid analysis was to be performed on a large number of samples; this required a method with higher throughput than was currently available. A 96 well plate method was developed which allowed a large number of samples to be analysed at the same time. In order to test the reliability across a range of membrane glycerolipids the 96 well plate method was compared to the standard method. Membrane glycerolipids were extracted from 4 samples of roots and shoots and the amount of each glycerolipid extracted was analysed.

2.7.1.2. *96 well plate method*

In a 1.5 ml Eppendorf 50 mg of previously frozen tissue was ground using a small pestle. Samples were placed in a 96 well plate containing 1.2 ml tubes. To each sample 1 ml of 9:1 ethanol/chloroform was added. The samples were then shaken for 1 hour at room temperature. After a short centrifugation (4000 rpm; 3 minutes) the supernatant containing the lipids was removed, transferred to a fresh glass vial, and evaporated under nitrogen. The total lipid extract was then resuspended in 150 µl of chloroform and stored under nitrogen at -20°C.

2.7.1.3. *Pestle and mortar method*

This method is adapted from the many protocols originally developed from the Bligh and Dyer method (Bligh and Dyer, 1959). Plant tissue was harvested and 50 mg of shoot or root material was heated for 10 minutes at 95°C in 1 ml of isopropanol. The samples were then ground using a pestle and mortar and transferred to a glass tube. A further 1 ml of isopropanol and a small amount of

BHT (butylated hydroxytoluene) was added. After which the samples were centrifuged and the supernatant (containing the lipids) was removed and retained. The pellet was resuspended in 1 ml of 1:1 isopropanol/chloroform and centrifuged. The supernatant was removed and the two supernatants were combined. The samples were then evaporated under a stream of nitrogen gas for 1 hour and then resuspended in 330 μ l of chloroform and stored under nitrogen at -20°C . Just prior to analysis, 10 μ l of this extract was added to 990 μ l of chloroform/methanol/ammonium acetate (330:665:35 v/v/v).

2.7.1.4. Comparison of methods

The extraction methods were both analysed using ESI-MS/MS (conditions described later section 2.7.2). As can be seen in Figure 2.6, lipids of different abundance within the plant resulted in the same quantity extracted from both methods. This shows that the two methods are comparable. The well plate method has a much higher throughput, meaning more samples can be analysed in the same amount of time. This was therefore used for all subsequent glycerolipid extractions.

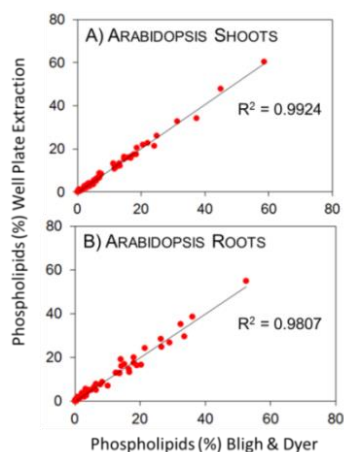


Figure 2.6. Comparison of methods used to extract glycerolipids. A standard lab protocol and a new high throughput method were compared. The amount of each phospholipid extracted is plotted for both of the extraction methods, and the degree of variation between the samples is represented by the R value.

2.7.2. ESI-MS/MS analysis of membrane glycerolipids

Using ESI-MS-MS, 140 molecular species of the membrane glycerolipids classes can be identified. Using either a precursor ion scan or neutral loss scan, these techniques can distinguish different head groups, number of carbon atoms and the number of double bonds present in the acyl chains. Table 2.3 shows the type of scan used and the size of the precursor ion or neutral loss fragment used for each of the scans as well as the polarity used for each glycerolipid class. An example of the fragments used in a precursor ion scan and the fragment used for analysis in a neutral ion scan can be seen in Figure 2.7.

Table 2.3 Mode of ESI-MS/MS used to analyse the various glycerolipid classes. Table adapted from (Welti *et al.*, 2002).

Lipids analysed	Polarity	Scan mode
PC/Lyso PC	[M+H] ⁺	Precursors of m/z 184 ⁺
PE/Lyso PE	[M+H] ⁺	Neutral loss of 141
PA/PG/Lyso PG	[M-H] ⁻	Precursors of m/z 153 ⁻
PI	[M-H] ⁻	Precursors of m/z 241 ⁻
PS	[M-H] ⁻	Neutral loss of 87
MGDG	[M+Na] ⁺	Precursors of m/z 243 ⁺
DGDG	[M+Na] ⁺	Precursors of m/z 243 ⁺

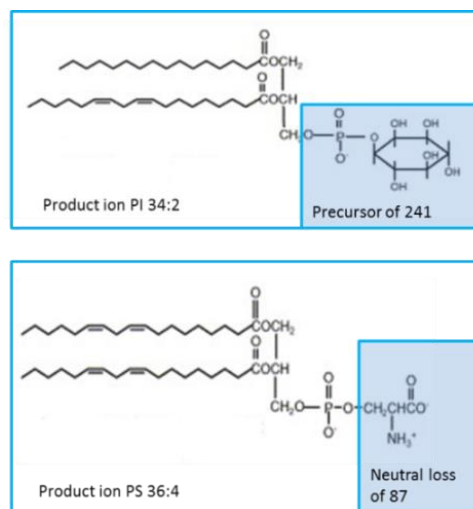


Figure 2.7. Fragments detected in neutral loss scan and precursor ion scan. PI is analysed using precursor ion scan. Highlighted in blue is the head group that is identified in Q3 so that Q1 can be scanned for ions that produce this head group size. PS is analysed using neutral loss scan. Highlighted in blue is the fragment size lost between Q1 and Q3, so that both Q1 and Q3 can be scanned to measure which molecules result in a loss of this size.

The samples were injected into the ESI source of the MS/MS using a CTC pal autosampler, model *HTS-xt*, at a rate of 15 $\mu\text{l}/\text{min}$. GS1 was set at 45 p.s.i., GS2 at 45 p.s.i., and curtain gas at 20 p.s.i. The source temperature was held at 100°C. The spray voltage was set to 5.5 kV for all classes except LPG which was set to -4.5kV. The collision energies and declustering potentials were different for the different glycerolipid classes and can be found in appendix I. The different mass ranges over which the scanning took place were dependent on the class of glycerolipid. The time taken for each scan and mass range can also be found in appendix I. ESI-MS/MS was first used to identify phospholipids using neutral ion scanning and precursor ion scanning by Brugger *et al.*, (1997). The method used here has been adapted from that developed by Welti *et al.*, (2002). An example of the spectrum produced from this analysis can be seen in Figure 2.8, it shows the masses of the precursor ions against the abundance of each. It shows that the peaks are clustered based on the total acyl chain lengths that it contains. The area under the peaks are then measured and the percentage each contributes to the total can then be analysed. Analysis of the raw data for membrane glycerolipid analysis was performed using the LipidView™ 1.2 software package. This software enables the profiling of lipids based on the parent and fragment ions and compares them to a known database. In this analysis, processing methods were used to select the mass range of the scan and the lipid class that is being identified. Additionally, this software package is able to add together isotopic forms of the various lipid classes. The benefit of the scanning technique is that for all compounds within a mass range are identified, and no prior knowledge of the molecular species in the sample is needed.

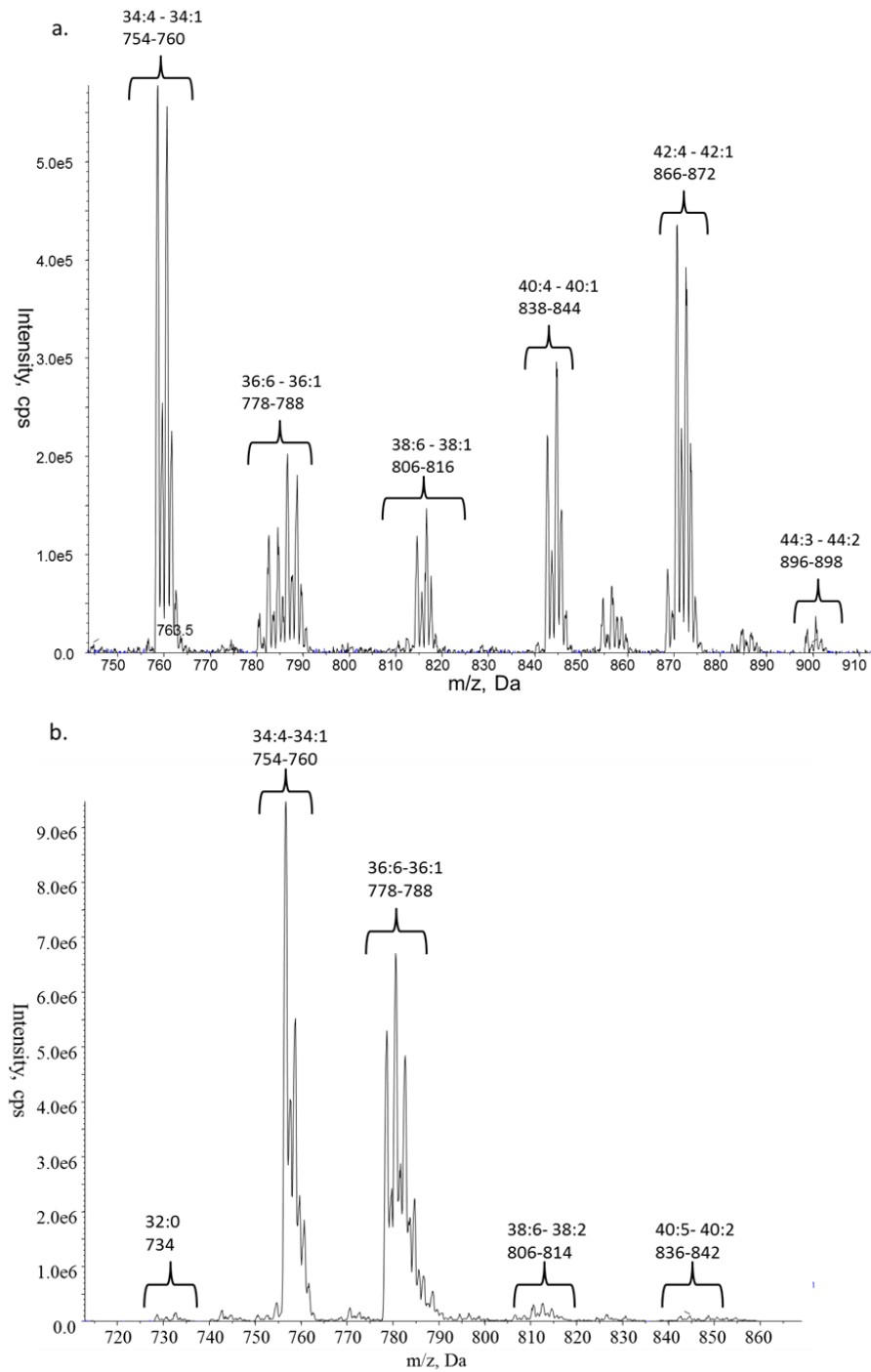


Figure 2.8 Glycerolipid profile of wild type shoots (a) the spectrum produced from PS which is analysed using a neutral ion scan. (b) the spectrum produced from PC which is analysed using a precursor ion scan.

Chapter 3. Lipidomic profiling of plants with mutations in the core components of the elongase

3.1. Introduction

Lipidomics is the detailed and comprehensive analysis of the complete spectrum of lipids in a tissue, organelle or cell. This information in conjunction with phenotypic analysis should reveal potential correlations that exist between the lipidome and the plant phenotype. The lipidomic characterisation of *Arabidopsis* lines which contain a mutation in a component of the microsomal fatty acid elongase complex or a construct designed to down regulate their expression were analysed here. The activity of the microsomal fatty acid elongase complex defines the cellular lipid population and requires global analytical methodology to capture the diversity.

3.1.1. Lipidomic analysis

Lipidomic analysis uses multiple techniques to identify and quantify the hundreds of chemically distinct lipids in cells so that their roles in cellular mechanisms can be investigated. Chromatography and Nuclear Magnetic Resonance have played a role in lipidomics. But it is developments in mass spectrometry that have enabled rapid advances in the field. ESI coupled with tandem mass spectrometry (ESI-MS/MS) and the use of scanning modes; MRM, precursor ion scan and neutral ion scan (as discussed in the Chapter 2), has been the biggest step forward in lipidomic research. It has allowed for the structural determination of complex lipids and has increased the sensitivity of both global and targeted lipid analyses (Blanksby and Mitchell, 2010). In addition, the use of automated samplers permits this analysis to take place on a large number of samples in a timely manner.

3.1.2. Comparative analysis of phenotypic variations between elongase mutants

Mutations in each of the core components of the elongase result in different root and shoot phenotypes and different combinations of phenotypes. This is surprising as they all affect the same enzymatic complex, and all result in decreases in the amount of VLCFAs (Zheng *et al.*, 2005, Bach *et al.*, 2008, Beaudoin *et al.*, 2009). The reasons for these phenotypic differences has previously not been investigated. Complete null mutations of both *kcr1* and *pas2* are embryo lethal so lines that showed partial reductions in gene activity had to be used to observe phenotypic variation (Bach *et al.*, 2008, Beaudoin *et al.*, 2009). Transgenic lines in which *KCR1* was downregulated by an RNAi construct developed by Beaudoin *et al.*, (2009) were used in this study. This construct was shown to specifically downregulate the *KCR1* gene. In comparison *pas2-1* mutants which are EMS (ethyl methane sulfonate) generated mis sense alleles of *PAS2*, show a partial reduction in gene activity (Harrar *et al.*, 2003). *cer10-2* is a complete null mutation. Steady state levels of the ECR gene transcript were recorded and showed that no transcript was produced for the *cer10* mutant (Zheng *et al.*, 2005). However complete loss of CER10 activity is not embryo lethal. *cer10-2* contains a T-DNA insertion in the second intron of the gene (Zheng *et al.*, 2005). A description of the different phenotypes that the different knockout/knockdown elongase lines result in can be found in Table 3.1, whilst some of the shoot and root phenotypes can be seen in Figure 3.1.

Table 3.1. Phenotypes that results from mutations in each of the core components of the elongase complex.

	<i>KCR RNAi</i>	<i>pas 2-1</i> (missense mutation, weak allele)	<i>cer10-2</i> (knockout mutation)
Flower buds fused	Yes	Yes	Yes
Reduction in primary root length	NO	60% reduced	35% reduced
Lack of lateral roots	Yes	Yes	No
Fused primary leaves	Yes	Yes	Yes



Figure 3.1. Phenotype of two week old elongase mutants showing a range of phenotypes.

Figure 3.1 shows the stage of growth when the plants were harvested. All three knockout/knockdown elongase lines displayed fused aerial organs, however the severity of the fusion differs. *pas2-1* shows the highest level of fusion followed by the *KCR RNAi* line, and *cer10-2* shows the lowest level of fusion. The *KCR RNAi* line appeared to show a lack of lateral roots and *pas2-1* seemed to show a reduction in the number of lateral root initiation events, whereas the *cer10-2* line looked to have the same density of lateral roots as wild type plants. Both *cer10-2* and *pas2-1* exhibited shorter primary roots, however, *cer10-2* showed a reduction in primary root length of 35% compared to a 60% reduction in *pas2-1*, based on an average of 4 plants (*pas2-1*= 3.9 cm, *cer10-2* =3.6 cm and WT=8.9 cm). No reduction in root length was seen in the *KCR RNAi* line.

Lipidomic analysis was used to investigate whether a lack of VLCFA in a specific lipid class or an accumulation of intermediates within the VLCFA pathway was responsible for the phenotypic differences seen between different knockout/knockdown elongase lines.

3.2. Results

Two week old plants were separated into root and shoot material and analysed separately for all lipid classes. Previously this analysis has taken place on whole plant material. Since different combinations of root and shoot phenotypes were observed it was reasoned that by analysing their lipid profiles separately, it would be possible to see if the elongase mutants cause different biochemical effects in the roots and shoots within the same mutant, and also between the roots and shoots of different mutants. Hence this separation could elucidate whether certain lipid

classes or a specific lipid compound in these tissues are responsible for a given phenotype.

3.2.1. Acyl-CoA profiling of wild type plants and elongase mutants

Acyl-CoA profiling is the analysis of cellular acyl-CoAs at any given time (a full list of the acyl-CoAs profiled can be found in appendix I). The results of all statistical analysis performed on the acyl-CoA data can be found in appendix II. Acyl-CoAs are separated on column via HPLC prior to detection using the MRM mode of the ESI-MS/MS instrument, the description of this can be found in section 2.4 and 2.5. The acyl-CoA pool is particularly important in the VLCFA mutants as acyl-CoAs and their derivatives are the substrates of each of the four reactions involved in VLCFA synthesis. The very long chain (VLC)-acyl-CoAs produced, are then channelled to the various lipid pools via distinct metabolic pathways.

The proportion of VLCFAs contained within the acyl-CoA pool was specifically examined. This procedure also allowed detection of any potential build-up of VLC-acyl-CoA intermediates in the elongase mutants analysed. These intermediates are likely to be 3-keto-acyl-CoAs in the case of *KCR RNAi* line and 3-hydroxy-acyl-CoAs in *pas2-1*, as these are substrates for the reactions catalysed by the mutants. The 2-enoyl intermediate, which would potentially build up in *cer10* could not be detected because it has the same mass as some of the unsaturated compounds and a standard was not available. The amount of acyl-CoA in the sample is very small, concentrations of 3-6 μM (Larson and Graham, 2001), since as soon as the acyl-CoAs are produced, they are swiftly channelled into the various lipid pools. Therefore the acyl-CoA pool is a very dynamic pool and can be difficult to obtain quantified data for.

3.2.1.1. Profiling of acyl-CoA intermediates of VLCFA synthesis

In the roots of the *KCR RNAi* line there was a build-up of 3-keto-acyl-CoA intermediates, with the total amount of 3-keto containing acyl-CoAs accounting for 21% of total acyl-CoAs in the *KCR RNAi* line. *pas2-1* shows an accumulation of the 3-hydroxy-acyl-CoA intermediate in the roots accounting for 34% of total acyl-CoAs, (Figure 3.2). These biosynthetic intermediates were seen to build up in 18, 20 and 22 carbon compounds (Figure 3.3); with the most substantial build up at 20 carbons. *pas2-1* showed a 14% build-up of 20 carbon hydroxy-acyl-CoA, and the *KCR RNAi* line had a build-up of 15% of 20 keto-acyl-CoA of the total acyl-CoAs analysed. The build-up was not as substantial in the shoots. In the *KCR RNAi* line the keto intermediate accounted for only 2% of the total acyl-CoAs measured in the shoots. The hydroxy intermediates accounted for 20% of the total in the shoots of *pas2-1*. There is a greater build-up of the keto intermediate in the *pas2-1* mutant than in the *KCR RNAi* line in the shoots. This could be explained by the reduced activity of the third reaction, (the dehydratase reaction catalysed by PAS2) in the pathway resulting in a build-up of precursors of the second reaction, as a result of a reduction in the speed of the next reaction in the pathway. This is also seen in *cer10* in the shoots, where the hydroxy intermediate builds up, the substrate for the reaction before the reaction catalysed by CER10. The build-up of intermediates in the shoots and the roots is shown in Figure 3.2.

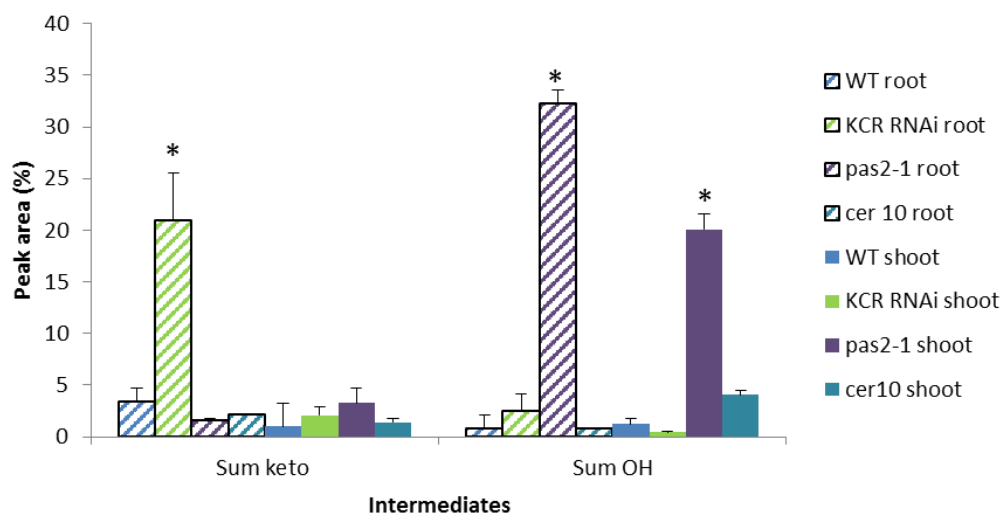


Figure 3.2 . The accumulation of intermediates of VLCFA synthesis within the acyl-CoA pool in the elongase mutants compared to wild type plants. Values are means of +/- standard error of 4 replicates. * Shows significant results based on ANOVA showing a F test p value of less than 0.05, and a difference in means greater than the least significant difference (LSD) values at 5% (degrees of freedom= 9).

3.2.1.2 The percentage of VLC-acyl-CoAs in wild type plants and elongase mutants

The acyl-CoA profiles showing the proportion of acyl-CoAs of saturated CoAs and intermediates can be seen in Figure 3.3 (a full list of the percentage of all acyl - CoAs analysed can be found in appendix II). Since the three mutant lines analysed are affected in VLCFA synthesis it was expected that the proportion of VLC-acyl-CoAs would be decreased. Figure 3.3a shows that in the roots there is a significant decrease in the proportion of acyl-CoA from 22 carbons for the *KCR RNAi* line and *pas2-1* and from 24 carbons in *cer10*. Figure 3.4 shows how the combined amount of VLC-acyl-CoA is affected in the knockout/knockdown elongase lines. No significant decrease was seen in the amount of acyl-CoAs containing 20 carbons or greater in the roots of any of the lines. This is the point that the intermediates in the pathway were shown to build up most substantially. This shows that the acyl-CoAs are extended to 20 carbons, with the same proportions as wild type. There is

however a significant decrease in the proportion of acyl CoA containing 22 carbons and greater when intermediates are included in the total and when they are not. The proportion of acyl-CoA containing 22 carbon chain lengths and greater is reduced compared to wild type plants by 62% in *KCR RNAi* line, 65% in *pas2-1* and 35% in *cer10* even when the proportion from the intermediates are considered in the roots.

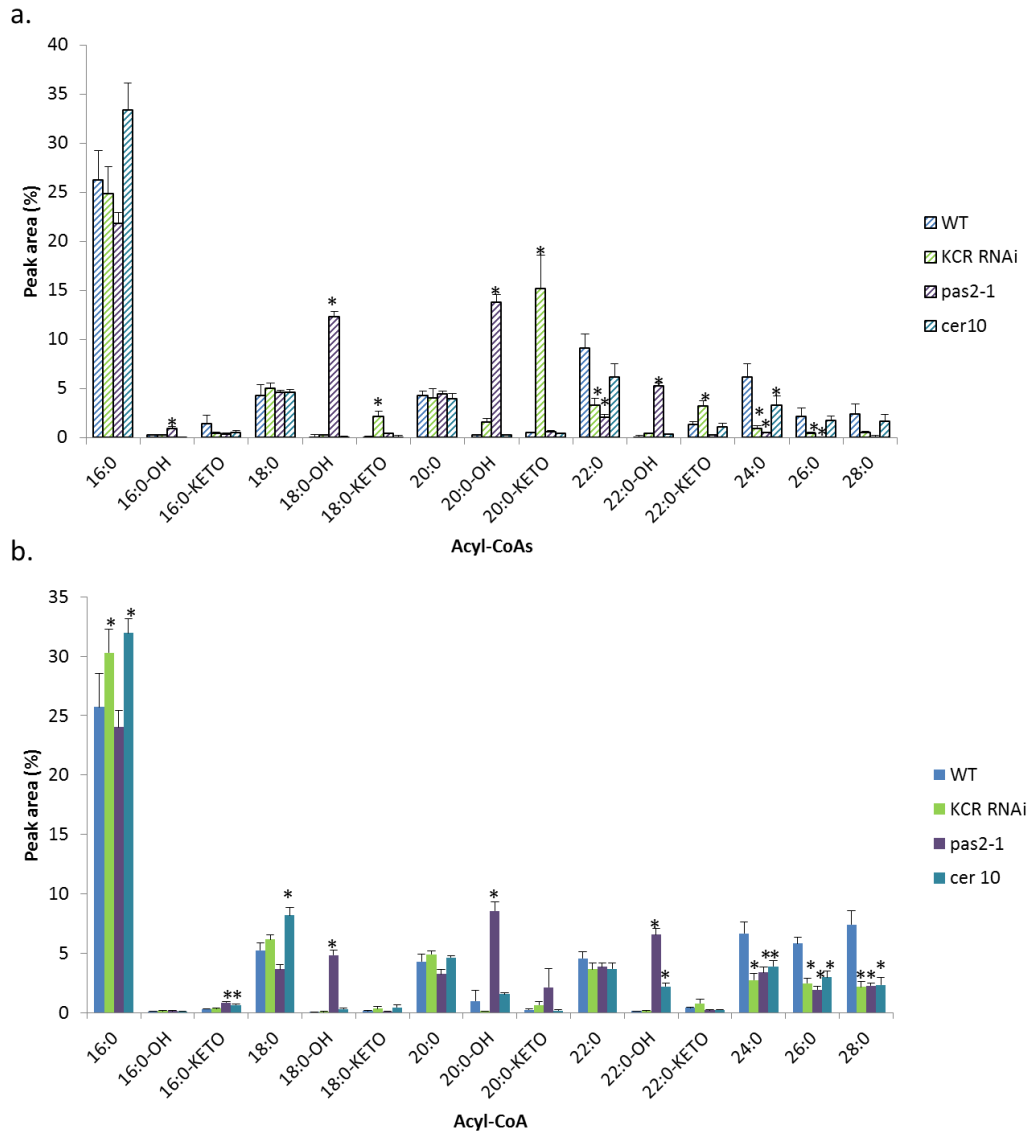


Figure 3.3. Acyl-CoA profile of saturated acyl-CoAs and intermediates within the VLC-acyl-CoA elongation pathway. (a). shows the acyl-CoAs in the roots and (b) shows the acyl-CoAs in the shoots, of elongase mutants and wild type plants. Values are means of +/- standard error of 4 replicates. * Shows significant results based on ANOVA showing a F test p value of less than 0.05, and a difference in means greater than the LSD values at 5% (degrees of freedom= 9).

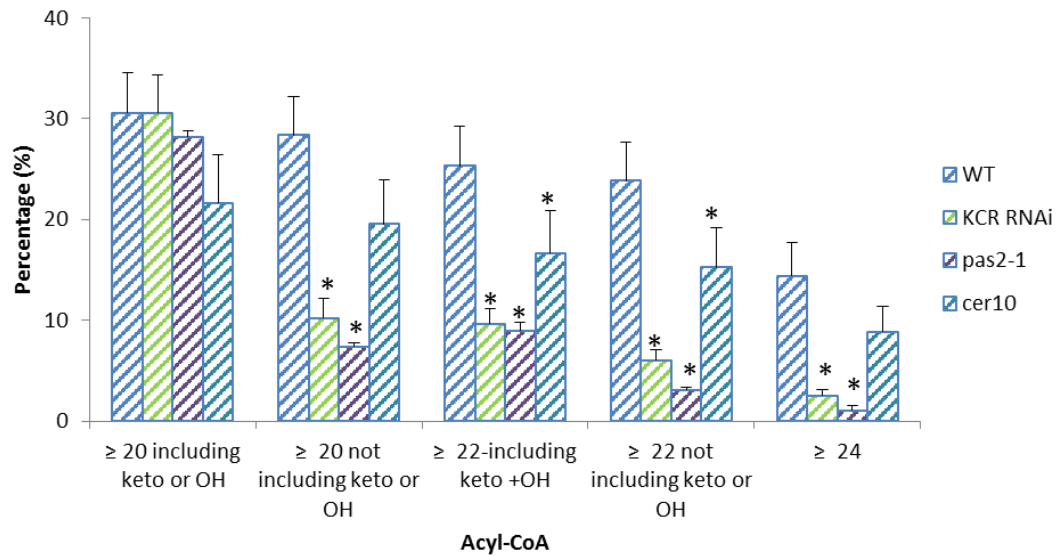


Figure 3.4. The proportion of VLC -acyl- CoAs in the roots of elongase mutants and wild type plants. Showing both fully elongated acyl-CoAs and intermediates within the pathway (3-keto and 3-hydroxy-CoAs). Values are means of +/- standard error of 4 replicates. * Shows significant results based on ANOVA showing a F test p value of less than 0.05, and a difference in means greater than the least significant difference values at 5% (degrees of freedom= 9).

A similar reduction in the proportion of VLC-acyl-CoAs in the shoots might be expected. However, as shown in Figure 3.2, a large build-up of the keto intermediate in the shoots was not seen and the hydroxy intermediate built up by 14% less than in the roots. This suggests that the knockout/knockdown elongase lines have slightly different effects in the shoots and the roots. It could be expected that the levels of VLC-acyl-CoAs are not reduced by as much in the shoots compared to the roots. Figure 3.3b shows that in the shoots there is a decrease from 24 carbons in all of the elongase mutants. This is different from the roots where a decrease was seen from 22 carbons in both *pas2-1* and the *KCR RNAi* line. It can be seen from Figure 3.5 how the total proportion of VLC-acyl-CoAs differ in the mutants compared to wild type plants. There was a significant decrease in the amount of acyl-CoA containing 20 carbons and greater in all of the genetic

disruptions if the intermediates are not included. However, due to the large amount of hydroxy intermediate that builds up in the *pas2-1* mutant there is not a significant decrease if this is included. *pas2-1* did show a significant decrease at 22 carbons and greater, with or without the intermediates being included in the total. The amount of VLC-acyl-CoAs at 22 carbons and greater including the intermediates were reduced by 49% in *KCR RNAi* lines, 22% in *pas2-1* and 37% in *cer10* in the shoots. *cer10* shows a similar reduction in the roots and shoots, whereas both *pas2-1* and the *KCR RNAi* line show a much greater reduction in the roots than the shoots. The same pattern is observed in chain lengths containing 24 carbons or greater, and again a much greater decrease is seen in the roots than the shoots except for *cer10*. *cer10* is also the only mutation of the core elongase complex not to show a lateral root phenotype.

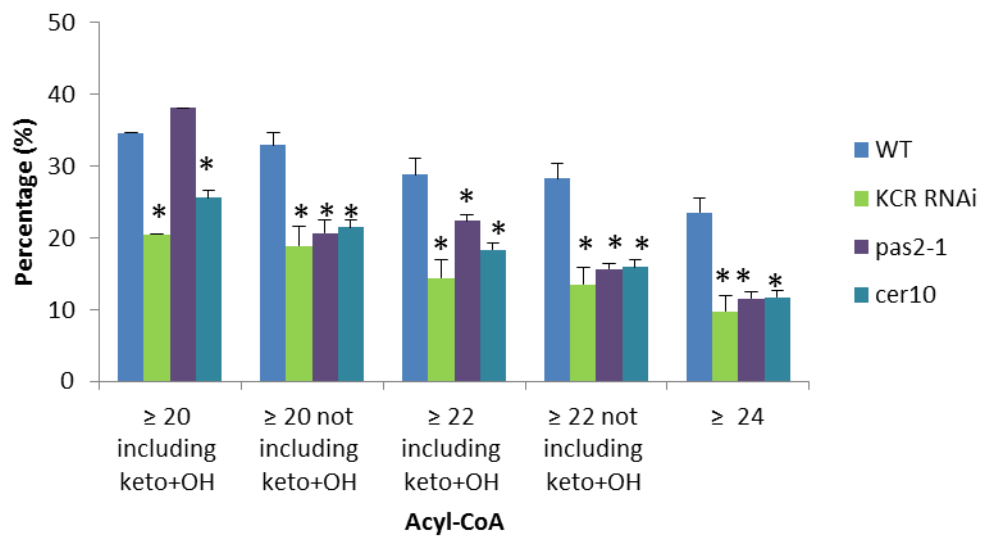


Figure 3.5 The proportion of VLC-acyl-CoAs in the shoots of elongase mutants and wild type plants. Showing both fully elongated acyl-CoAs and intermediates within the pathway (3-keto and 3-hydroxy-CoAs). Values are means of +/- standard error of 4 replicates. * Shows significant results based on ANOVA showing a F test p value of less than 0.05, and a difference in means greater than the least significant difference values at 5% (degrees of freedom= 9).

3.2.1.3. Quantity of acyl-CoAs detected in wild type plants and elongase mutants

Figure 3.6 shows that the patterns displayed as the percentage of the total acyl-CoAs detected are also seen in the quantity of acyl-CoAs detected. Figure 3.6 a and b shows that the quantity of acyl-CoA detected was not significantly different to wild type in *cer10* and the *KCR RNAi* line in the shoots and the roots, whereas *pas2-1* shows a decrease in the overall acyl-CoA pool. Figure 3.6 c and d shows that the intermediates in the *KCR RNAi* line build up in the roots significantly compared to wild type whereas in the shoots there is not a significant build up. *pas2-1* shows a build-up of intermediates greater than wild type in the shoots and the roots despite the fact that the acyl-CoA pool size has been reduced compared to wild type. This shows that a high proportion of the total acyl-CoA is in the form of the hydroxy intermediate. Intermediates are shown to build up in the *cer10* mutant, this is from the hydroxy intermediate as described previously in Figure 3.2. There is a decrease in the quantity of acyl-CoA containing chain lengths of 24 carbons and greater in both the roots and the shoots for all of the knockout/knockdown elongase lines.

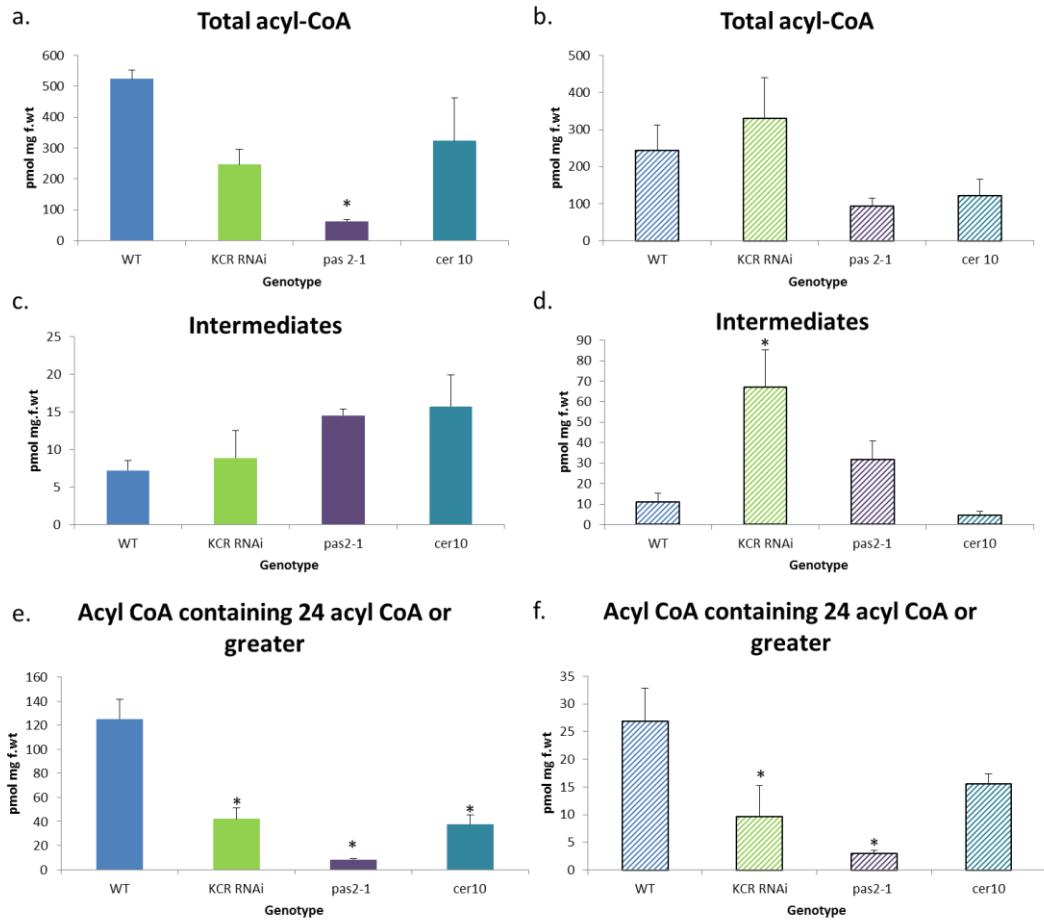


Figure 3.6. The quantity of acyl-CoA detected in the roots and shoots of elongase mutants compared to wild type plants. (a) The total quantity of acyl-CoA detected in the shoots, (b) the total quantity of acyl-CoA detected in the roots. (c) and (d) display the quantity of hydroxy and keto intermediates detected in the shoots (c) and in the roots (d). (e) and (f) show the quantity of acyl-CoAs containing a chain length of 24 carbons or greater in the shoots (e) and the roots (f). Values are means of \pm standard error of 3 replicates. * Shows significant results based on ANOVA showing a F test p value of less than 0.05, and a difference in means greater than the LSD values at 5% (degrees of freedom= 6).

3.2.2. Membrane glycerolipid profiling of wild type plants and elongase mutants

Membrane glycerolipids are a sink for VLCFAs, which are major components of the cellular membranes. They are also important signalling molecules and are important precursor molecules for the synthesis of other lipids. Precursor ion and neutral ion scanning using ESI-MS/MS allows profiling of glycerolipids to measure the acyl chain lengths attached to the various head groups. In *Arabidopsis*, PE and PS contain a significant proportion of VLCFAs, (Devaiah *et al.*, 2006). The acyl-

CoA data of the knockout/knockdown elongase lines showed a decrease in the proportion of VLC-acyl CoA, so the phospholipid pool was analysed to see if the phospholipids were reflective of this change. As shown in Figure 1.15 glycerolipids contain two acyl chains and the analysis performed here considers the combined number of carbons in these two chains. In addition it investigates differences when a VLCFA is present as one of these carbon chains.

3.2.2.1. Membrane glycerolipid profiling of the shoots of wild type plants and elongase mutants

The percentage of each of the different membrane glycerolipids, in the shoots of wild type plants and knockout/knockdown elongase lines, was investigated, (Figure 3.7). The wild type material analysed here showed a similar percentage of each of the glycerolipids to what has been reported previously for leaf material of 7 day old plants. One difference observed in this dataset is a higher proportion of PC and a lower proportion of DGDG compared to previously reported data (Wolti *et al.*, 2002, Yonghua Li-Beisson, 2013).

PC is the most abundant phospholipid and is also thought to be important in controlling the flux of fatty acids in the cell (Bates and Browse, 2012). No differences could be seen in the proportion that PC contributes to the total amount of phospholipids between wild type and elongase mutants, (Figure 3.7). In addition there was no difference in the contribution that each of the different chain length (those containing 34 or 36 carbon chain lengths) made to the total amount of PC. No PC molecules containing 38 carbon atoms could be detected meaning that no VLCFAs were present in this class. Amongst the other classes of glycerolipids there were differences between wild type and the elongase mutants in the proportion that

each class contributes to the total membrane glycerolipids in the shoots, but this was not the same for all of the mutants. For example, *cer10* shows an increase in the proportion of PA compared to wild type. However as all of the lines did not show the same changes it is not thought to be responsible for the phenotypes seen. The statistical analysis used to observe significant differences in classes and chain lengths can be found in appendix II.

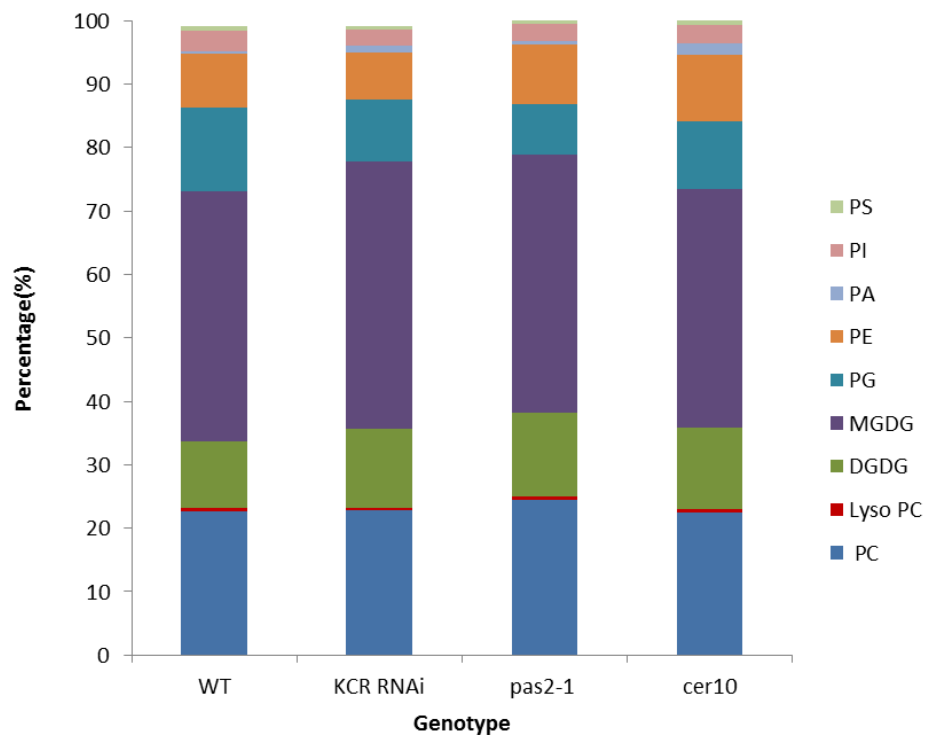


Figure 3.7. Membrane glycerolipid composition in the shoots of elongase mutants and wild type plants. Based on the mean of 4 values.

Analysis was performed to determine the proportion of phospholipids that contain VLCFA (those phospholipids that contain at least one acyl chain of 20 carbon atoms or greater). This was calculated by combining VLCFA containing PE and PS together as these were the only two classes where phospholipids that contained VLCFA were detected. Figure 3.8 shows that there is a significant decrease in all of

the knockout/knockdown elongase lines in the proportion of phospholipids containing VLCFA in the shoots compared to wild type plants. Compared to wild type, the *KCR RNAi* line decreased by 30%, *pas2-1* by 41% and *cer10* by 40% in the proportion of phospholipids containing VLCFAs.

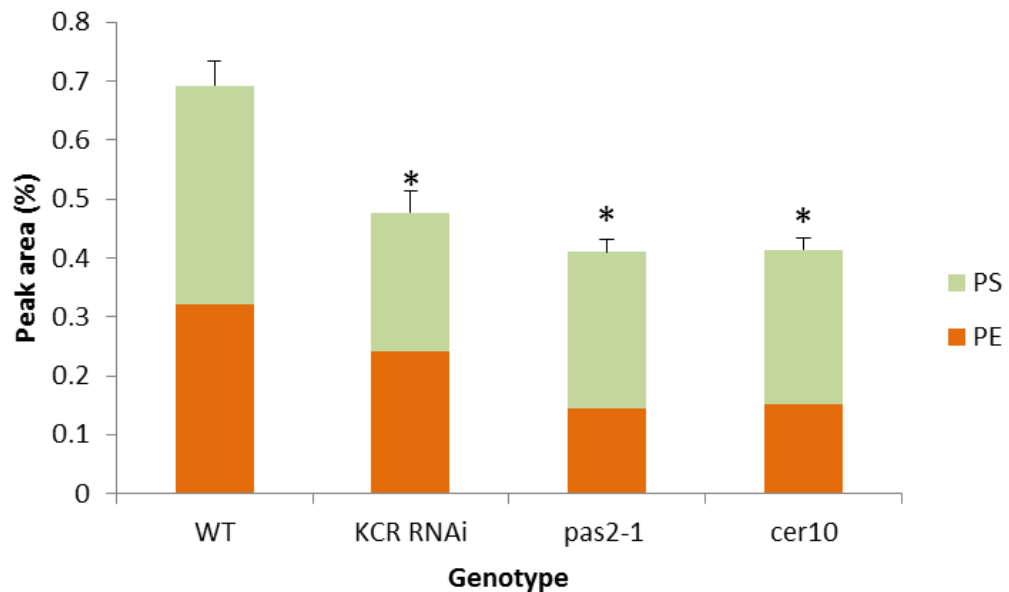


Figure 3.8 The proportion of phospholipids that contain a VLCFA in the shoots of elongase mutants and wild type plants. Values are means of +/- standard error of 4 replicates. * Shows significant results based on ANOVA showing a F test p value of less than 0.05, and a difference in means greater than LSD values at 5% (degrees of freedom= 9).

Since PS and PE contained VLCFA, the composition of these phospholipids was analysed in greater detail. Figure 3.9 shows how each of the different acyl chain lengths of PS contributed to the total amount of this phospholipid identified in the shoots. Molecular species containing 38 carbons were not significantly decreased in any of the elongase mutants and actually showed an increase in *pas2-1*. Whereas, all of the elongase mutants exhibited a significant decrease in the proportion of PS containing 40 carbon atoms or greater. It was shown that PS species containing 40 carbons chains and greater were composed of C24 or C26 acyl chains attached in

combination with a C18 fatty acid (Devaiah *et al.*, 2006). As illustrated in the acyl-CoA data (Figure 3.3), there is a significant decrease in all of the elongase mutants in C24 but not in C20 or C22 in the shoots. This suggests that the changes seen in the acyl-CoA pool are channelled into the phospholipid pool. PS also showed an increase in the proportion of the PS containing 34 or 36 acyl carbons in *cer10* and in 34 acyl carbons in *pas2-1*.

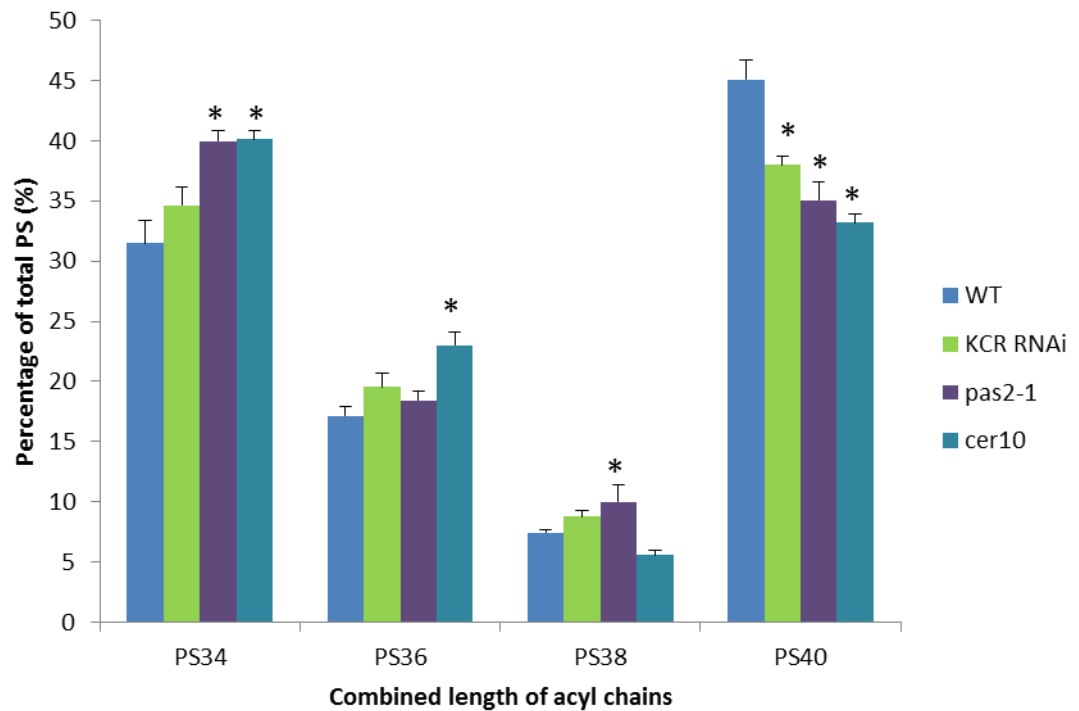


Figure 3.9. The proportion of each acyl chain length in the total amount of PS identified in the shoots in elongase mutants and wild type plants. Values are means of +/- standard error of 4 replicates. * Shows significant results based on ANOVA showing a F test p value of less than 0.05, and a difference in means greater than the LSD values at 5% (degrees of freedom= 9).

The PE profile of the mutants is similar to PS, as shown in Figure 3.10. There was a significant decrease in the proportion of PE molecules containing 38 carbons and greater in all of the elongase mutants. In the *KCR RNAi* line, VLCFA containing PE species were reduced by 13% (not a significant decrease), 59% in *pas2-1*, and 64% in *cer10* compared to wild type. In the PS profile a decrease was not seen in the

proportion of PS molecules containing 38 carbons but a decrease was seen in the proportion of PS containing 40 carbons and greater. The PE profiles, showed only one PE species that contained greater than 40 carbons. This species could not be detected in *pas2-1* and *cer10* and in *KCR RNAi* line only a very small amount could be detected, mirroring the profile of PS. However, unlike in the PS profile a decrease in the proportion of PE containing 38 carbon atoms was seen in all of the elongase mutants.

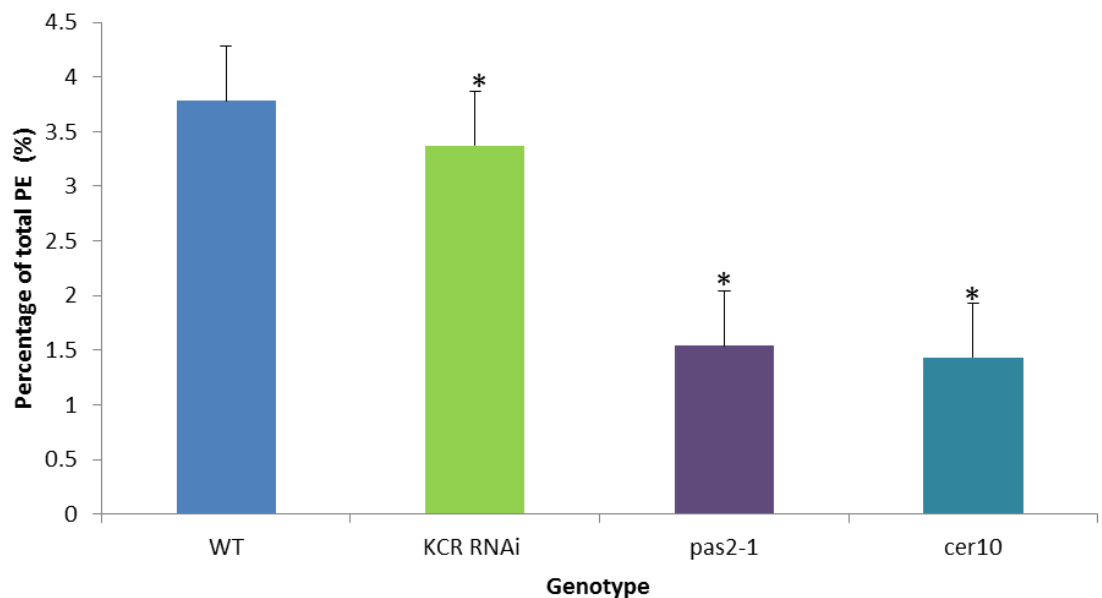


Figure 3.10 The proportion of PE containing a VLCFA as a percentage of the total amount of PE in the shoots of elongase mutants and wild type plants. Values are means of +/- standard error of 4 replicates. * Shows significant results based on ANOVA showing a F test p value of less than 0.05, and a difference in means greater than the LSD values at 5% (degrees of freedom= 9).

3.2.2.2. Membrane glycerolipid profiling of the roots of wild type plants and elongase mutants

The percentage that each glycerolipid class contributed to the total amount of membrane glycerolipids detected in the roots was analysed. The WT roots showed a similar profile to that detected previously for *Arabidopsis* roots (Yonghua Li-Beisson, 2013). *KCR RNAi* and *cer10* did not show any significant differences in

the proportion that any of the membrane glycerolipids contributed to the total compared to wild type plants. *pas2-1* contained a lower amount of PC (9% lower) and a higher amount of PG (1.7% higher). This can be seen in Figure 3.11. The statistical analysis used to observe significant differences in classes and chain lengths can be found in appendix II.

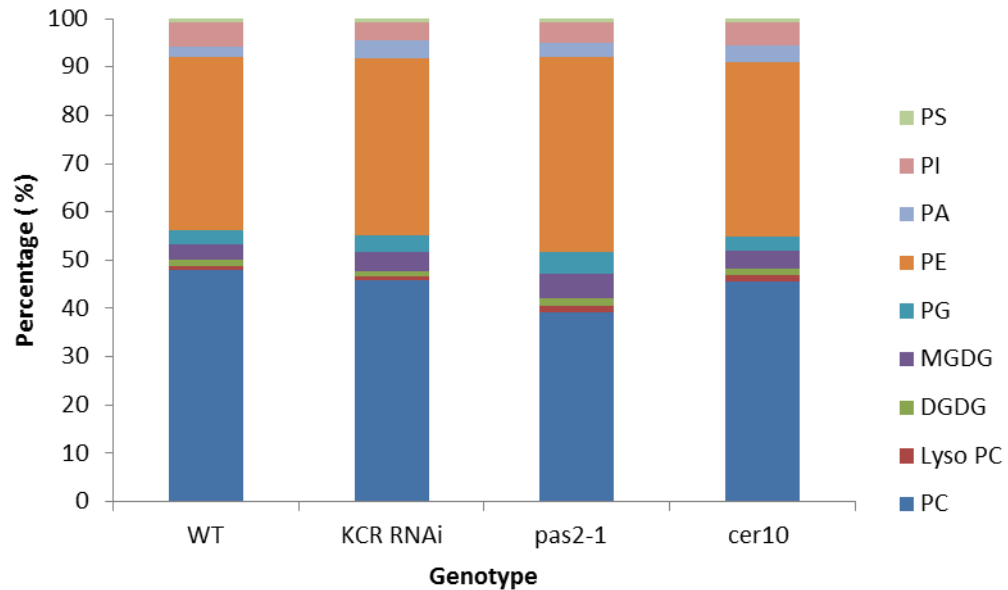


Figure 3.11 Membrane glycerolipid composition in the roots of elongase mutants and wild type plants. Values based on the mean of 3 replicates.

Figure 3.12 shows that, as in the shoots, there was a significant decrease in the proportion of phospholipids containing VLCFAs in *pas2-1* and in the *KCR RNAi* line. However, in contrast to the shoots, *cer10* did not show a statistically significant decrease in the roots. The *KCR RNAi* line exhibited a percentage decrease of 53%, *pas2-1* by 77% and in the case of *cer10* there was a more moderate decrease of 22% but this was not significant. *KCR RNAi* and *pas2-1* showed a larger percentage decrease in the roots than in the shoots, concurring with

the acyl-CoA data. *cer10* is the only mutant that displayed a less severe reduction in the roots than in the shoots.

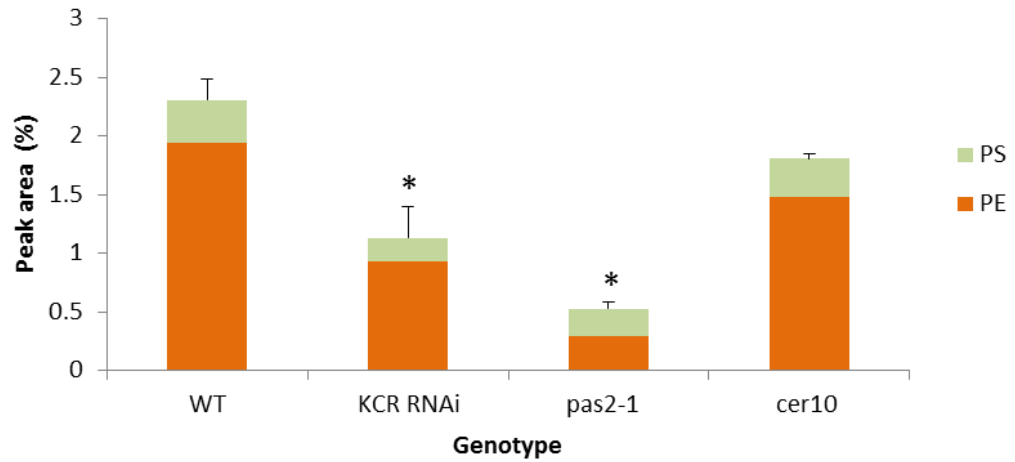


Figure 3.12. The proportion of phospholipids that contain a VLCFA in the roots of elongase mutants and wild type plants. Values are means of +/- standard error of 3 replicates. * Shows significant results based on ANOVA showing a F test p value of less than 0.05, and a difference in means greater than the LSD values at 5% (degrees of freedom= 6).

Figure 3.13 shows the PS profile of the roots. As previously shown for the shoots, there was a significant decrease in the amount of PS containing 40 carbon atoms and greater in *pas2-1* and the *KCR RNAi* line. However, unlike in the shoots there was not a significant decrease in *cer10*. The amount of PS containing 40 acyl carbons and greater as a percentage of the total amount of PS in the sample showed a decrease of 42% in the *KCR RNAi* line and is reduced by 30% in *pas2-1*. In the shoots there was a significant decrease in PS containing 40 carbons and greater, but not at 38 carbons. However, this pattern could not be seen in the roots as no PS molecules containing 38 carbons were detected in either the wild type plants or in the elongase mutants.

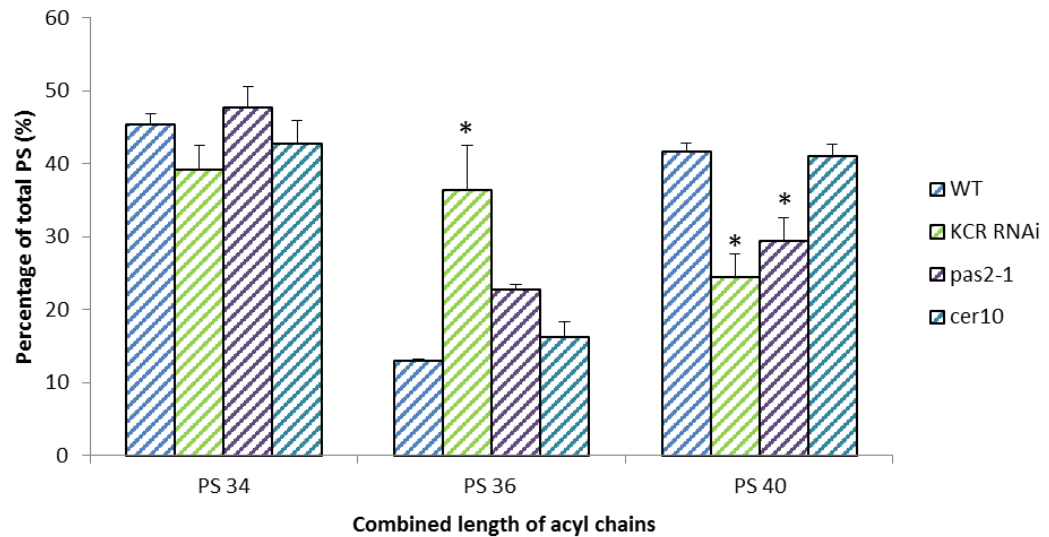


Figure 3.13 The proportion of each acyl chain length in the total amount of PS identified in the roots in the elongase mutants and wild type plants. Values are means of \pm standard error of 3 replicates. * Shows significant results based on ANOVA showing a F test p value of less than 0.05, and a difference in means greater than the LSD values at 5% (degrees of freedom= 6).

The PE profile showed a similar pattern to the PS profile in the roots (Figure 3.14).

The elongase mutants showed a significant decrease in the amount of PE containing a VLCFA. *KCR RNAi* exhibited a 55% decrease, *pas2-1* 87% and *cer10* by 25%, this is shown in Figure 3.14. These decreases are much greater than in the shoots for *pas2-1* and *KCR RNAi*; this is not the case for *cer10*. The percentage decrease in the case of *cer10* is much greater in the shoots than in the roots.

It has been shown previously in *pas2-1* roots, that the amount of PS and PE containing VLCFA was reduced so that there was nearly a complete absence of VLCFA containing PE and PS altogether (Bach *et al.*, 2011). This study correlates this decrease with the delay seen in cell plate formation and the role of VLCFAs in cytokinesis and speculates that this could be responsible for reduced primary root growth. Here we show that this effect also appears to occur in the shoots of *pas2-1* and in the *KCR RNAi* line in both the roots and the shoots. *cer10* has shown in the

proportion of phospholipid containing VLCFA that it exhibits a greater decrease in the shoots than in the roots, which is in contrast to the other two elongase mutants.

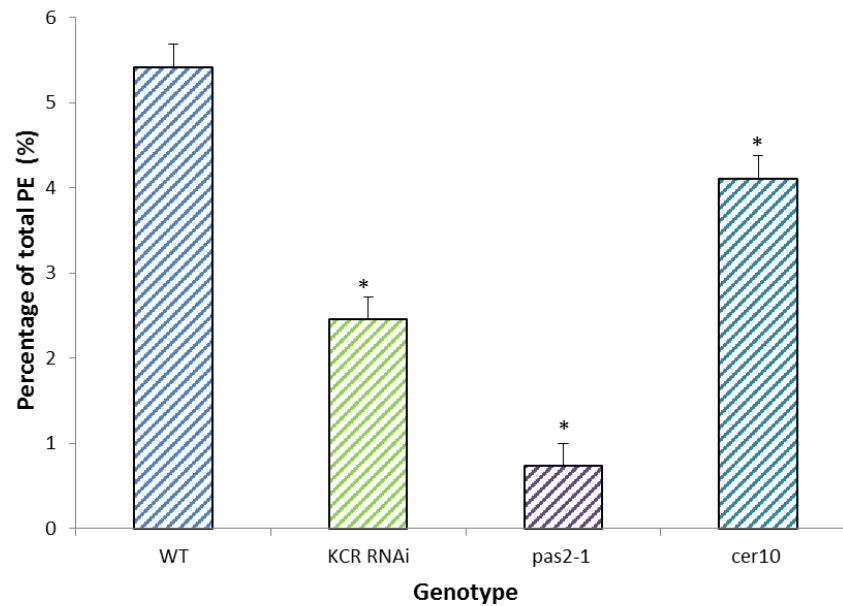


Figure 3.14. The proportion of PE containing a VLCFA as a percentage of the total amount of PE in the roots of elongase mutants and wild type plants. Values are means of +/- standard error of 3 replicates. * Shows significant results based on ANOVA showing a F test p value of less than 0.05, and a difference in means greater than the LSD values at 5% (degrees of freedom= 6).

3.2.3. Sphingolipid profiling of wild type plants and elongase mutants

Although sphingolipids are far less abundant than glycerolipids, they are a major component of the plasma membrane and tonoplast in plant cells and a major sink for VLCFAs from 20 to 26 carbons in length. An absence of VLCFAs containing sphingolipids has been shown to be embryo lethal in *Arabidopsis* (Markham *et al.*, 2011). In addition mutations in genes involved in sphingolipid metabolism, result in a number of phenotypes including a reduced root growth, reduction in plant size and altered golgi morphology (Sperling *et al.*, 2001, Dietrich *et al.*, 2008, Melser *et al.*, 2010, Roudier *et al.*, 2010, Markham *et al.*, 2011). Acyl-CoA profiling in this chapter has shown that the proportion of VLC- acyl-CoAs was reduced in the knockout/knockdown elongase lines. As the substrate for sphingolipid biosynthesis,

a reduction in VLCFA could result in a reduction in sphingolipids containing VLCFAs, which has been suggested previously to be responsible for a number of the phenotypes seen (Zheng *et al.*, 2005, Bach *et al.*, 2011, Markham *et al.*, 2011). For this reason the sphingolipid profile was analysed. The amount of GIPCs and GlcCers (complex sphingolipids), accounting for the highest amount of sphingolipids in *Arabidopsis*, as well as the amount of less abundant molecular species such as ceramides, hydroxycermides, (simple sphingolipids), and free LCBs and LCBPs were analysed.

3.2.3.1. Sphingolipid profiling of the shoots of wild type plants and elongase mutants

3.2.3.1.1. The quantity of each of the sphingolipid classes in the shoots

The contribution of each sphingolipid class to the total sphingolipid pool was measured in the shoots. It was shown that the proportion of each of the different classes of sphingolipids in wild type plants were similar to those that have previously been reported (Markham and Jaworski, 2007). As shown in Figure 3.15, all of the knockout/knockdown elongase lines resulted in a significant decrease in the total amount of sphingolipids, 23% in *KCR RNAi*, 10% in *pas2-1* and 15% in *cer10*. This was reported previously in the *KCR RNAi* line (Beaudoin *et al.*, 2009), and here it is shown that the other core elongase mutants also show a decrease. All the elongase mutants exhibited a decrease in the amount of GIPCs compared to wild type. *KCR RNAi* showed a decrease of 24%, 29% in *pas2-1* and 48% in *cer10* compared to wild type plants. There was also a decrease in the amount of GlcCer in all of the elongase mutants, 28% in *KCR RNAi*, 22% in *pas2-1* and 7% in *cer10*. It has been shown previously that there was a greater reduction in the amount of

GlcCer than GPCs in *pas2-1* (Bach *et al.*, 2008, Roudier *et al.*, 2010). This is not seen when just the shoots are analysed, instead a more general decrease in all complex sphingolipids is seen. *pas2-1* and *cer10* both show an increase in the total amount of both the ceramides and HCer. *pas2-1* showed an increase of 42% and 43%, in the ceramides and HCer respectively and *cer10* increases of 34% and 48% in the ceramides and HCer respectively. This was reported previously for the three *pas* mutants (Bach *et al.*, 2008, Roudier *et al.*, 2010). The *KCR RNAi* line did not show any significant changes compared to wild type in these two classes of sphingolipids.

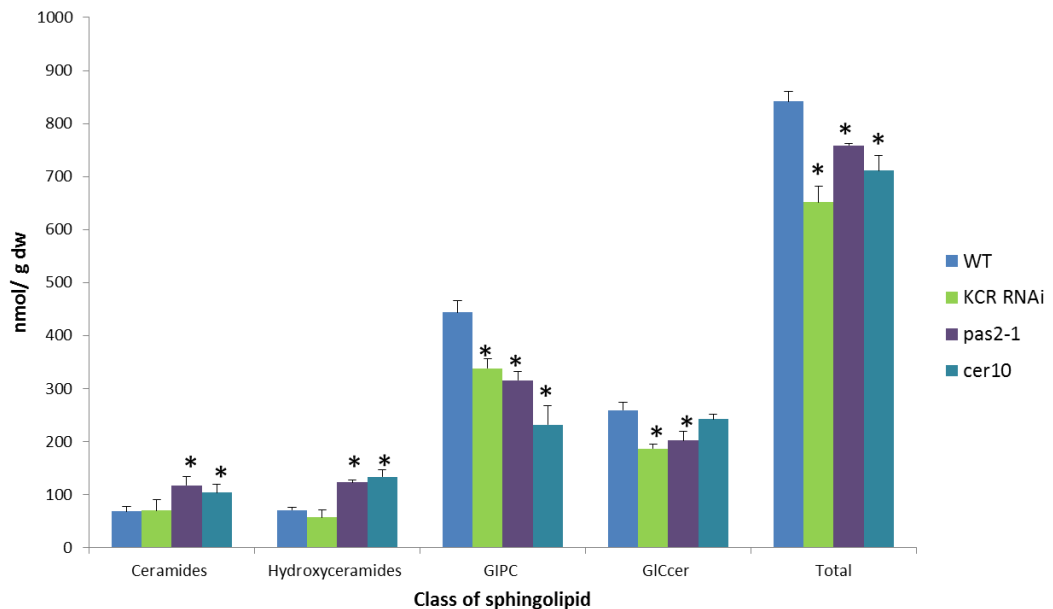


Figure 3.15. Sphingolipid composition in the shoots of elongase mutants and wild type plants Values are means of +/- standard error of 3 replicates. * Shows significant results based on ANOVA showing a F test p value of less than 0.05, and a difference in means greater than the LSD values at 5% (degrees of freedom= 6).

3.2.3.1.2. Percentage of sphingolipids containing VLCFAs in the shoots

The data was used to calculate the amount of each compound as a percentage of the total MS signal detected. The percentage of sphingolipids containing VLCFAs

across all the sphingolipid classes in the shoots was measured, (Figure 3.16a). Those that contained VLCFA (fatty acid with 20 carbons or greater) were compared between wild type and the knockout/knockdown elongase lines. The proportion of VLCFA shown in each of sphingolipid classes in wild type plants is similar to that previously reported (Markham and Jaworski, 2007). *pas2-1* and *cer10* shoots showed a decrease in the proportion of total sphingolipids containing VLCFA, 18% and 20% decrease respectively. However, a decrease was not seen in the *KCR RNAi* line.

Each class of sphingolipid was also measured individually to see if the decrease in the proportion of VLCFA could be seen in all classes and whether the decrease was of the same proportion in every class, shown in Figure 3.16 b-e. *cer10* (10%) and *pas2-1* (11%) both showed a significant decrease in the amount of VLCFA in GIPCs in the shoots. In contrast, *KCR RNAi* showed consistent levels of VLCFAs as wild type. *pas2-1* shows a significant decrease in GlcCer containing VLCFA, a decrease of 30% was observed. *cer10* also showed a significant decrease of 20%. A more substantial decrease in the proportion of VLCFAs can be seen in the GlcCer than in the GIPCs, as shown previously in *pas2-1* and here it is also shown for *cer10* (Bach *et al.*, 2008). The *KCR RNAi* line in contrast did not show any differences with wild type. The ceramides did not show any changes in the proportion of VLCFA in the shoots of the elongase mutants compared to wild type. The HCer were decreased in the proportion containing VLCFA in *pas2-1* by 19%, but no significant differences were seen in the *KCR RNAi* line or *cer10*.

The data suggests that the composition of sphingolipids is altered such that there is a reduction in the proportion of VLCFAs in complex sphingolipids, but in simple sphingolipids the proportion of VLCFAs remained more consistent with wild type in *pas2-1* and *cer10*. The *KCR RNAi* line however appears closer to wild type in its composition of all sphingolipid classes in the shoots.

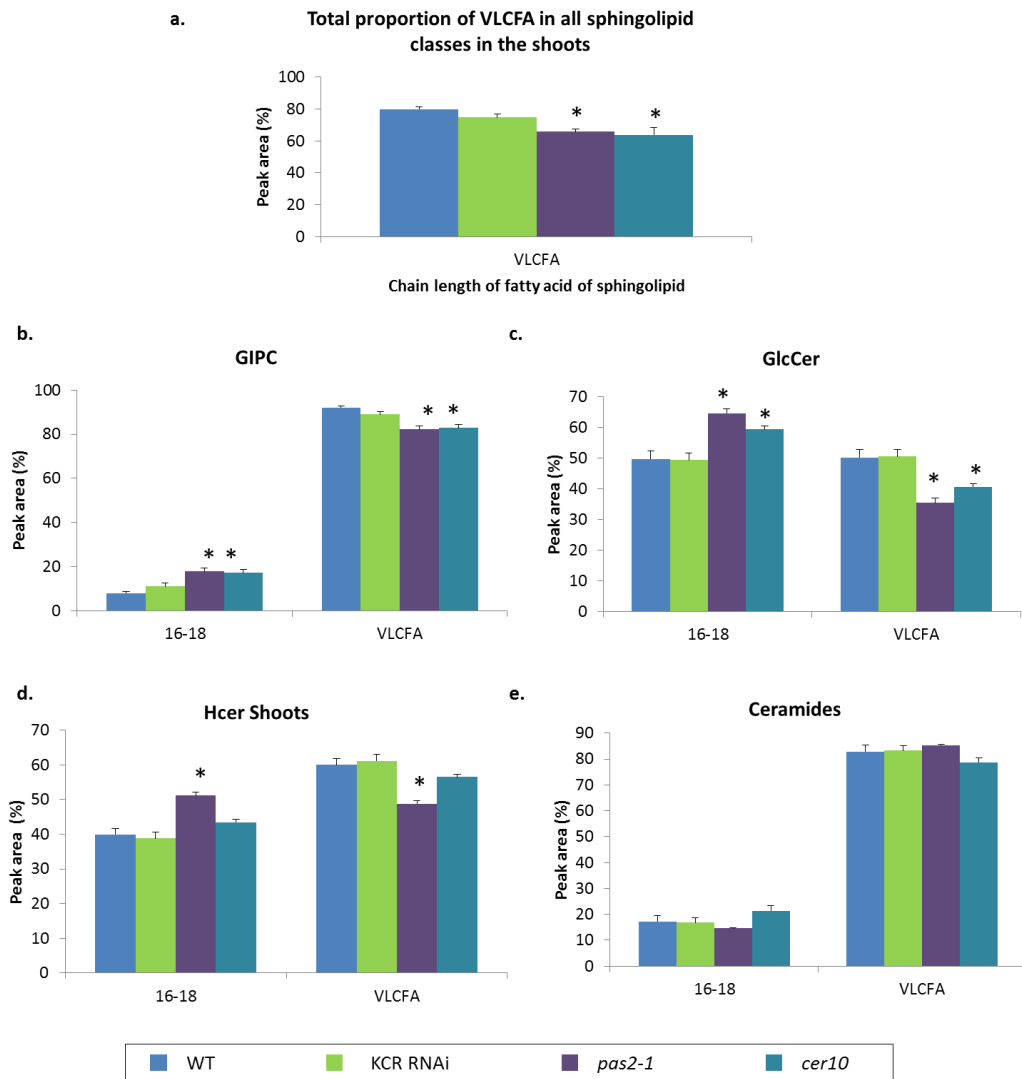


Figure 3.16. Percentage of different fatty acid chain lengths in the different sphingolipids classes in the shoots of elongase mutants and wild type plants. (a) total sphingolipids, (b) GIPC, (c) GlcCer, (d) Hcer, and (e) ceramides. Values are means of +/- standard error of 3 replicates. * Shows significant results based on ANOVA showing a F test p value of less than 0.05, and a difference in means greater than the LSD values at 5% (degrees of freedom= 6).

3.2.3.1.3. Quantity of sphingolipids containing VLCFAs in the shoots

The changes shown in the percentage of the total sphingolipids detected could then be compared with the quantity of sphingolipids in the sample, as shown in Figure 3.17, to see if the same patterns could be seen. All of the knockout/knockdown elongase lines resulted in a decrease in the amount of sphingolipids containing VLCFAs, Figure 3.17a. *KCR RNAi* exhibited a percentage decrease of 27%, *pas2-1* by 26% and *cer10* by 30%, this was observed previously for the *KCR RNAi* line (Beaudoin *et al.*, 2009) and mutations in the other two components of the elongase resulted in the same pattern in the shoots.

The quantity of VLCFA containing molecular species in each class of sphingolipid was analysed. The amount of GIPCs containing VLCFA was decreased in all of the mutants, *KCR RNAi* a decrease of 27%, *pas2-1* 36% and *cer10* a decrease of 53%. Decreases have been reported previously for the *KCR RNAi* line and *pas2-1* (Bach *et al.*, 2008, Beaudoin *et al.*, 2009). No differences could be seen in the amount of GIPCs containing 16-18 fatty acid chains. The percentage decrease in the quantity of GIPCs containing VLCFA is greater than the proportion changes of GIPCs containing VLCFA. This is due to a more general decrease in the total amount of GIPCs in the mutants. This suggests that the samples retain the proportions closer to wild type despite the decreases in total amounts. There was a decrease in GlcCer containing VLCFA in all of the elongase mutants in the shoots. GlcCer containing VLCFAs were decreased in *KCR RNAi* (28%), *pas2-1* (45%), and *cer10* (24%). As observed in the GIPCs, these absolute decreases were greater than seen in the proportions. This was again due to a decrease in the total amount of GlcCer in the mutants compared to wild type. The ceramides exhibited a different pattern to the

complex sphingolipids, in *pas2-1* and *cer10*, there was an apparent increase in the amount of VLCFA containing molecular species, however this was not significant. There was also an increase in the amount of ceramides containing 16-18 fatty acids in *pas2-1* and *cer10*. *KCR RNAi* shows similar quantities and proportions to wild type plants in the ceramide and H Cer pools. In *cer10* and *pas2-1* there was an increase in the amount of H Cer both at 16-18 carbon fatty acids and in those containing VLCFA. This explains the increase in the total amount of H Cer and ceramides in the samples. The pattern shown in the ceramides and the H Cer for *pas2-1* and *cer10* confirms that previously shown for *pas2-1* (Bach *et al.*, 2008).

The percentage differences in the quantities of sphingolipids containing VLCFAs observed between the knockout/knockdown elongase lines and wild type plants is summarised as a heat map shown in Table 3.2. The heat map shows that the greatest differences are in GIPCs and GlcCers containing VLCFAs. Previously it was shown that GlcCer exhibited a greater decrease than the GIPC pool in *pas2-1* (Bach *et al.*, 2008), which is shown here for *pas2-1* but not for the other elongase mutants. The ceramide and H Cer pools are seen to increase or remain close to wild type levels in all of the mutants as shown previously in *pas2-1* (Bach *et al.*, 2008). The quantity of sphingolipids containing 16-18 carbon fatty acids was increased in all sphingolipid classes for *pas2-1* and *cer10*. The *KCR RNAi* line exhibited a decrease in the amount of GlcCer and H Cer levels containing 16-18 carbon fatty acids and was consistent with wild type in Cer and GIPCs. The table shows the amount containing fatty acids of 22 carbons and greater and the amount containing 24 carbons and greater. It can be seen that the decreases or increases in the two chain lengths are similar in all of the knockout/knockdown elongase lines.

Table 3.2. Heat map to show the relative changes in chain lengths of fatty acids of the different sphingolipids classes between the shoots of wild type plants and elongase mutants. The red positive numbers show where the amounts were increased compared to wild type, and the blue negative number show where the amounts were decreased compared to wild type.

shoots	cer 16-18	cer 22	cer 24	Hcer 16-18	Hcer 22	Hcer 24	GlcCer 16-18	GlcCer 22	GlcCer 24	GIPC 16-18	GIPC 22	GIPC 24
KCR	0.04	0.04	0.03	-0.22	-0.17	-0.11	-0.29	-0.27	-0.22	0.07	-0.26	-0.29
pas2-1	0.43	0.42	0.43	0.59	0.30	0.32	0.01	-0.46	-0.43	0.37	-0.36	-0.36
cer10	0.56	0.29	0.29	0.53	0.46	0.45	0.10	-0.24	-0.21	0.10	-0.53	-0.54

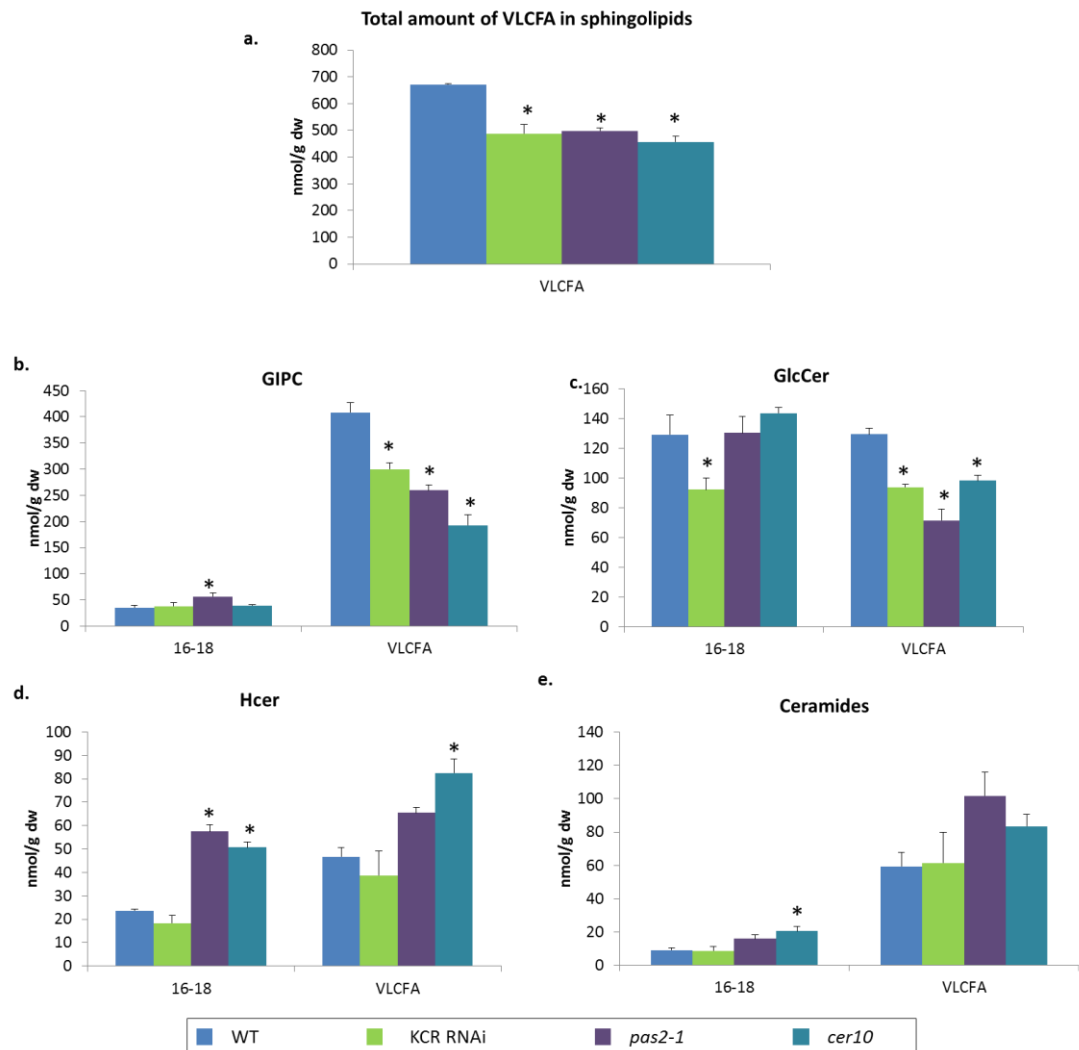


Figure 3.17. The quantity of different fatty acid chain lengths in the different sphingolipids classes in the shoots of elongase mutants and wild type plants. (a) total sphingolipids, (b) GIPCs, (c) GlcCer, (d) Hcer and (e) ceramides. Values are means of \pm standard error of 3 replicates. * Shows significant results based on ANOVA showing a F test p value of less than 0.05, and a difference in means greater than the LSD values at 5% (degrees of freedom= 6).

3.2.3.2. Sphingolipid profiling of the roots of wild type plants and elongase mutants

3.2.3.2.1. The quantity of each of the sphingolipid classes in the roots

The total amount of each class of sphingolipid and the total amount of all sphingolipids was measured in the roots, (Figure 3.18). Unlike in the shoots where all of the knockout/knockdown elongase lines showed a decrease in the total amount of sphingolipids, this was only evident in the *KCR RNAi* line. Total GIPCs were decreased in the *KCR RNAi* lines by 19%, and in *pas2-1* by 24%. There were no significant changes in the amount of GlcCer in the mutants. This is in contrast to the data obtained from the shoots, where *pas2-1* and the *KCR RNAi* line showed decreases. A significant increase in the total amount of ceramides of 47% was seen in the *pas2-1* line; a similar increase to that observed in the shoots. Similarly to the result obtained in the shoots, the *KCR RNAi* line, showed no differences in the quantity of ceramides. *cer10* roots contained very similar levels of ceramides to wild type roots in contrast to the data from the shoots. No significant changes could be seen in the hydroxyceramides, in contrast to the increase observed for *pas2-1* and *cer10* in the shoot material.

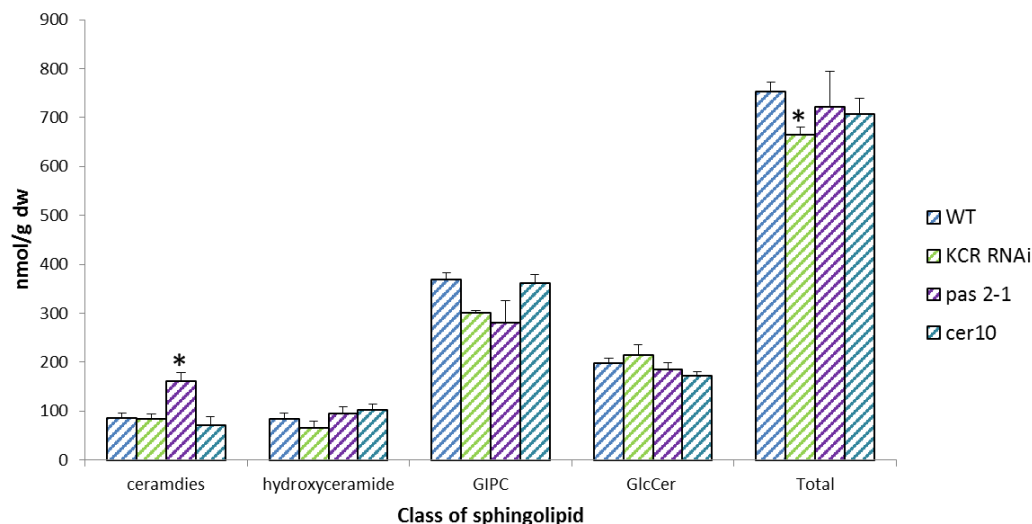


Figure 3.18 Sphingolipid composition in the roots of elongase mutants and wild type plants. Values are means of \pm standard error of 3 replicates. * Shows significant results based on ANOVA showing a F test p value of less than 0.05, and a difference in means greater than the least significant difference values at 5% (degrees of freedom= 6).

3.2.3.2.2. Percentage of sphingolipids containing VLCFAs in the roots

The percentage of sphingolipids containing VLCFA were analysed to see if patterns observed in the shoots were mirrored in the roots, shown in Figure 3.19. The total percentage of sphingolipids containing VLCFAs was significantly decreased in the roots in *pas2-1* by 25%, but was not significantly decreased in *cer10*. No significant decrease was seen in the levels of sphingolipids containing VLCFAs in the *KCR RNAi* line, as was the case in the data obtained from the shoots. The decrease in sphingolipids containing VLCFAs in *pas2-1* was similar to that displayed in the shoots, whereas *cer10* revealed a much lower decrease in the roots than the shoots. As in the shoots, the *pas2-1* roots showed a decrease in GIPCs containing VLCFAs (17% decrease). In contrast, both the *KCR RNAi* line and *cer10* do not show a significant decrease in the roots. The *KCR RNAi* line did not show a decrease in the shoots, *cer10* did. GlcCer containing VLCFAs show the same pattern in the roots as the shoots for *pas2-1*, but as for the GIPCs there was a greater decline (43%) in

the root than in the shoots. A significant decrease was not seen in the roots of the *KCR RNAi* lines (as was seen in the shoots). *cer10* also did not show a decrease in the roots, in contrast to the decrease that was seen in the shoots. In the ceramides *pas2-1* showed a decrease of 21% in the proportion of VLCFA, no difference was seen in *pas2-1* in the shoots. The *KCR RNAi* and *cer10* did not show a decrease, in line with data obtained from the shoots. Only *pas2-1* showed changes in the amount of HCer containing VLCFAs exhibiting a decrease of 38%.

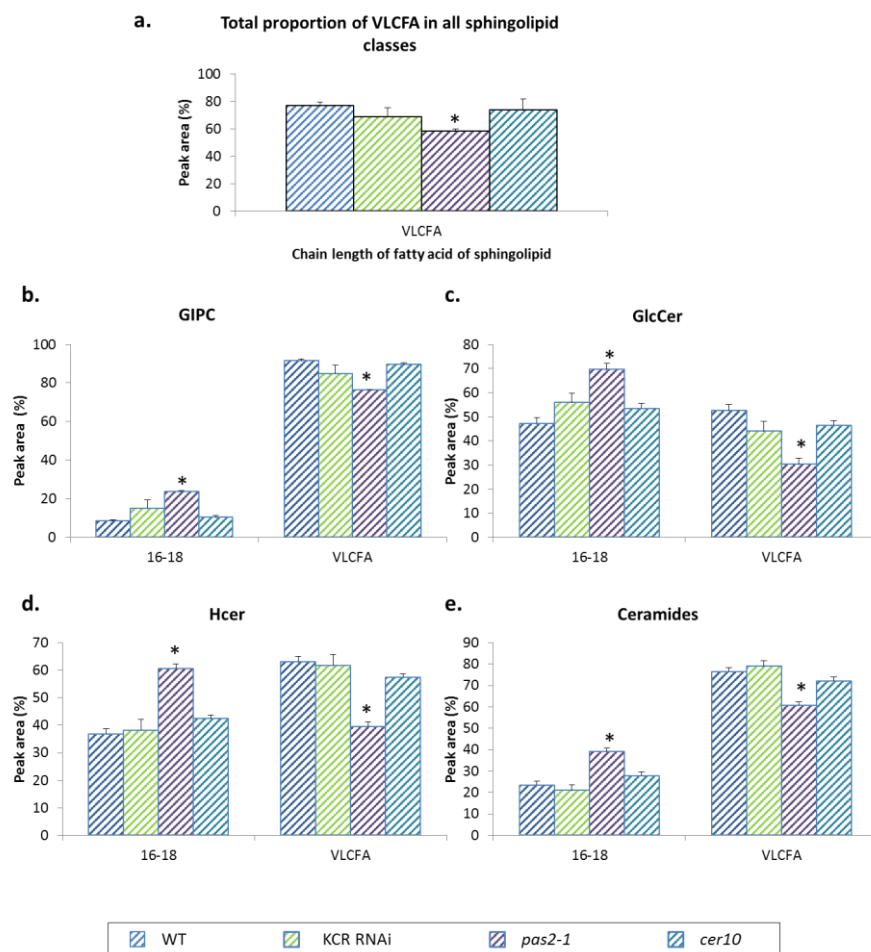


Figure 3.19 Percentage of different fatty acid chain lengths in the different sphingolipids classes in the roots of elongase mutants and wild type plants. (a) total sphingolipids, (b) GIPCs, (c) GlcCer, (d) Hcer, and (e) ceramides. Values are means of +/- standard error of 3 replicates. * Shows significant results based on ANOVA showing a F test p value of less than 0.05, and a difference in means greater than the LSD values at 5% (degrees of freedom= 6).

The sphingolipid data reflects that obtained for the acyl-CoA and phospholipid pools. The proportion of VLCFA in each class of sphingolipid was decreased more in the roots in *pas2-1* than in the shoots, and in *cer10* the opposite was seen, as was also seen in the phospholipid pool. The *KCR RNAi* line in both the acyl-CoA and the phospholipids showed decreases in the proportion of VLCFA in both roots and shoots, this was not seen in the sphingolipid data.

3.2.3.2.3. Quantity of sphingolipids containing VLCFAs in the roots

The quantitative data, shown in Figure 3.20 shows that the total amount of sphingolipids containing VLCFA showed a decrease in both *KCR RNAi* and *pas2-1*, by 20% and 28% respectively, a similar decrease to that seen in the shoots. No significant decrease was observed in the *cer10* line in the roots, which is in contrast to the data from the shoots. There is a significant decrease in the amount of GIPCs containing VLCFA in *pas2-1* and in the *KCR RNAi* line, 25% for *KCR RNAi* and 37% for *pas2-1*, which is a similar decrease to that detected in the shoots. In the percentage data the *KCR RNAi* line does not show a decrease, however it does show a decrease in the absolute amounts. This is due to a decrease in the total amount of GIPCs and suggests that *KCR RNAi* maintains the proportions of GIPCs chain lengths to match wild type despite the decrease in quantity. *cer10* roots did not show a decrease, unlike in the shoots. GlcCer containing VLCFA were decreased in all of the mutants in the roots consistent with the data obtained from the shoots. *pas2-1* and *cer10* exhibited a greater decrease in the roots than in the shoots, decreased by 51% and 30% respectively in the roots, whereas the *KCR RNAi* line shows a greater decrease in the shoots than in the roots, 15% decreased in the roots.

The ceramides containing VLCFA were increased by 31% in *pas2-1*. The *KCR RNAi* line showed no changes in ceramide composition in the roots, and *cer10* exhibited a non-significant decrease in the amount containing VLCFAs. *pas2-1* showed a decrease of 28% in the amount of HCer containing VLCFAs. The *KCR RNAi* line and *cer10* did not show any significant changes in the roots. These results are in contrast to those shown in the shoots, where both *pas2-1* and *cer10* resulted in a significant increase in HCer containing VLCFA.

Table 3.3 summaries these changes as a heat map. As in the shoots the greatest reductions are seen in the GlcCer and GIPCs. GIPCs showed a similar reduction in the roots as the shoots in both *pas2-1* and the *KCR RNAi* line, and a smaller reduction in *cer10* in the roots. GlcCer containing VLCFA show a similar reduction in the roots and the shoots in *cer10* and *pas2-1*, and a greater reduction in the shoots than the roots in the *KCR RNAi* line. HCer containing VLCFAs showed decreases, in *pas2-1*. In the shoots an increase was seen. *pas2-1* shows an increase in the amount of ceramides containing VLCFAs in the shoots and in the roots. Decreases are seen in the amount of ceramides containing VLCFA in the roots of *cer10* in contrast to the shoots where increases were seen. Increases can be seen in all the sphingolipid classes containing 16-18 carbon fatty acids for *pas2-1*, for *cer10* in all but GlcCer and for *KCR RNAi* in all but the HCer. As shown in the shoots, Table 3.3 shows that there is not a greater decrease in sphingolipids containing VLCFA as the chain length of the VLCFA increases.

Table 3.3 Heat map to show the relative changes in fatty acid chain lengths in total sphingolipid classes between the roots of wild type plants and elongase mutants. The red positive numbers show where the amounts were increased compared to wild type, and the blue negative number show where the amounts were decreased compared to wild type.

Roots	cer 16-18	cer 22	cer 24	Hcer 16-18	Hcer 22	Hcer 24	GlcCer 16-18	GlcCer 22	GlcCer 24	GIPC 16-18	GIPC 22	GIPC 24
KCR	0.06	-0.04	-0.06	-0.18	-0.24	-0.26	0.15	-0.13	-0.15	0.32	-0.25	-0.21
pas2-1	0.77	0.29	0.21	0.54	-0.29	-0.35	0.22	-0.52	-0.54	0.54	-0.37	-0.43
cer10	0.07	-0.23	-0.28	0.33	0.10	0.12	-0.09	-0.3	-0.29	0.18	-0.04	-0.03

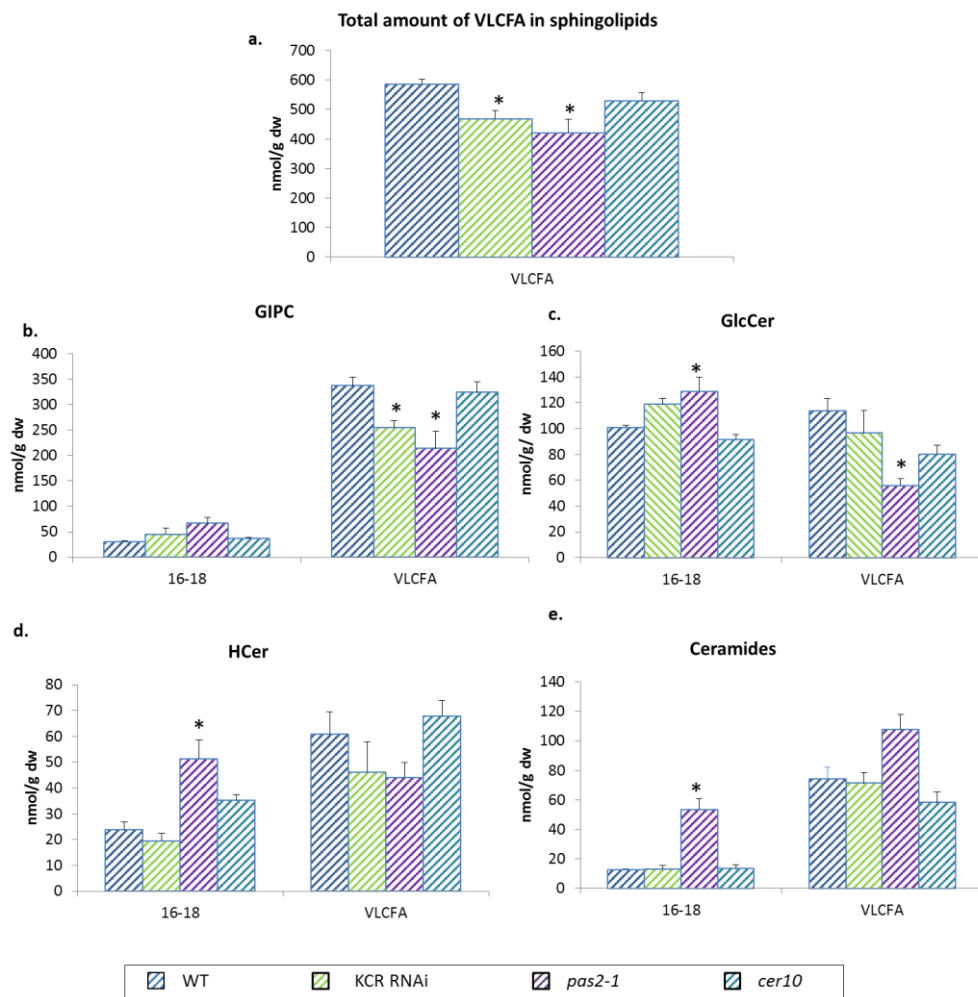


Figure 3.20. The quantity of different fatty acid chain lengths in the different sphingolipids classes in the roots of elongase mutants and wild type plants. (a) total amount of sphingolipids (b) GIPCs, (c) GlcCer, (d) HCer and (e) ceramides. Values are means of +/- standard error of 3 replicates. * Shows significant results based on ANOVA showing a p value of less than 0.05, and a LSD of less than 5% (degrees of freedom= 6).

3.2.3.3. Quantity of free LCBs and LCBPs of wild type plants and elongase mutants

The total amount of free LCBs (calculated by combining the amount of free LCB and free LCBP) in the sample were analysed to observe what effect a decrease in VLCFA has on this pool. In the shoots, shown in Figure 3.21a, there is a significant increase in the amount of free LCBs in *pas2-1* and *cer10*, of 61% and 47% respectively. The *KCR RNAi* line shows similar amounts to wild type plants. In the roots, Figure 3.21b, *pas2-1* again shows a 39% increase in the total amount, less than was shown in the shoots. *cer10* did not show a significant increase in the roots, and as shown in the other lipid classes tested, there is greater effect in the shoots than in the roots. The *KCR RNAi* line did show a significant increase in the roots (46%) in contrast to the shoots where no differences could be seen. The increase in the amount of free LCBs in this data, is thought to occur as a result of the decrease in the amount of VLCFA being produced. Due to a reduction in the amount of VLCFA, there would be an increase in the amount of free LCBs, as VLCFA would not be present for the LCB to combine with to form ceramides.

The proportion of each of the different LCB chains (d18:0,d18:1,t18:0 and t18:1) in the different sphingolipid classes were observed. It was shown that there were no differences in the proportion of any of the LCB chains in the shoots or the roots. It was also shown that this distribution of LCB chain lengths is similar to what has previously been reported (Markham and Jaworski, 2007). This data is shown in appendix II. All of the statistical analysis performed on the sphingolipid dataset can be found in appendix II.

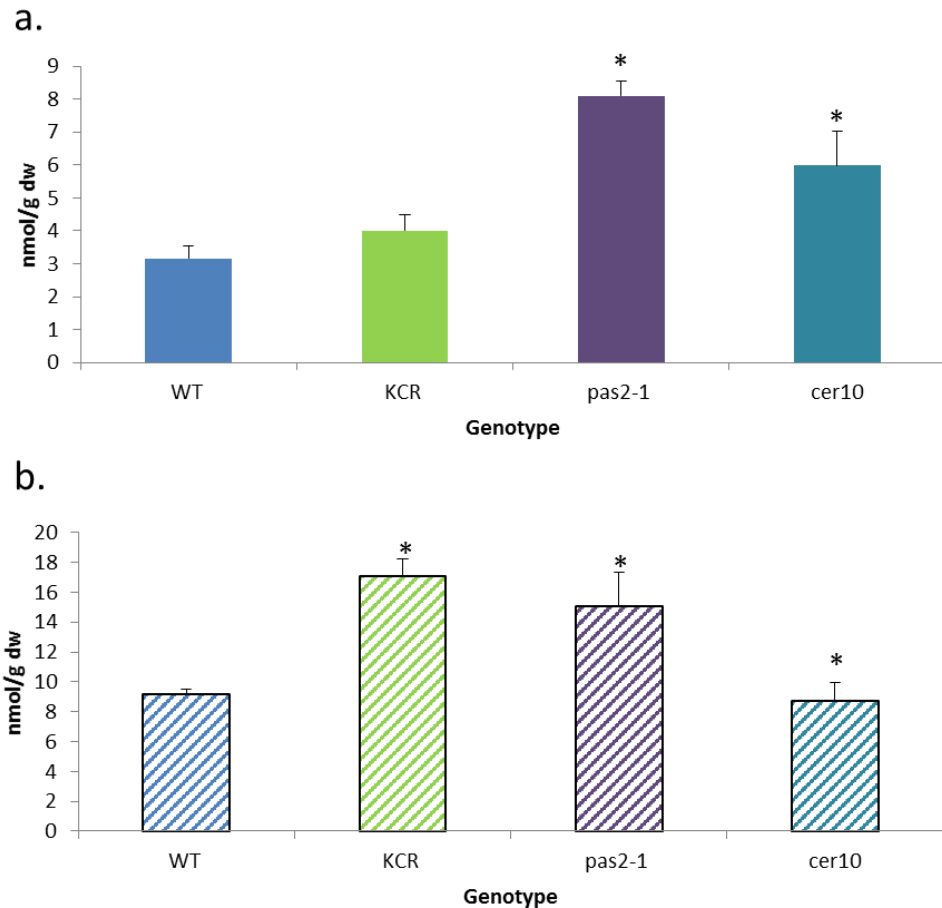


Figure 3.21. The total amount of free LCBs in the elongase mutants and wild type plants in (a) the shoots and (b) the roots. Values are means of +/- standard error of 3 replicates. * Shows significant results based on ANOVA showing a p value of less than 0.05, and a LSD of less than 5% (degrees of freedom= 6).

3.3. Discussion

This chapter describes the lipidomic profiling of lines carrying mutations in subunits of the core elongase complex, including analysis of the acyl-CoA, membrane glycerolipid and sphingolipid pools. Collectively the data shows that the proportion of VLCFA is decreased across all lipid classes tested, as summarised in Table 3.4. The acyl-CoA pool showed a reduction in the proportion of VLCFA and the subsequent analysis of sphingolipids and phospholipids were carried out to verify this decrease was transposed to these pools and whether the reduction was

the same across all lipid classes. It was then hoped that changes in the lipidome could be correlated with phenotypic differences seen.

3.3.1. Size of reductions in different lipid pools

There was a greater percentage decrease in the proportion of VLCFA in the phospholipid pool than was seen in the sphingolipid pool in both the shoots and the roots in all of the knockout/knockdown elongase lines. Sphingolipids containing VLCFAs have been shown to be essential in *Arabidopsis*, (Markham *et al.*, 2011), and so it is possible that sphingolipid homeostasis is maintained at the expense of pools that are able to tolerate more variation. As phospholipid containing VLCFAs account for such a small proportion of total phospholipids, less than 5%, it seems plausible that the plant can cope with reduced amount of phospholipids containing VLCFAs under normal growth conditions more than it can with a reduction in sphingolipids containing VLCFAs, which account for 75% of total sphingolipids; VLCFAs could be targeted accordingly.

Table 3.4. Heat map of the percentage differences in the proportion of VLCFA in each of the lipid classes analysed for each of the elongase mutants compared to wild type plants.

Shoots	Acyl CoAs containing C22 or greater	Acyl CoAs containing C24 or greater	Phospholipids VLCFA	Sphingolipids VLCFA
<i>KCR RNAi</i>	-50 %	-59 %	-32 %	0
<i>pas2-1</i>	-25 %	-52 %	-42 %	-12 %
<i>cer10</i>	-37 %	-39%	-41 %	-15 %
Roots	Acyl CoAs containing C22 or greater	Acyl CoAs containing C24 or greater	Phospholipids VLCFA	Sphingolipids VLCFA
<i>KCR RNAi</i>	-75 %	-83 %	-53 %	-8 %
<i>pas2-1</i>	-88 %	-93 %	-78 %	-32 %
<i>cer10</i>	-37 %	-39 %	-22 %	-5 %

3.3.2. Changes in the different sphingolipid pools

The reduction seen in the proportion of sphingolipids containing VLCFAs was not the same across all the sphingolipid pools, shown in Table 3.2 and 3.3. GlcCers showed a greater reduction than GIPCs in the proportion containing VLCFAs in some of the elongase mutants. This has been observed previously for *pas2-1* (Bach *et al.*, 2008), and *cer10* appears to produce a similar pattern in the proportion data and in the quantity data the same pattern is seen in the roots but not the shoots. *KCR RNAi* showed similar reductions in GIPCs and GlcCers containing VLCFAs in the roots and in the shoots. This suggests that when the proportion of VLCFAs is reduced, there might be preferential channelling occurring so that the proportion of GlcCers containing VLCFA are decreased more than the GIPCs containing VLCFAs particularly in the roots. This could be because GIPCs are more important for ensuring membrane homeostasis and function in plants. Lipid rafts are thought to contain higher proportions of GIPCs than GlcCer (Borner *et al.*, 2005). It has been suggested that lipid rafts have a number of important protein trafficking functions which are essential in plant development. It is possible that the plant retains the composition of GIPCs more closely to wild type than it does in GlcCers to reduce the effect on plants, due to the importance of these lipids. Changes are seen in the ceramides and HCer containing VLCFAs which differ between the shoots and the roots of the different mutants, and in some cases showed increases in the amount of VLCFAs compared to wild type which is in contrast to what is seen in the other sphingolipid classes. This suggests that channelling of VLCFA must occur to achieve this variation between classes.

3.3.3. Comparison of root and shoot data

For the first time the lipidomic analysis was performed on VLCFA mutants where the material for analysis was separated into shoots and roots to explain the differences in phenotypes seen between the elongase mutants. Differences are thought to be due to the different roles that lipids may play in the roots compared to the shoots. *pas2-1* had both shorter primary roots (60% reduction), and an apparent reduction in the number of lateral roots, the *KCR RNAi* line showed a lack of lateral roots but no change in primary root length. *cer10* displayed a reduction in primary root length (35%), but no change in lateral root density. All of the knockout/knockdown elongase lines exhibited a shoot phenotype, and at the point of harvest all three had fused aerial organs, but with different levels of severity, as was shown in Figure 3.1. As shown in Table 3.4, the *KCR RNAi* line and *pas2-1* both showed a greater decrease in the proportion of VLCFA in the roots than in the shoots in all lipid classes, in contrast *cer10* exhibited the same decrease as the shoots in the case of the acyl-CoA data and a lower decrease in the phospholipids and sphingolipids. This illustrates that the reductions are different in the shoots and the roots of the different knockout/knockdown elongase lines. This would suggest that lipids containing VLCFA might be regulated in the event of a decrease in the level of VLCFA, in both *pas2-1* and the *KCR RNAi* such that the decrease in the shoots is not as substantial as in the roots. This implies that the lipids containing VLCFA have a different or more necessary role in the shoots than in the roots that cannot be replaced by shorter chain fatty acids. What this function is, is unknown.

3.3.3.1. Explanation of the root phenotypes shown in elongase mutants

pas2-1 and the *KCR RNAi* line exhibit a lateral root phenotype. This decrease in lateral roots has been associated with the mistargeting of PIN1 the auxin efflux carrier. Previous work with *pas1* and double mutants of the ceramide synthase, *loh1 loh3*, has suggested that this is due to a decrease in the amount of sphingolipids containing VLCFAs (Roudier *et al.*, 2010, Markham *et al.*, 2011). In mutants which show a deficiency of VLCFA, PIN1 is not localised to the lateral membranes, but instead is diffused or aggregates in the cytosol (Roudier *et al.*, 2010); a situation which is thought to be responsible for the lack of lateral roots. It is thought that sphingolipid containing VLCFAs have an effect on the trafficking of specific proteins along the secretory pathway which could be responsible for the mislocalisation of PIN1 (Markham *et al.*, 2011). Both lines which show a lack of lateral roots (*KCR RNAi* and *pas2-1*), show a decrease in the total amount of sphingolipids containing VLCFA in the roots. In contrast, *cer10* which does not lack lateral roots, also does not exhibit a decrease in the total quantity of sphingolipids containing VLCFAs in the roots. This suggests that it could be a decrease in sphingolipids containing VLCFA that is responsible for this phenotype. *cer10* displays a decrease in the amount of GlcCer containing VLCFAs, but as *cer10* does not show a lateral root phenotype, it would seem more likely that GIPCs or HCer are responsible for the mistargeting of PIN1, since decreases are seen in *pas2-1* and *KCR RNAi*, but not in the *cer10* line in the amount containing VLCFAs. However PPMP, an inhibitor of GlcCer has been shown to also result in this mislocalization of PIN1 (Yang *et al.*, 2013). This suggests that this class may also be involved and an overall decrease in total sphingolipids containing VLCFA in the

roots could be responsible, or that one particular sphingolipid molecular species is responsible for this phenotype.

pas2-1 has shorter primary roots and previous work has suggested that this is the result of defects in cell plate formation in the last step of cell division (Bach *et al.*, 2011), resulting from changes in endomembrane dynamics. It has been shown previously that the proportion of PE and PS containing VLCFAs were reduced in *pas2-1* as were the levels of sphingolipids containing VLCFAs in GIPC and GlcCer (Bach *et al.*, 2008, Bach *et al.*, 2011). This pattern is also shown here in both the roots and the shoots, and in addition to *pas2-1* it is shown for the other elongase mutants in the shoots. However, *cer10* also showed shorter primary roots, but only showed a minor reduction in the proportion of PE and PS containing VLCFAs and the reduction it showed was not as great as seen in the *KCR RNAi* line, which did not show shorter primary roots. It therefore seems unlikely that the decrease in the proportion of PE and PS containing VLCFAs is responsible for the decrease in primary root length. Examining specifically the impact of sphingolipid quantities, a greater decrease is seen in the GlcCer pool in the roots in *cer10* and *pas2-1* than in the *KCR RNAi* lines; it could be the decrease in quantity in this pool that is responsible for the phenotype. GlcCer has previously been shown to affect the secretory pathway and golgi morphology which could affect the trafficking of material required for root growth (Melser *et al.*, 2010). In addition *pas2-1* showed a greater decrease in the pool than *cer10* and it could be that this greater decrease is responsible for the greater reduction in primary root length seen in *pas2-1* (65% reduction) compared to *cer10* (35% reduction). It has been shown previously that sterols are required for endocytosis during cell plate formation, (Men *et al.*, 2008,

Boutte *et al.*, 2010). *pas2-1* showed a delay in endocytosis in cell plate formation. As sterols and sphingolipids are the major components of lipid rafts it is possible that the correct composition and availability of lipid rafts is required for cell plate formation that subsequently results in this shorter primary root phenotype as a result of a delay in endocytosis. As suberin mutants also show a decrease in root length it cannot be ruled out that a decrease in suberin is responsible for this phenotype (Franke *et al.*, 2009). Suberin mutants show a decrease in root length but do not show changes in the root architecture. *cer10* only exhibited a shorter primary root which could be caused a decrease in suberin, whereas *pas2-1* which shows both shorter primary roots and a reduction in the number of lateral roots could be caused by a decrease in many different lipid classes.

3.3.3.2. Explanation of the fused aerial organ phenotype shown in elongase mutants

All three knockout/knockdown elongase lines displayed fused organs at the point of harvest, but with different levels of severity. It was been shown previously that this phenotype is not the result of a decrease in the total amount of wax or cutin (Voisin *et al.*, 2009). This phenotype could be a result of a protein that either stops cells adhering to one another, or a decrease or increase in a particular wax or cutin component that causes this fusion. This shows that the fusion phenotype could be caused by a decrease in a wax component synthesized from a VLCFA that cannot be synthesized in the mutants, or sphingolipids containing VLCFAs could be decreased such that these components are not transported to the outside of the cell.

The total amount of sphingolipids containing VLCFAs were shown to be reduced across all of the knockout/knockdown elongase lines in the shoots. In the GlcCer

pool *pas2-1* showed a greater decrease in the amount containing VLCFAs than in the other two elongase mutants. This suggests that a spectrum of reduction may affect the severity of the phenotype seen, as *pas2-1* also shows the most severe phenotype. It has previously been shown that GlcCer are involved in the secretory pathway, such that an increase in the amount of proteins transported within the secretory pathway resulted in an increase in the synthesis of GlcCer (Melser *et al.*, 2010). Decreases in GlcCer could therefore affect the correct functioning of the secretory pathway, preventing a component required to prevent fusion from being trafficked in the epidermal cells. Equally there were reductions in the proportion of phospholipids containing VLCFAs, but greater reductions were not seen in the *pas2-1* compared to the other mutants in this lipid pool but quantification of this data would be needed to show if the actual amounts of phospholipids containing VLCFAs are decreased more in *pas2-1*. In addition the wax composition of all of the elongase mutants should be performed to see if the fusion phenotype can be correlated with a change in a particular wax component.

3.3.3.3. Explanation of the reduction in cell size shown in elongase mutants

cer10 shows a reduction in the size of the aerial organs, and a smaller structure is seen in the other elongase mutants. New cell initiation was not comprised in *cer10*, and it is thought to be due to cell expansion defects (Zheng *et al.*, 2005). This phenotype is similar to that seen in the roots of *pas2-1* cells, where the reduction in primary root length was shown to be due to decreases in the size of the elongation and cell division zones as well as a delay in cell division caused by a possible delay in cell plate formation (Bach *et al.*, 2011). As was the case in *pas2-1*, *cer10* has been shown previously to result in the accumulation of endosomal compartments,

and the reduced size could be due to abnormal vesicle trafficking (Zheng *et al.*, 2005). This could be due to a defect in sphingolipid containing VLCFAs that play a role in vesicle trafficking. This reduction in size, as was seen in the roots where a reduction in primary root length was observed, could be due to the consistent decreases seen in all the elongase mutants in the amount of GlcCer containing VLCFAs.

Chapter 4. Lipidomic analysis of plants treated with herbicides that affect VLCFA synthesis

4.1. Introduction

The Herbicide Resistance Action committee (HRAC, www.hracglobal.com) classifies herbicides into groups according to their mode of action, chemical class and how similar the symptoms they generate are. Two groups have been classified as having a role in lipid biosynthesis. One group, the K₃ herbicides, are described as inhibitors of cell division and/or inhibitors of VLCFA biosynthesis. This group includes flufenacet which is part of the oxyacetamide chemical family. The second group the N herbicides are described as inhibitors of lipid synthesis. This group includes ethofumesate and benfuresate which are members of the benzofuran chemical family (Menne, 2014).

Previous research has shown that treatment with flufenacet resulted in reduced growth and fused organs in *Arabidopsis*. After application of flufenacet, the youngest leaves of the rosette leaves fused to each other. When the plants flowered, the inflorescences fused to themselves and to the surrounding uppermost cauline leaves (Lechelt-Kunze *et al.*, 2003). This is consistent with the phenotype seen in the *fiddlehead* mutant (Lolle *et al.*, 1992). Treatment with benfuresate and ethofumesate resulted in the same phenotype. The symptoms that occurred upon application of flufenacet were not long lasting, the flowers eventually returned to normal. In contrast when treated with benfuresate the plant symptoms persisted (Lechelt-Kunze *et al.*, 2003).

Gene expression profiles of plants treated with flufenacet or benfuresate were previously obtained using DNA chip hybridization using a 8247 gene array. As both herbicides are thought to affect lipid synthesis it was used to observe if any components of lipid synthesis were affected. Only one lipid biosynthesis gene was found to be upregulated in treated plants that was not also upregulated in plants treated with non-lipid affecting herbicides (Lechelt-Kunze *et al.*, 2003). This gene, At1g24470, was one of the two *KCR* genes identified in *Arabidopsis*, *KCR2* (Dietrich *et al.*, 2005). *KCR2* was not able to restore the embryo lethality of *kcr1* when placed behind the *KCR1* promoter, but this does not rule out the possibility of *KCR2* having a *KCR* activity later in development and the function of *KCR2* remains unknown. A promising target for the herbicides is thought to be the *KCS* enzymes. All three herbicides show an ability to carry out nucleophilic attack on a substrate (Jablonkai, 2003). *KCS* enzymes have an important cysteine at their active site, and it is possible that the herbicides attack this residue (Ghanevati and Jaworski, 2002).

Work by Trenkamp, (2004) further investigated the targets of action of these herbicides. When *KCS* enzymes were expressed in yeast which was grown in the presence of a herbicide, changes in its lipid profile were observed. Yeast cells grown in the presence of flufenacet did not produce VLCFA when they expressed any of the *KCS* enzymes tested (*FAE1*, *KCS1*, *KCS2*, *CER60* and *KCS20*). Eight other K_3 herbicides were also analysed in this way. Some prevented VLCFAs production in yeast cells expressing any of the *KCS* enzymes tested, and some only prevented VLCFAs production when certain *KCS* enzymes were expressed. Application of ethofumesate or benfuresate both induced the *fiddlehead* phenotype

in plants but did not inhibit the KCS enzymes they were tested with (Trenkamp, 2004). The N group of herbicides have previously been shown to inhibit VLCFAs synthesis (Abulnaja *et al.*, 1992), so it is likely that the target KCS of these herbicides were not tested in these experiment, only 6 of 21 were tested, or because they inhibit a different component of VLCFA biosynthesis.

4.2. Results

Plants were treated with herbicides known to affect VLCFA so that the effect of the herbicide on the plant could be observed. Lipidomic profiling was then performed on these plants to observe changes in the lipidome as a result of the treatment. It was hoped that correlations between phenotypes and changes in the lipidome could be made, to further support the correlations seen in Chapter 3.

4.2.1. Application of herbicides to wild type seeds

Herbicides known to affect VLCFA synthesis were added to plant growth media, preparation of which was described in sections 2.1.2. Col-0 wild type seeds were then grown on plates containing this media for 14 days. By adding the chemicals to the growth media it had an effect throughout plant development. To ascertain the appropriate concentration of herbicide that is needed to result in a phenotype, experiments were carried out based on the available literature. The three herbicides, flufenacet, ethofumesate and benfuresate, were previously used at a concentration of 100 μM to observe the effect they had on yeast cells expressing KCS enzymes (Trenkamp, 2004). At 100 μM and 20 μM both ethofumesate and benfuresate resulted in wild type plants displaying aerial organ fusions. Due to limited quantities of herbicide, a range of concentrations were used to try and establish the

lowest concentration that could be used but still result in a phenotype. Application of benfuresate at a concentration of 10 μM resulted in plants showing fused aerial organs but did not result in a phenotype at a concentration of 1 μM . A more consistent phenotype was obtained upon application of 20 μM of benfuresate and so 20 μM of benfuresate was chosen for further experiments. Ethofumesate resulted in fused primary leaves at a concentration of 1 μM and 2 μM but not at 0.5 μM . 2 μM of ethofumesate was applied due to the consistent phenotype achieved at this concentration. For flufenacet, a range of concentrations were tried to optimise the efficiency of treatment. With application of 100 μM and 20 μM of flufenacet the seeds germinated but did not develop further. A similar lack of growth was seen at 5 μM , 500 nM and 100 nM. Very low concentrations (10 nM) of flufenacet caused shorter primary roots but did not produce a shoot phenotype. Finally, 75 nM of flufenacet was chosen because plants exhibited both a shoot and a root phenotype. The phenotypes resulting from the application of the herbicides at the concentration chosen is shown in Figure 4.1.

Flufenacet inhibits KCS enzymes and it is thought that both ethofumesate and benfuresate also affect VLCFA synthesis (Abulnaja *et al.*, 1992, Trenkamp, 2004). However, the herbicides did not all produce the same phenotype. Ethofumesate and benfuresate treatment both resulted in fused primary leaves whereas, flufenacet produced both fused primary leaves and shorter primary roots. Flufenacet treated plants showed a 84% reduction in primary root length compared to untreated plants, based on an average of 4 plants, (untreated= 7.5cm, flufenacet= 1.2cm), this is shown in Figure 4.1.

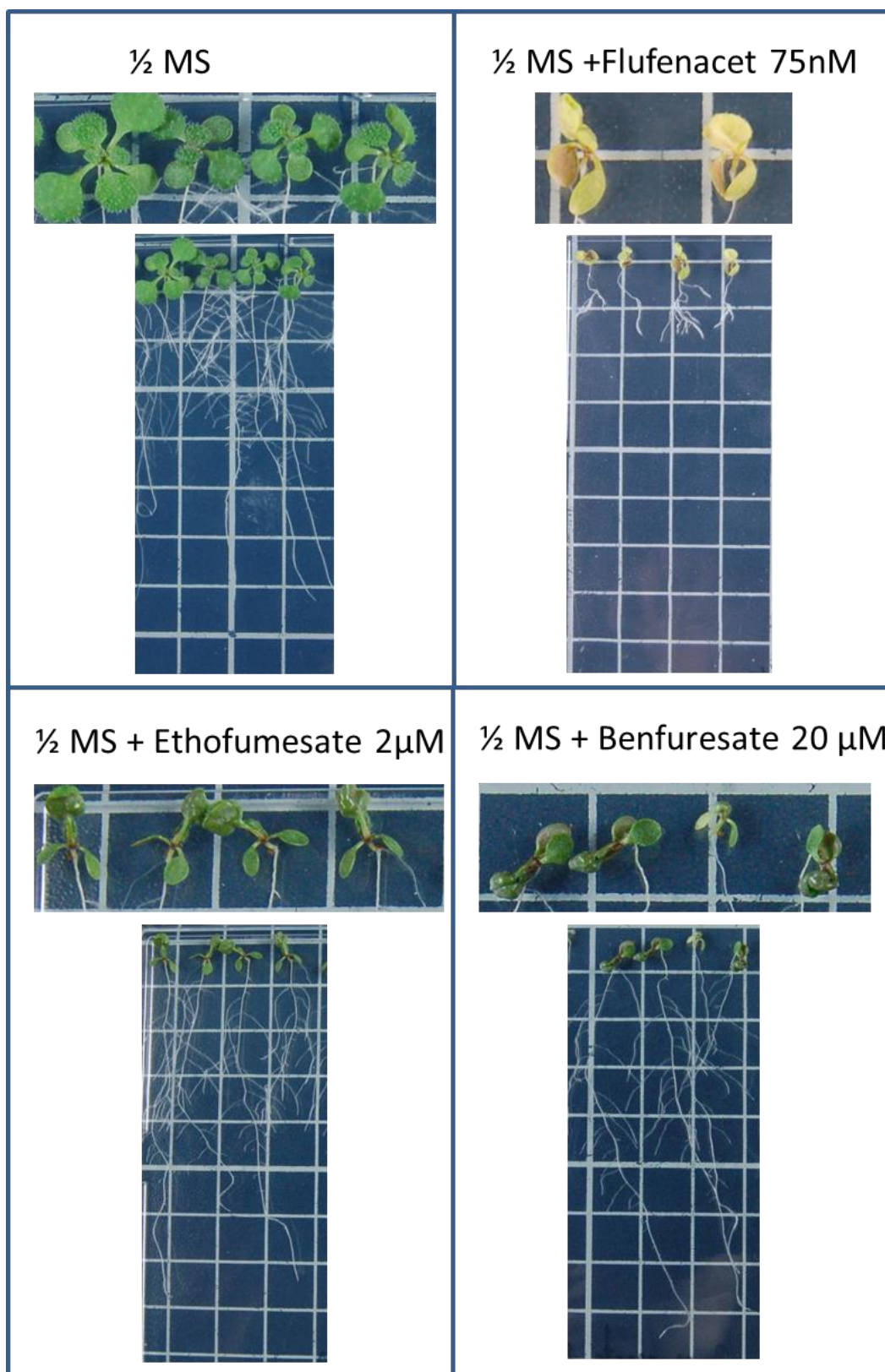


Figure 4.1 Phenotypes of plants treated with herbicides that affect VLCFA synthesis. Each square in the photograph is 1 cm².

4.2.2. Acyl-CoA profiling of plants treated with herbicides

Acyl-CoA analysis was performed on plants grown in the presence of herbicides to see if any differences could be seen with untreated plants. Acyl-CoA profiling, (Figure 4.2) showed that both ethofumesate and benfuresate treated plants have similar acyl-CoA profiles, in common with their similar phenotypes. A table of all the acyl-CoAs analysed and the proportion of each can be found in appendix III, along with all the statistical analysis performed on this dataset. Ethofumesate and benfuresate treated plants displayed a decrease in the proportion of acyl-CoAs containing 22 carbons and greater in the shoots compared to untreated plants as shown in Figure 4.2. The total proportion of VLC-acyl CoAs in the treated plants was analysed, shown in Figure 4.3. Untreated plants contain 33% acyl-CoAs containing 20 carbon chains or greater, compared to 9% in ethofumesate and 5% in benfuresate treated plants. A decrease can also be seen in the roots but it is not as substantial as in the shoots. Wild type roots contain 29% acyl-CoAs containing 20 carbon atoms or greater whereas benfuresate contains 19%, and ethofumesate contains 25%, showing a percentage decrease of 35% and 15% in the roots compared to a decrease of 73% and 85% in the shoots. The mode of action of these two herbicides is not known but it is thought to have a role in VLCFA synthesis (Abulnaja *et al.*, 1992). Based on the acyl-CoA data it would appear that the herbicides affect an enzyme involved in VLCFA synthesis that has a specific role in the shoots.

Flufenacet treated plants show a decrease in the proportion of VLC-acyl-CoAs from 20 carbons in the roots and longer than 22 carbons in the shoots compared to control plants, as shown in Figure 4.2. An increase can be seen in the amount of

20:0 in the shoots and 18:0 in the roots. This would suggest that in the shoots flufenacet treated plants are able to synthesise C20 species whereas in the roots the level of production is reduced. This could be due to differences in the expression pattern of the different KCS enzymes that flufenacet inhibits. Flufenacet contains 18% VLC- acyl-CoAs in the shoots, and 10% in the roots, shown in Figure 4.3. This is a much bigger decline when compared with untreated plants in the roots than in the other two herbicides. Flufenacet treated plants showed a smaller percentage decrease than the other two herbicides in the shoots. This data correlates with the phenotypes observed, only flufenacet showed a root phenotype and it also exhibited a much greater decrease of VLC-acyl-CoAs in the roots, whereas all three herbicides show a shoot phenotype and they all show a substantial decrease in the amount of VLC-acyl-CoAs in the shoots. Flufenacet was shown to inhibit KCS1, KCS2 (DAISY), KCS5 (CER60), KCS17, KCS18(FAE1) and KCS20 (Trenkamp, 2004) all of which have a role in cuticular wax synthesis and/or suberin synthesis. Acyl-CoAs greater than 26 carbons in the shoots were decreased by 72% in flufenacet treated plants compared to control plants. This confirms that flufenacet does inhibit KCS enzymes affecting wax synthesis as acyl-CoAs containing 26 carbons and greater are almost exclusively involved in wax synthesis.

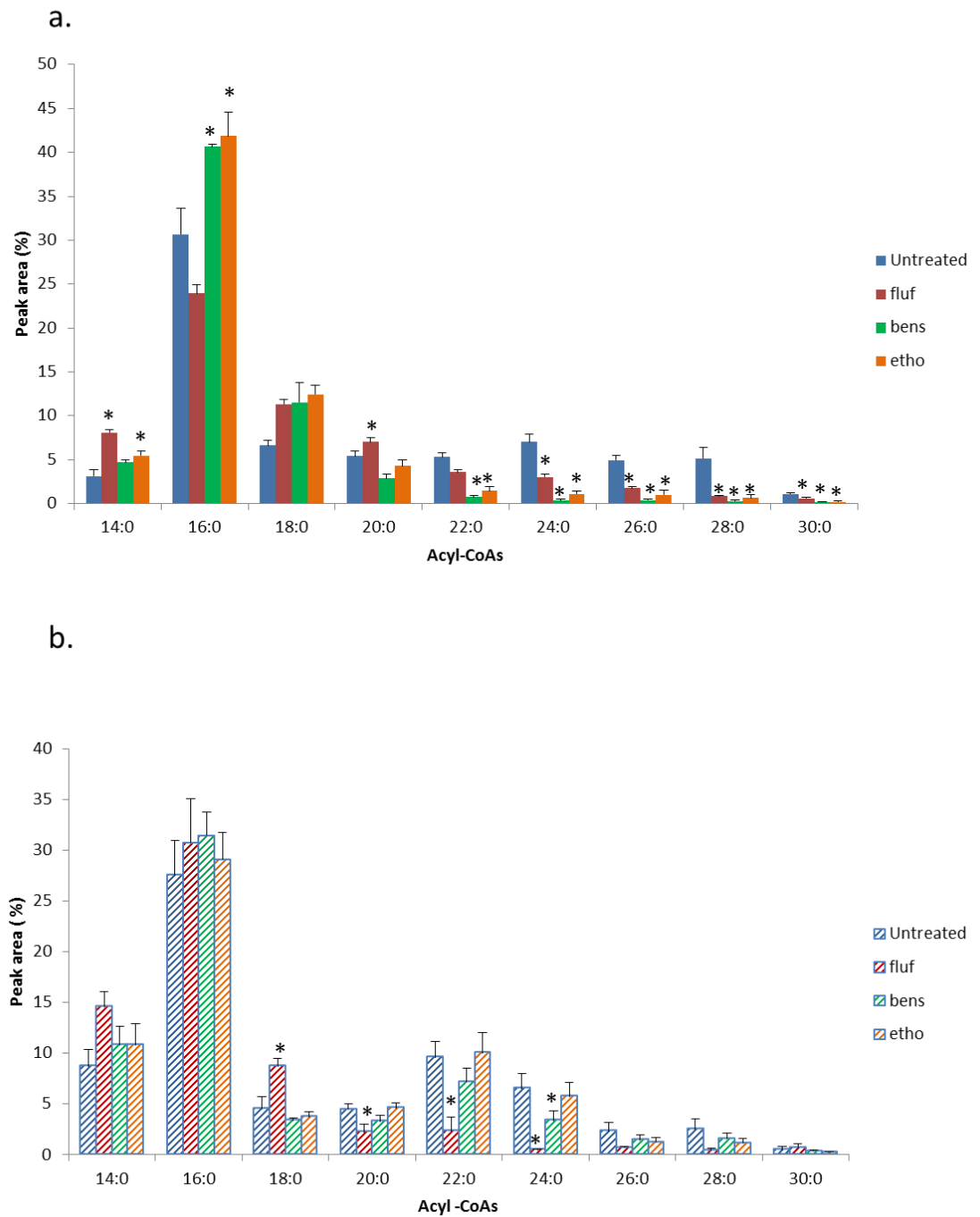


Figure 4.2 Acyl-CoA profiles of the roots and shoots of plants treated with herbicides. (a) The shoots of herbicide treated plants compared to untreated plants. (b) The roots of herbicide treated plants compared to untreated plants. Values are means of +/- standard error of 4 replicates. * Shows significant results based on ANOVA showing a F test p value of less than 0.05, and a difference in means greater than the LSD values at 5% (degrees of freedom= 9).

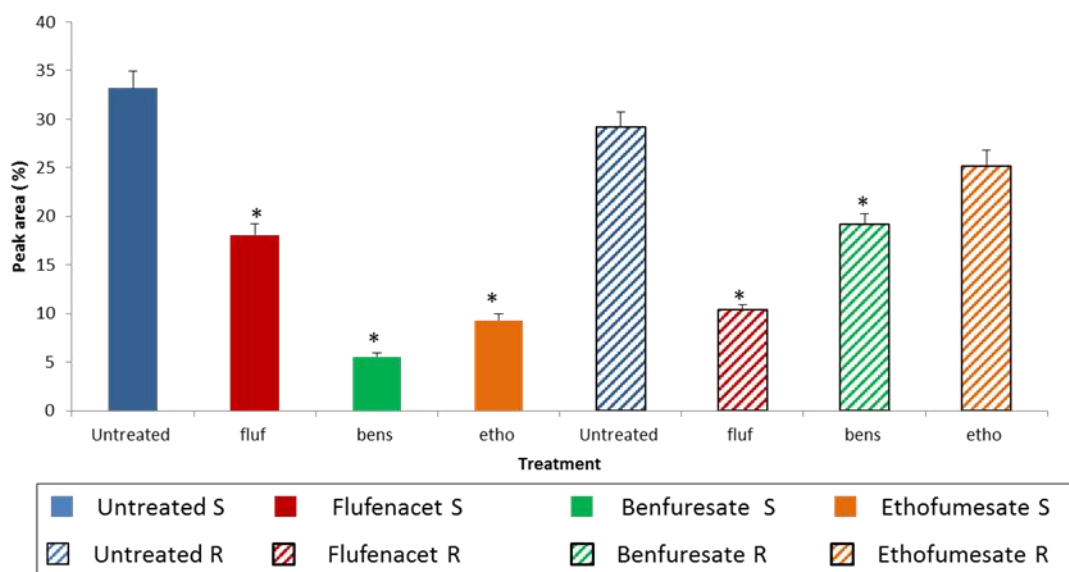


Figure 4.3 The percentage of total VLC-acyl-CoAs in herbicide treated plants. The analysis takes into consideration all those acyl-CoAs containing 20 carbon chain lengths and greater, both saturated and unsaturated compounds are included. Values are means of +/- standard error of 4 replicates. * Shows significant results based on ANOVA showing a F test p value of less than 0.05, and a difference in means greater than the LSD values at 5% (degrees of freedom= 9).

4.2.2.1. Quantity of acyl-CoA in herbicide treated plants

The quantity of acyl-CoA was measured to see if the effects seen in the percentage of the total amount of acyl-CoAs detected can also be seen in the quantified data. Figure 4.4 shows that although there are comparable total amounts of acyl-CoA in the herbicide treated plants to the untreated plants; decreases are seen in the quantity of VLC-acyl CoA in both the shoots and the roots. It is also shown that benfuresate and ethofumesate treated plants are decreased by greater amount in the shoots than in the roots as was the case with the percentage data. Flufenacet treated plants show a smaller decrease than the other two treatments in the shoots, whereas, in the roots it showed the most substantial decrease.

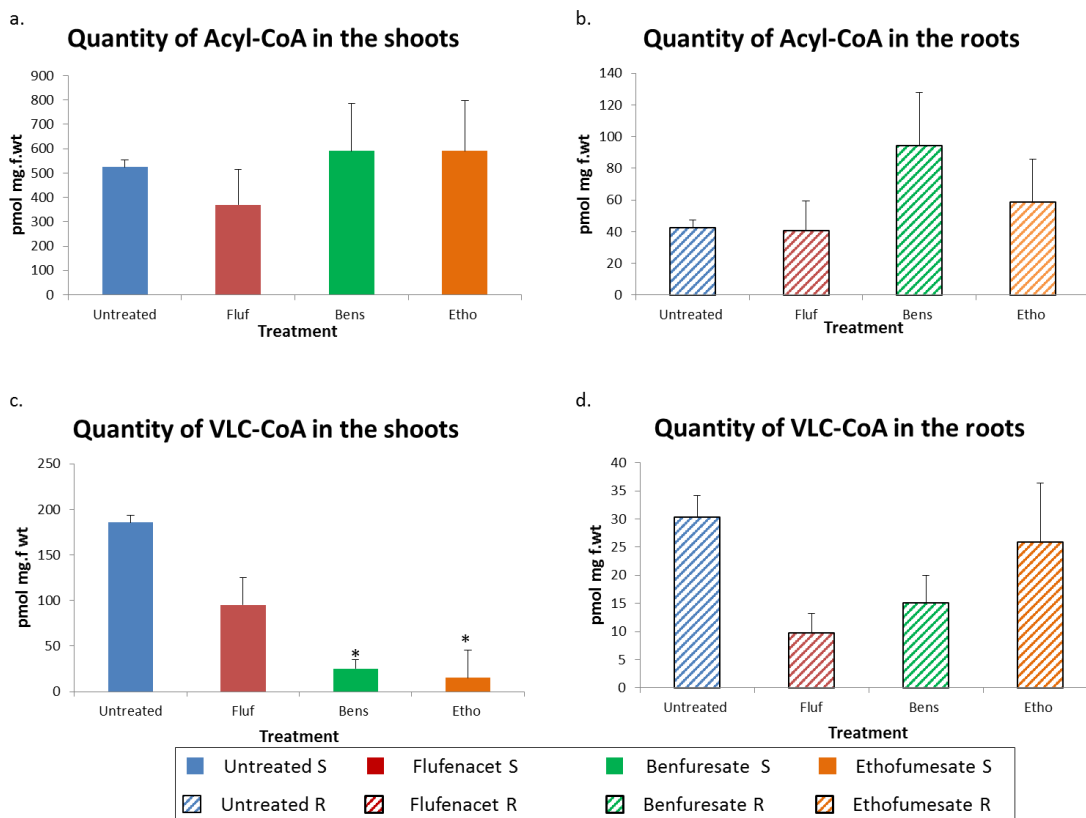


Figure 4.4 The quantity of acyl-CoA in herbicide treated plants. (a) shows the total quantity of acyl-CoA in the shoots, (b) shows the total quantity of acyl-CoA in the roots. (c) shows the quantity of acyl-CoA containing 20 carbons and greater in the shoots and (d) shows the quantity of acyl-CoA containing 20 carbons and greater in the roots. Values are based on the mean of 4 replicates +/- the SE. * Shows significant results based on ANOVA showing a F test p value of less than 0.05, and a difference in means greater than the LSD values at 5% (degrees of freedom= 9).

4.2.3. Membrane Glycerolipid profiling of plants treated with herbicides

As a result of the observation of a correlation between phenotype and the amount of VLC-acyl-CoAs, membrane glycerolipids were then analysed to see if a similar correlation could be seen. The contribution of each glycerolipid class to the total amount of glycerolipids in the shoots is shown in Figure 4.5. Flufenacet treated plants showed the greatest differences in the membrane glycerolipid composition compared to untreated plants. There was a significant difference in the contribution that every class made to the total amount of glycerolipids. There was an increase in the amount of PC (29% increase), and PE (55% increase) accompanied by

decreases in the amount of MGDG (37% decrease) and PG (53 % decrease) compared to untreated plants. The decreases seen are in lipid classes which have a function in the plastid (MGDG, PG) which would explain the chlorotic phenotype shown in Figure 4.1. Ethofumesate treated plants did not show significant changes in any of the classes compared to the untreated plants in terms of the proportion that they contributed to the total. Benfuresate treated plants only showed a significant increase in the proportion that PE contributed to the total (41% increase compared to untreated plants). As ethofumesate treated plants did not show any changes in the contribution of each class to the total, it would suggest that the changes in the proportion seen in the other herbicide treated plants are not responsible for the fused aerial organs. The results of the statistical analysis used to observe differences in the total amount of each class as well as differences in chain lengths can be seen in appendix III.

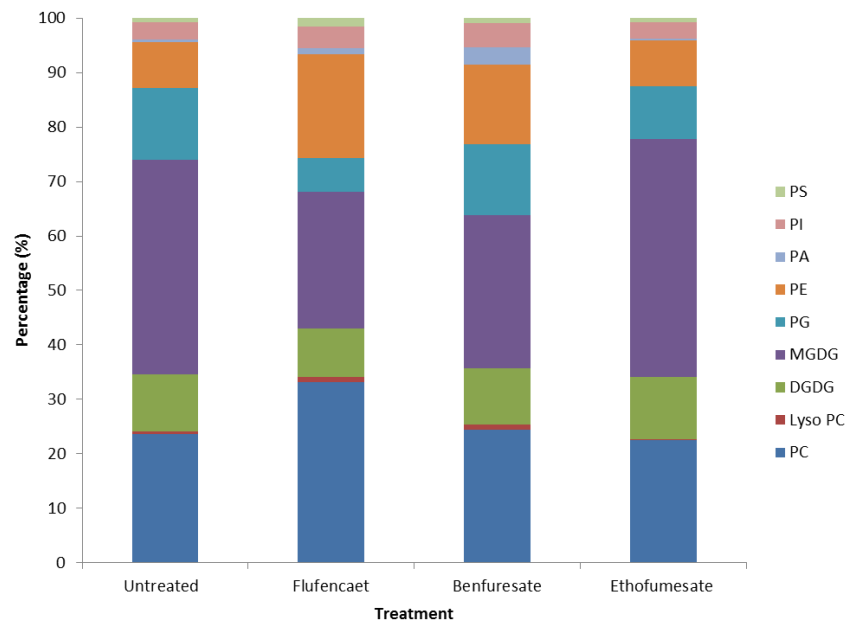


Figure 4.5 Membrane glycerolipid composition in the shoots of herbicide treated plants values are means of 4 replicates.

The same analysis was performed with the root data, as shown in Figure 4.6. As observed in the shoots, plants treated with ethofumesate did not show significant changes in the membrane glycerolipid composition. Flufenacet treated plants did not show any significant changes in the roots in contrast to the data from the shoots, this is due to the fact that the decreases that were seen in the shoots are in plastid lipids that are not present in high amounts in the roots, which was thought to result in the percentage increases in PC and PE. Benfuresate treated plants showed a significant difference in many of the membrane glycerolipid classes in the roots. Decrease were seen in the amount of PC (24% decrease) and an increase in the amount of PA (34% increased), PI (42% increased), and PE (15% increased).

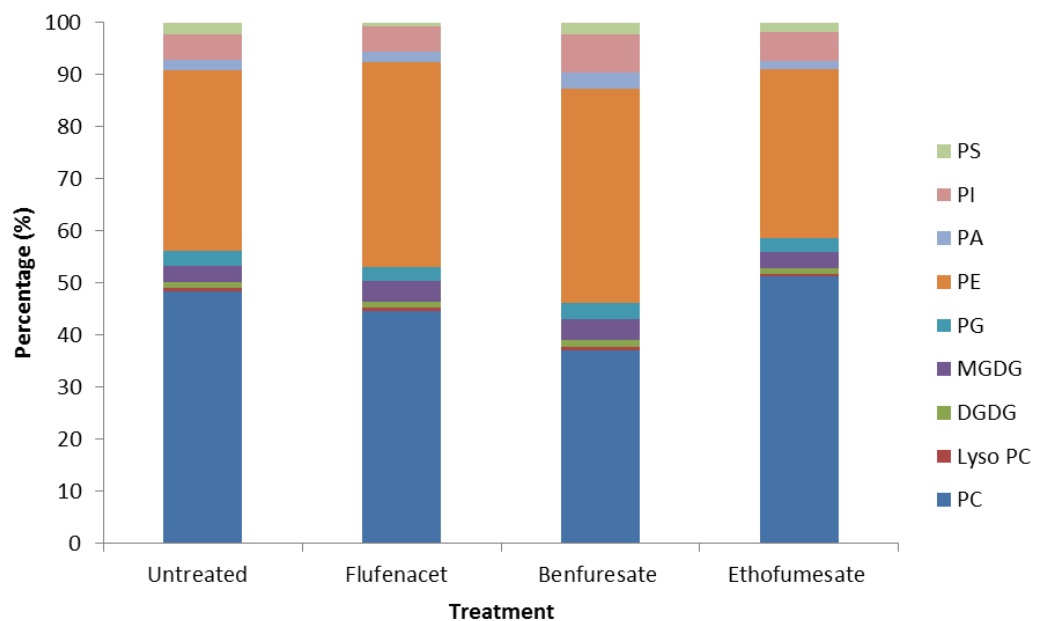


Figure 4.6 Membrane glycerolipid composition in the roots of herbicide treated plants values are means of 3 replicates.

The fatty acid chain lengths, within the phospholipid classes were examined. Although all chain lengths were observed for differences with wild type, (the results of which can be found in appendix III), the percentage of VLCFA will be discussed

here. In the roots there was a significant decrease in the amount of phospholipids containing VLCFA in both ethofumesate and flufenacet treated plants but not in benfuresate treated plants compared to untreated plants, (Figure 4.7). Ethofumesate showed a percentage decrease of 23% compared to wild type and a 10% decrease was seen in benfuresate. In comparison flufenacet showed a 72% decrease in the roots. This exhibited the same trend as in the acyl-CoA data, where the decrease in flufenacet treated plants was much larger than in the other two herbicides. This shows a correlation between the phenotype and the lipidomic data. Flufenacet treated plants showed a reduction in the amount of PE and PS containing VLCFA, whereas benfuresate and ethofumesate treated plants only showed reductions in the amount of PE.

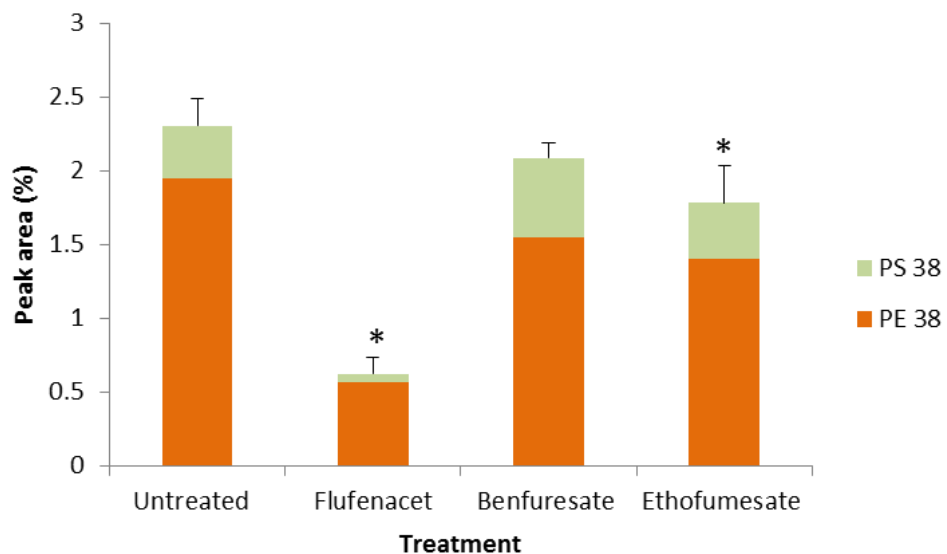


Figure 4.7 The proportion of phospholipids that contain a VLCFA in the roots of herbicide treated plants. Values are means of \pm standard error of 3 replicates. * Shows significant results based on ANOVA showing a F test p value of less than 0.05, and a difference in means greater than the least significant difference values at 5% (degrees of freedom= 6).

The situation in the shoots appears more complicated. Ethofumesate and benfuresate both showed a significant decrease in the percentage of VLCFA in PE

and PS whereas flufenacet treated plants did not. A decrease of 54% in benfuresate and 42% in ethofumesate was observed compared to untreated plants (Figure 4.8a). However benfuresate and flufenacet treated plants also contained VLCFA in other classes which were not detected in untreated plants. In benfuresate treated plants VLCFA could be detected in PC, which accounted for 6% of the total PC, in PG accounting for 7.5% of the total PG, and in PA accounting for 1% of the total. Flufenacet showed VLCFA in PA accounting for 1% of the total PA. As a result of this, benfuresate showed a significant increase in total VLCFA containing phospholipids in the shoots, (Figure 4.8b). It contained 4 times the amount of phospholipids containing VLCFAs than untreated plants did. These additional phospholipids containing VLCFAs were not seen in the roots. Due to this, where a fused aerial organ phenotype was observed, a decrease was not observed in the percentage of phospholipids containing VLCFAs in all herbicide treated plants.

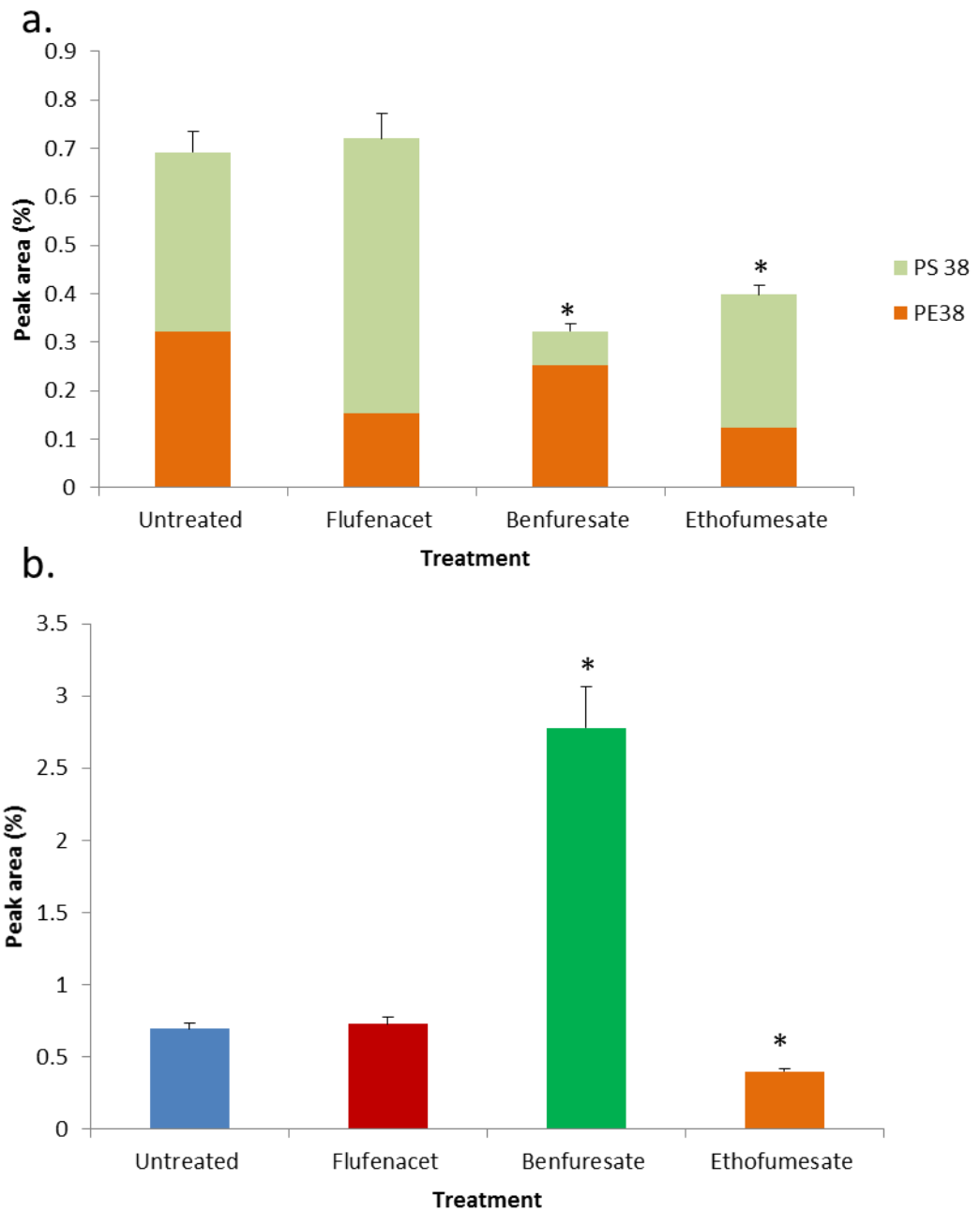


Figure 4.8 The proportion of phospholipids that contain a VLCFAs in the shoots of herbicide treated plants. (a) The percentage of VLCFA in PE and PS. (b) Total VLCFA in all phospholipid classes. Values are means of +/- standard error of 4 replicates. * Shows significant results based on ANOVA showing a F test p value of less than 0.05, and a difference in means greater than the LSD values at 5% (degrees of freedom= 9).

4.2.4. Sphingolipid profiling of plants treated with herbicides

A correlation has been shown between the percentage of VLC-acyl-CoAs present in a tissues and the phenotype seen in that tissue in the plants treated with herbicides. However the phospholipid pool showed while a decrease was seen in the proportion of phospholipids containing VLCFA in the roots where a root phenotype was observed, this was not the case in the shoots. Sphingolipid profiling was carried out to see what affect a decrease in VLC-acyl CoAs had on this lipid pool. All statistical analysis of the sphingolipid data presented in this chapter can be found in appendix III.

4.2.4.1. Total amount of sphingolipids in herbicide treated plants

The total quantity of sphingolipids was measured in the herbicide treated plants. It was shown that there was no significant difference in the total amount of sphingolipids in the shoots or in the roots (Figure 4.9). Within the classes there were no significant differences in the amount of each class of sphingolipid in the roots and the shoots of ethofumesate treated plants compared to untreated plants. Flufenacet and benfuresate treated plants showed an increase in the amount of ceramides in the shoots. It has also been shown that the proportion of each of the different LCB/LCBPs within the sphingolipid molecule is similar between untreated plants and plants treated with herbicides (data shown in appendix III).

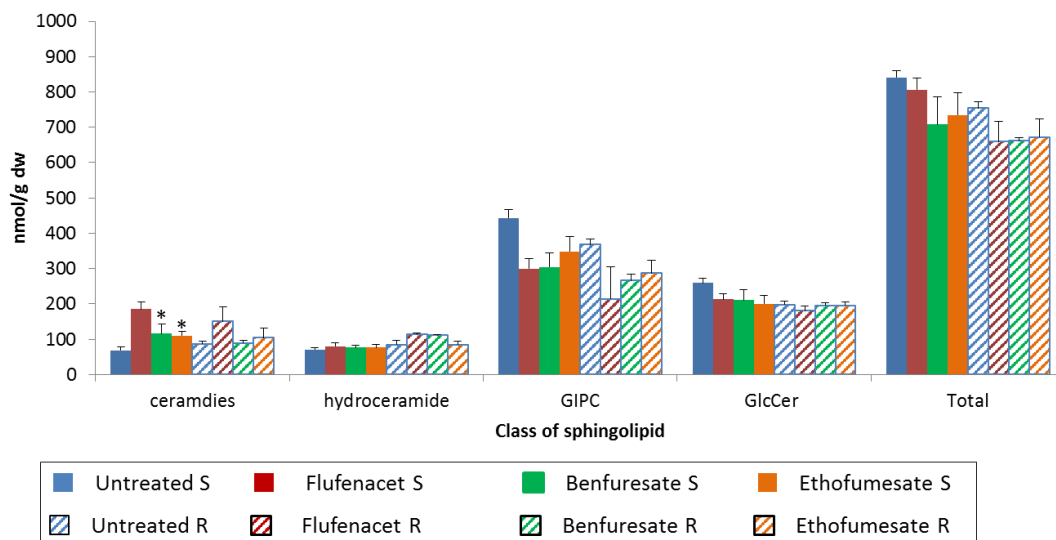


Figure 4.9 Sphingolipid composition in the shoots and roots of herbicide treated plants. Values are means of +/- standard error of 3 replicates. * Shows significant results based on ANOVA showing a F test p value of less than 0.05, and a difference in means greater than the LSD values at 5% (degrees of freedom= 6).

4.2.4.2. Percentage of sphingolipids containing VLCFA in herbicide treated plants

The total proportion of sphingolipids containing VLCFAs, (Figure 4.10a) showed a decrease in the shoots of all the herbicide treated plants compared to untreated plants. All treated plants showed a greater percentage decrease in the amount of fatty acids containing 24 carbons and greater, than those containing 22 carbons and greater compared to untreated plants. At 24 carbons and greater flufenacet treated plants showed a decrease of 45%, benfuresate a decrease of 76% and ethofumesate a decrease of 55%. The roots exhibited a similar reduction in flufenacet treated plants, which showed a decrease of 84%. Benfuresate and ethofumesate treated plants also showed a reduction in the roots of 15%, which was not as substantial as that shown in the shoots. As was observed in the acyl-CoA pool, a decrease in the proportion of VLCFA is seen most substantially in the shoots of the plants that show a shoot phenotype, and in both the roots and the shoots, where a phenotype is observed in both.

The proportion of VLCFA in each of the different sphingolipid classes was measured, (Figure 4.10 b-e). GIPCs containing VLCFA, (Figure 4.10b) were reduced in their proportions in all three of the herbicides in the shoots, with ethofumesate and benfuresate more strongly affected than flufenacet. A percentage decrease of 74% was seen for benfuresate treated plants, 60% for ethofumesate treated plants and 43% for flufenacet treated plants, for fatty acids of 24 carbons and greater. In addition a greater percentage decrease was seen in those sphingolipids containing fatty acids with a chain length of 24 carbons and greater, than in those containing 22 carbons and greater by approximately 20% in all three of the herbicide treated plants. This reduction was not observed in the roots for benfuresate and ethofumesate treated plants. In contrast, the same pattern was seen in the roots for plants treated with flufenacet.

The proportion of GlcCer containing VLCFA, (Figure 4.10c) showed the same pattern as in the GIPC pool. A decrease is seen in the shoots of all herbicide treated plants. In addition, as was the case with GIPCs there was a smaller percentage decrease in GlcCer containing fatty acids with a chain lengths of 22 carbons and greater, than those containing 24 carbons and greater. A decrease was not observed in the roots treated with ethofumesate and benfuresate. Whereas, flufenacet treated plants did show a decrease in the amount of GlcCer containing VLCFAs in the roots. This shows that both classes of complex sphingolipids show a reduction in the proportion of VLCFA in the shoots where only a shoot phenotype is observed, and in the roots and in the shoots were phenotypes are observed in both.

In the ceramides and HCer, (Figure 4.10 d and e) a reduction in the proportions of VLCFA in the shoots was observed. A decrease of 68% was seen in ceramides containing VLCFAs in benfuresate treated plants, and ethofumesate treated plants showed a 42% reduction in the amount containing fatty acids with a chain length of 24 carbons and greater. A smaller decrease of 31% was observed in flufenacet treated plants. The roots did show a decrease in ceramides containing VLCFA in ethofumesate and benfuresate treated plants but by a much reduced percentage decrease, of 18% in both, than that seen in the shoots. Flufenacet produced a substantial decrease in the roots. All of the herbicide treated plants showed a decrease in the amount of HCer containing VLCFA in the shoots. In the roots both ethofumesate and benfuresate treated plants showed minor decreases whereas flufenacet showed a substantial decrease.

This shows that in all sphingolipid classes and in the total amount of sphingolipids the same pattern is seen as in the acyl-CoA data: where a phenotype is seen, there is a decrease in the proportion of sphingolipids containing VLCFAs.

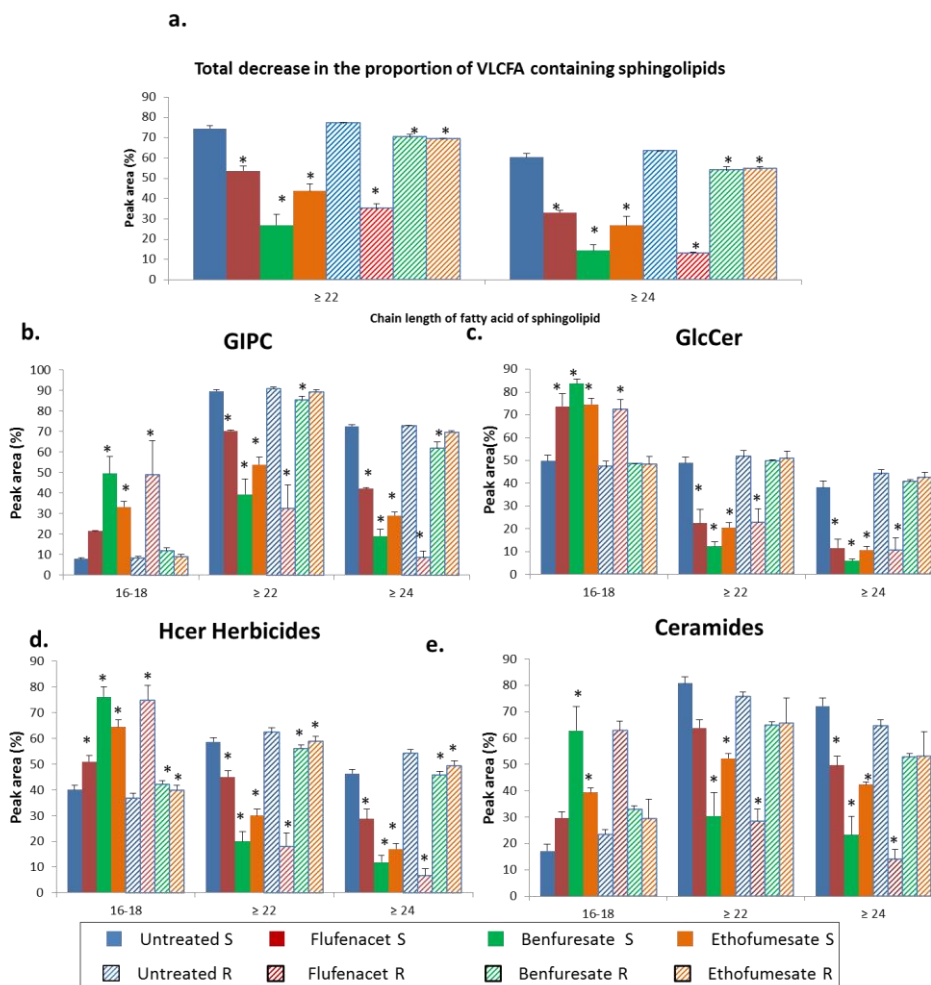


Figure 4.10 Percentage of different fatty acid chain lengths in the different sphingolipids classes in the shoots and roots of herbicide treated plants compared to untreated plants. (a) the total amount of sphingolipids, (b) GIPCs, (c) GlcCer (d) Hcer and (e) Ceramides. Values are means of +/- standard error of 3 replicates. * Shows significant results based on ANOVA showing a F test p value of less than 0.05, and a difference in means greater than the least significant difference values at 5% (degrees of freedom= 6).

4.2.4.3. The quantity of sphingolipids containing VLCFAs in herbicide treated plants

The sphingolipid data was quantified to see if the amounts of VLCFA containing sphingolipids were reduced in the herbicide treated plants compared to the untreated plants. Figure 4.11a shows that there is a significant decrease in all of the herbicide treated plants in the shoots and in the roots in the amount of sphingolipids containing VLCFAs. The decrease in the roots is not as substantial as the shoots in ethofumesate and benfuresate treated plants, whereas a greater decreases is seen in

the flufenacet treated plants in the roots than in the shoots. GIPCs containing VLCFA were reduced in the shoots of all of the herbicide treated plants, (Figure 4.11b) and a greater percentage decrease was seen in fatty acids with a chain length of 24 carbons and greater, than with 22 carbons and greater. Treated plants showed a decrease of 83% in benfuresate, ethofumesate a decrease of 69% and flufenacet showed a smaller decrease of 57%. There was an increase in the amount of GIPCs containing fatty acids with 16 or 18 carbons in the shoots of all the herbicide treated plants. In the roots, ethofumesate and benfuresate treated plants showed a decrease of 26% and 39% respectively compared to untreated plants in the amount of GIPCs containing VLCFAs, which is substantially smaller decrease than in the shoots. Flufenacet treated plants showed an increase in the GIPCs containing 16-18 carbon fatty acids and a reduction in those containing VLCFA in the roots, as was shown in the shoots. GlcCer containing VLCFA (Figure 4.11c) showed the same pattern in the shoots as shown in the GIPCs but in the roots a decrease is only seen in flufenacet treated plants. HCer containing VLCFA, (Figure 4.11d) followed the same pattern as the GlcCer containing VLCFA for ethofumesate and benfuresate treated plants, decreases were seen in HCer containing VLCFA in the shoots but not in the roots. Flufenacet treated plants did not show any significant differences with the untreated plants in the shoots, but in the roots there was an increase in short length fatty acids and a decrease in VLCFA. Different patterns were seen in the amount of ceramides containing VLCFA across all three herbicide treated plants, (Figure 4.11e). Benfuresate treated plants showed an increase in the amount of ceramides containing 16-18 carbon chains and a decrease in those containing VLCFAs in the shoots and did not show any changes in the roots. Ethofumesate

treated plants did not show any differences with untreated plants in the roots or in the shoots unlike the other sphingolipid classes. In flufenacet treated plants an increase was observed in all chain lengths of ceramides in the shoots and in the roots there were increases in 16-18 chain length fatty acids, with a decrease in those containing VLCFAs.

The percentage differences between treated and untreated plants in the total quantities of sphingolipids can be seen in the heat map shown in Table 4.1. Decreases in the quantities of sphingolipids containing 24 carbon fatty acids and greater are seen in all sphingolipid classes in all herbicide treated plants in the shoots, except for flufenacet which does not show a decrease in ceramides containing VLCFAs. There is also an increase in all sphingolipid classes in the amount containing 16-18 fatty acids. The most substantial decreases are seen in the complex sphingolipids, GIPCs and GlcCer in the shoots. In the roots of flufenacet treated plants the same pattern is seen as in the shoots, both in the increase in those containing 16-18 carbons and decreases in those containing 24 carbons and greater. The complex sphingolipids also show the most substantial changes in the roots of flufenacet treated plants. Ethofumesate and benfuresate roots do show the same pattern as in the shoots but the changes are much less substantial. Both benfuresate and ethofumesate treated plants showed a decrease in all classes of sphingolipids in the amount of VLCFA in the shoots. In the knockout/knockdown elongase lines decreases were not seen in the ceramides and HCer containing VLCFAs in the shoots. In addition there is a greater percentage decrease compared to untreated plants as the chain length of the VLCFA increases, which was not seen in the knockout/knockdown elongase lines.

Table 4.1 Heat map of the relative changes of plants treated with herbicides compared to untreated plants. The red positive numbers show where the amounts were increased compared to untreated plants, and the blue negative number show where the amounts were decreased compared to untreated plants.

	Shoots			Roots			Shoots			Roots		
	cer 16-18	cer 22	cer 24	Hcer 16-18	Hcer 22	Hcer 24	GlcCer 16-18	GlcCer 22	GlcCer 24	GIPC 16-18	GIPC 22	GIPC 24
Fluf	0.79	0.54	0.37	-0.05	0.05	-0.07	0.17	-0.61	-0.74	0.49	-0.48	-0.57
Bens	0.92	-0.43	-0.52	0.58	-0.63	-0.73	0.27	-0.81	-0.88	0.77	-0.71	-0.83
Etho	0.79	-0.02	-0.10	0.47	-0.39	-0.52	0.14	-0.68	-0.79	0.70	-0.53	-0.69
Fluf	0.86	-0.31	-0.61	0.71	-0.59	-0.83	0.33	-0.63	-0.80	0.79	-0.7	-0.9
Bens	0.39	-0.09	-0.13	0.36	0.16	0.11	-0.06	-0.13	-0.16	0.03	-0.32	-0.39
Etho	0.57	-0.06	-0.12	0.11	0.05	0.09	0.20	-0.02	-0.04	-0.14	-0.24	-0.26

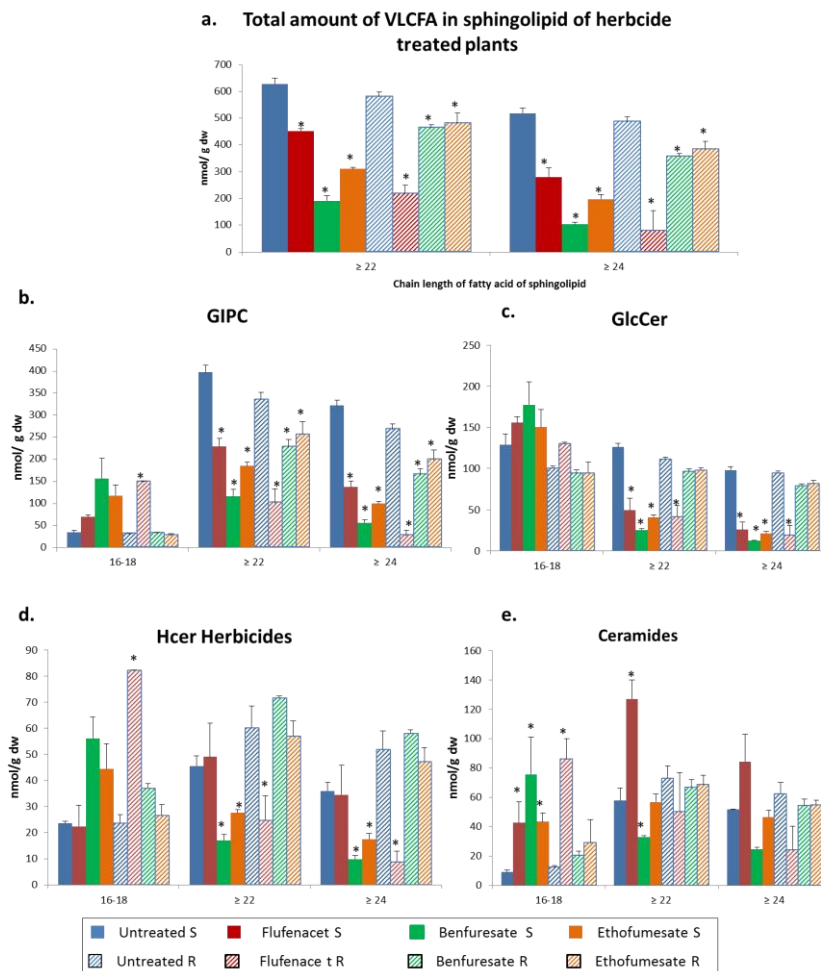


Figure 4.11 The quantity of different fatty acid chain lengths in the different sphingolipids classes in the shoots and roots of herbicide treated plants compared to untreated plants. (a) the total sphingolipids (b) GIPCs, (c) GlcCer, (d) Hcer and (e) ceramides. Values are means of +/- standard error of 3 replicates. * Shows significant results based on ANOVA showing a F test p value of less than 0.05, and a difference in means greater than the LSD values at 5% (degrees of freedom=6).

4.3. Discussion

It has been shown here that it is possible to use herbicides that affect VLCFA synthesis to produce similar phenotypes to those seen in the knockout/knockdown elongase lines. Lipidomic profiling of these treated plants can be used to complement the patterns seen in the elongase mutants to provide further evidence for correlations between phenotype and changes in the lipidome. Benfuresate and ethofumesate treated plants showed a shoot phenotype of fused aerial organs but did not have an observable root phenotype. Flufenacet treated plants had the same shoot phenotype but in addition also had shorter primary roots. This mimicked the effect that was seen in the elongase mutants, where mutants of the VLCFA elongase complex all resulted in decreases in VLCFA but did not all show the same phenotype.

4.3.1. Correlating phenotypes with lipidomic results

The herbicide treated plants have shown a clear correlation between phenotype and lipidomic profiling. In most cases where a phenotype is seen there is a decrease in the proportion of VLCFAs in that tissue. Benfuresate and ethofumesate treated plants displayed a shoot phenotype and a substantial decrease in the proportion of all VLCFA containing lipids analysed in the shoots. With the exception of the phospholipid pool in which benfuresate treated plants showed a large percentage increase in the proportion of the phospholipids containing VLCFAs compared to untreated plants in the shoots. In the roots of benfuresate and ethofumesate treated plants, which did not have a root phenotype, a decrease was seen in the proportion of VLCFA compared to wild type across all lipid classes. However this percentage decrease is not as substantial as that observed in the shoots, as shown in Table 4.2.

Table 4.2 Heat map of the percentage differences of the lipid classes between herbicide treated plants and untreated plants.

	Acyl CoAs containing C22 or greater	Acyl CoAs containing C24 or greater	Phospholipids VLCFA	Sphingolipids containing C22 or greater	Sphingolipids containing C24 or greater
Shoots					
Flufenacet	-62%	-69%	5%	-28%	-46%
Benfuresate	-92%	-93%	75%	-74%	-76%
Ethofumesate	-83%	-85%	-42%	-40%	-55%
	Acyl CoAs containing C22 or greater	Acyl CoAs containing C24 or greater	Phospholipids VLCFA	Sphingolipids containing C22 or greater	Sphingolipids containing C24 or greater
Roots					
Flufenacet	-62%	-68%	-73%	-47%	-76%
Benfuresate	-36%	-42%	-10%	-9%	-15%
Ethofumesate	-18%	-32%	-23%	-13%	-15%

In contrast flufenacet treated plants, which displayed both a root and a shoot phenotype, showed a decrease in VLCFAs in all lipid classes in both the roots and the shoots (except for the phospholipids in the shoots). All three herbicide treated plants showed a greater reduction in the proportion of VLCFA in the acyl-CoA pool and in the sphingolipid pool compared to the knockout/knockdown elongase lines. A greater reduction is also seen in the quantities of the sphingolipid pools. A greater reduction is again seen in the quantity of GlcCer than the GIPCs containing VLCFAs in the shoots. This would reinforce the statement in Chapter 3, suggesting that there is preferential channelling of VLCFA into certain classes of sphingolipids when there is a reduction in the amount of VLCFAs as shown previously for *pas2-1* (Bach *et al.*, 2008). However unlike in the elongase mutants, there was a decrease in sphingolipids containing VLCFAs in all of the sphingolipid pools in the benfuresate and ethofumesate treated plants in the shoots. In the elongase mutants no decreases or a much reduced decrease was seen in the quantity of HCer and ceramides containing VLCFA. This would suggest that the channelling that occurs in the elongase mutants does not take place in the herbicide treated plants, or that it does

not occur to the same extent. If the herbicides do affect the KCS enzymes, the data here would suggest that it could be the presence of a particular KCS enzyme in the elongase complex that is responsible for the channelling.

Flufenacet treatment has an effect on both roots and shoots and was shown previously to inhibit a number of KCS enzymes (Trenkamp, 2004). The KCS enzymes it inhibits have roles in the shoots and in the roots. It could therefore be expected to have a phenotype in both. The wide range of KCS enzymes that it inhibits could also explain why a much lower concentration of this herbicide was needed to generate a phenotype compared to the other two herbicides. The greater the number of KCS enzymes that are inhibited, the lower the amount of acyl-CoA generated of the correct length, degree of saturation, and in the correct location to be channelled into the various lipid pools. Hence the greater the effect on the plant. There are 21 different KCS enzymes which have some degree of overlapping functions and tissue specificities (Joubes *et al.*, 2008). Since flufenacet inhibits such a variety of KCS enzymes the amount of acyl-CoA could be reduced to such an extent that it would be embryo lethal, it has been shown previously that VLCFAs are essential for plant development (Bach *et al.*, 2008, Beaudoin *et al.*, 2009). This would explain why high concentrations of flufenacet resulted in plants that showed severely stunted growth, or that did not grow at all when higher concentrations than used in this analysis were used.

4.3.2. Effect of increasing chain length

The herbicide treated plants showed a greater decrease in the amount of sphingolipid containing VLCFA as the chain length of the VLCFA increased. This was not seen in the knockout/knockdown elongase lines in Chapter 3, as shown in

Table 3.2 and 3.3. In the elongase mutants this could be attributed to the fact that particular chain lengths of sphingolipids were important for ensuring homeostasis of the plants. When the levels of VLCFA are reduced in these lines, the plant may preferentially synthesise certain chain lengths of VLCFA due to the importance of them for sphingolipid metabolism. Flufenacet has been shown to inhibit at least 6 KCS enzymes, which show different substrate specificities. The 21 different KCS enzymes result in the synthesis of different chain lengths of VLCFAs. It is possible in the herbicide treated plants that increased chain lengths of VLCFAs cannot be produced as all the KCS enzyme capable of producing this chain length are inhibited in that tissue. In contrast, in the knockout/knockdown core elongase lines the expression of a particular KCS enzyme capable of producing these essential chain lengths of VLCFA for sphingolipids could have an increased expression, to try and maintain the sphingolipid pool as much as possible. Differential expression of KCS enzymes has been shown previously under different stress conditions (Joubes *et al.*, 2008). In addition herbicide treated plants showed a greater reduction in the amount of VLCFA in the sphingolipid pool than the elongase mutants. This could again be explained by an increased expression of the KCS enzyme that produces VLCFA for sphingolipids in the elongase mutants which cannot occur in the herbicide treated plants.

4.3.3. Explaining the fused aerial organ phenotype

All three herbicides show a similar shoot phenotype of fused aerial organs, this was also seen in the knockout/knockdown elongase lines. In the elongase lines it was thought that it was a decrease in the GlcCer containing VLCFA that could be responsible for the fused organ phenotype. Further proof of that can be seen in the

plants treated with herbicides, as all three herbicides show substantial decreases in the amount of GlcCer containing VLCFAs. In the elongase mutants however, it was speculated that the greater decrease seen in *pas2-1* in the sphingolipid pool was responsible for the more severe phenotype. None of the plants treated with herbicides (used at the concentration here) resulted in as severe of phenotype as *pas2-1*, however, the reduction in the amount of GlcCer containing VLCFAs is greater in the herbicide treated plants than in *pas2-1*. The data from the herbicides therefore seems to suggest that if this more severe phenotype in *pas2-1* is due to a greater decrease in sphingolipids containing VLCFA it must be due to a decrease in a particular sphingolipid not a class of sphingolipid. Also a number of the phenotypes seen in *pas2-1* are thought to arise due to decreased levels of VLCFA during embryo development. It is possible that the severe phenotypes of *pas2-1* are not seen in the herbicide treated plants as they do not have an effect on VLCFA synthesis during embryo development.

4.3.4. Explaining the root phenotype

Flufenacet treated plants did show a root phenotype, in the knockout/knockdown elongase lines this was correlated with a reduction in sphingolipids containing VLCFAs. The short primary root phenotype that is seen in the *pas2-1* and *cer10* was correlated with a greater reduction in GlcCer containing VLCFAs than was seen in the *KCR RNAi* line, which does not have a reduction in primary root length. Flufenacet treated plants showed a greater reduction than both *cer10* and *pas2-1* in the quantity of GlcCer containing VLCFAs. In addition the reduction seen in the other two herbicide treated plants, that did not produce a root phenotype, showed a smaller decrease than seen in *pas2-1* and *cer10*. This shows a correlation between

plants showing a shorter primary root and a lack of GlcCer containing VLCFAs. Flufenacet shows a greater reduction in primary root length than *pas2-1*. Flufenacet treated plants also showed a greater reduction in GlcCer containing VLCFA than *pas2-1*, suggesting that the lower the level of GlcCer containing VLCFA the greater the effect on primary root length. Further support of this comes from the fact that *pas1* plants, show a greater reduction in primary root than wild type plants when exposed to fumonisin, an inhibitor of ceramide synthesis. A higher concentration of inhibitor caused a greater reduction in root length in *pas1* and caused a reduction in primary root length in wild type plants. This suggests that as the level of sphingolipids decreases the root length decreases. LOH1 and LOH3 catalyse the binding of LCBs and VLCFAs to produce ceramides. Double mutants resulted in a complete absence of sphingolipids containing VLCFA and there was no root growth. This suggests that sphingolipids containing VLCFA have a role in primary root growth (Markham *et al.*, 2011).

4.3.5. Role of the herbicides

It has been suggested previously that all three herbicides have an effect on KCS enzymes (Jablonkai, 2003, Trenkamp, 2004). It was shown that flufenacet has an effect on VLCFA production when KCS enzymes were expressed in yeast. Benfuresate and ethofumesate did not affect VLCFA production when incubated with a number of KCS enzymes in yeast. If benfuresate and ethofumesate do affect the KCS enzymes they must only affect KCS enzymes that have a much higher level of expression in the shoots than in the roots, of which there are a number of candidates, KCS3, KCS6 and KCS10 (Joubes *et al.*, 2008). These enzymes were not tested in the previous study and are likely candidates. However, the herbicides must

affect an enzyme that does not show any redundant activity with another KCS enzyme due to the severe reduction in VLCFAs that has been shown here. The other KCS enzymes, not tested previously, could be tested in the same way as previously done by Trenkamp, (2004) to observe if benfuresate and ethofumesate have an effect on any KCS enzymes. It is possible that the herbicides affect VLCFA biosynthesis specifically in the shoots by affecting another component of VLCFA synthesis. Additionally it is possible that the plants treated with these herbicides do not show a root phenotype because the compounds are degraded in the roots or bind to an unrelated compound in the roots, such that they are not available to inhibit the KCS enzymes. It is possible that at higher concentrations these herbicides could have resulted in a root phenotype. Flufenacet had been shown previously to affect a KCS enzyme with expression in the roots, KCS2, and in the shoots, KCS5. As such the reduction in VLCFA in the shoots and the roots was to be expected (Trenkamp, 2004, Joubes *et al.*, 2008).

Chapter 5. Forward genetic screen to identify novel genes involved in VLCFA metabolism

A forward genetic screen was conducted to identify new components of VLCFA metabolism. This would lead to a greater understanding of the role of VLCFAs in *Arabidopsis* growth and development. By using a mutant of VLCFA synthesis both suppressor and enhancer mutants of that gene can be identified to discover other genes involved in various aspects of VLCFA metabolism.

5.1. Introduction

5.1.1. Genetic background for the forward genetic screen

The forward genetic screen was conducted in the *cer10-1* background, which encodes for the fourth component of the elongase complex. *cer10-1* seeds were mutagenized, with the aim to identify both suppressor mutations and enhancer mutations. A suppressor mutation would result in a plant exhibiting more phenotypic traits of wild type plants than *cer10-1*. An enhancer mutation would show phenotypes more severe than *cer10-1*. *cer10-1* was chosen as the background for the screen because it has a stable phenotype that is easy to observe, such as the fused flower bud phenotype shown in Figure 1.10. Phenotypes such as these were easy to trace such that when they became more or less severe potential suppressor and enhancer mutations could be identified. Null mutations of *cer10*, unlike the other core components of the elongase, are not embryo lethal and it is thought that there is another gene capable of carrying out the function of *cer10*. It was hoped that by carrying out the screen in *cer10* it could lead to the identification of this additional elongase component.

5.1.2. Principles of ethyl methane sulfonate mutagenise

In a forward genetic screen, mutations are introduced into the genome of the plant of interest, in this case *cer10-1*, by mutagenesis and then their progeny are screened for changes in the phenotype of interest. The phenotypes of interest used here were plants that showed phenotypic traits that were characteristic of suppressor or enhancer mutations of *cer10-1*. Ethyl Methane sulfonate (EMS) is the most widely used chemical mutagen in *Arabidopsis*, because of its high mutagenicity and low mortality (Moller, 2007). EMS treatment generates point mutations distributed randomly throughout the *Arabidopsis* genome (Greene *et al.*, 2003). EMS alkylates guanine (G) resulting in mispairing to thymine (T) instead of cytosine (C). This results in C/G to T/A (adenine) substitutions in the genetic code. This can then result in amino acid changes (Greene *et al.*, 2003). The reaction can be seen in Figure 5.1. EMS produces point mutations with different degrees of severity so that not all of the mutations are loss of function mutations. Reduced function and altered function mutations can also be produced for example.

The diploid cells of the fully developed embryos which are covered by the seed coat are targets for mutagenesis. Mutations in the genome of each cell that is mutagenized will be independent of any other cells that are mutagenized. As only two cells in *Arabidopsis* contribute to the germ line only mutations derived from these cells will be detected in later generations grown from that seed. As only one cell from the two germ cells that will form the M₁ plant will contain any given mutation, it means 50% of the resulting M₂ seeds will be derived from the germ line cell that contains the mutation and half will not. In the resulting M₂ population the ratio for homozygotes of the mutation will be 7:1, 4:0 obtained from the non-

mutagenized half and 3:1 from the half that was originally mutagenized (Moller, 2007).

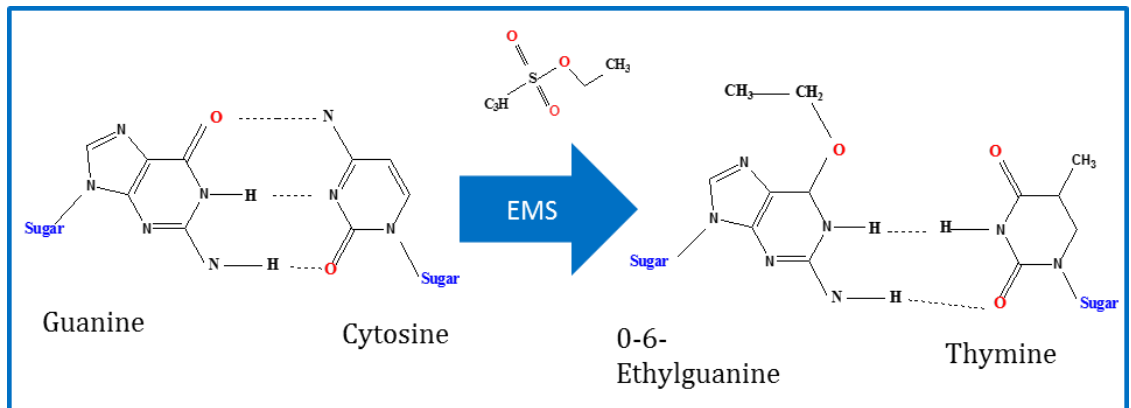


Figure 5.1 The effect of EMS on the genetic code. EMS alkylates guanine resulting in mispairing in the genetic code. Guanine is converted to 0-6-Ethylguanine which then bonds with thymine resulting in a G/C to T/A change.

5.2. Methods

5.2.1. Genotyping of TILLING lines

TILLING lines were received from the Arabidopsis Biological Resource Centre. Genomic DNA was extracted using the CTAB DNA extraction method (discussed in section 2.3.1). PCR was also carried out using the standard PCR conditions, discussed in section 2.3.3. Genotyping was performed using derived cleaved amplified polymorphic sequence (dCAPS) primers, the sequence of which can be seen in Table 5.1 along with the list of restriction enzymes that were used to cut the resulting PCR product.

Table 5.1 The sequence of dCAPS primers used for the genotyping of TILLING lines. The base that has been changed in the sequence is shown in red, and the restriction enzyme used to cut the resulting sequence is shown in blue.

dCAPS primers – KCR

KCR5460F – AACCTTATACTCGTTGCTCGTAACCC**G** WILD TYPE *HpaII*

KCR5460R- CAAGTTATTGATCAACTCTTCATCAACC

KCR2473F- CCTCAGATCTTTCTACATCTACTTCC

KCR2473R- ATATCTCCAGAGAAATCCATCACAC**CCG** WILD TYPE *AgeI*

KCR2957F- GTCTACATGTTGAGTATAAGAAGA**CTG** WILD TYPE *BFI*

KCR2957R- GAGATTCAATAAACAACATTTTACAC

dCAPS primers –PAS2

PAS2G5SF- GTTCTCGCGTATTCACCTTCCATGG**CC** WILD TYPE – *NaeI*

PASG5SR- CTGAGCAAGCTGGAGAGGCTTCTCAATGGC

PAS2S8F- CCCAAAATTCTGGAAGTTGGGGGTTGATAATGTCG

PAS2S8R – AGAGAGTGAGGTACACGCGCCGGACAG**GCG** WILD TYPE- *NspII*

5.2.2. Mutagenesis

5000 *cer10-1* seeds (Ler Arabidopsis ecotype) were incubated overnight in a water solution containing 0.1% potassium chloride. These seeds were then soaked with 0.1M sodium phosphate, pH 5, 5% dimethyl sulphoxide and 100 mM ethyl methanesulfonate (EMS) for 4 hours, before being rinsed repeatedly with 100mM sodium thiosulphate for 15 minutes. The seeds were then left to dry overnight and planted into pools of 20 plants. Seeds from these pools were sown alongside Ler and *cer10-1* plants so that phenotypic differences could easily be seen.

5.2.3. Analysis of plant cuticle

5.2.3.1. Toluidine blue staining for defects in the waxy cuticle

35 ml of 0.05 % (w/v) Toluidine Blue was poured onto plates containing ten day old plants for 2 minutes. The plates were then washed twice with 35 ml of sterile water.

5.2.3.2. Qualitative and quantitative wax analysis

5.2.3.2.1. Extraction of stem waxes for analysis

800 mg of stem was collected from five week old plants. 5 ml of chloroform was added to the samples and the samples were inverted for 1 minute after which the

chloroform was extracted into a new tube. The chloroform was evaporated under nitrogen, and the samples were then stored at -20°C. 100 µl of bis-N-N-(trimethylsilyl) trifluoroacetamide 1% Trimethylsilyl (BSTFA+TMS; sigma) was added to each sample. For one hour the samples were incubated at 85°C. 100 µl of heptane was then added. This would transform all the hydroxy containing compounds into the corresponding trimethylsilyl (TMS) derivatives so that they can be detected by the MS.

5.2.3.2.2. Analysis of flower waxes using thin layer chromatography

500 mg of flower material was collected and a chloroform extraction was performed as for the stem wax extraction above. The chloroform was again evaporated under nitrogen. 120 µl of chloroform with standards was then added to each sample. The standard used for flower wax quantification contained 500 nM of C₂₄ alkane, 50 nM C₃₂ wax ester, 100 nM C₁₅ ketone, 100 nM of C₂₀ primary alcohol, and 100 nM C₂₄ fatty acids. The samples were then heated at 40°C for 20 minutes before being loaded onto pre-equilibrated thin layer chromatography (TLC) plates. The plates were equilibrated with the solvent that was used in the chromatography. The TLC plates used here were Whatmann™ Absorption 60Å Silica Gel TLC plates (supplied by Fisher Scientific). The TLC plate is then added to the TLC tank which had previously been equilibrated with the solvents for 1 hour. The solvents used were hexane:diethylether:acetic acid (80:15:1 v/v/v). Once the migration front of the solvent had reached the top of the plate, the TLC plate was sprayed with primuline and visualized under UV light. The individual bands of different chemical groups could then be seen and pencil lines were drawn around each of them, as can be seen in Figure 5.2. The bands were scrapped off and stored in glass tubes at -20°C.

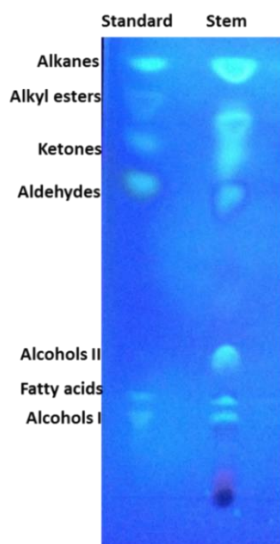


Figure 5.2 TLC plate showing the separation of the wax components.

The compounds were then extracted from the silica by adding 1 ml of chloroform to each of the glass tubes, which were left for 10 minutes at room temperature. The chloroform was then extracted and added to a new tube. A second 1 ml of chloroform was added to the extracted TLC band which was once again removed and added to the first extraction. The chloroform was then evaporated under a stream of nitrogen gas. The primary alcohol (alcohol I) and secondary alcohols (alcohol II), and fatty acids were then derivatised with 100 μ l BSTFA+ TMS and were then heated to 85°C for 1 hour. 100 μ l of heptane was then added to each sample. The alkanes, ketones, aldehydes and the wax esters did not need derivatising and heptane was added straight to the samples. The heptane was added to these compounds so that each standard was present at 1 M concentration.

5.2.3.2.3. Identification of the components present in wax using GC-MS

The components of stem and flower wax were identified using Gas Chromatography Mass Spectrometry (GC-MS) the same method was used for both stem and flower waxes. The capillary column that was used for the GC analysis was

the capillary GC (30m in length, 0.25mm internal diameter, with a film thickness of 0.25 μm supplied by aligent). Helium was used as the carrier gas at an inlet pressure regulated for a constant flow of 1ml/min. The initial oven temperature was set at 50°C for 1 minute, which rose by 50°C per minute to 200°C, followed by an increase of 3°C per minute up to 325°C. This method was used for the stem wax samples and all of the flower wax components except the ketones and the wax esters, where the method was adapted for a longer run time so that it was possible to see compounds of a longer carbon length. In this case the temperature was held at 325°C for 10 minutes. The compounds were then identified by MS. The fragmentation pattern of the compounds would allow for identification of the chemical groups and chain length of the compounds.

5.2.3.2.4. Quantitative and qualitative analysis of wax composition using GC-FID

The proportion of each compound was studied using capillary GC with Flame Ionisation Detection (FID) under the same GC conditions as stated above. The mol % of each compound was calculated by normalising each peak area with the molecular weight, as the intensity of FID signal is dependent on the size of the molecule.

To quantify the amount of flower wax components present single compounds were quantified against the internal standard. For the stem analysis all of the compounds were quantified against an external standard. This was done by extracting the peak area of each of the compounds and the standard. Each sample area could then be corrected depending on the recovery of the standard. The peak areas were normalised for each sample using, the molecular weight (as in the mol % calculation), the amount of material used, and the total volume of the sample. This

gave a value of the total amount of each of the wax components in the sample which can be combined to give the total amount of wax. An example of the spectra produced both for flower and stem wax is shown in Figure 5.3.

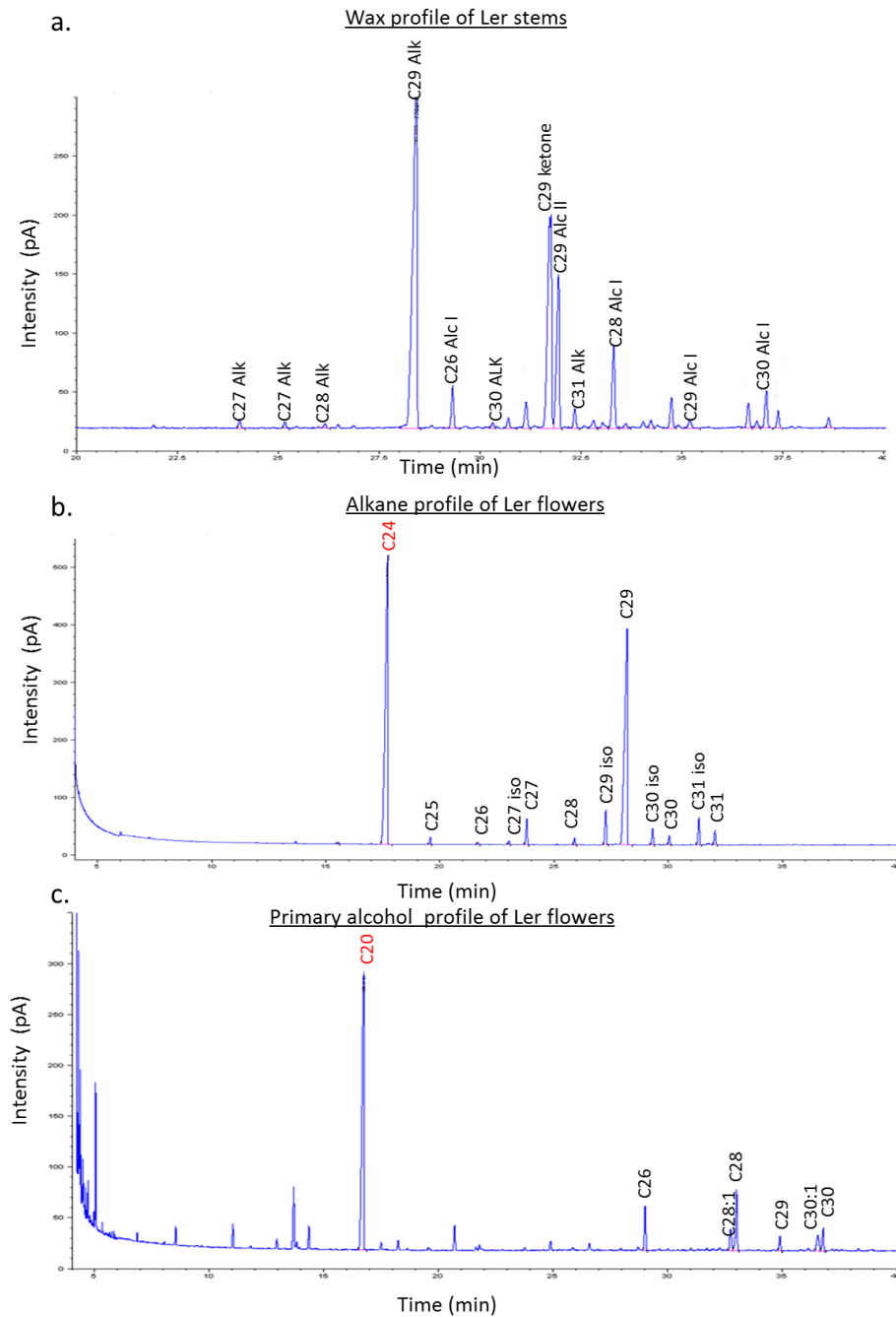


Figure 5.3 Wax profiles of flowers and stems obtained by GC-FID analysis. a. the total wax profile of ler stems. b, and c show the alkanes and primary alcohols of Ler flowers after separation by TLC.

5.3. Results

5.3.1. Designing a suppressor/enhancer genetic screen for VLCFA metabolism

A genetic screen was designed to find other genes that are involved in VLCFA metabolism. To do this, an already characterised VLCFA mutant is mutagenized with EMS to create a mutant population. Initially mutations of *PAS2* and *KCR1* were considered as the most suitable candidates to perform the forward genetic screen. Null mutations of *KCR1* and *PAS2* are embryo lethal, but lines with reduced levels of expression are available: *pas2-1* (Bach *et al.*, 2008) and the *KCR1 RNAi* lines (Beaudoin *et al.*, 2009). The *pas2-1* mutation is leaky meaning that the function of the gene is reduced but the enzyme is present at lower levels and some VLCFAs can still be produced. Hence the resulting phenotype is not as severe as the null mutation. The *KCR RNAi* line reduces the expression of the *KCR* gene. The phenotype and characteristics of each of these lines can be found in sections 1.6.2 and 1.6.3. The *KCR1 RNAi* lines were not reliable enough to be used in a screen as, the severity of their phenotype changed between generation and a stable phenotype could not be obtained. The *pas2-1* mutation was too severe. For example it often produced sterile flowers which would make it difficult to perform a genetic screen if there was a reduction in the number of offspring produced.

5.3.1.1. TILLING lines

TILLING (targeting induced local lesions in genomes) lines received from the Arabidopsis Biological Resource Centre (www.arabidopsis.org) were attractive candidates to find weaker mutations of these two genes. The TILLING lines were originally generated using a combination of EMS induced mutagenesis with high throughput screening for point mutations using denaturing high performance liquid

chromatography (DHPLC) (McCallum *et al.*, 2000). This resulted in the availability of a number of point mutations for each gene in the *Arabidopsis* genome. A number of TILLING lines were received for both *KCR1* and *PAS2*.

5.3.1.1.1. Isolating a homozygous *KCR* TILLING line

The stocks received for the *KCR1* gene can be seen in Table 5.2. Out of the 12 TILLed alleles received, only 4 resulted in a non-synonymous mutation. A non-synonymous mutation is a mutation that does result in an amino acid change in the protein sequence. The amino acid changes that the TILLING lines produced can be seen in Figure 5.4. As shown in Figure 5.4 all of the mutations are outside of the active site and are not in the important NADH-binding motif, suggesting that they were not likely to result in the embryo lethal phenotype seen in *kcr1* (Beaudoin *et al.*, 2009). It can also be seen that these mutations affect amino acids residues conserved across different species suggesting that they may be important for function generally.

Table 5.2. TILLING lines received for *KCR1*. Those shown in red are the lines that did not result in a synonymous mutation.

Stock	Effect	Zygoty
CS92957	G228E	Hetero
CS93417	F18=	Homo
CS93586	Intron	Hetero
CS93121	K225=	Homo
CS93750	V108=	Hetero
CS92096	G132R	Hetero
CS92473	T106I	Hetero
CS95460	D86N	Homo
CS95792	A68=	Homo
CS95786	L20=	Hetero
CS96082	L41=	Hetero

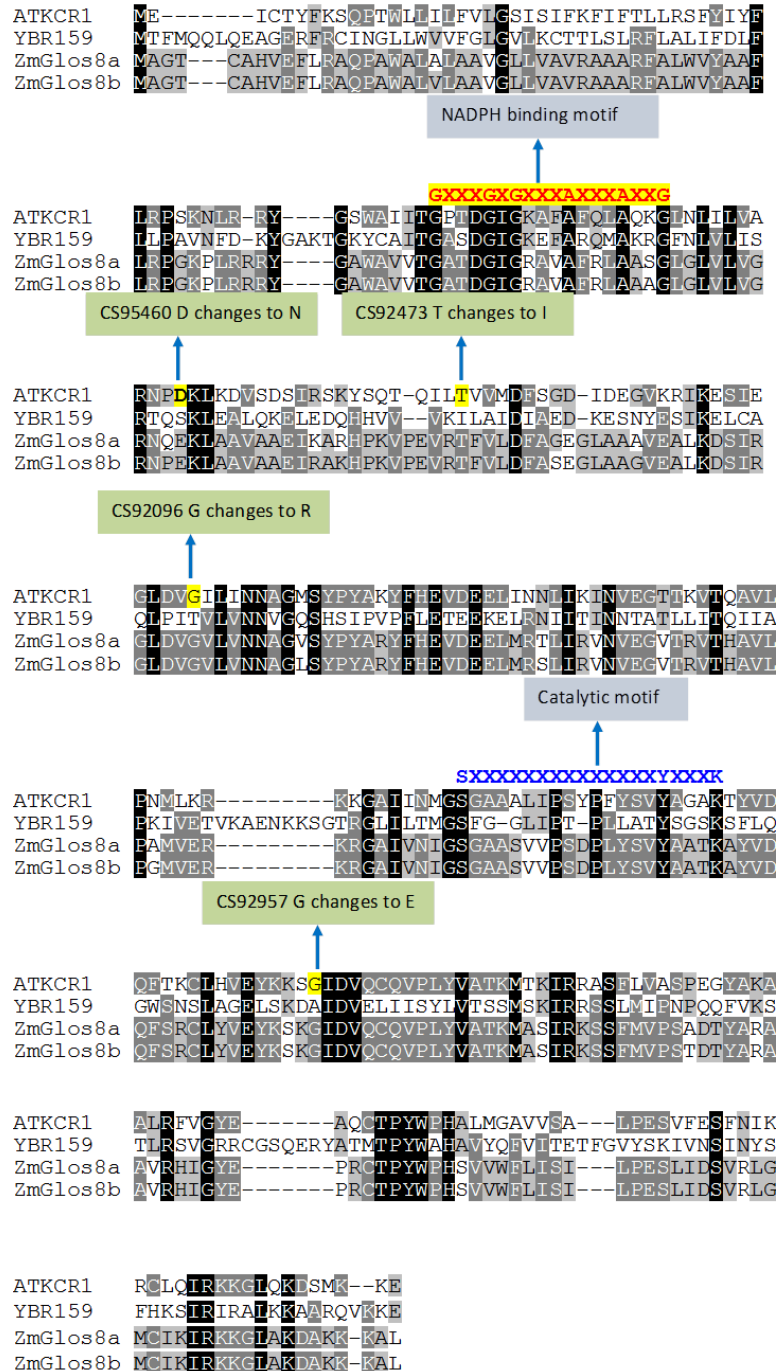


Figure 5.4 Position of the TILLING mutations in the amino acid sequence of KCR1. Amino acid sequence-comparisons of KCR proteins from different organisms, AtKCR1 from *Arabidopsis*, YBR159 from *S. Cerevisiae*, and GL8a and GL8b from *Z. mays*. The NADH binding motif (GX3GXG3AX3AX2G), and the essential catalytic motif (SX14YX3K) are also shown.

Some of the stocks that were received were heterozygous so first homozygotes of the mutations had to be isolated. Seeds were collected from these heterozygous plants and were sown to generate a mixed population that homozygous plants could

be isolated from. This involved using dCAP primers to determine the genotype of the plant within the mixed population. dCAP primers are designed to introduce a mutation into the DNA sequence of the gene of interest which is PCR amplified. This mutation along with the single nucleotide polymorphism (SNPs) that already exists between the TILLING lines and wild type plants creates a restriction site. The PCR products are incubated with the restriction enzyme which cuts either only the wild type strand or only the mutant strand (Neff *et al.*, 1998). The primers were designed using dCaps Finder 2.0 output (<http://helix.wustl.edu/dcaps/dcaps.html>), which gave a list of possible restriction sites which could be created. These restriction enzymes, were then checked to see if they cut anywhere else in the *KCR* gene sequence using the web based program, web cutter (<http://rna.lundberg.gu.se/cutter2/>). The dCAP primers used can be seen in Table 5.1, along with the restriction enzymes. All of the primers except CS92096 resulted in the generation of a restriction site in only the wild type PCR product, and therefore the restriction enzyme only cut the wild type product. The opposite was the case for CS92096. The wild type *KCRI* gene sequence is shown in Figure 5.5a, the binding site of the dCAP primers in the wild type *KCR* sequence are also shown. Figure 5.5b shows how the dCAP primers result in the generation of a restriction site in only the wild type strand and how this can be used to determine the genotype of the plant. The electrophoresis gel shown in Figure 5.5c shows a difference in the product size between wild type and the TILLING lines, showing that the restriction enzyme has just cut the PCR product generated from wild type DNA. Both products of the restriction digest cannot be seen as one of the products is smaller than can be detected on this gel (~30bp).

Forward genetic screen to identify novel genes involved in VLCFA metabolism

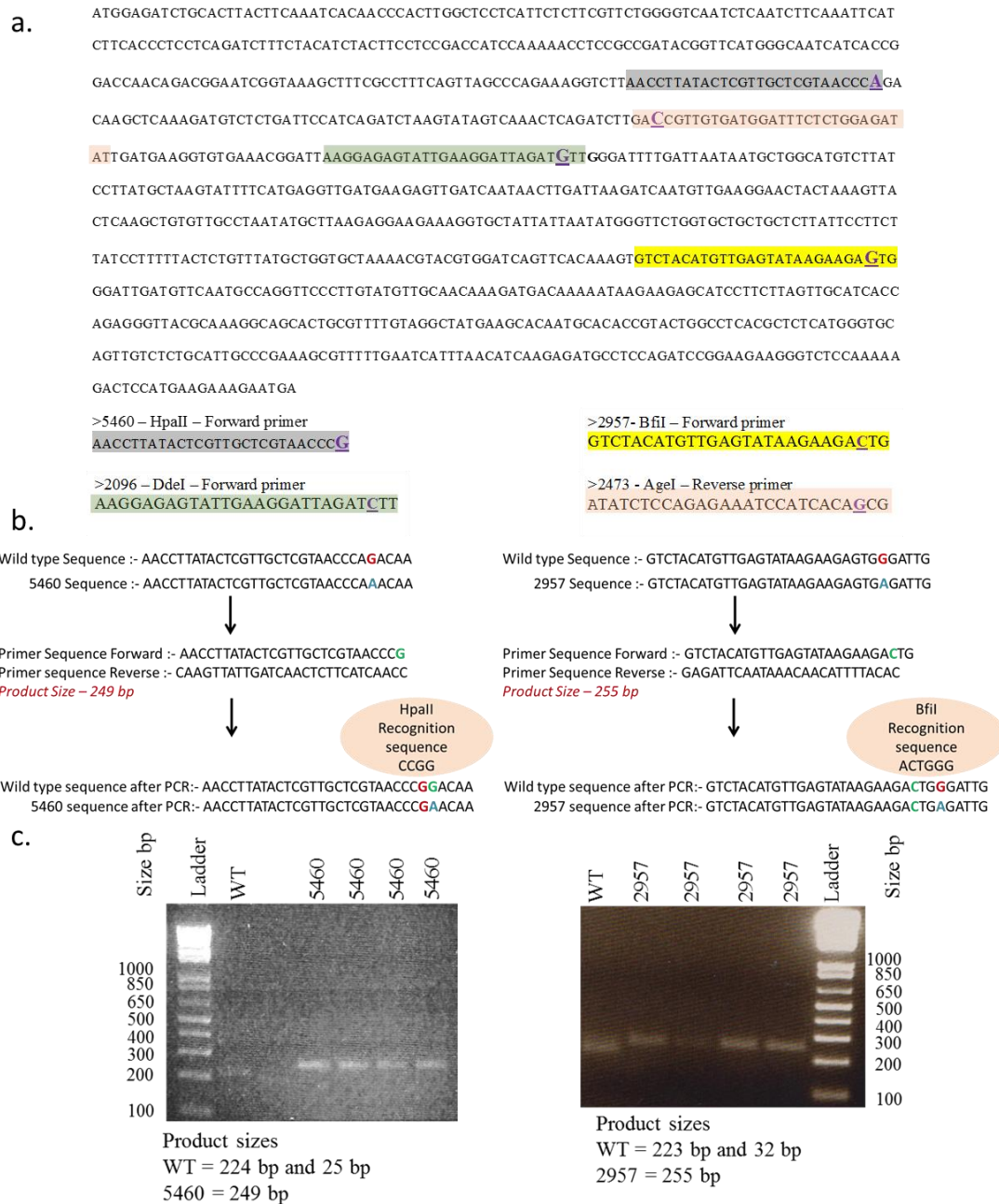


Figure 5.5. dCAP primers used to determine the genotype of TILLING lines. **a.** The *KCR1* gene sequence of *Arabidopsis*, showing the position of the dCAP primers and the nucleotide substitutions that occur. In both the *KCR* sequence and the primer sequences the nucleotide that is changed is underlined and in purple. **b.** shows the difference in sequences between the TILLING lines CS95460 and CS92957 and wild type, and how the primer sequences result in the generation of a restriction site in only the wild type DNA. **c.** Restriction digest of the TILLING lines using a 2.5% agarose gel. It can be seen that only the WT sequence was cut, and therefore the four 2957 and 5460 lines were homozygotes. The restriction enzymes used were BfiI for 2957 and HpaII for 5460.

Homozygotes of CS92957, CS95460 and CS92473 did show a phenotype of a lack of lateral roots (data not shown) as shown previously in the *KCR RNAi* lines (Beaudoin *et al.*, 2009). However this phenotype was not present after the first backcross so could not be used in a genetic screen. It was thought that this phenotype was the result of an unrelated mutation that was not in the *KCR* gene.

5.3.1.1.2. Isolating a homozygous *PAS2* TILLING line

TILLING lines were also obtained for *PAS2* (Table 5.3). Three of the stocks received resulted in a non-synonymous mutation. CS93669 and CS93511 were reported to result in an amino acid change at position 5 and 8 respectively. The S8F stock received did not have a mutation at position 8, and the *PAS2* sequence was the same as wild type, so no further analysis took place. Once homozygotes of G5S were obtained no phenotype was visible. In the case of the third non synonymous mutation, a stop codon was introduced, Q28*, and thus it would be expected to be an embryo lethal mutation since the absence of the *PAS2* enzyme is embryo lethal (Bach *et al.*, 2008). For this reason Q28* wasn't investigated any further.

Table 5.3. TILLING lines for *PAS2*. Those shown in red are the lines that did not result in a synonymous mutation.

Stock	Effect	Zygoty
CS93088	Intron	Homo
CS93422	Intron	Hetero
CS93432	Intron	Hetero
CS93511	G5S	Hetero
CS93541	Intron	Homo
CS92040	Intron	Hetero
CS93669	S8F	Hetero
CS93961	Q28*	Hetero
CS94001	Intron	Homo
CS92339	Intron	Hetero
CS93881	L53=	Hetero
CS94643	Intron	Homo

5.3.1.2. Identifying an inducible phenotype in the TILLING lines

Due to a lack of observable phenotype in the TILLING lines it was decided to try and induce a phenotype in the KCR TILLING lines. It has been shown that stress conditions can affect the expression level of various KCS, KCR and ECR enzymes (Joubes *et al.*, 2008). For example low temperature has been shown to result in a decrease in expression of KCR, ECR and many KCS enzymes whereas, high salt conditions have been shown to increase expression of KCR and ECR and has different effects on different KCS enzymes (Joubes *et al.*, 2008). In the case of salt stress where the expression of KCR is increased, if there was any reduction in activity as a result of the mutation in the TILLING lines the effect of salt maybe more severe due to its inability to increase function in high salt conditions. A similar effect could occur on varied temperature conditions. For this reason the KCR TILLING lines were subjected to temperature variation (30°C and 10°C). However the mutant plants did not appear different from the WT plants grown in the same conditions, (data not shown).

Herbicides known to affect VLCFA synthesis were also applied at a concentration just below the levels required to create a phenotype in wild type plants to see if the TILLING lines were more susceptible to the chemicals which could result in a shoot or root phenotype. The herbicides used were the same as those used in the Chapter 4. The concentrations that were used were as follows, flufenacet 0.5 nM, ethofumesate 0.5 µM and benfuresate 10 µM. Although some of the chemicals did result in some of the mutants showing stunted growth, it did not occur consistently so could not be used for a genetic screen. Conducting a forward genetic screen using chemical inhibitors is generally not ideal as it can lead to the selection of non-

Forward genetic screen to identify novel genes involved in VLCFA metabolism

specific mutations. A gene expression study used to see what genes were upregulated upon application of flufenacet and benfuresate shown that most genes were not specific to lipid synthesis and were involved in general wound response. It was therefore possible that the mutants identified could be involved in general defence or would be detoxifying mutants, rather than suppressors or enhancers of the elongase gene mutation. For these reasons the use of chemicals was no longer considered. Figure 5.6 shows the TILLING lines grown alongside WT plants on plates containing the different herbicides.

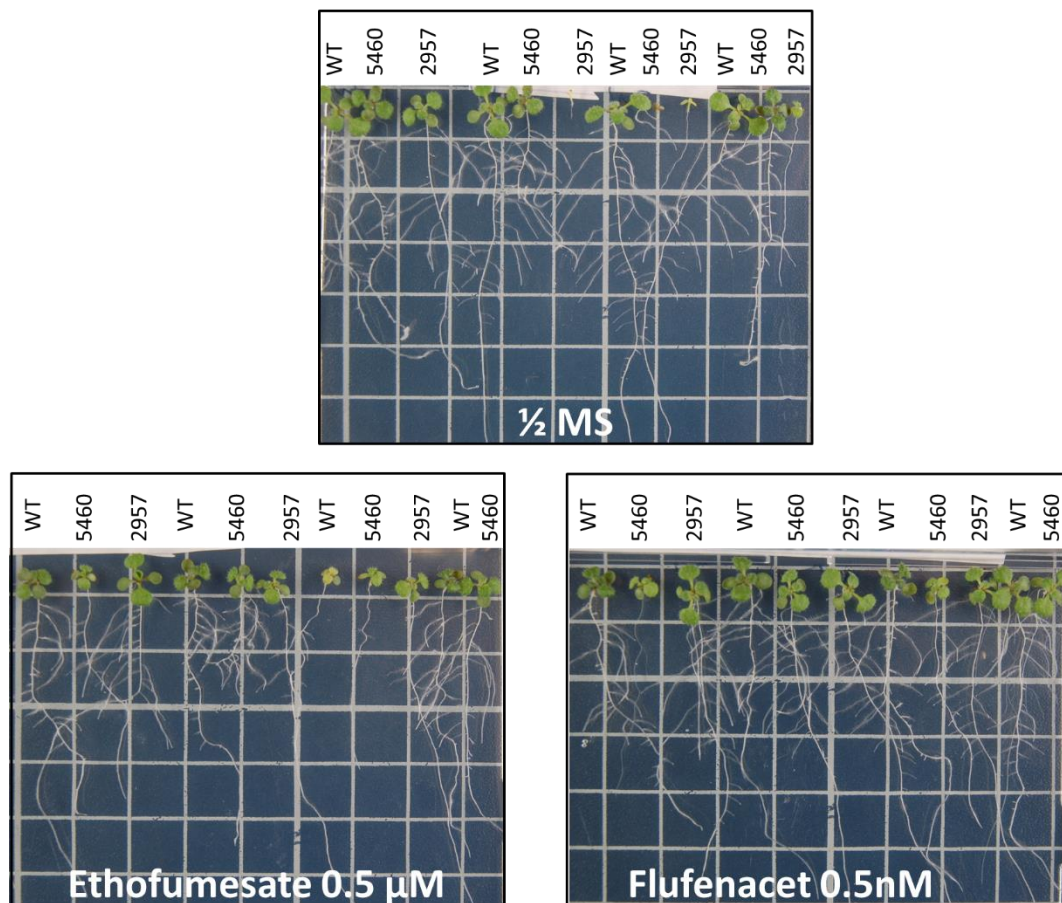


Figure 5.6 TILLING lines grown in the presence of herbicides. 8 day old seedlings arranged WT, 5460, 2957 4 times across the plate. No consist difference can be seen between the TILLING lines and the wild type plants.

5.3.1.3. *cer10-1* as the background for the genetic screen

Due to the absence of an observable phenotype to score in the *PAS2* and *KCR* TILLING lines we decided to carry out the EMS screen using a mutant of *CER10* (*cer10-1*) the last component of the elongase complex encoding the enoyl-CoA reductase, discussed in section 1.6.4. Although *cer10-1* displays morphological phenotypes at all developmental stages such as downward pointing cotyledons and curled leaves, floral bud fusion and reduced height of the fully grown plants are the easiest traits to score. The reason that the TILLING lines were initially considered over *cer10-1* is that mutants of *PAS2* and *KCR1* have shown previously to have a root phenotype. *cer10-1* does not show a root phenotype compared to its parent line Ler. If the TILLING lines had shown a root phenotype they could have been grown on plates and screened after 2 weeks. This would have required a shorter growth time and less space than is needed with *cer10-1* to observe the flower and height phenotype (plants have to be at least 4 weeks old to observe these phenotypic traits). As no appropriate alternative to *cer10-1* could be found this became the best option.

cer10-1 is in the Ler background and was obtained from an x-ray mutagenized population (Koornneef *et al.*, 1989). *cer10-1* has a 5kb deletion and/or rearrangement located in the promoter region, the 5'-untranslated region and at least 90 bp downstream of the translation start of the gene (Zheng *et al.*, 2005). *cer10-1* plants are smaller in size, have crinkled and smaller leaves, the inflorescences of the mutant are shorter, and the flower buds are also smaller and fused together, these phenotypes are stable and easy to observe making it a good candidates to be used for a genetic screen.

cer10-1 seeds were mutagenized with EMS to create a mutant population, with the aim of identifying additional components of VLCFA metabolism. This population was then searched for both enhancer and suppressor mutations of this original mutant. Plants in which these phenotypes were weaker were considered as potential suppressor mutations, this involved looking for mutations that made the plant appear more like wild type than *cer10-1* plants, for example increased height. It was thought that finding an enhancer mutation would be more difficult as the other two ubiquitously expressed components of the elongase complex are embryo lethal. Therefore if the levels of VLCFA are reduced any further than is already the case in *cer10-1* then it could be embryo lethal. Also, mutants of other already characterised elongase genes such as KCS enzymes could have potentially been identified which would have been eliminated by sequencing but this would still have been time consuming. Enhancer mutations would include fused aerial organs, or glossy or curly stems as seen in the *KCR RNAi* line (Beaudoin *et al.*, 2009), or any other phenotype that has been associated previously with VLCFA mutants. A table of the phenotypes that were associated with suppressor or enhancer mutants can be seen in Table 5.4.

Unlike *pas2* and *kcr1*, *cer10* null mutations are not embryo lethal suggesting that the *Arabidopsis* genome contains another gene with redundant activity. There are two close homologs of CER10 in *Arabidopsis* At5g16010 (DET2) and At2g38050 (TSC13-like). It was initially thought that these genes might have ECR activity and might be responsible for *cer10* mutant viability. Before attempting to cross the mutants in *Arabidopsis* to check for lethality of the double mutants, these genes were expressed in the yeast *tsc13* mutant to verify whether they can functional

complement this mutant. However these two genes did not complement the *tsc13* mutant in yeast (unpublished data), so were ruled out as orthologs of CER10. Therefore it is now thought that when absent this function is carried out by an unrelated gene. One hope of the screen was to find out what this other gene is and how its expression is regulated.

Table 5.4. Phenotypic traits used to identify both suppressor and enhancer mutations.

Suppressor	Enhancer
Less crinkled and larger leaves	Fused aerial organs
Larger less fused flower buds	Curly stems
Restored fertility	Glossy stems and sterile
Increased Size	Root phenotype

5.3.2. Conducting an EMS screen in the *cer10-1* mutant background

The steps taken to produce the mutagenized population can be seen in Figure 5.7. 5000 seeds were mutagenized with EMS. The seeds were grown to produce M₁ plants which were heterozygous for the induced mutation. These M₁ plants were then grouped into pools of 20 plants. The seeds were collected from the self-fertilised M₁ plants and the screening took place on the M₂ plants that could contain homozygous plants encoding recessive suppressor/enhancer mutations. The mutations produced by EMS are mainly recessive so the M₂ population would contain homozygous alleles for the mutated gene within the mixed population whereas the M₁ plants would be heterozygous for the gene. As stated earlier it is expected that any given recessive mutation in the M₂ generation will be present in the ratio 7:1 from the seeds that are produced from the M₁ plant. It was important that the number of M₂ plants grown would make it statistically likely that the mutations were present. For a 95% chance (i.e.3 SD), 500 plants were grown for each pool to give the best chance of observing the most mutations in the given

space. This would mean, 25 seeds on average would have been planted for each of the 20 M_1 plants in the pool. 1 in 8 of the 25 seeds would be homozygous for any given mutation, so you would expect to observe each mutation 3 times in the M_2 population. This assumes that the same number of seeds were produced from each plant, and that the same number of seeds were sown from each plant, both of which were unlikely but it does mean that a mutation should have appeared more than once in the pool. This gave an indication when a true mutation had been identified and this observed phenotype was more likely to be seen in the M_3 population as it is caused by a mutation rather than a phenotype that is a result of something that has just occurred to a single plant.

If a recessive homozygote plant had been selected in the M_2 population all of the plants in the M_3 population would have appeared the same, as all of the plants would have been homozygous for the mutation. If however a heterozygous plant has been selected in the M_2 population due to a dominant mutation being selected, the M_3 population would still have been segregating.

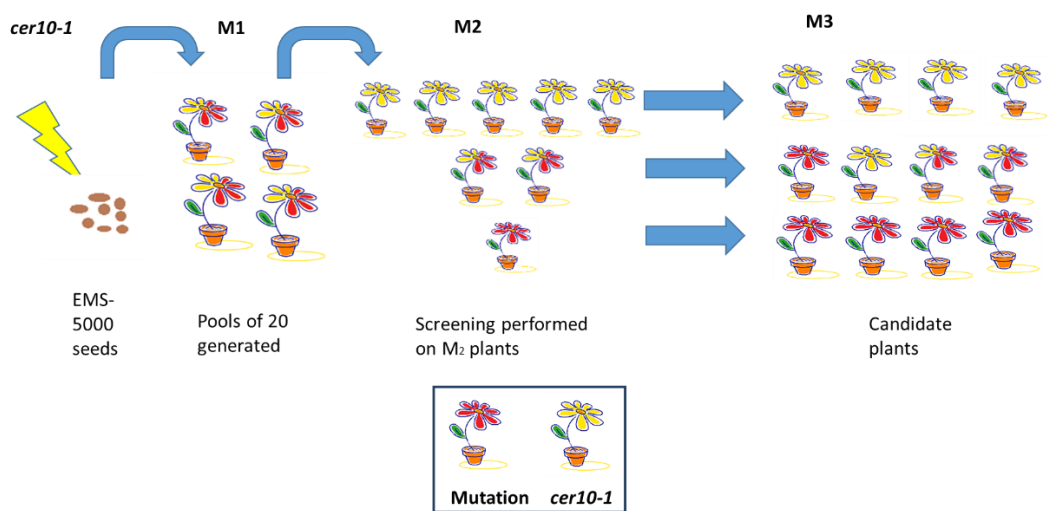


Figure 5.7. The steps taken in an EMS screen.

5.3.3. Screening of *cer10-1* M₂ pools for suppressor/enhancer mutations

20 of a total of 120 pools were screened for potential candidate mutations. This is a much reduced number of pools than would be expected. This was due to; a large number of M₁ seeds not germinating, some plants died at different stages in the life cycle of the plant, and a number of M₁ plants did not produce any seeds so M₂ plants could not be generated from them. The screening took place with 5 week old plants that were grown in soil. A number of potential enhancer mutations were identified that showed flower buds that were more tightly fused than in *cer10-1*. These plants were infertile and produced no seeds. In addition to this a number of potential suppressor mutations were found where the phenotype was no longer observed within the M₃ population. Two potential suppressor candidates were identified from two separate pools where the observed phenotype was stable throughout the M₃ population. Within the M₂ population two plants were identified that displayed the same suppressed phenotype for each of the suppressor candidates. One suppressor mutant, suppressor 36, had flower buds and fertility comparable to wild type but still maintained the reduced size of the *cer10-1* mutant, shown in Figure 5.8. The second suppressor mutant, suppressor 80, shows restored size of aerial organs but the flower buds remain fused, shown in Figure 5.9. The two suppressors were crossed to Ler plants. Both suppressors did not show a phenotype in the F₁ plants. Within the F₂ population, Ler, *cer10-1* and suppressor plants were identified but no additional phenotypes were present. Both suppressor phenotypes were not observed more than expected according to Mendelian genetics, for this reason it is expected that the suppressor mutants do not have an effect on wild type plants.

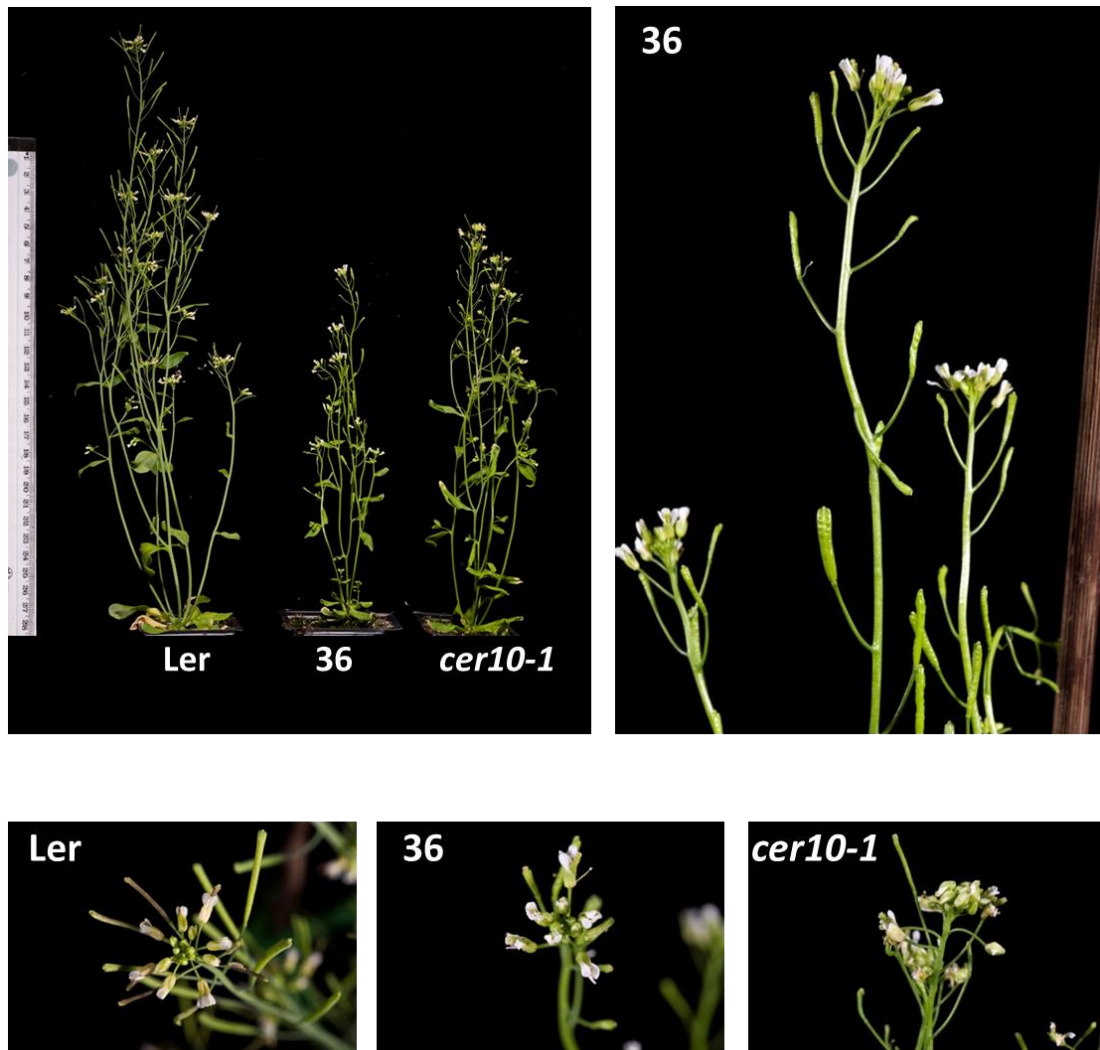


Figure 5.8. Phenotype of suppressor 36. Restored fertility and unfused flower buds can be seen. Suppressor 36 is still the same height as *cer10-1*, and therefore reduced compared to wild type.

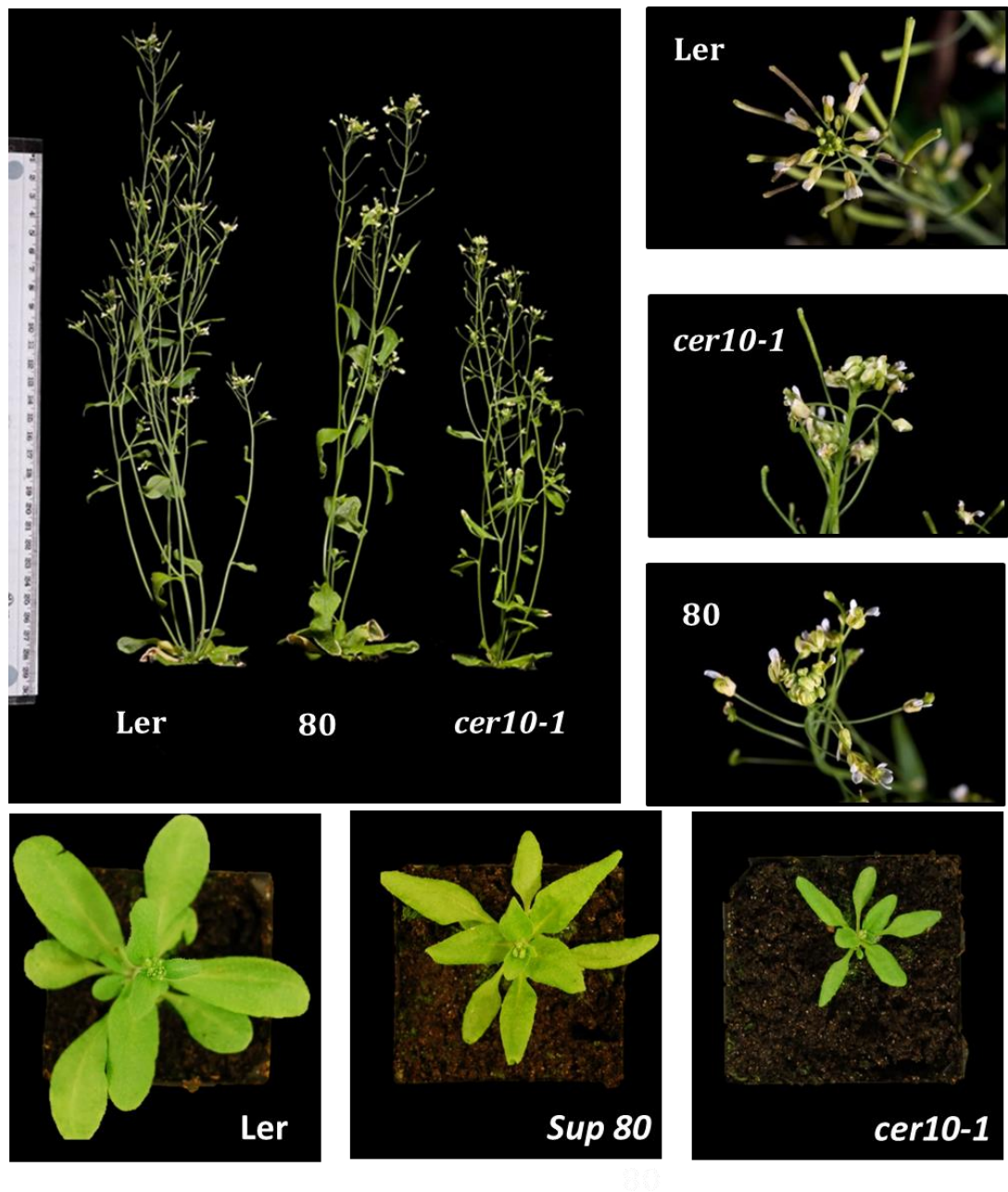


Figure 5.9. Phenotype of suppressor 80. Restored height and leaf area can be seen, suppressor 80 is much more similar in height to Ler than it is to *cer10-1*. The flower buds however are still fused.

5.3.4. Phenotypic characterisation of *cer10-1* suppressor lines

Figure 5.9 shows that suppressor 80 has a greater height than *cer10-1* and the plants also showed larger leaves than *cer10-1*. To quantify this 4 plants were measured at five weeks old, as at this point the plants had reached their final height. *cer10-1*

plants were on average 25% shorter than Ler plants, and suppressor 36 was not significantly different in height from *cer10-1*. Suppressor 80 had a height that was on average 8% shorter than Ler and there was not a significant difference between the height of Ler and suppressor 80, shown in Figure 5.10a.

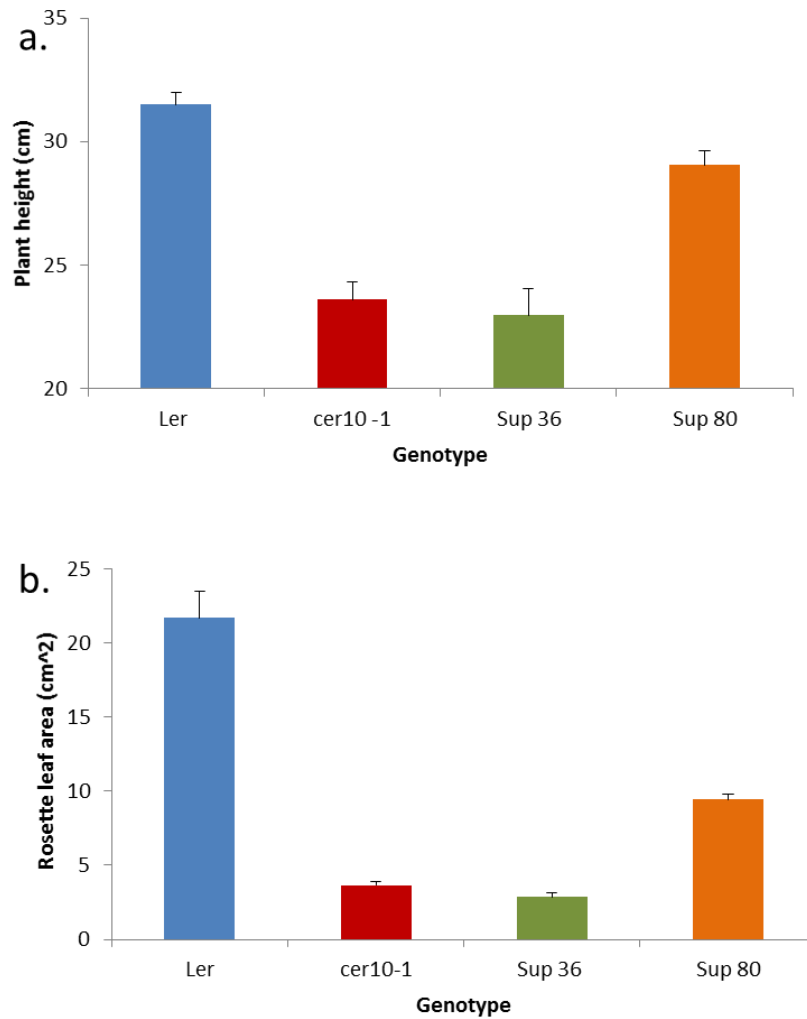


Figure 5.10 Phenotypic traits of suppressor plants (a) Height of plants and (b) rosette leaf area of suppressor and Ler plants. Values are means of +/- standard error of 4 replicates.

A similar pattern was shown in the rosette leaf area, shown in Figure 5.10b. The rosette leaf area was measured on three week old plants as the rosette leaves were healthy and easiest to record at this age. Although suppressor 80 rosette leaf area is

still 55% less than Ler, *cer10-1* is 74% less than Ler, and suppressor 80 leaf area is three times as much as *cer10-1*. This suggests that the rosette leaf area has been partially restored. Suppressor 36 had a 77% reduction in leaf area compared to Ler, and there was not a significant difference between *cer10-1* and suppressor 36.

5.3.5. Acyl-CoA profiling of *cer10-1* suppressor lines

The observed suppression of the *cer10-1* phenotypes described above could be due to many different factors and not just due to changes in lipid metabolism. Since the proportion of VLC-acyl-CoAs were shown to be reduced in the *cer10* mutant in Chapter 3, the acyl-CoAs of the suppressors were measured to see if the proportion of VLC-acyl-CoAs in the suppressors differed to *cer10-1* and whether the levels were restored to wild type levels. This would suggest that the mutations identified are suppressors of *cer10-1* and have a role in VLCFA metabolism.

Two week old suppressor plant material was separated into roots and shoots because, as shown in the previous lipidomics chapters, the phenotype of plants as well as the lipidomic profile is often organ specific. As was illustrated in Chapter 3, *cer10* showed a decrease in the proportion of total acyl-CoAs containing 22 carbon chains and greater in the shoots and in the roots, Figure 3.4 and 3.5. As shown in Figure 5.11a, there is an equal proportion of total VLC-acyl-CoAs in suppressor 80 and in Ler in the shoots, whereas suppressor 36 shows equal proportions to *cer10-1*. There is a 26% reduction in *cer10-1* and suppressor 36 compared to suppressor 80 and Ler, in acyl-CoAs with chain lengths of 24 carbons or greater. This shows that the proportion of VLCFA has been restored in suppressor 80. Figure 5.11b shows the proportion of VLC-acyl-CoAs in the roots, *cer10-1* does not show a significant

difference with Ler, in terms of the proportion of VLC-acyl-CoAs, and the two suppressors show a similar amount of VLC-acyl-CoAs as both *cer10-1* and Ler.

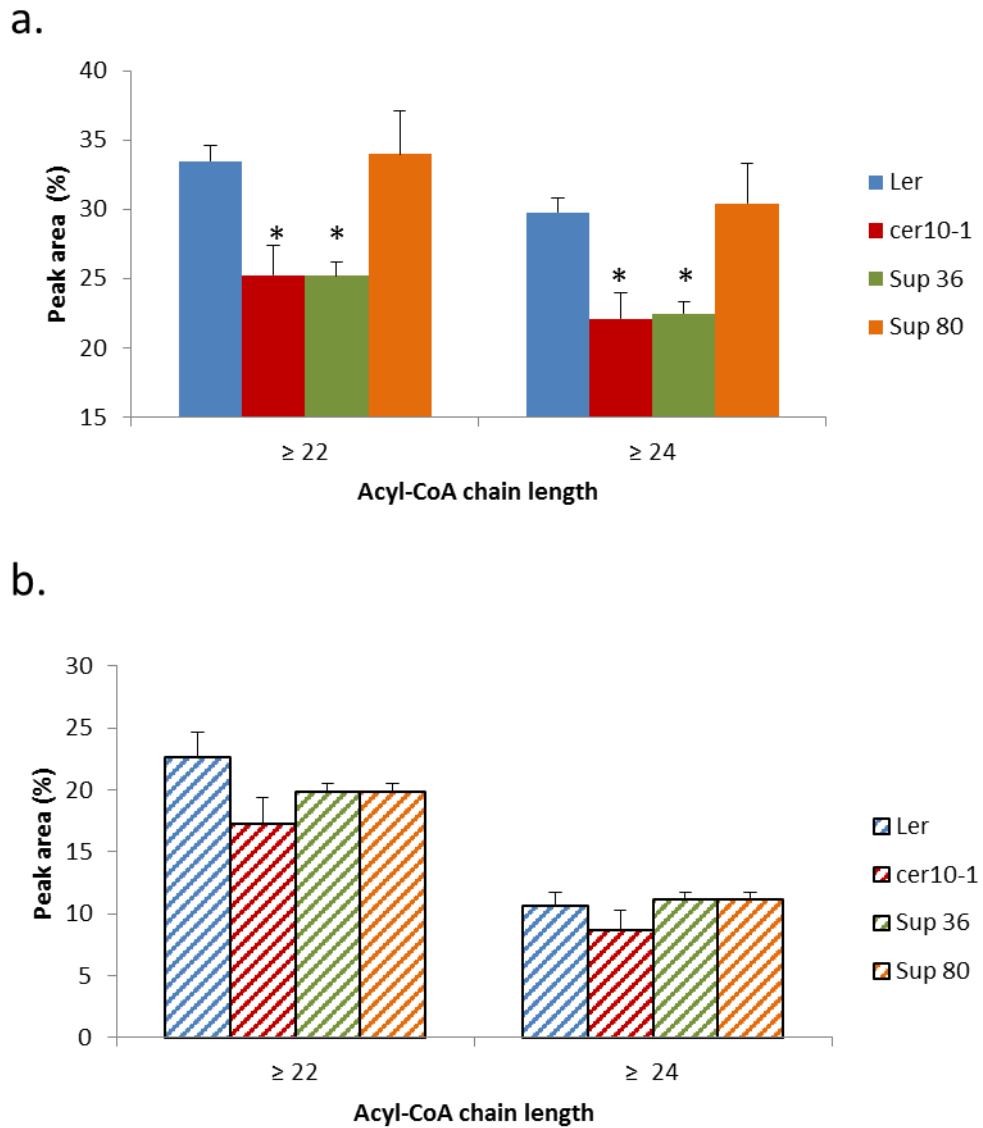


Figure 5.11. The proportion of VLC-acyl-CoAs in the suppressor mutants. (a) in the shoots and (b) in the roots. Showing the amount of acyl-CoAs containing 22 carbons or greater and the amount containing 24 carbons or greater in carbon chain length. Values are means of +/- standard error of 4 replicates. * Shows significant results based on ANOVA between Ler and samples, showing a F test p value of less than 0.05, and a difference in means greater than the LSD at 5% (degrees of freedom=9).

However the patterns shown in Figure 5.11 are not seen in all acyl CoAs measured.

Suppressor 36 exhibited an increase in the proportion of C24:0 (~20%) and C30:0

acyl-CoAs (~32%) in the shoots compared to *cer10-1* whereas the proportion of all other saturated VLC-CoAs showed non-significant decreases or showed consistent proportions with *cer10-1* (Figure 5.12a). The roots showed a similar effect, there is an increase in C24 (~12% increase in C24:0) and in C30 (~40% increase). All other VLCFAs exhibited non-significant decreases or amounts consistent with wild type in the roots.

As shown in Figure 5.11, suppressor 80 shows a significant increase in the total amount of acyl CoAs containing 22 carbons and greater in fatty acid chain length. However, as seen in Figure 5.12, a significant increase is only seen in 26:0 and 30:0, of all the chain lengths measured, although all chain lengths do show increases there is a large amount of variability in the data. Suppressor 80 does not show any significant changes in the roots compared to *cer10-1*. The acyl-CoA analysis therefore suggested that the suppressor mutations did change the composition of acyl-CoAs compared to *cer10-1*. However the composition of the acyl-CoA pool was not the same as wild type and any restoration of acyl-CoAs that did occur was tissue and chain length specific. Figure 5.12 only shows selected acyl-CoAs that were measured, the whole profile of acyl-CoAs that were recorded in Chapter 3 and 4 were also observed here, the results on the graph show the most interesting acyl-CoAs. The proportion of all the acyl-CoAs measured can be found in the appendix IV, as well as the results of statistical analysis that was performed.

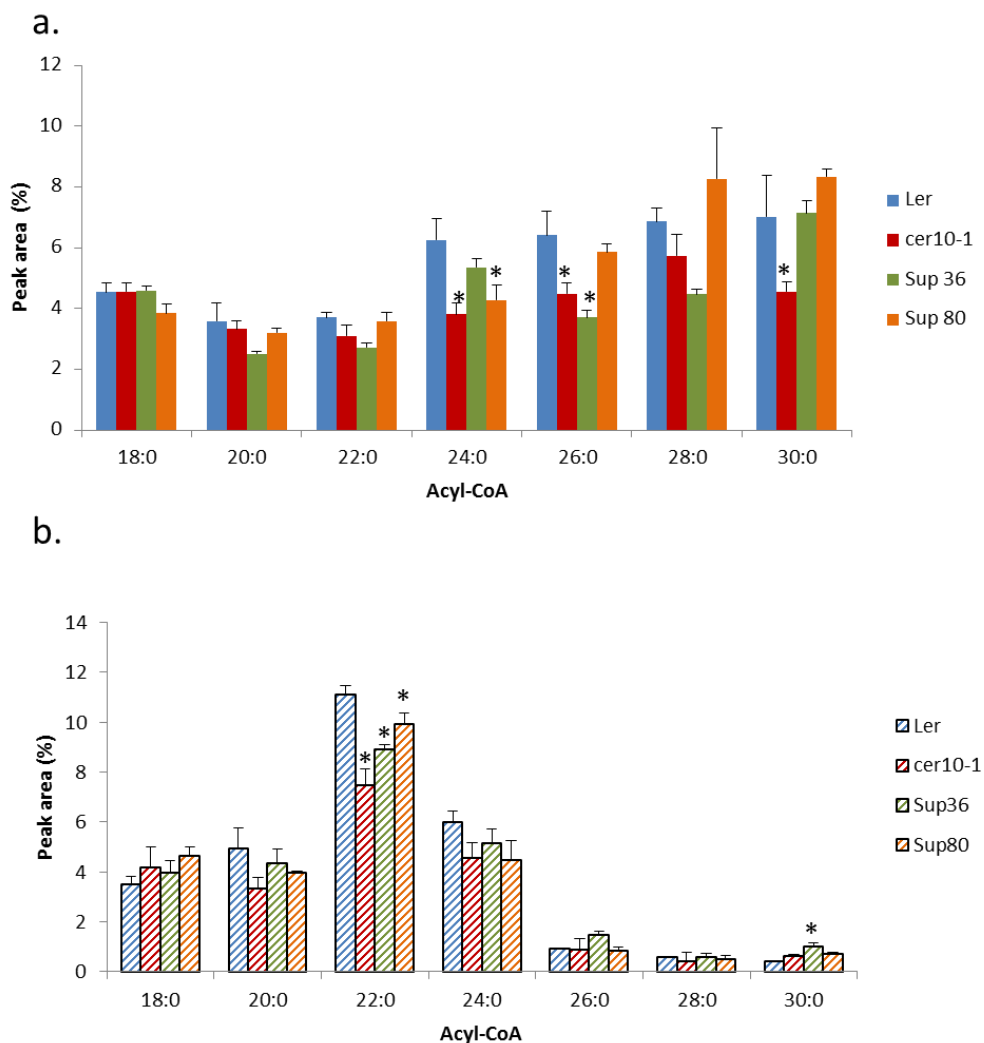


Figure 5.12. Acyl-CoA profiling of suppressor plants. (a) shoots and (b) roots, measured on 14 day old plants. Values are means of +/- standard error of 4 replicates. * Shows significant results based on ANOVA between Ler and samples, showing a F test p value of less than 0.05, and a difference in means greater than the LSD at 5% (degrees of freedom=9).

5.3.6. Wax analysis of *cer10-1* suppressor lines

5.3.6.1. Toluidine blue test

The main sink for acyl-CoAs greater than C26:0 in the shoots is cuticular wax. It has previously been reported that *cer10-1* shows a 60% reduction in stem wax (Zheng *et al.*, 2005). Suppressor 80 shows an increase in acyl-CoAs greater than C26:0, so it is expected that the levels of wax could have been restored in the suppressor. The toluidine blue test was used to see if the cuticle had been affected.

The cuticle acts as a hydrophobic barrier, therefore plants that do not have a fully functional cuticle, i.e. the composition of it has been altered, it is possible for hydrophilic dyes such as toluidine blue to penetrate and stain the plant. This is the basis of the test developed by Tanaka *et al.*, (2004) which used already characterized cuticle mutants, such as *fdh* mutant and various *cer* mutants and looked at the characteristic staining patterns that resulted. *cer10-1* was shown to have staining on the trichomes, a class V staining pattern.

As can be shown in Figure 5.13, the wild type, Ler, did not show any staining showing that it has a fully functional hydrophobic cuticle as would be expected. *cer10* has been shown previously to only have staining on the trichomes (Tanaka *et al.*, 2004), whereas in the growth conditions used here as can be seen in Figure 5.13, there was more substantial patchy staining, class II staining pattern. Suppressor 36 still shows patchy staining like *cer10-1*, although the amount of staining did appear to be reduced slightly. Suppressor 80 however did not show any staining like Ler, this suggest that the hydrophobic functionality of the cuticle of suppressor 80 had been restored. This correlates with the acyl-CoA data shown in Figure 5.12a, which showed that the proportion of acyl-CoA containing greater than 26 carbons had increased in proportion compared to *cer10-1*, as the wax component of the cuticle is thought to be a major sink of acyl-CoAs of this length.

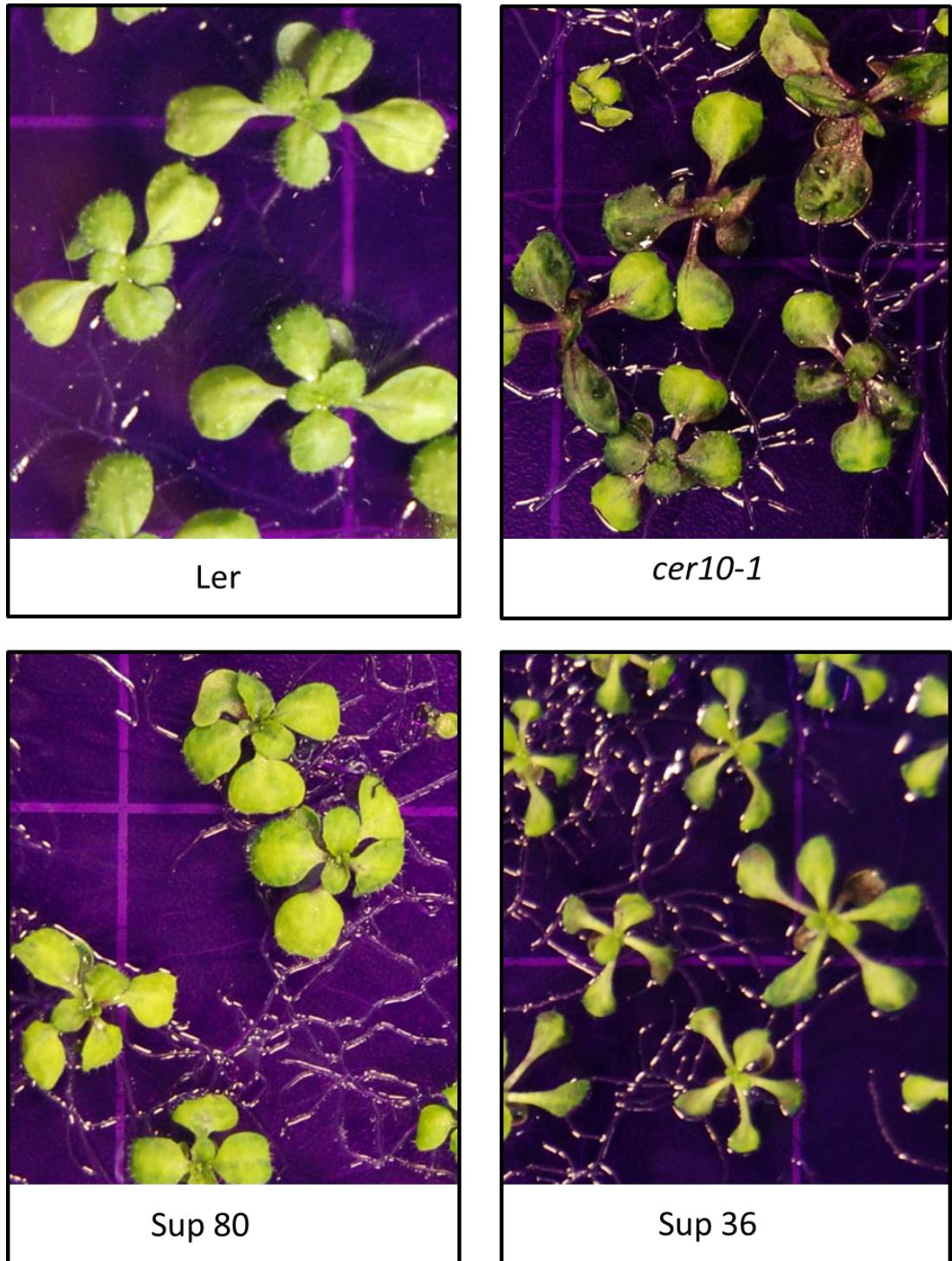


Figure 5.13 Toluidine blue test performed on the suppressor mutants to test the functionality of the cuticle.

5.3.6.2. Quantitative wax analysis of the stems of *cer10-1* suppressor plants

Of the two components of the cuticle, the cutin and the cuticular wax, only the wax contains VLCFA so these two results, from the Toluidine blue test and acyl-CoA data would suggest that cuticular wax content has been restored in suppressor 80. Detailed wax analysis was performed to see whether the composition of the wax had been affected, as well as whether the total amount of wax had been restored. The composition and quantity of the wax from the stems of suppressor 80 was compared with Ler and *cer10-1*. The stems of suppressor 36 were also analysed, since it showed an increase of C30:0 acyl-CoAs in the stems compared to *cer10-1*.

The total amount of wax was calculated by adding each of the individual wax components that could be detected together. The stems of *cer10-1* showed a 72% reduction in the amount of wax on the stems compared to Ler, previously this line was shown to result in a reduction of 60% compared Ler (Zheng *et al.*, 2005). The two suppressors showed a similar dramatic reduction in the total amount of wax, suppressor 36 showed a 73% reduction and suppressor 80 showed a 58% reduction, shown in Figure 5.14.

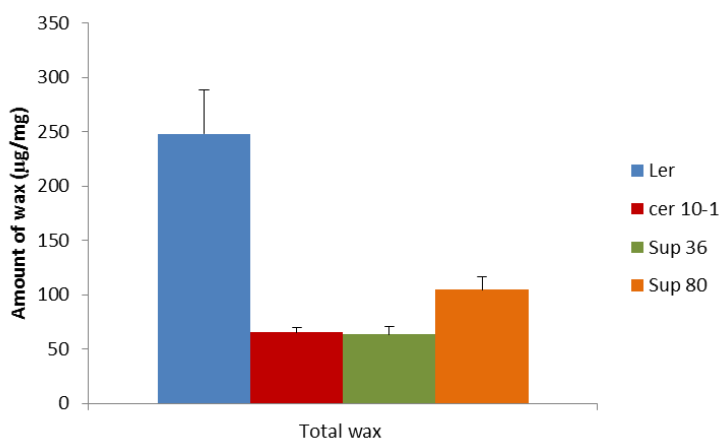


Figure 5.14. The total amount of wax in the two suppressor stems compared to Ler and *cer10-1*. Values are means of +/- standard error of 4 replicates.

It was then analysed whether there was a significant increase in the suppressor mutants compared to *cer10-1*, (Figure 5.15a). Suppressor 80, showed a 30% increase in total wax compared to *cer10-1*. Increases are shown in each of the wax components, but the most substantial increases were in the secondary alcohols, a 36% significant increase, (Figure 5.15e) and a significant increase of 59% in the ketones (Figure 5.15d), however the amounts still showed a substantial decrease compared to Ler. Suppressor 80 did not show a statistically significant increase in the total amount of primary alcohols, and within the different chain lengths it only showed an increase in C29, which is a minor component of the total. In the alkane component of wax, suppressor 80 showed a significant increase of 31% in the amount of alkanes containing 29 carbons, and there was a significant increase in the total amount of alkanes of 23%. No significant differences were seen in the total amount of wax or in the amount of any of the wax components or chain lengths between suppressor 36 and *cer10-1*. The results of the statistical analysis can be seen in appendix IV.

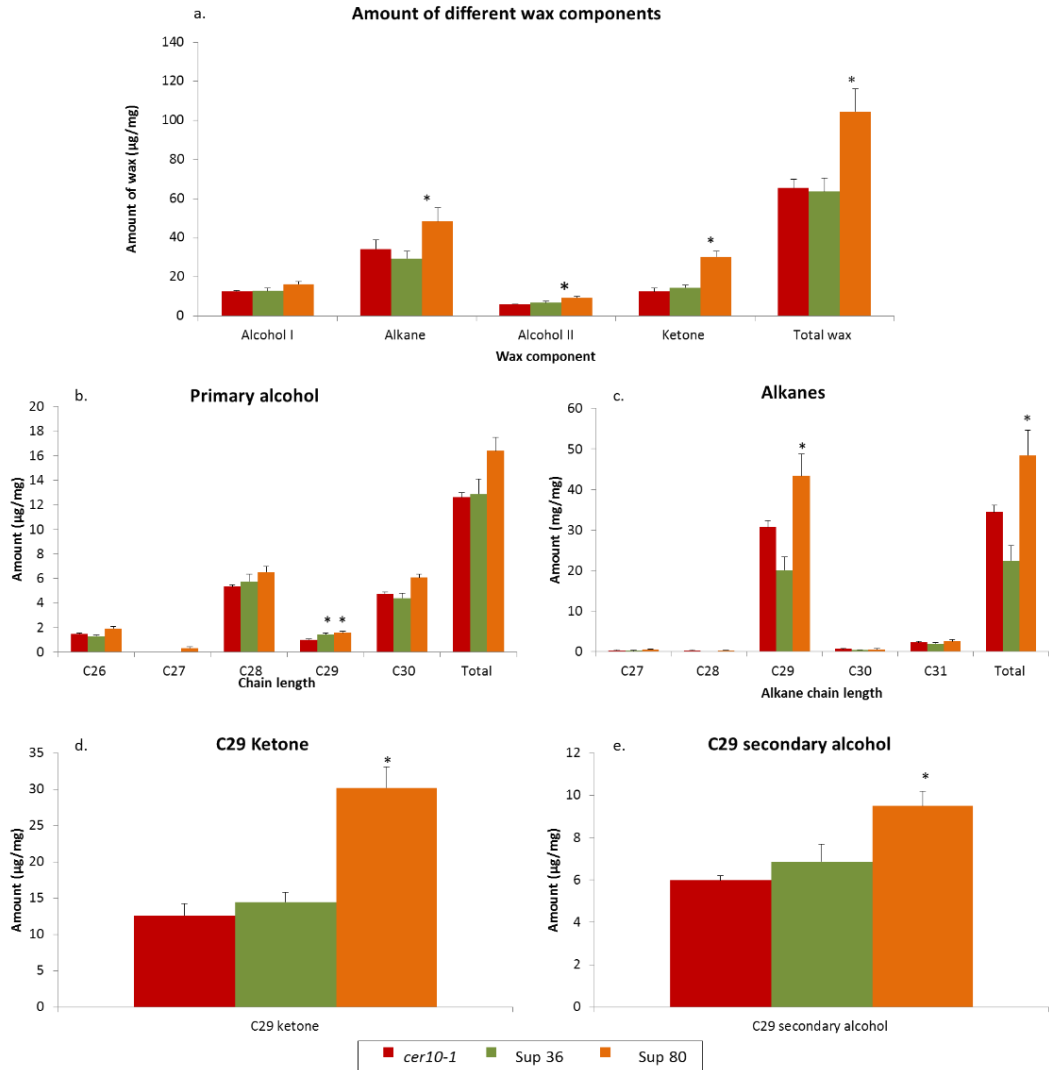


Figure 5.15. Quantity of stem wax components in suppressor plants compared to *cer10-1*. The amount of, (a) each of the wax components (b) primary alcohols, (c) alkanes, (d) ketone, and (e) secondary alcohol. Values are means of \pm standard error of 4 replicates. * Shows significant results based on ANOVA showing a F test p value of less than 0.05, and a difference in means greater than the LSD at 5% (degrees of freedom=6).

5.3.6.3. Wax composition of fused and unfused flowers

The composition of wax from the flowers of suppressor 36 were also analysed. The reason for observing the wax composition of suppressor 36 is that unlike *cer10-1* it has unfused flower buds. Fused flower buds are thought to be caused by defects in the epidermal cells but what causes this fused phenotype is not well understood. However a number of VLCFAs mutants show fused flowers, *fdh*, *KCR RNAi* and

cer10 (Pruitt *et al.*, 2000, Zheng *et al.*, 2005, Beaudoin *et al.*, 2009), so it is known that a reduction in amounts of VLCFA can cause this phenotype. Although it is not thought that a decrease in total wax levels are responsible for the fused phenotype (Voisin *et al.*, 2009), the composition and quantities of the different wax components could be affected in the mutants resulting in fused flower buds. Flower wax was extracted from suppressor 36 and Ler and compared with suppressor 80 and *cer10-1* to see if the fusion of the flower buds could be attributed to any component of the wax, be it quantity or composition.

It was not possible to use the same approach as was used for stem wax analysis. This is because analysing all the wax components at once on the GC-FID resulted in many of the compounds co-migrating due to the higher level of complexity of flower waxes compared to stem waxes. In addition a number of the components of flower waxes were present in quantities too small to be detected without prior separation. Instead the components of flower wax were first separated on a TLC plate, and each wax component was then individually analysed on the GC-FID and GC-MS. However, due to poor separation on the TLC plate and the lack of available standards it was not possible to analyse the total amount of flower wax. However, it was possible to analyse the amount of alkanes and primary alcohols. *cer10-1* showed a reduction in the total amount of primary alcohols, 37%, and alkanes, 60% reduction, compared to Ler and these amounts were not restored in suppressor 36, as shown in Figure 5.16. This shows that a decrease in the amount of these classes is not responsible for the fused flower phenotype.

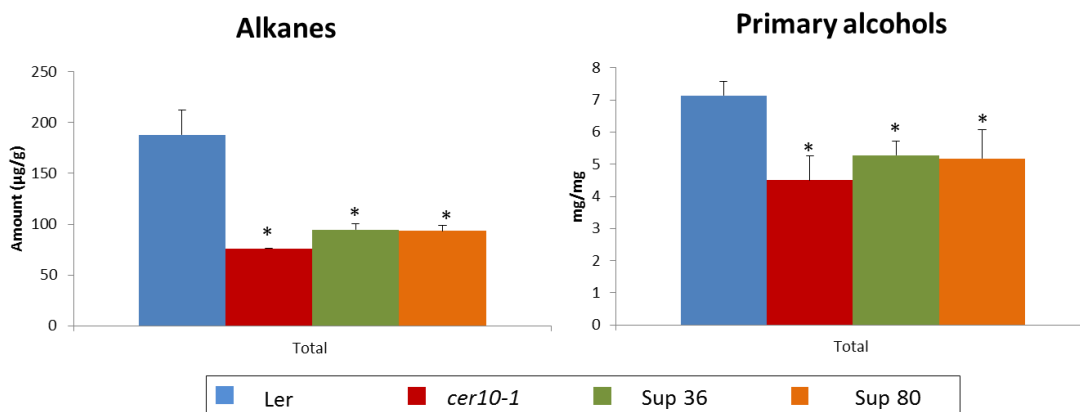


Figure 5.16. Total amount of alkanes and primary alcohols in the flowers of the suppressor mutants. Values are means of \pm standard error of 3 replicates. * Shows significant results based on ANOVAs showing a F test p value of less than 0.05, and a difference in means greater than the LSD at 5% (degrees of freedom=6).

The proportion that each of the different alkanes and primary alcohol chain lengths contributed to the total amount of each class was analysed to see if any differences were observed. C29 alkane, which is the most abundant alkane, showed no differences in proportion between plants with fused and unfused flower buds (data shown in appendix IV). There were differences in C30 alkanes which showed a lower proportion in suppressor 36 and Ler compared to *cer10-1* and suppressor 80, this was the only alkane where a correlation between fused and unfused flower buds could be seen, shown in Figure 5.17a. There was an increase of 24% in *cer10-1* compared to Ler. As this is a minor lipid compound it seems unlikely that this could be responsible for the fused phenotype, and in terms of actual quantities of alkane, in suppressor 36, the amount of C30 was still reduced compared to Ler, and showed the same amount as *cer10*.

Suppressor 36 did however produce a different pattern from Ler, *cer10* and suppressor 80 in its proportions of iso alkanes. An iso alkane contains a single methyl branch within the alkane molecule, at the α carbon within the carbon chain.

Suppressor 36 showed an increase in the proportion of C31 iso alkane (29% increased compared to *cer10-1*) and a substantial decrease in the proportion of C30 iso alkane (80% decreased compared to *cer10-1*). This can be seen in Figure 5.17 b-c. The same pattern was observed in the quantitated data, Figure 5.17d. There is an increase of 39% in C31 iso alkane and a decrease of 70% of C30 iso alkane compared to *cer10-1*. However the increase in C31: iso alkane is still 22% reduced compared to Ler.

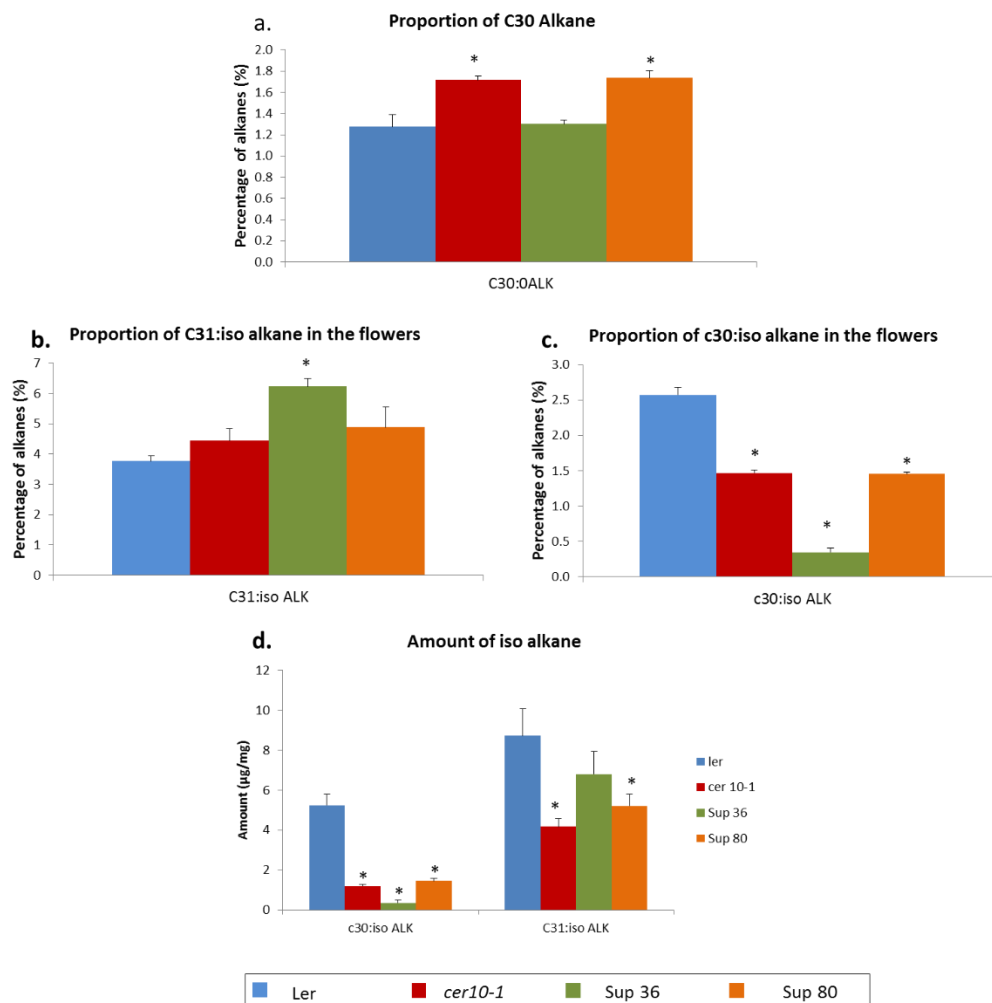


Figure 5.17. Quantity and percentage of alkanes in the flowers of the suppressor mutants. (a) the proportion of C30:0 alkane, (b) the proportion of C31 iso alkane, (c) the proportion of C30 iso alkane and (d) the amount of iso alkanes. Values are means of +/- standard error of 3 replicates. * Shows significant results based on ANOVA showing a F test p value of less than 0.05, and a difference in means greater than the LSD at 5% (degrees of freedom=6).

5.4. Discussion

5.4.1. Evaluation of *cer10-1* as a background for the genetic screen

cer10-1 was a good choice of background for the forward genetic screen to be performed in since, the phenotypic changes were easy to score and two interesting candidate suppressor mutants were identified. As expected it was difficult to isolate enhancer mutations of *cer10-1*, those that were identified did not produce any seeds so no further experiments could be performed.

There were however technical difficulties with the screen being performed in *cer10-1*, most notable the amount of space required to screen each pool, and how laborious and time consuming growing the plants to five weeks old was. For this reason only 20 of the 120 pools were screened, a larger number of potential suppressors could have been identified if more pools had been screened. To speed up this process a biochemical screen could be performed using the lipidomics platform discussed in Chapters 3 and 4. Using one of the lipid classes that showed reductions in *cer10*, the M₂ plants could then be screened for restoration of these levels to wild type levels or further reductions. The wax levels have been shown here to be reduced strongly in *cer10-1*, by 70%. However the protocol used to analyse cuticular wax is time consuming, and would need to be made more high throughput for this to be possible. This could be done using the toluidine blue test, to find suppressor mutants with restored cuticle. However this approach would only identify wax mutants and not mutants of general VLCFA metabolism. Chapter 3 showed that the levels of phospholipids containing VLCFAs were reduced in the shoots of *cer10*. As discussed in Chapter 2 this method is now high throughput and material can be grown on plates for two weeks for this analysis and low quantities

of tissue are required. It is possible that further pools could be screened for changes in the phospholipid profile compared to *cer10* in order to identify both suppressor and enhancer mutations which would greatly speed up the screening process.

The gene responsible for carrying out the function of CER10 in the absence of it was not identified. This was expected as it is thought that the plants would be embryo lethal, as the other two ubiquitously expressed components of the elongase are. It was possible that a mutation could have resulted in a reduced function of this protein such that the plants were still viable. However it would be expected that the plant would have much reduced levels of VLCFA, such that like *pas2-1* it would be unable to grow without the presence of sucrose and would not germinate directly in soil (Faure *et al.*, 1998). As the screening was performed in soil it would be unlikely to be identified even if the mutation was not lethal. In addition the reduced fertility of all of the elongase mutants would mean that it would be likely that very little, or in fact no seeds would be produced, this would mean further analysis would not be possible. If the M₁ plants had not been separated into pools, it is possible that more enhancer mutations might have been identified. Mutations resulting in very sick M₂ plants or that were embryo lethal could have been identified and the heterozygotes of the mutation could have been analysed further. The resulting M₂ plants from the M₁ plants could have been grown in more favourable conditions for example at higher humidity or in the presence of sucrose.

5.4.2. Explaining the candidate suppressor mutations

The two candidate suppressors that were identified, suppressor 80 and suppressor 36, were isolated from two separate pools and result in the restoration of different aspects of the *cer10* phenotype. Each suppressor line showed differences compared

to *cer10* in their acyl-CoA profile, suggesting that the mutations do have an effect on VLCFA metabolism and the restored phenotypes are not due to an unrelated function.

5.4.2.1. Explaining the phenotype of *cer10-1* suppressor 80

Suppressor 80, showed a restoration of the proportion of VLC-acyl-CoAs in the shoots, showing the same proportion of total VLC-acyl-CoAs of 22 carbons or greater in length as Ler. It also exhibited an increase in the total amount of wax, compared to *cer10-1*, although these levels have not been restored to Ler levels. This suggests that the level of VLCFAs has been increased in suppressor 80 compared to *cer10-1*. Suppressor 80 shows an increased height and increased leaf area compared to *cer10-1*, and these phenotypic restorations could be explained from an increased level of VLCFA, or by an increase in a particular chain length of VLCFA.

It has been shown previously that different levels of reduction in VLCFAs result in different phenotypes. This has been shown with herbicides that affect VLCFA levels, such that large reductions result in organ fusions due to uncontrolled cell division as seen in *pas2-1*. Whereas smaller decreases in VLCFA levels result in a smaller increase in cell division such that they have a larger leaf area (Nobusawa *et al.*, 2013). Different phenotypes resulting from different level of VLCFA reductions are also seen in the *KCR RNAi* lines. High levels of reduction in the *KCR RNAi* lines result in both glossy stems and fused organs, whereas lower levels of reduction only result in fused organs (Beaudoin *et al.*, 2009). If it is true that the different phenotypes observed are dependent on the level of reduction of VLCFAs, then it is

possible in suppressor 80 that an increase in the level of VLCFA means that the growth retardation phenotype seen in *cer10* plants is no longer observed, but the increase in VLCFA levels is not great enough to restore the flower bud phenotype. Figure 5.11 shows that the proportion of VLC-acyl CoAs in suppressor 80 is restored to wild type levels. Quantified data could be obtained to see if the actual quantities of VLCFAs are completely restored or whether a partial restoration in actual amounts could explain the restoration of only specific phenotypes. It is also possible that it is an increase in a specific chain length of VLCFA that is responsible for only certain phenotypes being restored; this will be discussed further below.

Plant organ growth is controlled by inter-cell-layer communication, and it is thought that signals from the epidermis control growth of ground tissues (Savaldi-Goldstein *et al.*, 2007). It is possible that these signals are not transported in the VLCFA mutants, possibly as a result of defects in sphingolipid trafficking, such that VLCFA mutants are smaller in size but when the levels of VLCFA are restored in suppressor 80 wild type growth is seen.

The reduced size of the organs of *cer10* was thought to be due to cell expansion defects as a result of defects in sphingolipid containing lipid rafts (Zheng *et al.*, 2005). It was shown in Chapter 3 that *cer10* does result in a reduction in the amount of sphingolipids containing VLCFAs in the shoots. Auxin is known to play many roles in cell expansion (Perrot-Rechenmann, 2010), and it is possible as stated in Chapter 3 that auxin is not distributed correctly due to defects in trafficking caused by a reduction in sphingolipids containing VLCFAs (Roudier *et al.*, 2010). This

could result in the cell expansion phenotype shown in *cer10*. It is possible that the restored levels of VLCFA in suppressor 80 means that the levels of sphingolipid containing VLCFAs have been restored so that this cell expansion phenotype is restored and a greater size of aerial organs is seen.

Mutations in other signalling pathways result in phenotypes similar to those seen in suppressor 80. Brassionsteroid (BR) catabolic mutants and plants overexpressing BR biosynthetic genes showed increased growth, including phenotypes that are shown in suppressor 80 such as larger rosette leaves and taller plants. The table produced by Vriet *et al.*, (2012) compiles a list of BR mutants and overexpressors that result in these enhanced growth phenotypes. As these plants show an increase in VLCFA it was expected that the increase in these proportion is responsible for the restored phenotype seen but an effect on other signalling pathways cannot be ruled out. It is possible that changes are seen in the VLCFA levels as a result of the mutation that has an indirect effect on VLCFA levels.

5.4.2.2. Explaining the phenotype of *cer10-1* suppressor 36

The wax level and composition of suppressor 36 was measured to see if the unfused flower bud phenotype, could be correlated with any changes in the wax profile of suppressor 36 compared to *cer10-1*. Only a reduction in the proportion of C30 alkane was shown to be common to Ler and suppressor 36 that was not seen in *cer10-1*. Suppressor 36 also showed changes in the proportion that C30 and C31 isoalkane made to the total. These minor lipid classes could affect cell adhesion and therefore result in the unfused flower buds. In addition the quantity of ketones, secondary alcohols and wax esters and the proportion that they contribute to the

total amount of wax was not analysed in the flower waxes. These levels could be restored in suppressor 36 and be responsible for the unfused flower buds. Standards of these compounds should be located or synthesized and improvements in the TLC technique made in order for these components of flower wax to be analysed in the mutants. It was not possible to analyse the wax esters in either the stems or the flowers of the suppressors. The analysis should therefore be performed again with more material to identify any changes in the wax esters that could be responsible for the phenotypes.

5.4.2.3. Differences are seen in the chain lengths that are restored in the two suppressors

It is possible that the increases in specific chain lengths shown in Figure 5.12 in suppressor 36 and suppressor 80 are responsible for the restoration of these specific phenotypes. As C24:0 is restored in the shoots of suppressor 36, which does show unfused flower buds, but is not in suppressor 80, which doesn't show unfused flower buds, this chain length could be responsible for this phenotype. The wild type levels of a particular chain length of VLCFA could explain the different restored phenotypes seen in the two suppressors. Sphingolipid and membrane lipid analysis would show whether the increases in particular chain lengths is transferred to these pools, this could help correlate the changes in phenotypes with a restored level of a particular lipid.

Chapter 6. Identifying the gene responsible for the suppressor phenotype

Once the *cer10-1* suppressor mutants isolated in Chapter 5 had been identified and characterised the next step was to identify the mutated gene in the genome. The identification of the gene would make it possible to understand the effect of the mutation on wild type plants in the absence of the *cer10* mutation. This would confirm whether the mutation is a true suppressor of VLCFA reduction and what other effects it may have on plant growth and development. Two different approaches were used to identify the position of the mutation; map based cloning and next generation sequencing (NGS).

6.1.1. Map based cloning

Map based cloning, also known as positional cloning or mapping, can be used to identify a mutated gene of interest. This approach has been used widely to identify genes responsible for mutant phenotypes in *Arabidopsis* (Chang *et al.*, 1988, Chang and Meyerowitz, 1991), especially the type of mutation generated by EMS, such as the mutant lines from Chapter 5. Map based cloning first involves the creation of an outcrossed F₂ population. This requires the crossing of two different accessions of *Arabidopsis* and collecting the seeds from this cross to produce F₁ plants. Seeds are collected from the F₁ plants to produce an F₂ population. The steps taken to generate a F₂ population are shown in Figure 6.1 a-c. According to Mendelian genetics, a population of F₂ hybrid plants should exhibit a 1:2:1 ratio of, homozygous parental type 1: heterozygous: homozygous parental type 2, for any point in the genome. The process of map-based cloning utilises this fact.

Plants with the phenotype of interest are selected from the F₂ population. Provided the phenotype is the result of a recessive mutation, by selecting plants based on the phenotype of interest, the genomic region responsible has to be the same as in the parental line (ie homozygous for parental type 1), the rest of the genome not under selection would be segregating according to Mendelian rules. It is possible to test an F₂ population at various points in the genome using molecular markers that are characteristic of a particular accession, so that a map of the level of homozygosity across that genome can be determined. Based on the principle that the closer to the site of the mutation the lower the frequency at which genetic recombination would have occurred, a region of high homozygosity for parental type 1 would be identified as the region in which the mutation is located, shown in Figure 6.1d.

A huge range of markers are now available to map the *Arabidopsis* genome across different accessions. The Col-0 accession was sequenced to produce the original *Arabidopsis* genome sequence (*Arabidopsis* Genome, 2000), however other accessions including Landsberg erecta (Ler) have subsequently been sequenced and polymorphisms that exist between the different accessions have been identified. Markers are then designed around these polymorphism which aim to distinguish between the accessions (Konieczny and Ausubel, 1993). It is now most common to use molecular markers based around sites such as insertion / deletion sequences (INDEL) and cleaved amplified polymorphic sequences (CAPs) which are both PCR markers. These markers produce results that are easy to analyse by PCR and electrophoresis to produce quick and reliable results, where it is possible to see differences between accessions (Konieczny and Ausubel, 1993, Bell and Ecker, 1994).

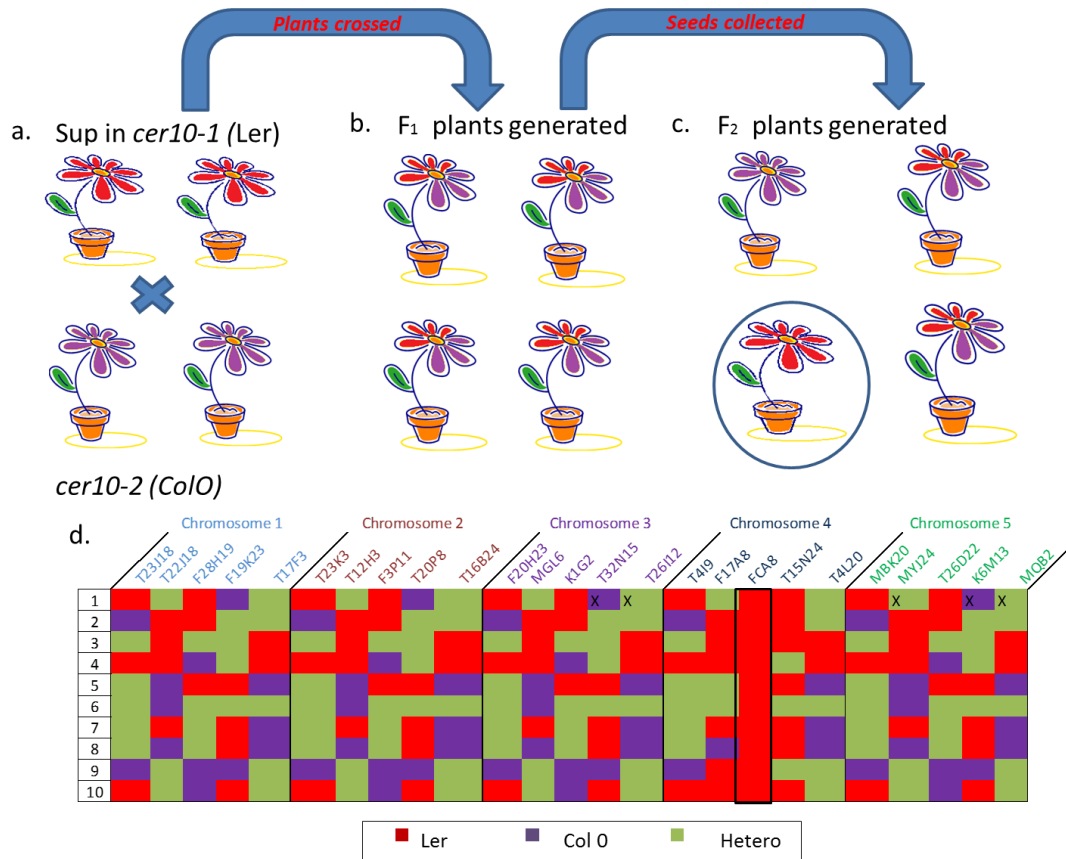


Figure 6.1. Generation of a F₂ population (based on the material used in this chapter). (a) Ler plants were outcrossed to Col-0 (b) F₁ plants were generated, (c) an F₂ segregating population was created. (d) the allele frequency across the genome of an F₂ plant selected for a phenotype of interest. The mutation would be located on chromosome 4, based on the use of markers suggested by (Hou *et al.*, 2010).

6.1.2. Next generation sequencing and SHOREmap

It is thought that by using the map based cloning method, it is possible to identify a gene responsible for a phenotype within a year (Jander *et al.*, 2002). Affordable genome resequencing has resulted in this being a much quicker method. The resequencing of the genome can be performed using the illumina sequencing by synthesis (SBS) approach which results in large numbers of short high quality reads being produced quickly and at an affordable cost. The background of how SBS works can be found in Figure 6.2. The SHORE pipeline was developed that allowed the short reads generated by SBS to be mapped to a reference genome. SNPs and 1-3 bp indels can be identified from the alignment of the sequences (Ossowski *et al.*,

2008). SHOREmap is an extension of this pipeline that uses the sequencing data from a pool of recombinants, provided from the illumina platform, to combine genome wide genotyping and candidate gene sequencing in a single step. This has greatly decreased the time needed to find a list of candidate mutations (Schneeberger *et al.*, 2009). The principles of this method is that the different SNPs that are present between the two parents of the recombinant population can be used to map the allele frequency within the F₂ population in much the same way as map based cloning. SHOREmap plots the allele frequency along the chromosome to produce a SHOREmap interval plot. This identifies local skews in the parental allele frequencies, which are introduced as a result of phenotypic selection of the mutant phenotype within a population of recombinants (skew towards the background the suppressor mutation was introduced into). This directs the analysis to an interval, that can be screened for unique SNPs using the same sequencing data used to create the plots (Schneeberger *et al.*, 2009).

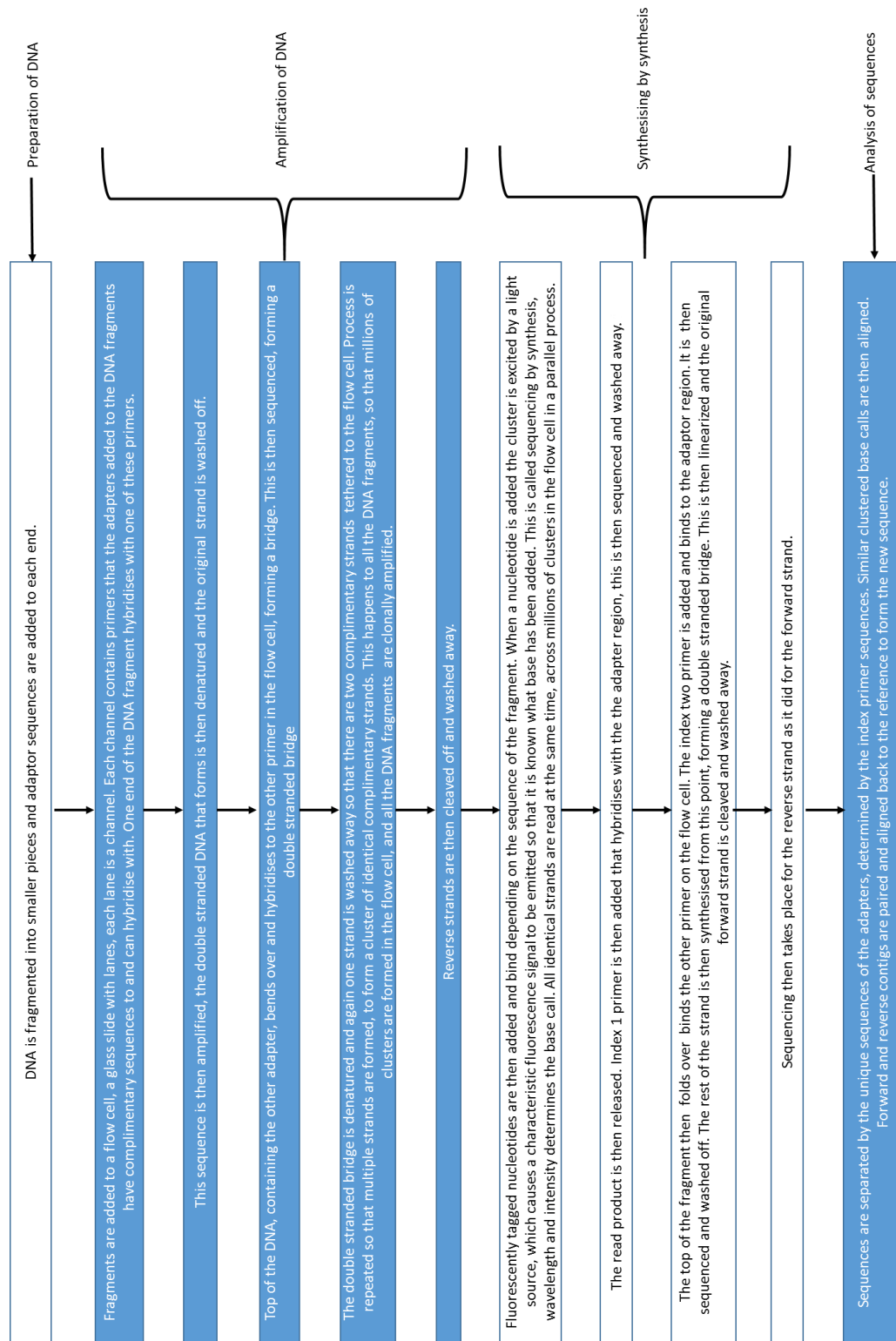


Figure 6.2. Paired end illumina next generation sequencing. Information obtained from (illumina, 2014)

6.2. Methods

6.2.1. Generation of an F₂ population

M₃ plants of suppressor lines 36 and 80, in the *cer10-1*(Ler) background were crossed to *cer10-2* (Col-0). The *cer10-2* line contains a mutation in the same gene as *cer10-1* but in the Col-0 background. The position of each of the mutations can be seen in Figure 6.3. The *cer10-2* line contains a T-DNA insertion in the second intron of the gene, as well as a deletion and a duplication of the region flanking the T-DNA insertion (Zheng *et al.*, 2005). Seeds were collected from these crossed plants, and grown to produce F₁ plants which were allowed to self-fertilize and the seeds were collected. These seeds were sown to produce the F₂ population. The steps taken to produce an F₂ population can be seen in Figure 6.1 a-c.

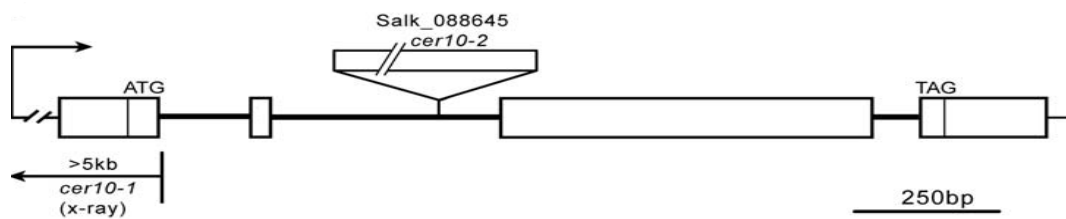


Figure 6.3. The structure of the *CER10* gene and position of the two *cer10* mutations. White boxes show the exons of the gene. Figure taken from (Zheng *et al.*, 2005).

6.2.2. Methods used for map based cloning

6.2.2.1. Quick DNA extractions

Roughly 0.5 cm² of leaf material was ground in 50 µl of 0.25 M sodium hydroxide (Fisher), and incubated at 96°C for 30 seconds. 50 µl of 0.25 M hydrochloric acid and 25 µl of 0.5 M Tris HCl pH 8 0.25% (v/v) IGEPAL-CA-630 (Octylphenoxypolyethoxyethanol) was added to each sample. The samples were then incubated at 96°C for 2 minutes, and stored at -20°C. This protocol was modified from that by Klimyuk *et al.*, (1993).

6.2.2.2. Primers and PCR conditions for mapping markers

A set of 25 evenly distributed INDEL markers, as suggested by Hou *et al.*, (2010) as part of the Arabidopsis mapping platform (AMP), were used to genotype the two mutations. The location on the chromosomes of each of these markers can be seen in Figure 6.4. These markers consist of primer pairs that produce different product sizes in Col-0 and Ler. The list of primer sequences can be found in appendix V. A 30 second extension time was used for all of the primers; the other PCR conditions were the same as those discussed in section 2.3.2. The annealing temperatures used can be found in appendix V. Additional markers were identified to further define the genomic region of interest. Information regarding these additional primers can also be found in appendix V.

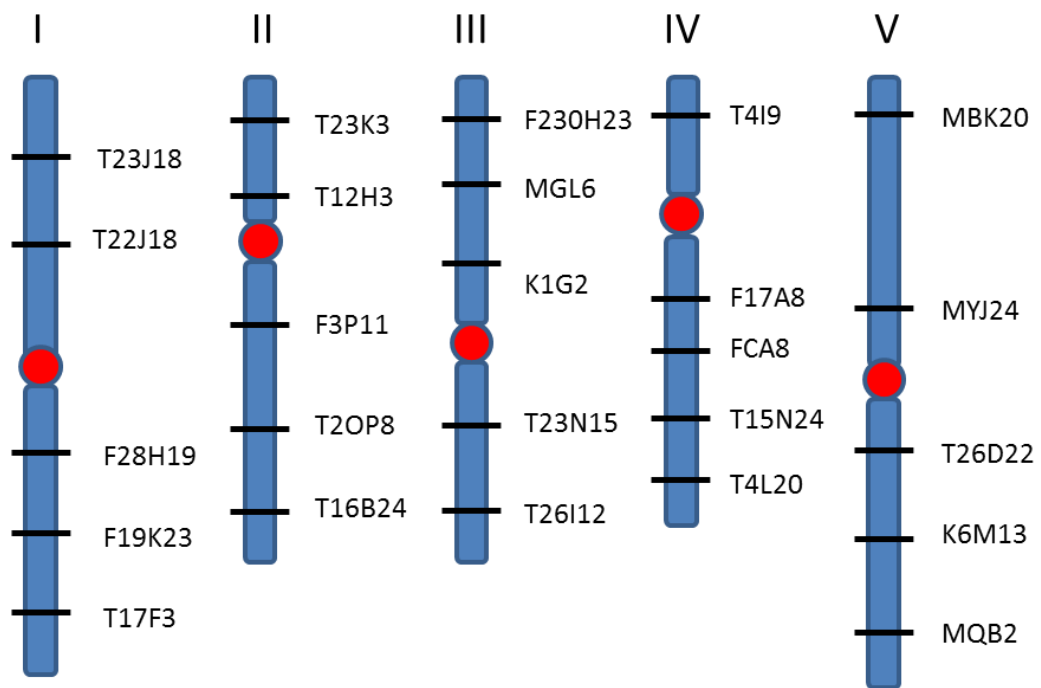


Figure 6.4. 25 evenly distributed INDEL markers used to genotype *Arabidopsis* plants. The position of the markers along the 5 chromosomes is shown. Diagram modified from (Hou *et al.*, 2010).

6.2.3. Preparation of DNA for NGS

6.2.3.1. Collection of F₂ material

A leaf was collected from each of the plants selected from the F₂ population. Roughly the same size leaf was taken from each plant to ensure each F₂ plant was equally represented. DNA was extracted from groups of 10 leaves. All of the DNA extractions were combined to form the final sample to be sent for NGS. The individual DNA extractions from the pools of 10 leaves were normalised by volume so that each pool was equally represented.

6.2.3.2. Extraction of DNA for NGS

6.2.3.2.1. CTAB DNA extractions

The DNA was first extracted using the CTAB extraction protocol, as described in section 2.3.1. This protocol was scaled up according to the weight of material used in the extraction.

6.2.3.2.2. DNeasy®Plant Mini kit extraction protocol

To purify the DNA further and to remove any RNA that was still present, the extracted DNA was purified using the DNeasy®Plant Mini kit (Qiagen), according to the manufacturer's instructions. A minor modification was made to this protocol in that the initial incubation with RNase was extended to 30 minutes.

6.2.3.2.3. Ethanol precipitation

After the first two extraction protocols the samples had a lower than desired 260/280 wavelength ratio (lower than 1.8) than was recommended for DNA samples to be used in NGS (data obtained from nanodrop reading, ND-1000 spectrophotometer). This is the ratio of DNA to other molecules in the sample such as proteins. For this reason an ethanol precipitation was performed to further purify the DNA. To the final volume of DNA, 1/10 volume of 3M sodium acetate (pH 5.5) was added to the sample along with 2.5 x volumes of 100% ethanol. Samples were

then incubated on ice for 1 hour. The samples were then centrifuged at 14,000 rpm for 20 minutes. The ethanol was removed and an equal volume of 70% ethanol was added. Samples were incubated on ice for 15 minutes and were then centrifuged at 14,000 rpm for 10 minutes. The ethanol was extracted and the samples were air dried to remove any trace ethanol, before being resuspended in nuclease free water (Qiagen). Samples were quantified using a Qubit® 2.0 Fluorometer (Invitrogen™, Life Technologies). The Qubit uses Molecular Probes® dyes which bind specifically to dsDNA and emit a signal when they bind. This gives information on the amount of dsDNA available for sequencing.

6.2.3.3. Validation of *cer10-1* and *cer10-2* mutations

The same PCR conditions as those described in section 2.3.2, were used to check the purity of both parental DNA lines, *cer10-1* and *cer10-2* before they were sent for NGS. PCR was carried out using primers which did not produce a product in the mutant lines, (negative PCR). Both sets of primer pairs were designed such that one primer of the pair binds in the area that is deleted in the mutants, such that no product is produced in the mutant, shown in Figure 6.5. The primer sequences used for these reactions can be found in Table 6.1.



Figure 6.5. The position of the primers used to detect the purity of the mutant lines.

Table 6.1. List of primers used for validating mutations and the conditions used for the PCR.

Primers used for validation of mutations	Annealing temperature and extension time
<i>cer10-1</i> for ATTCCTCATCTGGGTCT	- Annealing temperature 49°C
<i>cer10-1</i> rev AACGCTTCTTGCAGATCA	- Extension time 30 seconds
<i>cer10-2</i> for ACACAGTTTTGGATTTGAATTA	- Annealing temperature 52°C
<i>cer10-2</i> rev GTAGGAAACTTGTGGCCCC	- Extension time 40 seconds

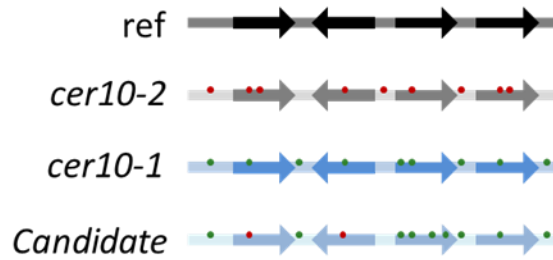
6.2.3.4. Identification of SNPs from the NGS data

The analysis of the sequencing data was performed by Professor Antony Hall's group within the University of Liverpool Genomic Centre. The steps taken to analyse the sequencing data to find the candidate SNPs in the suppressor mutant, can be found in Figure 6.6. The short reads from the sequencing data of the parental lines were first mapped to the TAIR10 *Arabidopsis* sequence, (Figure 6.6a), to identify any SNPs that were different from the reference genome, using the SHORE pipeline (Ossowski *et al.*, 2008). From this, 1300 SNPs were found in *cer10-2* sequence, and ~541,400 SNPs were identified in the *cer10-1* sequence. The two bulked segregate populations were then mapped to the *cer10-1* reference sequence that was produced from the first alignment.

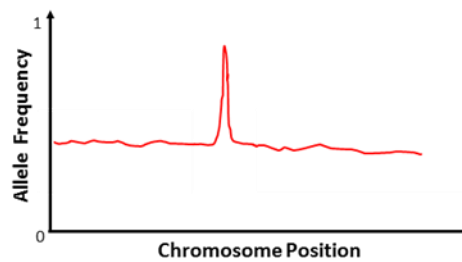
A SHOREmap plot was generated from this data (Figure 6.6b), which is a plot of the homozygous SNPs of Ler and Col-0 across each of the chromosomes. The plots were used to identify regions which showed conserved SNP homozygosity between the bulked DNA samples of the F₂ plants and the *cer10-1* parental line, as this was the line the suppressor mutation was originally isolated from. This involved identifying the area of highest allele frequency. The frequencies of allele SNPs were identified across the chromosome at 200,000 bp, using sliding window analysis. Within this identified region of highest allele frequency, SNPs were identified where the suppressor mutants differed to the parental genomes, this was used to generate a list of candidate SNPs, Figure 6.6c. The SNPs were then analysed so the effect of the SNPs on the amino acid sequence could be determined Figure 6.6d.

Identifying the gene responsible for the suppressor phenotype

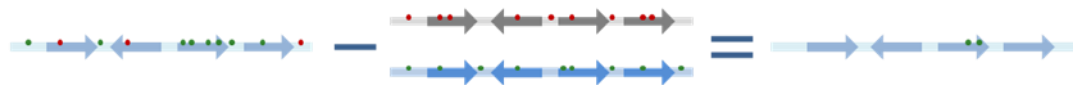
a. Map the data to the reference genome, and identify any SNPs.



b. Generate a plot of the allele frequency, compared to *cer10-1*, across each of the chromosomes. A candidate region is identified with a high allele frequency.



c. Remove the SNPs from the parental lines from the candidate region



d. Identify the effect of the SNPs from within that candidate region

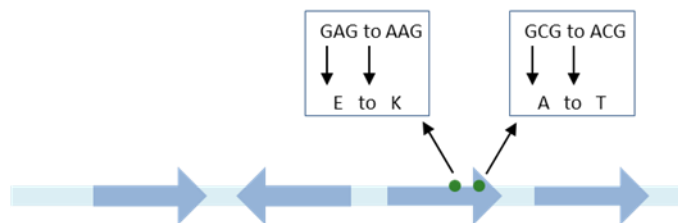


Figure 6.6. The SHOREmap pipeline to identify the SNPs in the suppressor mutants. Diagram modified from Uchida *et al.*, (2014).

6.3. Results

6.3.1. Generating a F₂ population for suppressor 36 and suppressor 80

The F₂ mapping population was generated by crossing the M₃ suppressor lines (Ler), to *cer10-2* (Col-0). Crosses were successful regardless of whether the M₃ plant was used as the maternal or paternal parent. The F₁ plants were observed for the suppressor 36 and 80 phenotypes, however none were detected, suggesting that the mutations were recessive in both cases. The F₁ plants generated were analysed to ensure the cross was successful by using one of the INDEL markers, the result of this test is shown in Figure 6.7. Plants where the suppressor phenotype was observed were selected from the F₂ population. Within the F₂ population the phenotype of suppressor 36 was easy to observe as the unfused flower buds were easy to distinguish from the fused flower buds seen in the rest of the plants within the F₂ population, as shown in Figure 6.8.

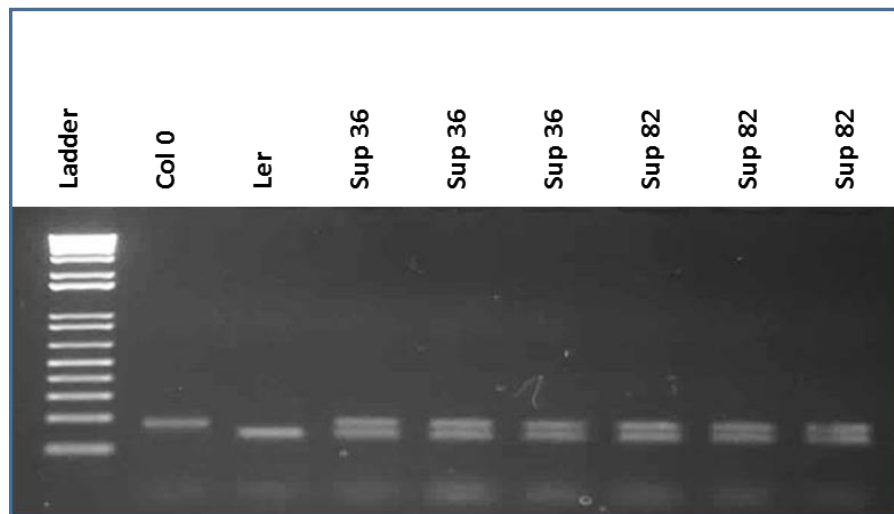


Figure 6.7. Genotyping F₁ plants. T26D22 one of the INDEL mapping primers used to show that the cross between *cer10-1* and *cer10-2* was successful and the F₁ plants were heterozygous.

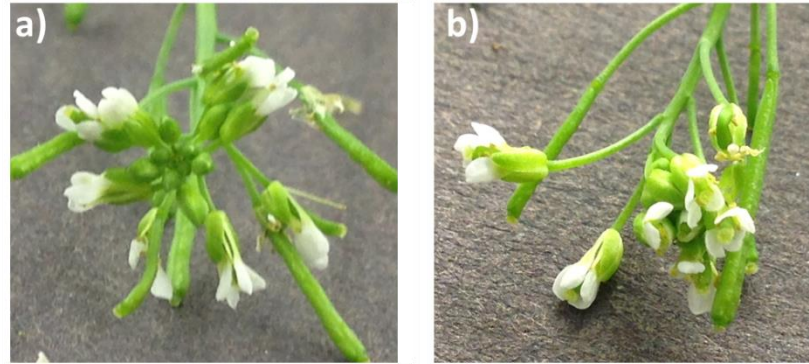


Figure 6.8. Floral phenotype of plants within the F₂ population of suppressor 36. (a) The unfused flower phenotype of suppressor 36 (b) the fused flower buds characteristic of *cer10-1*.

Selecting plants exhibiting the suppressor 80 phenotype in the F₂ population was more difficult. Suppressor 80 showed taller plants with a larger leaf area than *cer10-1*. However as *cer10-2* plants are taller than *cer10-1* it was difficult to observe what was due to the effects of the mutation and what was the result of the differences between accessions. For this reason only plants which were taller than *cer10-2* were selected based on height. An example of an F₂ suppressor 80 plant that was selected can be seen in Figure 6.9.



Figure 6.9 A suppressor 80 plant selected from the F₂ population.

6.3.2. Molecular mapping of the *cer10-1* suppressor mutants

6.3.2.1. Mapping Suppressor 36

Within the F₂ suppressor 36 population, seven individuals, from a population of forty plants, were initially selected as they exhibited the suppressor phenotype. These individuals were analysed with the 25 markers, shown in Figure 6.4. The number of Ler, Col-0 and heterozygous alleles for each marker was recorded for each F₂ plant. Chi squared tests were used to look for areas which showed a significant deviation from the expected result (1:2:1, Ler:hetero:Col-0). The genotypic results from these initial 25 markers tested with 7 individual F₂ plants can be found in appendix V, along with the chi squared results for each of the markers. The chi squared results showed that only two markers at the top of chromosome 2 resulted in a significant deviation ($p < 0.05$), T23K3 and T12H3. An image of the electrophoresis agarose gel of these two markers is shown in Figure 6.10.

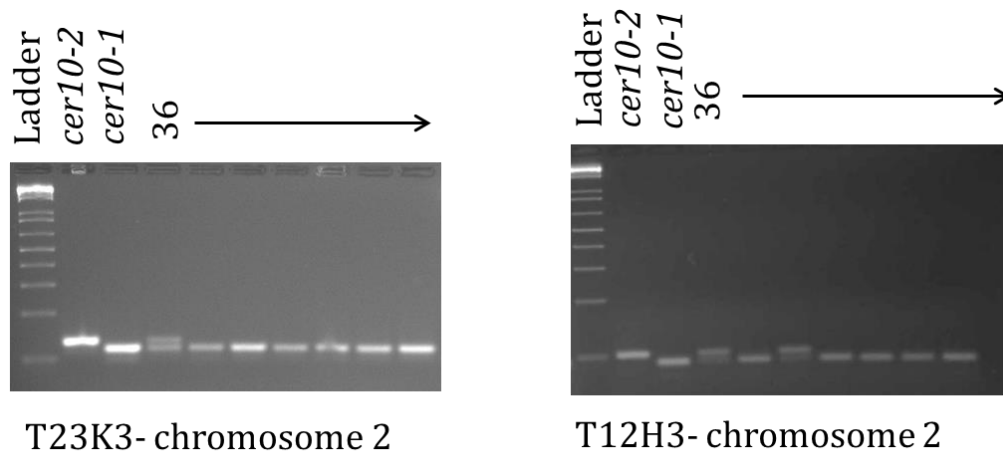


Figure 6.10. The genotyping results for suppressor 36, showing the two markers that showed significant results from a chi-squared test. *cer10-2* (Col 0) and *cer10-1* (Ler) were used as controls.

The top of chromosome 2 was therefore considered as a potential region in which this suppressor mutation could be located. In order to map the mutation to a smaller region of the chromosome, additional markers were obtained for the region between the two markers at the top of chromosome 2 and a greater number of individuals

Identifying the gene responsible for the suppressor phenotype

from the F₂ population were analysed (50-100 individuals). The position of the chosen markers on chromosome 2 can be seen in Figure 6.11. Chi squared test showed that all of the additional markers resulted in a significant deviation from the expected result, as shown in Table 6.2. These results suggested that the initial pass was accurate and the suppressor mutation is at the top of chromosome 2. However the additional markers did not reduce the candidate region containing the mutation any further, as all of the markers tested produced a highly significant result (p value < 0.001). Therefore map based cloning suggested that the mutation responsible for the phenotype in suppressor 36 was at the top arm of chromosome 2.

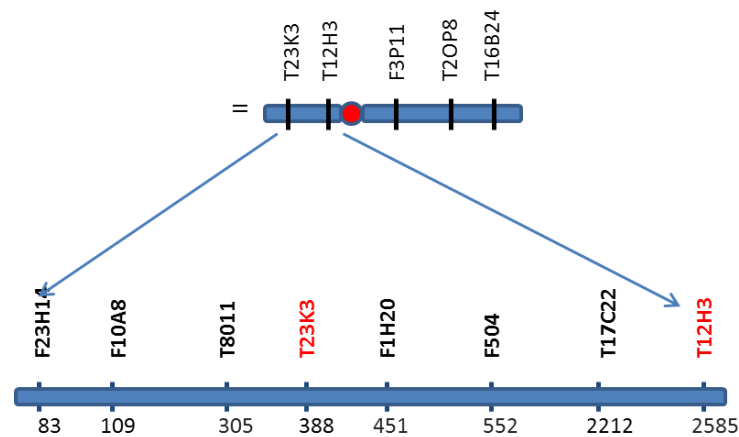


Figure 6.11 The position of additional markers used for genotyping suppressor 36. The name of the primers can be seen on the top line and the numbers show how many bases (kbp) along the chromosome the markers are.

Table 6.2. Chi-squared results for suppressor 36. The number of individuals in the test is shown by 'n', the result of the chi squared test ' χ^2 ' (on 2 d.f) and the p- values show where the results were significant.

Marker	Distance (kbp)	Ler (%)	Col-0 (%)	Het (%)	Individuals analysed (n)	χ^2 statistic	p-value
F23H14	83	66.27	2.41	31.33	83	79.27	<0.001
F10A8	109	46.75	2.60	50.65	77	30.04	<0.001
T8011	305	50.00	3.75	46.25	80	34.68	<0.001
T23K3	388	50.00	3.77	46.23	106	45.91	<0.001
F14H20	451	78.00	10.00	12.00	50	75.12	<0.001
F504	553	52.73	5.45	41.82	55	26.05	<0.001
T17C22	2212	22.22	51.11	26.67	45	17.31	<0.001
T12H3	2584	58.97	17.95	23.08	39	24.44	<0.001

6.3.2.2. *Mapping Suppressor 80*

From the suppressor 80 F₂ population, eleven individuals were selected from a population of 72 plants and analysed using the 25 mapping primers. Chi Squared tests were used to determine if any of the markers produced a significant deviation from the expected result. Two markers produced a significant result, shown in appendix V. The marker TI2H3 at the top of chromosome 2 was significantly different from the expected distribution, but due to an increase in the number of individuals that were Col-0 at that point, not Ler as would be expected if the suppressor mutation was in that location. The second marker which produced a significant result was at the bottom of chromosome 2, T16B24 which did have a higher than expected Ler homozygosity at that point. More individuals were selected from the segregating F₂ population and analysed with this marker, which also produced a highly significant result <0.001. A further five markers were identified and obtained for analysis around this region. The position of these additional markers can be found in Figure 6.12 and the sequences of these markers can be seen in appendix V. The additional markers also showed a significant result, shown in Table 6.3. This was not because of the large number of Ler individuals, as would be the case if the mutation was in that area. This could mean that the mutation is very close to T16B24 and the other markers used were too far away from this marker to produce a significant result. The Arabidopsis mapping platform did not show any markers closer to T16B24, so it was not possible to determine whether this was the location of the mutation. Map based cloning for suppressor 80 suggested that the mutation could be at the bottom of chromosome 2 but no further information was obtained using map based cloning to see if this was the case.

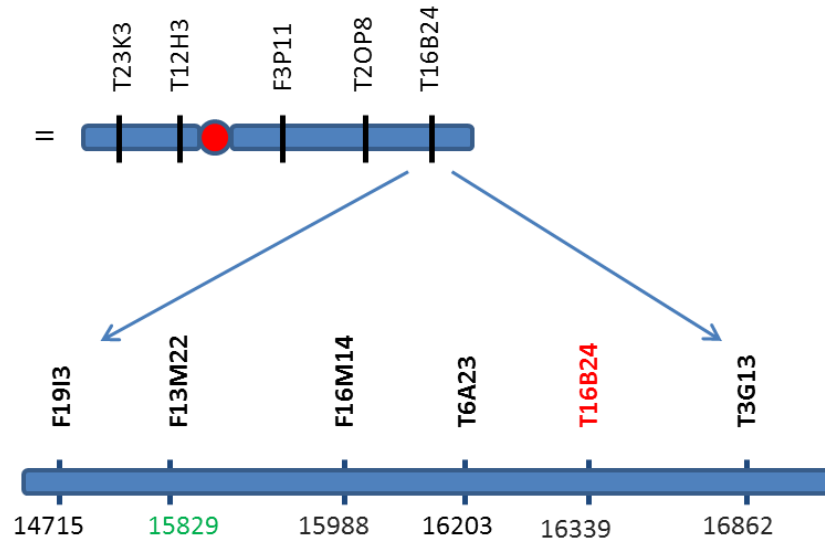


Figure 6.12 The position of additional markers used for genotyping suppressor 80. The name of the primers can be seen on the top line and the numbers show how many bases (kbp) along the chromosome the markers are.

Table 6.3. Chi-squared results for suppressor 80. The number of individuals in the test is shown by 'n', the result of the chi squared test ' χ^2 ' (on 2 d.f) and the p-values show where the results were significant.

Marker	Distance (kbp)	Ler (%)	Col 0 (%)	Het (%)	Individuals analysed (n)	χ^2 statistic	p value
F19I3	14715	0	32.14	67.86	28	9.36	<0.05
F13M22	15829	0	0	0	0	NA	NA
T6A23	16203	0	0	0	0	NA	NA
F16M14	15988	30.91	38.18	30.91	55	8.6	<0.05
T16B24	16339	71.11	2.22	26.67	45	52.51	<0.01
T3G12	16862	40	40	20	25	9	<0.05

6.3.3. Next generation sequencing results

Mapping suggested a 2500kbp region in which the mutation of suppressor 36 was likely to be. Mapping did not give a strong indication of where in the genome the suppressor 80 mutation might be positioned. Whole genome sequencing of the suppressors was adopted to identify the position of the suppressor mutations. NGS was performed by the University of Liverpool Genomic Centre.

A large number of F₂ plants displaying the suppressor phenotype were selected from the segregating populations. The DNA was extracted from these plants and all of the individual DNA extractions were pooled together. For suppressor 36, 119 individual F₂ plants were selected and for suppressor 80, DNA from 84 individuals was extracted. The two pools of F₂ suppressor DNA were sequenced by the illumina Hiseq platform, with paired end reads of 100bp, using the SBS approach. This generated 111 million reads for suppressor 36 and 108 million reads for suppressor 80. The resulting average depth of coverage was 149x for suppressor 36 and 138x for suppressor 80. This depth of coverage allowed for sensitive and accurate SNP calling. It was essential that a high coverage was attained for the two suppressor lines, so that the frequencies of alleles within the population could be determined. This would be used to identify the position of the mutation. For this reason, Hiseq illumina was used due to the higher number of reads it produces and higher output which can be achieved compared to other sequencing platforms.

The mutant parental lines *cer10-1* and *cer10-2* were also sequenced. This was because little was known about the exact position of the *cer10-1* mutation. By sequencing the mutant genome the exact position of the mutation could be determined. This would allow for easier genetic characterisation of the mutant in the future. In addition it was not known to what degree the two lines would defer from the reference *Arabidopsis* sequences of Col-0 and Ler. Sequencing these genomes allowed for more accurate SNP calling in the suppressor mutants.

The DNA of the parental lines were sequenced using the Miseq illumina platform. This did not produce as many reads as the Hiseq platform, but it was more cost

effective. It was decided that this would be sufficient for the sequencing of the *cer10-1* and *cer10-2*, as these genomes would not differ by as many SNPs as the two suppressor mutants. Also, it was not essential that a high depth of coverage was achieved, as allele frequency would not need to be determined. A total of 12 million reads were produced for *cer10-1*, with an average depth of coverage of 17.4x. For the *cer10-2* line, 18 million reads were produced, with an average depth of coverage of 23.6x. The two parent sequences resulted in over 99% coverage of the reference genome.

6.3.3.1. Candidate SNP identification in *cer10-1* suppressor 36

Suppressor 36 showed 880 homozygous SNPs that were not found in either parental lines, and 31,863 heterozygous SNPs. However a large number of identical SNPs were identified in both suppressor lines. This could be explained by the fact that both bulked suppressor populations were sequenced to a greater depth of coverage than the two parental lines. Some SNPs between the parental line and the reference genome may not have been identified, but these SNPs could then have been identified in both suppressor lines. For this reason the SNPs conserved across the two suppressor lines were also removed from the candidate lists. When these SNPs were removed, suppressor 36 had 560 unique homozygous SNPs and 17,004 unique heterozygous SNPs. Figure 6.13 shows the SHOREmap plots generated for suppressor 36. An area of conserved homozygosity with the *cer10-1* parental lines was identified on chromosome 2 at 3Mbp, and the candidate window identified was 600kbp in size. It has been reported that the candidate window size is related to the number of individuals used for sequencing (James *et al.*, 2013), the candidate window identified here was of a good size, as the number of SNPs identified within

Identifying the gene responsible for the suppressor phenotype

it was manageable. From this region a list of unique homozygous SNPs was generated, this can be found in appendix V. The SNPs which occurred within intergenic regions were removed from this list. The potential candidates within coding regions are shown in Table 6.4.

Table 6.4. Candidate SNPs identified in suppressor 36 which are in a coding region.

Position	%reads showing alternate	Position in gene	Gene name	synonymous or non-synonymous	amino acid of reference	amino acid after
2623760	82	intronic/non coding	AT2G06570			
3617716	94	CDS	AT2G07981	Nonsyn	*	Y
3620208	81	CDS	AT2G08986	Nonsyn	V	M

The first SNP identified is in AT2G06570, within a noncoding region of the gene so it was not considered. The second gene which contained a SNP was AT2G07981. This gene encodes a protein of unknown function of 413 amino acids in length. The sequencing data shows that the SNP results in a stop codon being changed to a tyrosine residue. The nucleotide sequence, shows that this change would result in a further 7 amino acids being added to the end of the sequence until the next stop codon code is reached. These extra residues are YDLMSCV, which is a hydrophobic addition. This could have a substantial effect. This protein was shown to be located in the nucleus and the cytosol, determined using the subcellular location of proteins in Arabidopsis database (SUBA).

The third candidate SNP is in the coding region of AT2G08986, which codes for a protein of unknown function of 1218 amino acids in size. The amino acid change takes place at position 448. This results in an amino acid change of valine to proline, both amino acids are hydrophobic but the two amino acids differ in properties, and this is not considered a conservative amino acid change. The protein

Identifying the gene responsible for the suppressor phenotype

was shown to be present in the cytosol, determined using SUBA. In the future these two mutations would be analysed in more detail and are considered the most likely position of the mutation based on the sequencing results. Basic local alignment search tool (BLAST) was used to see if homologs of these two genes could be identified in yeast, however homologs of high similarity were not found. Tissue specific expression data was not available for either of these genes.

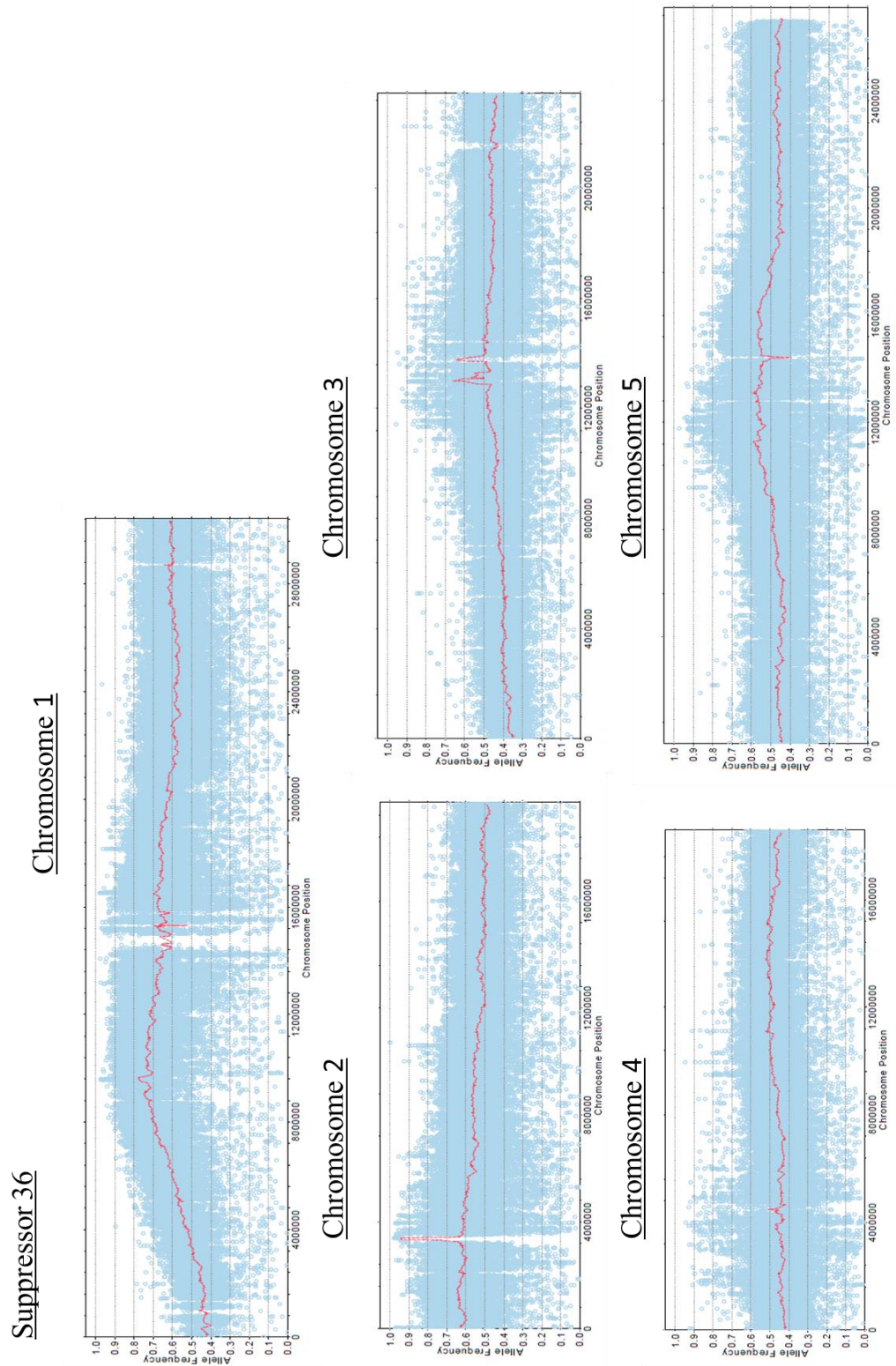


Figure 6.13 SHOREmap plots for suppressor 36. The allele frequency is plotted against the distance along the chromosome. Blue dots show the single markers, and the red line shows the window markers which is composed of the sum of the single markers divided by the total number of markers.

6.3.3.2. Candidate SNP identification in *cer10-1* suppressor 80

Analysis of the sequence of suppressor 80 revealed 259 unique homozygous SNPs and 11,126 unique heterozygous SNPs. The SHOREmap plots which were produced from the sequencing data for suppressor 80 highlighted the same candidate region as was identified for suppressor 36, at 3Mbp (million base pairs) on chromosome 2 (Figure 6.14). From this candidate window, a list of SNPs were generated which can be found in appendix V. The SNPs identified within the intergenic regions were removed, a list of the remaining potential candidate SNPs are shown in Table 6.5.

Table 6.5. Candidate SNPs identified in suppressor 80 which are in a coding region.

Position	%reads showing alternate allele	Position in gene	Gene name	synonymous or non-synonymous	amino acid of reference	amino acid after base change
3251022	82	CDS	AT2G07777	Nonsyn	A	E
3290052	100	Splice site	AT2G07681			
3385678	84	CDS	AT2G07706	Syn	V	V
3385688	84	CDS	AT2G07706	Nonsyn	G	D
3385694	83	CDS	AT2G07706	Nonsyn	P	L
3615628	80	noncoding	AT2G07981			
3623164	88	noncoding	AT2G08986			

The first candidate SNP was located in AT2G07777, which codes for ATP synthase 9 which was not thought to be responsible for the phenotype of the suppressor mutant, so will not at this point be considered as a potential candidate. A SNP was identified within AT2G07681, which encodes for a cytochrome C assembly protein (TAIR), however, this SNP is not in a coding region so will not be considered. Three SNPs were identified within AT2G07706. The first SNP resulted in a nucleotide change that produced a synonymous mutation, so can be disregarded. The other two SNPs however, produced non-synonymous mutations. This gene encodes for a protein of unknown function of 504 amino acids in length. The first

amino acid change of glycine to aspartic acid is a substantial change, of an uncharged small amino acid, to a polar amino acid which is charged. The second non-synonymous mutation resulted in a change from proline to lysine, again, this is a substantial change. These two amino acid changes are separated by a single amino acid and are at the start of the protein sequence. The genes AT2G07981 and AT2G08986 which encode for proteins of unknown function, both have SNPs which occur within their introns. As these are within intronic regions, they will not be considered in the first instance. Only the mutation within the gene AT2G07706 will be considered initially as this appears like the most likely potential candidate. This protein was shown to be strongly localised in the cytosol, determined using SUBA. Protein searches have shown that this is a plant specific protein. The Arabidopsis eFP browser showed low levels of expression in the rosette leaves where the phenotype of *cer10-1* is suppressed in suppressor 80, making this a likely candidate.

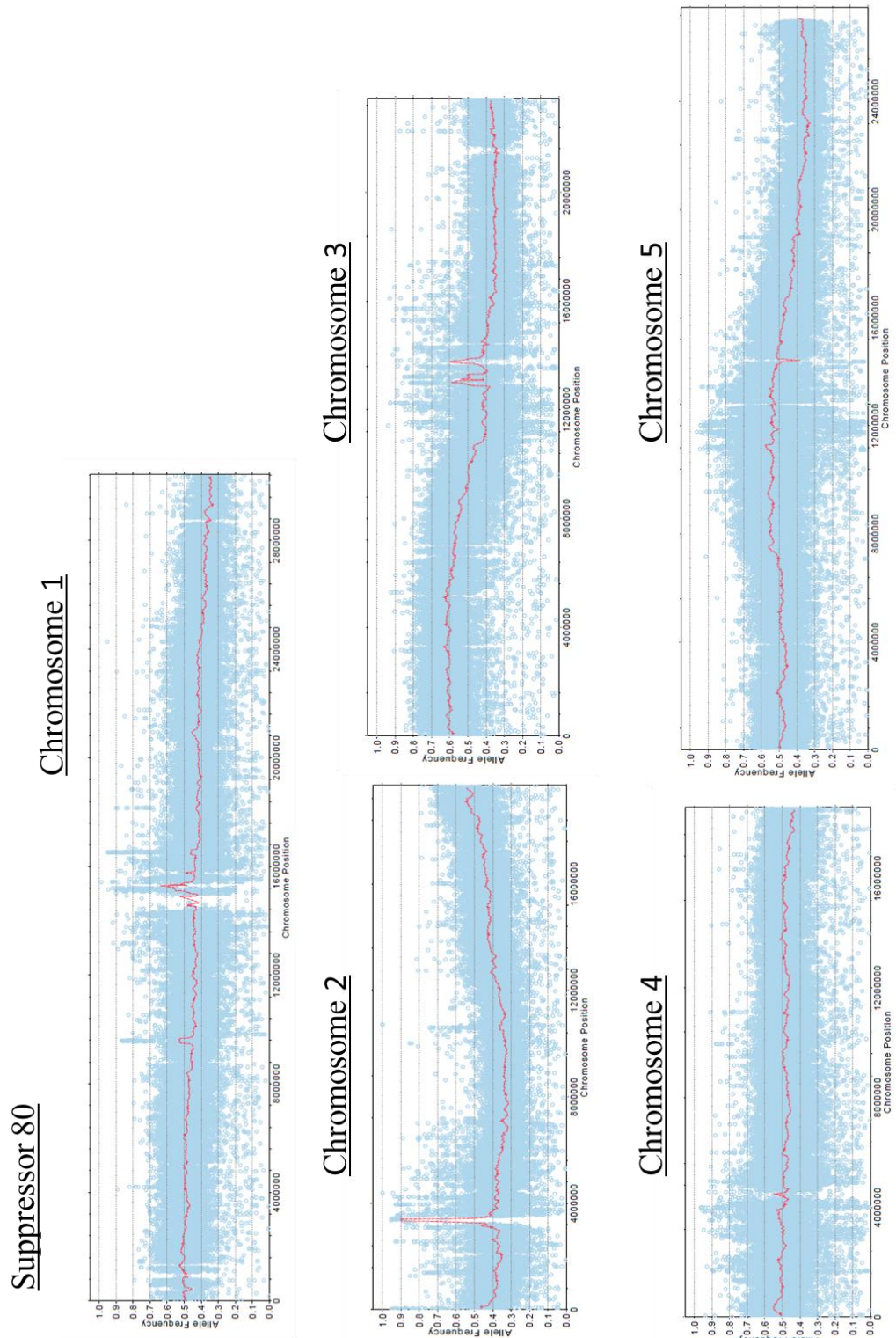


Figure 6.14. SHOREmap plots for suppressor 80. The allele frequency is plotted against the distance along the chromosome. Blue dots show the single markers, and the red line shows the window markers which is composed of the sum of the single markers divided by the total number of markers.

6.4. Discussion

6.4.1. Evaluation of rough mapping

The candidate region for suppressor 36 has been identified as being located on the top arm of chromosome 2, between 3.1-3.7 Mbp. The same location was identified from both the map based cloning and the NGS data. The map based cloning was able to narrow the position of the mutation to an arm of a chromosome. Although the rough mapping did suggest the same location for the mutation as was identified from the analysis of the NGS data, fine mapping the mutations would have been a time consuming process.

The use of additional markers did not narrow the interval any further, as the closest marker used in this study to the region identified from the sequencing data, was primer pair T12H3 located at 2585 kbp on chromosome 2, still 600 kbp away from the candidate interval identified by SHOREmap. The Arabidopsis mapping platform, shows that there are additional CAPs and PCR markers which are closer to the candidate region that could have been used for genotypic analysis. However as there were multiple regions on chromosome 2 with a high proportion of homozygosity towards Ler, covering an area of 2.5Mbp, it would have been a time consuming and expensive process to genotype this region in greater depth. On average, 61 individuals were used for rough mapping and less individuals were used for marker T12H3, this was due to the primer pairs often not producing a product from the PCR. It is possible that if more individuals had been analysed the map based cloning approach would have been more successful.

NGS also identified the candidate window for the SNP responsible for the suppressor 80 phenotype on the top arm of chromosome 2. This was not identified from the map based cloning and in order to locate the position of the mutation using mapping would have taken considerable more time.

6.4.2. Difficulties with the identification of plants within the F₂ populations

The identification of candidate plants exhibiting the suppressor 80 phenotype within the F₂ segregating population was difficult. The phenotype of suppressor 80 showed an increased height of plants and increased leaf area. Due to the increased height of *cer10-2* compared to *cer10-1*, the phenotype of suppressor 80 was more difficult to identify from the surrounding plants. For this reason, for easier identification of candidate plants, it may have been more suitable to backcross the mutation into *cer10-1* and then sequence the mutation, using the pipeline described by Hartwig *et al.*, (2012). A large number of false positives may explain why the map based cloning was unsuccessful for this suppressor mutant. However the NGS data would suggest that this is not the case as the percentage of reads showing the candidate SNPs in the interval region is high, 90%, and the allele frequency in the candidate region is high, 90%. This suggests that few false positive were selected for.

6.4.3. Evaluation of the NGS sequencing data

The NGS data has suggested that the mutations of the two suppressors are located within the same region on chromosome 2. There were a high number of SNPs which the two suppressor mutants had in common, 50% across the whole genome. This could be explained by the higher coverage of the suppressor mutants compared to the parent alleles, such that some SNPs present in the parent are not being called in the suppressor pools as a result of the different sequencing platforms used. This could result in SNPs that are present in the parental lines compared to the reference genome not being identified in the parent but that were identified in the two suppressor pools. If the parent lines had been sequenced at the same coverage as the segregating populations it may have resulted in better SNP calling, and a clearer list of candidates for the suppressor mutants. The decision was taken to remove the

SNPs that the two suppressor mutants had in common, because phenotypic data shown in Chapter 5 would suggest that the mutations do not affect the same gene. However the suppressor mutants should now be crossed to rule out the possibility that they are two different alleles of the same gene.

It has been shown previously that two mutations of the same gene can result in different phenotypic changes. For example, in the different *KCR RNAi* lines some shown fused flower buds and some had fused flower buds and glossy stems. This is thought to be due to the different levels of reduction in VLCFAs (Beaudoin *et al.*, 2009). An additional example of observing different phenotypes depending on the severity of the reduction in VLCFA levels was shown when herbicides that affected VLCFA levels were applied to plants. When a low concentration of herbicides was used there was an increase in cell division such that there was an increase in plant size, whereas a higher concentration resulted in smaller plants, with callus like structures as a result of uncoordinated cell division (Nobusawa *et al.*, 2013). As the SHOREmaps of the suppressor mutants are so similar, it is possible that they affect the same gene but result in different phenotypes. This would mean that the number of candidate SNPs would be higher, as the SNPs removed that the two suppressors had in common could also be considered.

6.4.4. Future work

The NGS data has produced a list of candidate genes that may be mutated and therefore be responsible for the suppressor phenotype. The next step would be to validate the results from the NGS. The region around the SNP would be PCR amplified for both the suppressor mutant and parent lines and then be sequenced using 454 sequencing or by using dCAP markers to validate the results of the sequencing (Neff *et al.*, 1998). In addition quantitative PCR could be performed to see if the level of expression of these genes had been affected. If the SNPs are

Identifying the gene responsible for the suppressor phenotype

confirmed, lines with mutations in these genes would be identified from Salk collections. Salk lines were created using *Agrobacterium* which was used to transfer DNA (T-DNA) to create insertion events across the *Arabidopsis* genome so that nearly every gene has a Salk line created for it. This means that the effect of a mutation in any gene can be observed (Alonso *et al.*, 2003). The lines which would be obtained for further analysis of each of the candidate genes are shown in Table 6.6. These plants would then be crossed to the *cer10-1* plant to see if the same phenotype is produced in the offspring as shown in Chapter 5 indicating that the same gene is dysfunctional in both the SALK and suppressor mutant. This approach would only be suitable for loss of function mutations. However, as these mutations might not result in a complete loss of function a different approach could be used. The WT allele of the candidate gene could be cloned and then overexpressed in the suppressor line. This should reverse the suppression and restore the *cer10-1* phenotype, which would confirm that the mutation in this gene does result in the suppressed phenotype.

Table 6.6. List of the Salk lines that would be ordered for the SNPs identified in the suppressor mutants.

Gene	Suppressor line	Salk line	Type of mutation
AT2G07981	36	SALK_070409	Homozygous knockout line
AT2G07981	36	SALK_035841	Homozygous knockout line
AT2G07981	36	SALK_052067	Homozygous knockout line
AT2G08986	36	SALK_066680	Homozygous knockout line
AT2G08986	36	SALK_111790	Homozygous knockout line
AT2G08986	36	SALK_108524	Homozygous knockout line
AT2G07706	80	SALK_073532	Heterozygous - exon
AT2G07706	80	SALK_071601	Heterozygous - exon

Chapter 7. General discussion

Mutations in the biosynthesis of VLCFAs result in a number of different phenotypes. The KCS enzymes are responsible for determining the carbon chain length of the final elongation product and have tissue specific expression patterns (Millar and Kunst, 1997). It has been shown previously that differences in chain lengths and expression pattern can be responsible for the different phenotypes. For example, KCS2 (Daisy) is expressed in the roots and mutants showed a decrease in root length (Franke *et al.*, 2009) whereas, KCS6 is expressed in the epidermis and mutants had waxless stems (Millar *et al.*, 1999). The aim of this thesis was to explain the different phenotypes that result from mutants of the core components of the elongase complex by analysing their lipidome. All of the core components of the elongase (defined as the keto-reductase, the dehydratase and the enoyl-reductase) are expressed ubiquitously in the plant. Therefore, one would expect all mutants to result in a general ubiquitous reduction in the amount of VLCFA and as a consequence, display the same phenotype. However this has been shown previously not to be the case (Zheng *et al.*, 2005, Bach *et al.*, 2008, Beaudoin *et al.*, 2009).

Additionally, a forward genetic screen was conducted to try and isolate new interacting partners in VLCFA biosynthesis. This would lead to a greater understanding of VLCFA biosynthesis, potentially providing information about how VLCFA are synthesised and channelled into the various lipid groups and how this channelling is regulated. An increased knowledge of how VLCFAs are synthesised and incorporated into different lipid pools has important implications for understanding their role in plant development, interactions with their

environment, response to pest and pathogens as well as for metabolic engineering and future biotechnology applications.

7.1. Correlating changes in the lipidome with phenotypic traits

In Chapter 3 it was shown that the different knockout/knockdown elongase lines all had fused aerial organs; however, the severity of these phenotypes differed. *pas2-1* showed the most severe fusion, followed by the *KCR RNAi* line used in this study and finally the *cer10* mutant. The root phenotype also differed between these lines, the *KCR RNAi* line and *pas2-1* both showed a reduction in the number of lateral roots whereas *cer10* did not. *pas2-1* and *cer10* both showed shorter primary roots whereas the *KCR RNAi* line did not. From this phenotypic analysis it was clear that *pas2-1* showed the most severe phenotype both in the shoots and in the roots.

In Chapter 4 similar phenotypes were shown in plants treated with herbicides that are known to affect VLCFA synthesis (Abulnaja *et al.*, 1992). Flufenacet has been shown previously to inhibit the activity of various KCS enzymes using yeast as a heterologous expression system (Trenkamp, 2004). Flufenacet was shown in Chapter 4 to produce a root phenotype (shorter primary roots), and a shoot phenotype (fused aerial organs). Benfuresate and ethofumesate are also thought to affect VLCFA synthesis (Abulnaja *et al.*, 1992) but their mode of action is not known. Plants treated with these herbicides showed the same shoot phenotype as flufenacet treated plants but did not have a root phenotype.

The combined aim of both of these chapters was to use lipidomic profiling to find correlations between a particular phenotypic trait and changes in the lipidome. Previous work with mutants of the core elongase complex has shown that the level

of VLCFAs is reduced in these mutants, as are the lipid classes that they are components of (Zheng *et al.*, 2005, Bach *et al.*, 2008, Beaudoin *et al.*, 2009). By performing lipidomic analysis on material that has been separated into roots and shoots, for the first time it has been possible to investigate whether the effects observed in VLCFA containing lipid pools were the same in both fractions. It was thought that refining the analysis in this way might help understand some of the reasons for the different phenotypes seen in the different elongase mutants.

The data presented in Chapters 3 and 4 did show correlations between changes in the lipidome and phenotypic traits. This was most clearly seen in the herbicide treated plants. Flufenacet treated plant, which exhibited a root and a shoot phenotype, showed a decrease in the proportion of VLCFA containing lipids in all the lipid classes analysed in both the roots and the shoots. In contrast, benfuresate and ethofumesate treated plants did not show a root phenotype and VLCFAs were only decreased by minor amounts in the roots in all of the lipid classes analysed, whereas large reductions were seen in the shoots. This showed that where an observable phenotype was seen as was a decrease in the proportion of VLCFAs.

7.1.1. Explaining the different root phenotypes shown in the elongase mutants

It was possible to show correlations between changes seen in a particular sphingolipid class and specific phenotypes in the roots. Decreases were seen in the amount of sphingolipids containing VLCFAs in mutant roots which showed a reduction in lateral roots, which was not seen in those mutants that did not show a lateral root phenotype. Additionally specific decreases were seen in the GIPC and HCEr containing VLCFAs in these mutants, which could be responsible for the phenotype. This phenotype is also seen in sterol mutants (Willemsen *et al.*, 2003)

and as sterols and sphingolipids are the major components of lipid rafts it is possible that a change in their composition or the availability of lipid rafts could be responsible for this phenotype. Those mutants which showed a shorter primary roots showed decreases in the GlcCer containing VLCFAs which was not seen in mutants that did not show shorter primary roots. This data correlated with a decrease in GlcCer containing VLCFAs seen in the flufenacet treated plants which also showed shorter primary roots. It has been shown that the shorter the primary root the greater the reduction in GlcCer containing VLCFA. It is possible that the greater the reduction in GlcCer containing VLCFAs the shorter the primary roots.

7.1.2. Explaining the fused aerial organs shown in elongase mutants

Both the knockout/knockdown elongase lines and the herbicide treated plants showed fused aerial organs. All of these plants showed reductions in the proportion of VLCFAs in the shoots in nearly all of the lipid classes tested. A number of causes of this phenotype in VLCFA mutants have been suggested previously. It was shown that fused organs were not due to changes in the total amount of cutin or wax (Voisin *et al.*, 2009), which could mean that it is due to changes in the amount of individual components of the wax or cutin. Evidence for this comes from investigations with mutants of bodyguard (*BDG*) which encodes for a protein that has a role in cuticle synthesis and shows fused organs (Kurdyukov *et al.*, 2006). *bdg* shows an increased amount of wax but does not show an equal increase in all wax components. Alkanes were disproportionally increased. This is also seen in the *fdh* mutant, which shows fused organs and an increase in total wax but again this increase is mainly in alkanes (Voisin *et al.*, 2009). This would suggest that the fusion could be due to changes in the wax composition rather than the total amount.

bdg was shown to have an altered cuticular surface. Transmission electron microscope studies showed areas of electron dense material and areas of less dense material (Kurdyukov *et al.*, 2006). It has recently been suggested that a reduction in both cutin and wax are required for a fused phenotype (Weng *et al.*, 2010). As cutin does not contain any VLCFAs, it is possible that the changes seen in the cuticle structure are a result of a decrease in VLCFA levels which prevent the transport of cutin to the outside of the cell. Plants which show a reduction in VLCFA would also show a decrease in wax components as VLCFA are the precursors of all wax components. This combined decrease could then result in the fused phenotype. The fused phenotype could also be due to a protein required to prevent fusion not being transported to the outside of the cell. This could occur as a result of changes in the cuticle structure preventing transport, or as a result of a decrease in sphingolipids containing VLCFA that have a role in trafficking of proteins. GlcCer have been shown to be required for the correct functioning of the secretory pathway and the transport of certain proteins (Melser *et al.*, 2010). All plants that showed fused phenotypes showed a decrease in the amount of GlcCer containing VLCFA and it is possible that this results in trafficking defects which results in fused organs.

7.1.3. The role of lipid rafts

Lipid rafts are an attractive hypothesis for the cause of many of the phenotypes, particularly because a number of the phenotypes have been associated with defects in trafficking. For example, the trafficking of PIN1 is associated with the lateral root phenotype (Markham *et al.*, 2011), and the trafficking of proteins for cell plate formation has been suggested to be responsible for shorter primary roots (Bach *et al.*, 2011). Lipid rafts have been associated with a wide range of cellular processes

such as protein sorting during exocytosis and endocytosis and in signal transduction pathways (Simons and Toomre, 2000). Many of which could be used to explain the phenotypes shown here. Lipid rafts are thought to contain sterols and sphingolipids. The fact that the elongase mutants showed a decrease in sphingolipids containing VLCFA and the phenotypes that were seen in VLCFA mutants are also observed in sterol mutants, (fused aerial organs, cell expansion phenotypes and root phenotypes), suggests that changes in lipid raft composition is an attractive hypothesis for a number of the phenotypes seen (Schrack *et al.*, 2000, Willemsen *et al.*, 2003, Men *et al.*, 2008, Boutte *et al.*, 2010). It should be remembered that the existence of these lipid rafts in vivo has not been unequivocally proven. Doubts remain over the existence of lipid rafts due to the methods used for extraction and purification of lipid rafts and the difficult in visualizing them in cells (Munro, 2003). This should be considered when trying to draw conclusions on the phenotypes seen.

7.2. The importance of sphingolipids containing VLCFAs

It was thought that sphingolipids containing VLCFA were essential for survival of yeast. Mutations in both condensing enzymes of the elongase complex involved in VLCFA synthesis in yeast, *elo2* and *elo3*, resulted in a lethal phenotype. Double mutants are unable to synthesise sphingolipids containing VLCFA and this is thought to be responsible for the lack of viability (Oh *et al.*, 1997). The presence of C26 VLCFA has been shown to be an essential requirement for the formation of lipid rafts and in stabilizing the raft at the plasma membrane in fungus (Eisenkolb *et al.*, 2002). C26 has also been shown to be important for protein trafficking and protein stability at the plasma membrane in yeast (David *et al.*, 1998). This

suggested that sphingolipids containing VLCFAs were essential in yeast. However it has recently been shown that yeast cells can survive without sphingolipids containing VLCFA. Mutations in the ceramide synthase genes, *lag1* and *Alac1* cause a reduction in the amount of complex sphingolipids containing C26 fatty acids. When this function was replaced by the human *Lass5* gene which shows specificity towards C16-18 fatty acids the yeast cells could survive with ceramides containing shorter chains. However it was shown that the cells still needed VLCFA to survive (Cerantola *et al.*, 2007). This study showed that there was an increase in the amount of PI containing VLCFA and it is possible that when there is a decrease in the amount of sphingolipids, PI compensates for this decrease and partially restores functionality. This shows that yeast cells do seem to adapt to a decrease in sphingolipid containing VLCFA and suggests that the lipid classes are tightly connected to one another.

It was therefore observed whether chain length played an important function in plant sphingolipids. Sphingolipids containing VLCFAs have been shown to be essential in plants and unlike in yeast cannot survive by only containing sphingolipids with 16-18 fatty acids (Markham *et al.*, 2011). It seems plausible therefore, that when the levels of VLCFAs are reduced the plant tries to produce as much of these essential sphingolipids containing VLCFA as possible to ensure survival. Results obtained with the core elongase mutants, show that there was a smaller reduction in the proportion of VLCFA in sphingolipids than both the phospholipid and the acyl-CoA pools. In addition the decrease did not become more substantial with increasing VLCFA chain length. In contrast, herbicide treated plants showed a greater reduction in the amount of sphingolipids containing

VLCFA than was shown in the phospholipid pool. In addition within the sphingolipid pool there was a greater reduction as the chain length of the VLCFA increased. Since these herbicides are believed to affect KCS enzymes; the plant may be unable to produce these longer length sphingolipids as a result of the inhibition of KCS enzyme capable of producing them. This could mean that the core elongase mutants upregulate certain KCS enzymes capable of producing fatty acids for channelling into the sphingolipid pool as a response to a decrease in VLCFAs. This would explain why in Chapter 3 the reduction in the sphingolipid pool was not as substantial as that of the other lipid pools. This would ensure that sphingolipid homeostasis is maintained due to the vital importance of it, but this cannot happen in herbicide treated plants, due to the inhibition of the KCS required for this. The KCS enzymes are thought to be the rate limiting step in VLCFA synthesis, so an increase in the expression could result in an increase in the amount of a fatty acid required for sphingolipid synthesis being produced (Millar and Kunst, 1997). Additionally there could be a physical interaction between a particular KCS and the ceramide synthase such that the VLCFA are channelled straight into the sphingolipid pool. This KCS could be inhibited in the herbicide treated plants.

Although the herbicide treated plants do show differences in the reduction of VLCFA between the different sphingolipid pools, all the classes showed reductions in the shoots (except flufenacet which did not show a reduction in the ceramides containing VLCFA). In contrast in the core elongase mutants, the amount of GlcCers and GIPCs containing VLCFAs were reduced but the ceramides and HCer showed no decreases or minor decreases in the amount containing VLCFAs, and in some cases actually showed increases. This would suggest that the core elongase

mutants have an additional level of channelling of VLCFA into the different sphingolipid classes that does not occur or has a reduced efficiency in the herbicide treated plants. The channelling of VLCFAs into the different sphingolipid pools could once again be controlled by changing the expression of different KCS enzyme, or by a physical interaction, that cannot occur in the herbicide treated plants. The data here suggests that VLCFA are channelled into particular lipid classes when the levels are reduced and that this could be controlled by the KCS enzymes.

In flufenacet and benfuresate treated plants there was an increase in the proportion of phospholipids containing VLCFA in classes that do not contain VLCFA in wild type plants. It is possible that this is a compensatory effect due to the decrease in the sphingolipid pool. It has been shown in yeast that when the proportion of sphingolipid containing VLCFA decreases there is an increase in the amount of phospholipids containing VLCFAs (Cerantola *et al.*, 2007). It is possible that this effect occurs in plants. The herbicide treated plants may not be as affected by the reduction in the sphingolipid containing VLCFAs, despite the large decreases that are seen, due to the fact that the additional phospholipid containing VLCFAs that it produces can perform a similar function to sphingolipids.

The expression of the KCS enzymes could be measured in the herbicide treated plants using real time PCR to see what effect the herbicides has on the expression of the 21 KCS enzymes. This could show the point of action of both benfuresate and ethofumesate which is currently unknown. It could also be observed whether the expression of the various KCS enzymes changes in the elongase mutants which

could explain the channelling seen in these mutants when the level of VLCFAs are decreased. The plants could also be treated with herbicides throughout the plant life cycle to see what phenotypes are seen throughout development. For example, whether the plants show fused flowers and whether they exhibit any fertility problems. The herbicide treated plants do not show more severe phenotypes, in 2 week old seedlings, than the elongase mutants despite a greater reduction in sphingolipids and a greater reduction with increasing chain length of the VLCFA. Observing the effect of the herbicides throughout the life of the plant could show what the effect these differences have.

7.3. A greater reduction in VLCFA results in more severe phenotypes

It has been suggested in this thesis that, as might be expected, the greater the reduction in VLCFA the more severe the phenotype. *pas2-1* shows the most severe shoot and root phenotype compared to both *cer10* and the *KCR RNAi* line used in this study. It also showed the greatest level of reduction in the lipid pools. For example, in Chapter 3 it was suggested that the fused aerial organs might be due to a decrease in the amount of GlcCer containing VLCFAs. *pas2-1* shows the greatest reduction of the three mutants, and also shows the greatest amount of fusion. *pas2-1* and *cer10* both showed shorter primary roots, but *pas2-1* showed a greater reduction in root length than *cer10*. This phenotype is correlated with a decrease in the amount of GlcCer containing VLCFA which is reduced more in *pas2-1*. Flufenacet treated plants which showed even shorter primary roots have been shown to contain an even greater reduction in GlcCer containing VLCFA than in *pas2-1*. This strongly suggests that it is the magnitude of the decrease in a particular lipid that is responsible for the severity of the phenotype seen. In the shoots

however, the herbicides showed a greater reduction in the amount of GlcCer containing VLCFA than *pas2-1* but did not result in the same severity of phenotype. Therefore it could be due to specific lipid molecular species, rather than a whole class of sphingolipids that is responsible. Analysis of the data generated in greater details would be required to see whether specific molecular species are decreased in all of the mutants and herbicide treated plants, which also shows a correlation between severity of phenotype and the amount of reduction in the shoots.

Previously it has been demonstrated that the level of reduction in VLCFA is important in determining the phenotype that is observed. In multiple *KCR RNAi* lines, displaying different levels of reduction, it was shown that the greatest reduction was always associated with the most severe phenotypes (Beaudoin *et al.*, 2009). In this example the different phenotype seen could be explained by different expression patterns of KCS enzymes. The *KCR RNAi* lines all showed fused flower buds associated with the activity of KCS10 (FDH) but did not all show glossy stems associated with a decrease in the expression of KCS6 (Beaudoin *et al.*, 2009). It has been shown that expression of KCS6 is greater than that of KCS10 (Joubes *et al.*, 2008). When the levels of VLCFA are reduced, KCS6 greater level of expression could mean that it outcompetes KCS10 activity resulting in VLCFAs being available for wax synthesis but are reduced in the lipid required to prevent organ fusion, such that the mutants do not show glossy stems but do display the organ fusion phenotype. However when the levels of VLCFA are reduced further there are inadequate amounts of VLCFA to prevent either of these phenotypes from occurring.

Recent work by Nobusawa *et al.*, (2013) with herbicides that affect VLCFA shows that depending on the level of reduction of VLCFA the resulting phenotypes are very different. It was shown that a high level of reduction results in phenotypes such as *pas2-1* where there is uncoordinated cell division that results in the formation of callus like structures. Whereas, lower level of reduction results in larger leaves and thicker hypocotyls as a result of an increase in cell division but not to the extent that is shown in *pas2-1* (Nobusawa *et al.*, 2013).

7.4. The identification of additional components of VLCFA biosynthesis

Chapter 3 shows that mutations in the core components of the elongase do not show the same level of reduction in the proportion of VLCFAs in all lipid classes tested. This would suggest that VLCFAs are channelled into a particular lipid class when the levels are reduced as initially suggested by Bach *et al.*, (2008). This could require additional interacting protein partners involved in the channelling of VLCFA to the specific lipid pools, or components that play a role in the regulation of different KCS enzymes. Such components have not yet been identified. A forward genetic screen was used to identify novel genes involved in VLCFA regulation and metabolism. Additionally it could lead to the identification of genes which have an indirect effect on lipid metabolism. The screen was performed in *cer10*, and the resulting EMS population was searched for enhanced or suppressed phenotypes of *cer10*. Two candidate mutants, which were shown to suppress different aspects of the *cer10* phenotype, were identified from these pools. Through limited characterisation of their lipidomic profiles, it was shown that both suppressors have changes in their VLCFA composition compared to *cer10*, suggesting that the mutations identified do affect VLCFA synthesis. Suppressor 80

showed a restored proportion of VLC-acyl-CoAs in the shoots and an increase in the level of wax compared to *cer10* in the stems. Suppressor 36 had restored proportions of 24:0 and 30:0 acyl-CoA in both the roots and the shoots. The two suppressor mutants that were isolated from the forward genetic screen showed different phenotypes and showed changes in the proportion of different chain lengths of acyl-CoAs. It is possible that these different phenotypes are the result of differences in the chain lengths that were restored in the mutant.

7.4.1. Regulation of the chain lengths of VLCFAs that are synthesised

The restoration of two distinct phenotypic traits of *cer10* shown by the two suppressors could be due to the restored levels of a particular fatty acid chain lengths, especially in suppressor 36 which showed increased amounts of C24 and C30 acyl-CoAs only. As KCS enzymes are responsible for determining the length and possibly the fate of the product of the elongation reaction it is possible that the mutations have an effect on this component. In addition, the point of action of benfuresate and ethofumesate is not known but it is expected that they have an effect on KCS enzymes. It is possible, however, that another level of regulation is involved in determining the chain length of the VLCFA that is produced and both the herbicides and suppressor mutants could affect this additional regulating component. It was shown that CER2 and CER2-LIKE1 work with CER6 (KCS 6) in order for C30 and C32 VLCFA to be produced in yeast (Haslam *et al.*, 2012). It is not known how these proteins have an effect on the chain length of fatty acids produced but it seems possible that other such proteins could have a role regulating the activity of other KCSs. Alternatively, PAS1 was suggested to stabilize the elongase complex such that when it is absent there is a reduction in the level of

VLCFA, showing another protein that it involved in VLCFA elongation (Roudier *et al.*, 2010). If such a stabilising protein lost its function it is possible that only certain chain lengths of fatty acids could be produced. Or such a protein could be up or down regulated as a result of a mutation which again could result in an increase in the production of certain chain lengths. It has also been seen that the MYB30 transcription factor regulates VLCFA biosynthesis for activation in the HR response. VLCFA or VLCFA derivatives, potentially sphingolipids, are thought to be cell death messengers in plants, and VLCFA biosynthesis is thought to be the first target of these transcription factors (Raffaele *et al.*, 2008). This shows another level of regulation of VLCFA synthesis, and additional transcriptional factors could be discovered that regulate VLCFA chain length. These examples show that there are additional components of VLCFA synthesis that are yet to be discovered. If the suppressor mutant affected a gene that regulated the chain length of the VLCFA that is produced, this could explain why only certain chain lengths show wild type proportions. It could be that this chain length is responsible for the restoration of a specific phenotype. Additionally, if the suppressor mutation affected a mechanism that controlled the channelling of VLCFA into different lipid pools, if that lipid pool is responsible for a specific phenotype this could explain why only certain phenotypes are restored.

7.4.2. Identification of an additional Enoyl-CoA Reductase activity

A null mutation of *cer10* is not embryo lethal, unlike the other two core components of the elongase. It was therefore speculated that there is another unrelated protein capable of carrying out the function of CER10 (ECR activity). It was hoped that the forward genetic screen would lead to the identification of the gene responsible for

this function. However for the reasons discussed in Chapter 5 this was not possible. Data presented in Chapter 3 showed that *cer10* resulted in a greater reduction in both the phospholipids and sphingolipids containing VLCFA in the shoots than the roots. This could suggest that the redundant gene shows a higher level of expression in the roots than in the shoots.

The enzyme responsible for the ECR (CER10) activity in mammals, TER has been shown to have a dual function. In addition to its role in VLCFA synthesis it was shown to have a role in the glycerophospholipid pathway in which sphingosine-1-phosphate is converted to 16:0 acyl-CoA (Wakashima *et al.*, 2014). The data from Chapter 3 was used to see if there was a build-up of any free LCB-P in the *cer10* mutant to see if any additional function of CER10 could be detected in plants. As shown in the appendix VI there is some evidence to suggest that t18:0-P does build up specifically in *cer10* but not in the other core elongase mutants. Further analysis would be needed to see if this dual function does really occur in plants.

In order to identify the gene responsible for the additional ECR activity in *Arabidopsis*, a large scale homology search of the *Arabidopsis* genome might identify unrelated proteins with potential reductase activities capable of catalysing the function of CER10 in VLCFA synthesis. As discussed in Chapter 5, the two closest homologous of CER10 have been tested for activity in yeast by functional complementation and were shown not to carry out this activity as they did not complement the *tsc13* mutant. A wider search of the genome would therefore be necessary. This could be done in a similar way to previously performed in yeast to identify the KCR activity (Beaudoin *et al.*, 2002). In that study the *Saccharomyces*

cerevisiae genome was searched for potential protein sequences that were likely to encode for an oxidoreductases activity. Mutants of the potential candidate were then produced to see if the mutants lost the ability to elongate polyunsaturated fatty acids in yeast (fatty acids not normally present in yeast). Yeast strains containing mutations in the already characterised *ECR* gene, *tsc13*, could be transformed with candidate genes from *Arabidopsis* to see if yeast survives on FOA selection plates. The identification of a potential candidate for the enoyl CoA reductase activity could be based on the same observations originally used to identify the *ECR* gene in yeast. Those observations were the build-up of substrate (enoyl CoA), homology to other enzymes capable of reducing an α - β double bond to a carbonyl group, and its physical interaction with the other elongase components in yeast (Han *et al.*, 2002). The hypothesis that the gene is thought to have a higher level of expression in the roots than the shoots should facilitate its identification.

7.5. Future work

The quantity of sphingolipids containing VLCFAs appears to be of vital importance in explaining the phenotypes seen in the mutants affected in VLCFA metabolism. Sphingolipid analysis was performed on three replicates for each genotype and herbicide treatment. Further replicates are necessary to refine the analysis and confirm these patterns. In order to see if a particular class of sphingolipid is responsible for the phenotypes seen, mutants of the enzymes involved in the synthesis of GlcCer and GIPCs could be used to see if these phenotypes are also present in these mutants. A similar approach to that used by Roudier *et al.*, (2010) and Markham *et al.*, (2011), in which the expression of the DR5 auxin response promoter and PIN1 distribution was monitored, could be used for mutants of

enzymes specific to the GIPC or the GlcCer pathway. This would show if auxin distribution which is thought to explain the lateral root phenotype is affected. It would then be possible to determine whether a reduction in a particular class of sphingolipid is responsible for the reduction in lateral roots or if it is an effect that is caused by a reduction in many different sphingolipid classes at the same time.

The lipidomic analysis in Chapters 3 and 4 showed a strong correlation between phenotype and changes in the lipidomic profiles. To further correlate the lipidomic profile of mutants and their displayed phenotype it would be important to study different phenotypes arising from mutants of different KCS enzymes. Lipidomic analysis of these mutants would show whether it is possible to link phenotypes to changes in a particular lipid class and whether the correlation shown here in the knockout/knockdown core elongase lines are also seen in these mutants.

The discovery of both *CER2* and *CER2* –*LIKE 1*, *PAS1* and *MYB30* would suggest that there are a number of other genes involved in the regulation of VLCFA synthesis. Identification of additional proteins involved in VLCFA biosynthesis and those involved in the subsequent channelling to different lipid pathways should lead to a greater understanding of VLCFA biosynthesis. It was only possible to screen 20 of 120 M₂ pools from the *cer10* forward genetic screen. More of these pools should be screened so that further components of VLCFA synthesis and components involved in channelling the products of VLCFA synthesis can be identified. The two suppressor mutants identified in Chapter 5 could be characterised further such that the role they play in VLCFA biosynthesis can be determined. Both mutations seem to show restoration of certain chain lengths of VLCFA in the acyl-CoA pool

and in the wax analysis. Further lipidomic characterisation of the pools that VLCFA are components of, phospholipids, sphingolipids, and triacylglycerols would show if the mutations have an effect on the elongase complex or more specifically on a particular lipid class. If these mutations do affect the elongase complex the lipidomic characterisation of these additional lipid pools will show, as seen in the wax analysis, if only certain chain lengths are affected. This will show whether an increase in a particular chain length, or specific channelling to a lipid class is responsible for the restored phenotypes seen in Chapter 5. The candidate SNPs identified to be the cause of the phenotypes in suppressor 36 and 80 should be confirmed to try and identify two new genes that have a novel role in VLCFA metabolism.

7.6. Conclusions

The work presented in this PhD thesis contains novel data and original results which will be useful to further our understanding of the role of VLCFAs in plant growth and development.

Comprehensive lipidomic profiling of plants with genetically or chemically induced reductions in VLCFA content provided some indication about which lipid classes may be responsible for the different morphological phenotypes observed in the fatty acid elongase mutants. The lipidomic data generated has provided an extensive list of changes in the lipidome of elongase mutants and highlighted marked differences between shoot and root tissues. Analysis of these tissues separately allowed correlations to be established between some morphological and biochemical phenotypes. These analyses also indicated that reduced levels of VLCFAs are

preferentially channelled to specific lipid classes as suggested initially by results obtained with the *pas2-1* mutant (Bach *et al.*, 2008).

The EMS population generated will be useful to identify additional genes involved in VLCFA metabolism. Screening only 17% of this population during this PhD already allowed the identification of two suppressor mutations that are thought to have an effect in the regulation and/or synthesis of VLCFAs. Limited biochemical characterisation of these mutant lines revealed only partially restored levels of VLCFAs with specific differences observed between tissues and in fatty acid chain lengths. Further characterisation of these mutant lines will be required to determine the effect of these mutations on the lipidome and how it correlates with the phenotypes observed. Cloning and functional characterisation of the genes should contribute to improve our understanding of VLCFA metabolism.

References

Aach, H. and Heise, K. P. (1998). *On the compartmentation of triacylglycerol synthesis in developing seeds of Brassica Napus*. Botanica Acta **111**(2): 123-129.

Aarts, M. G., Keijzer, C. J., Stiekema, W. J. and Pereira, A. (1995). *Molecular characterization of the CER1 gene of Arabidopsis involved in epicuticular wax biosynthesis and pollen fertility*. Plant Cell **7**(12): 2115-2127.

Abulnaja, K. O., Tighe, C. R. and Harwood, J. L. (1992). *Inhibition of fatty-acid elongation provides a basis for the action of the herbicide, ethofumesate, on surface wax formation* Phytochemistry **31**(4): 1155-1159.

Ahmed, S. N., Brown, D. A. and London, E. (1997). *On the origin of sphingolipid/cholesterol-rich detergent-insoluble cell membranes: physiological concentrations of cholesterol and sphingolipid induce formation of a detergent-insoluble, liquid-ordered lipid phase in model membranes*. Biochemistry **36**(36): 10944-10953.

Alonso, J. M., Stepanova, A. N., Leisse, T. J., Kim, C. J., Chen, H. M., Shinn, P., Stevenson, D. K., Zimmerman, J., Barajas, P., Cheuk, R., Gadrinab, C., Heller, C., Jeske, A., Koesema, E., Meyers, C. C., Parker, H., Prednis, L., Ansari, Y., Choy, N., Deen, H., Geralt, M., Hazari, N., Hom, E., Karnes, M., Mulholland, C., Ndubaku, R., Schmidt, I., Guzman, P., Aguilar-Henonin, L., Schmid, M., Weigel, D., Carter, D. E., Marchand, T., Risseuw, E., Brogden, D., Zeko, A., Crosby, W. L., Berry, C. C. and Ecker, J. R. (2003). *Genome-wide insertional mutagenesis of Arabidopsis thaliana*. Science **301**(5633): 653-657.

Arabidopsis Genome, I. (2000). *Analysis of the genome sequence of the flowering plant Arabidopsis thaliana*. Nature **408**(6814).

Bach, L. and Faure, J.-D. (2010). *Role of very-long-chain fatty acids in plant development, when chain length does matter*. Comptes Rendus Biologies **333**(4): 361-370.

Bach, L., Gissot, L., Marion, J., Tellier, F., Moreau, P., Satiat-Jeunemaitre, B., Palauqui, J.-C., Napier, J. A. and Faure, J.-D. (2011). *Very-long-chain fatty acids are required for cell plate formation during cytokinesis in Arabidopsis thaliana*. Journal of Cell Science **124**(19): 3223-3234.

Bach, L., Michaelson, L. V., Haslam, R., Bellec, Y., Gissot, L., Marion, J., Da Costa, M., Boutin, J. P., Miquel, M., Tellier, F., Domergue, F., Markham, J. E., Beaudoin, F., Napier, J. A. and Faure, J. D. (2008). *The very-long-chain hydroxy fatty acyl-CoA dehydratase PASTICCINO2 is essential and limiting for plant development*. Proceedings of the National Academy of Sciences of the United States of America **105**(38): 14727-14731.

Barthlott, W. and Neinhuis, C. (1997). *Purity of the sacred lotus, or escape from contamination in biological surfaces*. Planta **202**(1): 1-8.

References

Basu, S., Kaufman, B. and Roseman, S. (1968). *Enzymatic synthesis of ceramide-glucose and ceramide-lactose by glycosyltransferases from embryonic chicken brain.* Journal of Biological Chemistry **243**(21): 5802-5804.

Bates, P. D. and Browse, J. (2012). *The significance of different diacylglycerol synthesis pathways on plant oil composition and bioengineering.* Frontiers in Plant Science **3**.

Baud, S., Bellec, Y., Miquel, M., Bellini, C., Caboche, M., Lepiniec, L., Faure, J. D. and Rochat, C. (2004). *gurke and pasticcino3 mutants affected in embryo development are impaired in Acetyl-CoA Carboxylase.* Embo Reports **5**(5): 515-520.

Baud, S., Guyon, V., Kronenberger, J., Wulleme, S., Miquel, M., Caboche, M., Lepiniec, L. and Rochat, C. (2003). *Multifunctional Acetyl-CoA Carboxylase 1 is essential for very long chain fatty acid elongation and embryo development in Arabidopsis.* Plant Journal **33**(1): 75-86.

Beaudoin, F., Gable, K., Sayanova, O., Dunn, T. and Napier, J. A. (2002). *A Saccharomyces cerevisiae gene required for heterologous fatty acid elongase activity encodes a microsomal beta-keto-reductase.* Journal of Biological Chemistry **277**(13): 11481-11488.

Beaudoin, F., Wu, X., Haslam, R., Markham, J., Zheng, H., Napier, J. and Kunst, L. (2009). *Functional characterization of the Arabidopsis β -Ketoacyl-Coenzyme A reductase candidates of the fatty acid elongase.* Plant physiology **150**: 1174-1191.

Beeler, T., Bacikova, D., Gable, K., Hopkins, L., Johnson, C., Slife, H. and Dunn, T. (1998). *The Saccharomyces cerevisiae TSC10/YBR265w gene encoding 3-Ketosphinganine Reductase is identified in a screen for temperature-sensitive suppressors of the Ca²⁺-sensitive csg2 Delta mutant.* Journal of Biological Chemistry **273**(46): 30688-30694.

Bell, C. J. and Ecker, J. R. (1994). *Assignment of 30 microsatellite loci to the linkage map of Arabidopsis.* Genomics **19**(1): 137-144.

Bellec, Y., Harrar, Y., Butaeye, C., Darnet, S., Bellini, C. and Faure, J. D. (2002). *Pasticcino2 is a protein tyrosine phosphatase-like involved in cell proliferation and differentiation in Arabidopsis.* Plant Journal **32**(5): 713-722.

Benkova, E., Michniewicz, M., Sauer, M., Teichmann, T., Seifertova, D., Jurgens, G. and Friml, J. (2003). *Local, efflux-dependent auxin gradients as a common module for plant organ formation.* Cell **115**(5): 591-602.

References

Bernard, A., Domergue, F., Pascal, S., Jetter, R., Renne, C., Faure, J. D., Haslam, R. P., Napier, J. A., Lessire, R. and Joubes, J. (2012). *Reconstitution of plant alkane biosynthesis in yeast demonstrates that Arabidopsis ECERIFERUM1 and ECERIFERUM3 are core components of a very-long-chain alkane synthesis complex.* Plant Cell **24**(7): 3106-3118.

Bernard, A. and Joubes, J. (2013). *Arabidopsis cuticular waxes: Advances in synthesis, export and regulation.* Progress in Lipid Research **52**(1): 110-129.

Bird, D., Beisson, F., Brigham, A., Shin, J., Greer, S., Jetter, R., Kunst, L., Wu, X., Yephremov, A. and Samuels, L. (2007). *Characterization of Arabidopsis ABCG11/WBC11, an ATP binding cassette (ABC) transporter that is required for cuticular lipid secretion.* Plant Journal **52**(3): 485-498.

Blakeslee, J. J., Bandyopadhyay, A., Lee, O. R., Mravec, J., Titapiwatanakun, B., Sauer, M., Makam, S. N., Cheng, Y., Bouchard, R., Adamec, J., Geisler, M., Nagashima, A., Sakai, T., Martinoia, E., Friml, J., Peer, W. A. and Murphy, A. S. (2007). *Interactions among PIN-FORMED and P-glycoprotein auxin transporters in Arabidopsis.* Plant Cell **19**(1): 131-147.

Blanksby, S. J. and Mitchell, T. W. (2010). *Advances in mass spectrometry for lipidomics.* Annual Review of Analytical Chemistry **3**: 433-465.

Bligh, E. G. and Dyer, W. J. (1959). *A rapid method of total lipid extraction and purification* Canadian Journal of Biochemistry and Physiology **37**(8): 911-917.

Bonaventure, G., Salas, J. J., Pollard, M. R. and Ohlrogge, J. B. (2003). *Disruption of the FATB gene in Arabidopsis demonstrates an essential role of saturated fatty acids in plant growth.* Plant Cell **15**(4): 1020-1033.

Borner, G. H. H., Sherrier, D. J., Weimar, T., Michaelson, L. V., Hawkins, N. D., MacAskill, A., Napier, J. A., Beale, M. H., Lilley, K. S. and Dupree, P. (2005). *Analysis of detergent-resistant membranes in Arabidopsis. Evidence for plasma membrane lipid rafts.* Plant Physiology **137**(1): 104-116.

Bourdenx, B., Bernard, A., Domergue, F., Pascal, S., Leger, A., Roby, D., Pervent, M., Vile, D., Haslam, R. P., Napier, J. A., Lessire, R. and Joubes, J. (2011). *Overexpression of Arabidopsis ECERIFERUM1 promotes wax very-long-chain alkane biosynthesis and influences plant response to biotic and abiotic stresses.* Plant physiology **156**(1): 29-45.

Boutte, Y., Frescatada-Rosa, M., Men, S. Z., Chow, C. M., Ebine, K., Gustavsson, A., Johansson, L., Ueda, T., Moore, I., Jurgens, G. and Grebe, M. (2010). *Endocytosis restricts Arabidopsis KNOLLE syntaxin to the cell division plane during late cytokinesis.* Embo Journal **29**(3): 546-558.

References

Brandwagt, B. F., Mesbah, L. A., Takken, F. L. W., Laurent, P. L., Kneppers, T. J. A., Hille, J. and Nijkamp, H. J. J. (2000). *A longevity assurance gene homolog of tomato mediates resistance to *Alternaria alternata* f. sp *lycopersici* toxins and fumonisin B(1)*. Proceedings of the National Academy of Sciences of the United States of America **97**(9): 4961-4966.

Brown, D. A. and Rose, J. K. (1992). *Sorting of GPI-anchored proteins to glycolipid-enriched membrane subdomains during transport to the apical cell surface*. Cell **68**(3): 533-544.

Browse, J., Kunst, L., Hugly, S. and Somerville, C. (1989). *Modifications to the two pathway scheme of lipid metabolism based on studies of arabidopsis mutants*. Biological Role of Plant Lipids. P. Biacs, K. Gruiz and T. Kremmer, Springer US: 335-339.

Browse, J., McCourt, P. and Somerville, C. R. (1985). *A mutant of Arabidopsis lacking a chloroplast specific lipid* Science **227**(4688): 763-765.

Brugger, B., Erben, G., Sandhoff, R., Wieland, F. T. and Lehmann, W. D. (1997). *Quantitative analysis of biological membrane lipids at the low picomole level by nano-electrospray ionization tandem mass spectrometry*. Proceedings of the National Academy of Sciences of the United States of America **94**(6): 2339-2344.

Bure, C., Cacas, J. L., Wang, F., Gaudin, K., Domergue, F., Mongrand, S. and Schmitter, J. M. (2011). *Fast screening of highly glycosylated plant sphingolipids by tandem mass spectrometry*. Rapid Communications in Mass Spectrometry **25**(20): 3131-3145.

Cacas, J. L., Furt, F., Le Guedard, M., Schmitter, J. M., Bure, C., Gerbeau-Pissot, P., Moreau, P., Bessoule, J. J., Simon-Plas, F. and Mongrand, S. (2012). *Lipids of plant membrane rafts*. Progress in Lipid Research **51**(3): 272-299.

Cerantola, V., Vionnet, C., Aebischer, O. F., Jenny, T., Knudsen, J. and Conzelmann, A. (2007). *Yeast sphingolipids do not need to contain very long chain fatty acids*. Biochemical Journal **401**(1): 205-216.

Chang, C., Bowman, J. L., DeJohn, A. W., Lander, E. S. and Meyerowitz, E. M. (1988). *Restriction fragment length polymorphism linkage map for Arabidopsis thaliana*. Proceedings of the National Academy of Sciences of the United States of America **85**(18): 6856-6860.

Chang, C. and Meyerowitz, E. M. (1991). *Plant genome studies: restriction fragment length polymorphism and chromosome mapping information*. Current Opinions in Genetic Development **1**(1): 112-118.

References

Chao, D.-Y., Gable, K., Chen, M., Baxter, I., Dietrich, C. R., Cahoon, E. B., Guerinot, M. L., Lahner, B., Lue, S., Markham, J. E., Morrissey, J., Han, G., Gupta, S. D., Harmon, J. M., Jaworski, J. G., Dunn, T. M. and Salt, D. E. (2011). *Sphingolipids in the root play an important role in regulating the leaf ionome in Arabidopsis thaliana*. Plant Cell **23**(3): 1061-1081.

Cheesbrough, T. M. and Kolattukudy, P. E. (1984). *Alkane biosynthesis by decarbonylation of aldehydes catalysed by a particulate preparation from Pisum-sativum* Proceedings of the National Academy of Sciences of the United States of America-Biological Sciences **81**(21): 6613-6617.

Chen, M., Han, G. S., Dietrich, C. R., Dunn, T. M. and Cahoon, E. B. (2006). *The essential nature of sphingolipids in plants as revealed by the functional identification and characterization of the Arabidopsis LCB1 subunit of Serine Palmitoyltransferase*. Plant Cell **18**(12): 3576-3593.

Chen, M., Markham, J. E., Dietrich, C. R., Jaworski, J. G. and Cahoon, E. B. (2008). *Sphingolipid long-chain base hydroxylation is important for growth and regulation of sphingolipid content and composition in Arabidopsis*. Plant Cell **20**(7): 1862-1878.

Chen, X., Goodwin, S. M., Boroff, V. L., Liu, X. and Jenks, M. A. (2003). *Cloning and characterization of the WAX2 gene of Arabidopsis involved in cuticle membrane and wax production*. Plant Cell **15**(5): 1170-1185.

Clough, S. J. and Bent, A. F. (1998). *Floral dip: a simplified method for Agrobacterium-mediated transformation of Arabidopsis thaliana*. Plant Journal **16**(6): 735-743.

Costaglioli, P., Joubes, K., Garcia, C., Stef, M., Arweiler, B., Lessire, R. and Garbay, B. (2005). *Profiling candidate genes involved in wax biosynthesis in Arabidopsis thaliana by microarray analysis*. Biochimica Et Biophysica Acta-Molecular and Cell Biology of Lipids **1734**(3): 247-258.

David, D., Sundarababu, S., Gerst, J. E. and Gerst, J. E. (1998). *Involvement of long chain fatty acid elongation in the trafficking of secretory vesicles in yeast*. Journal of Cell Biology **143**(5): 1167-1182.

Denic, V. and Weissman, J. S. (2007). *A molecular caliper mechanism for determining very long-chain fatty acid length*. Cell **130**(4): 663-677.

Dennis, M. W. and Kolattukudy, P. E. (1991). *Alkane biosynthesis by decarbonylation of aldehyde catalysed by a microsomal preparation from botryococcus-braunii*. Archives of Biochemistry and Biophysics **287**(2): 268-275.

References

Devaiah, S. P., Roth, M. R., Baughman, E., Li, M. Y., Tamura, P., Jeannotte, R., Welti, R. and Wang, X. M. (2006). *Quantitative profiling of polar glycerolipid species from organs of wild-type Arabidopsis and a PHOSPHOLIPASE D alpha 1 knockout mutant*. Phytochemistry **67**(17): 1907-1924.

Dietrich, C. R., Han, G., Chen, M., Berg, R. H., Dunn, T. M. and Cahoon, E. B. (2008). *Loss-of-function mutations and inducible RNAi suppression of Arabidopsis LCB2 genes reveal the critical role of sphingolipids in gametophytic and sporophytic cell viability*. Plant Journal **54**(2): 284-298.

Dietrich, C. R., Perera, M., Yandeu-Nelson, M. D., Meeley, R. B., Nikolau, B. J. and Schnable, P. S. (2005). *Characterization of two GL8 paralogs reveals that the 3-ketoacyl reductase component of fatty acid elongase is essential for maize (Zea mays L.) development*. Plant Journal **42**(6): 844-861.

Domon, B. and Aebersold, R. (2006). *Review - Mass spectrometry and protein analysis*. Science **312**(5771): 212-217.

Dormann, P. (2005). Plant lipids- Biology, Utilisation and manipulation

Dörmann, P. (2001). *Galactolipids in Plant Membranes*. eLS, John Wiley & Sons, Ltd.

Dubots, E., Botte, C., Boudiere, L., Yamaryo-Botte, Y., Jouhet, J., Marechal, E. and Block, M. A. (2012). *Role of phosphatidic acid in plant galactolipid synthesis*. Biochimie **94**(1): 86-93.

Dunn, T. M., Lynch, D. V., Michaelson, L. V. and Napier, J. A. (2004). *A post-genomic approach to understanding sphingolipid metabolism in Arabidopsis thaliana*. Annals of Botany **93**(5): 483-497.

Eigenbrode, S. D. and Espelie, K. E. (1995). *Effects of plant epicuticular lipids on insect herbivores*. Annual Review of Entomology **40**: 171-194.

Eisenkolb, M., Zenzmaier, C., Leitner, E. and Schneiter, R. (2002). *A specific structural requirement for ergosterol in long-chain fatty acid synthesis mutants important for maintaining raft domains in yeast*. Molecular Biology of the Cell **13**(12): 4414-4428.

References

Fahy, E., Subramaniam, S., Brown, H. A., Glass, C. K., Merrill, A. H., Murphy, R. C., Raetz, C. R. H., Russell, D. W., Seyama, Y., Shaw, W., Shimizu, T., Spener, F., van Meer, G., VanNieuwenhze, M. S., White, S. H., Witztum, J. L. and Dennis, E. A. (2005). A comprehensive classification system for lipids. *Journal of Lipid Research* **46**(5): 839-861.

Faure, J. D., Vittorioso, P., Santoni, V., Fraiser, V., Prinsen, E., Barlier, I., Van Onckelen, H., Caboche, M. and Bellini, C. (1998). The PASTICCINO genes of *Arabidopsis thaliana* are involved in the control of cell division and differentiation. *Development* **125**(5): 909-918.

Fiebig, A., Mayfield, J. A., Miley, N. L., Chau, S., Fischer, R. L. and Preuss, D. (2000). Alterations in CER6, a gene identical to CUT1, differentially affect long-chain lipid content on the surface of pollen and stems. *Plant Cell* **12**(10): 2001-2008.

Franke, R., Hofer, R., Briesen, I., Emsermann, M., Efremova, N., Yephremov, A. and Schreiber, L. (2009). The DAISY gene from *Arabidopsis* encodes a fatty acid elongase condensing enzyme involved in the biosynthesis of aliphatic suberin in roots and the chalaza-micropyle region of seeds. *Plant Journal* **57**(1): 80-95.

Frentzen, M., Heinz, E., McKeon, T. A. and Stumpf, P. K. (1983). Specificities and selectivities of glycerol-3-phosphate acyltransferase and monoacylglycerol-3-phosphate acyltransferase from pea and spinach chloroplasts. *European Journal of Biochemistry* **129**(3): 629-636.

Friml, J., Vieten, A., Sauer, M., Weijers, D., Schwarz, H., Hamann, T., Offringa, R. and Jurgens, G. (2003). Efflux-dependent auxin gradients establish the apical-basal axis of *Arabidopsis*. *Nature* **426**(6963): 147-153.

Fujino, Y. and Ohnishi, M. (1982). Speices of Sphingolipids in Rice Grain. *Proceedings of the Japan Academy Series B-Physical and Biological Sciences* **58**(2): 36-39.

Gable, K., Garton, S., Napier, J. A. and Dunn, T. M. (2004). Functional characterization of the *Arabidopsis thaliana* orthologue of Tsc13p, the enoyl reductase of the yeast microsomal fatty acid elongating system. *Journal of Experimental Botany* **55**(396): 543-545.

Gable, K., Han, G., Monaghan, E., Bacikova, D., Natarajan, M., Williams, R. and Dunn, T. M. (2002). Mutations in the yeast LCB1 and LCB2 genes, including those corresponding to the hereditary sensory neuropathy type I mutations, dominantly inactivate Serine Palmitoyltransferase. *Journal of Biological Chemistry* **277**(12): 10194-10200.

Gable, K., Slife, H., Bacikova, D., Monaghan, E. and Dunn, T. M. (2000). Tsc3p is an 80-amino acid protein associated with Serine Palmitoyltransferase and required for optimal enzyme activity. *Journal of Biological Chemistry* **275**(11): 7597-7603.

References

Ghanevati, M. and Jaworski, J. G. (2002). *Engineering and mechanistic studies of the Arabidopsis FAE1 beta-ketoacyl-CoA synthase, FAE1 KCS.* European Journal of Biochemistry **269**(14): 3531-3539.

Givan, C. V. (1983). *The source of acetyl Coenzyme-A in chloroplasts of higher-plants.* Physiologia Plantarum **57**(2): 311-316.

Gray, J. E., Holroyd, G. H., van der Lee, F. M., Bahrami, A. R., Sijmons, P. C., Woodward, F. I., Schuch, W. and Hetherington, A. M. (2000). *The HIC signalling pathway links CO₂ perception to stomatal development.* Nature **408**(6813): 713-716.

Greene, E. A., Codomo, C. A., Taylor, N. E., Henikoff, J. G., Till, B. J., Reynolds, S. H., Enns, L. C., Burtner, C., Johnson, J. E., Odden, A. R., Comai, L. and Henikoff, S. (2003). *Spectrum of chemically induced mutations from a large-scale reverse-genetic screen in Arabidopsis.* Genetics **164**(2): 731-740.

Greer, S., Wen, M., Bird, D., Wu, X. M., Samuels, L., Kunst, L. and Jetter, R. (2007). *The cytochrome p450 enzyme CYP96A15 is the midchain alkane hydroxylase responsible for formation of secondary alcohols and ketones in stem cuticular wax of arabidopsis.* Plant Physiology **145**(3): 653-667.

Grilley, M. M., Stock, S. D., Dickson, R. C., Lester, R. L. and Takemoto, J. Y. (1998). *Syngomycin action gene SYR2 is essential for sphingolipid 4-hydroxylation in Saccharomyces cerevisiae.* Journal of Biological Chemistry **273**(18): 11062-11068.

Han, G., Gable, K., Kohlwein, S. D., Beaudoin, F., Napier, J. A. and Dunn, T. M. (2002). *The Saccharomyces cerevisiae YBR159w gene encodes the 3-Ketoreductase of the microsomal fatty acid elongase.* Molecular Biology of the Cell **13**: 360A-360A.

Han, G., Gupta, S. D., Gable, K., Niranjankumari, S., Moitra, P., Eichler, F., Brown, R. H., Jr., Harmon, J. M. and Dunn, T. M. (2009). *Identification of small subunits of mammalian Serine Palmitoyltransferase that confer distinct acyl-CoA substrate specificities.* Proceedings of the National Academy of Sciences of the United States of America **106**(20): 8186-8191.

Han, J., Clement, J. M., Li, J., King, A., Ng, S. and Jaworski, J. G. (2010). *The cytochrome P450 CYP86A22 is a fatty acyl-CoA omega-hydroxylase essential for estolide synthesis in the stigma of Petunia hybrida.* Journal of Biological Chemistry **285**(6): 3986-3996.

Hanada, K. (2003). *Serine Palmitoyltransferase, a key enzyme of sphingolipid metabolism.* Biochimica Et Biophysica Acta-Molecular and Cell Biology of Lipids **1632**(1-2): 16-30.

References

Hanada, K., Kumagai, K., Yasuda, S., Miura, Y., Kawano, M., Fukasawa, M. and Nishijima, M. (2003). *Molecular machinery for non-vesicular trafficking of ceramide*. Nature **426**(6968): 803-809.

Harrar, Y., Bellec, Y., Bellini, C. and Faure, J. D. (2003). *Hormonal control of cell proliferation requires PASTICCINO genes*. Plant Physiology **132**(3): 1217-1227.

Hartwig, B., James, G. V., Konrad, K., Schneeberger, K. and Turck, F. (2012). *Fast isogenic mapping-by-sequencing of ethyl methanesulfonate-induced mutant bulks*. Plant Physiol **160**(2): 591-600.

Harwood, J. L. (1988). *Fatty-acid metabolism*. Annual Review of Plant Physiology and Plant Molecular Biology **39**: 101-138.

Harwood, J. L. (1996). *Recent advances in the biosynthesis of plant fatty acids*. Biochimica Et Biophysica Acta-Lipids and Lipid Metabolism **1301**(1-2): 7-56.

Haslam, T. M. and Kunst, L. (2013). *Extending the story of very-long-chain fatty acid elongation*. Plant Science **210**: 93-107.

Haslam, T. M., Manas-Fernandez, A., Zhao, L. and Kunst, L. (2012). *Arabidopsis ECERIFERUM2 is a component of the fatty acid elongation machinery required for fatty acid extension to exceptional lengths*. Plant physiology **160**(3): 1164-1174.

Haynes, C. A., Allegood, J. C., Sims, K., Wang, E. W., Sullards, M. C. and Merrill, A. H., Jr. (2008). *Quantitation of fatty acyl-coenzyme As in mammalian cells by liquid chromatography-electrospray ionization tandem mass spectrometry*. Journal of Lipid Research **49**(5): 1113-1125.

Hooker, T. S., Millar, A. A. and Kunst, L. (2002). *Significance of the expression of the CER6 condensing enzyme for cuticular wax production in Arabidopsis*. Plant physiology **129**(4): 1568-1580.

Hou, X. H., Li, L. C., Peng, Z. Y., Wei, B. Y., Tang, S. J., Ding, M. Y., Liu, J. J., Zhang, F. X., Zhao, Y. D., Gu, H. Y. and Qu, L. J. (2010). *A platform of high-density INDEL/CAPS markers for map-based cloning in Arabidopsis*. Plant Journal **63**(5): 880-888.

Hulskamp, M., Kopczak, S. D., Horejsi, T. F., Kihl, B. K. and Pruitt, R. E. (1995). *Identification of genes required for pollen-stigma recognition in Arabidopsis thaliana*. Plant Journal **8**(5): 703-714.

illumina (2014). *Sequencing by synthesis technologies*

References

Jablonkai, I. (2003). *Alkylating reactivity and herbicidal activity of chloroacetamides*. Pest Management Science **59**(4): 443-450.

James, D. W. and Dooner, H. K. (1990). *Isolation of EMS-induced mutants in Arabidopsis altered in seed fatty-acid composition*. Theoretical and Applied Genetics **80**(2): 241-245.

James, D. W., Lim, E., Keller, J., Plooy, I., Ralston, E. and Dooner, H. K. (1995). *Directed tagging of the Arabidopsis fatty-acid elongation-1 (FAE1) gene with the maize transposon activator*. Plant Cell **7**(3): 309-319.

James, G. V., Patel, V., Nordstrom, K. J. V., Klasen, J. R., Salome, P. A., Weigel, D. and Schneeberger, K. (2013). *User guide for mapping-by-sequencing in Arabidopsis*. Genome Biology **14**(6).

Jander, G., Norris, S. R., Rounsley, S. D., Bush, D. F., Levin, I. M. and Last, R. L. (2002). *Arabidopsis map-based cloning in the post-genome era*. Plant Physiol **129**(2): 440-450.

Jenik, P. D. and Barton, M. K. (2005). *Surge and destroy: the role of auxin in plant embryogenesis*. Development **132**(16): 3577-3585.

Jenks, M. A., Tuttle, H. A., Eigenbrode, S. D. and Feldmann, K. A. (1995). *Leaf epicuticular waxes of the eceriferum mutants in Arabidopsis* Plant physiology **108**(1): 369-377.

Jetter, R. and Schaffer, S. (2001). *Chemical composition of the Prunus laurocerasus leaf surface. Dynamic changes of the epicuticular wax film during leaf development*. Plant Physiology **126**(4): 1725-1737.

Joubes, J., Raffaele, S., Bourdenx, B., Garcia, C., Laroche-Traineau, J., Moreau, P., Domergue, F. and Lessire, R. (2008). *The VLCFA elongase gene family in Arabidopsis thaliana: phylogenetic analysis, 3D modelling and expression profiling*. Plant Molecular Biology **67**(5): 547-566.

Kalscheuer, R. and Steinbuchel, A. (2003). *A novel bifunctional wax ester synthase/acyl-CoA:diacylglycerol acyltransferase mediates wax ester and triacylglycerol biosynthesis in Acinetobacter calcoaceticus ADP1*. Journal of Biological Chemistry **278**(10): 8075-8082.

Kent, C. and Carman, G. M. (1999). *Interactions among pathways for phosphatidylcholine metabolism, CTP synthesis and secretion through the Golgi apparatus*. Trends in Biochemical Sciences **24**(4): 146-150.

Kim, H. U. and Huang, A. H. (2004). *Plastid lysophosphatidyl acyltransferase is essential for embryo development in Arabidopsis*. Plant Physiol **134**(3): 1206-1216.

References

Kim, H. U., Li, Y. and Huang, A. H. (2005). *Ubiquitous and endoplasmic reticulum-located lysophosphatidyl acyltransferase, LPAT2, is essential for female but not male gametophyte development in Arabidopsis.* Plant Cell **17**(4): 1073-1089.

Kim, J., Jung, J. H., Lee, S. B., Go, Y. S., Kim, H. J., Cahoon, R., Markham, J. E., Cahoon, E. B. and Suh, M. C. (2013). *Arabidopsis 3-Ketoacyl-Coenzyme a synthase is involved in the synthesis of tetracosanoic acids as precursors of cuticular waxes, suberins, sphingolipids, and phospholipids.* Plant Physiology **162**(2): 567-580.

Kimberlin, A. N., Majumder, S., Han, G., Chen, M., Cahoon, R. E., Stone, J. M., Dunn, T. M. and Cahoon, E. B. (2013). *Arabidopsis 56-amino acid Serine Palmitoyltransferase-interacting proteins stimulate sphingolipid synthesis, are essential, and affect mycotoxin sensitivity.* Plant Cell **25**(11): 4627-4639.

Kinney, A. J., Clarkson, D. T. and Loughman, B. C. (1987). *The regulation of phosphatidylcholine biosynthesis in rye (Secale cereale) roots. Stimulation of the nucleotide pathway by low temperature.* Biochemical Journal **242**(3): 755-759.

Klimyuk, V. I., Carroll, B. J., Thomas, C. M. and Jones, J. D. G. (1993). *Alkali treatment for rapid preparation of plant-material for reliable PCR analysis.* Plant Journal **3**(3): 493-494.

Kohlwein, S. D., Eder, S., Oh, C. S., Martin, C. E., Gable, K., Bacikova, D. and Dunn, T. (2001). *Tsc13p is required for fatty acid elongation and localizes to a novel structure at the nuclear-vacuolar interface in Saccharomyces cerevisiae.* Molecular and Cellular Biology **21**(1): 109-125.

Kolattukudy, P. E. (1980). *Bio-polyester membranes of plants-cutin and suberin.* Science **208**(4447): 990-1000.

Konieczny, A. and Ausubel, F. M. (1993). *A procedure for mapping Arabidopsis mutations using codominant ecotype-specific PCR-based markers.* Plant Journal **4**(2): 403-410.

Koorneef, M., Hanhart, C. J. and Thiel, F. (1989). *A genetic and phenotypic description of eceriferum (CER) mutants in arabidopsis-thaliana.* Journal of Heredity **80**(2): 118-122.

Kunst, L., Browse, J. and Somerville, C. (1988). *Altered regulation of lipid biosynthesis in a mutant of Arabidopsis deficient in chloroplast glycerol-3-phosphate acyltransferase activity.* Proceedings of the National Academy of Sciences of the United States of America **85**(12): 4143-4147.

Kunst, L. T., D and Underhill, E. (1992). *Fatty acid elongation in developing seeds of Arabidopsis thaliana.* Plant physiological Biochemistry **30**(4): 425-434.

References

Kurdyukov, S., Faust, A., Nawrath, C., Bar, S., Voisin, D., Efremova, N., Franke, R., Schreiber, L., Saedler, H., Metraux, J. P. and Yephremov, A. (2006). *The epidermis-specific extracellular BODYGUARD controls cuticle development and morphogenesis in Arabidopsis*. Plant Cell **18**(2): 321-339.

Lai, C., Kunst, L. and Jetter, R. (2007). *Composition of alkyl esters in the cuticular wax on inflorescence stems of Arabidopsis thaliana cer mutants*. Plant Journal **50**(2): 189-196.

Lardizabal, K. D., Metz, J. G., Sakamoto, T., Hutton, W. C., Pollard, M. R. and Lassner, M. W. (2000). *Purification of a jojoba embryo wax synthase, cloning of its cDNA, and production of high levels of wax in seeds of transgenic arabidopsis*. Plant Physiol **122**(3): 645-655.

Larson, T. and Graham, I. (2001). *Technical Advance: A novel technique for the sensitive quantification of acyl CoA esters from plant tissues*. The Plant journal **25**(1): 115-125.

Lechelt-Kunze, C., Meissner, R. C., Drewes, M. and Tietjen, K. (2003). *Flufenacet herbicide treatment phenocopies the fiddlehead mutant in Arabidopsis thaliana*. Pest Management Science **59**(8): 847-856.

Lee, S.-B., Jung, S.-J., Go, Y.-S., Kim, H.-U., Kim, J.-K., Cho, H.-J., Park, O. K. and Suh, M.-C. (2009). *Two Arabidopsis 3-ketoacyl CoA synthase genes, KCS20 and KCS2/DAISY, are functionally redundant in cuticular wax and root suberin biosynthesis, but differentially controlled by osmotic stress*. Plant Journal **60**(3): 462-475.

Lefebvre, B., Furt, F., Hartmann, M. A., Michaelson, L. V., Carde, J. P., Sargueil-Boiron, F., Rossignol, M., Napier, J. A., Cullimore, J., Bessoule, J. J. and Mongrand, S. (2007). *Characterization of lipid rafts from Medicago truncatula root plasma membranes: A proteomic study reveals the presence of a raft-associated redox system*. Plant Physiology **144**(1): 402-418.

Lemieux, B., Miquel, M., Somerville, C. and Browse, J. (1990). *Mutants of Arabidopsis With Alterations in Seed Lipid Fatty-Acid Composition*. Theoretical and Applied Genetics **80**(2): 234-240.

Li, F., Wu, X., Lam, P., Bird, D., Zheng, H., Samuels, L., Jetter, R. and Kunst, L. (2008). *Identification of the wax ester synthase/acyl-coenzyme A: Diacylglycerol acyltransferase WSD1 required for stem wax ester biosynthesis in Arabidopsis*. Plant Physiology **148**(1): 97-107.

Liang, H., Yao, N., Song, L. T., Luo, S., Lu, H. and Greenberg, L. T. (2003). *Ceramides modulate programmed cell death in plants*. Genes & Development **17**(21): 2636-2641.

References

Lolle, S. J., Berlyn, G. P., Engstrom, E. M., Krolkowski, K. A., Reiter, W. D. and Pruitt, R. E. (1997). *Developmental regulation of cell interactions in the Arabidopsis fiddlehead-1 mutant: A role for the epidermal cell wall and cuticle.* Developmental Biology **189**(2): 311-321.

Lolle, S. J., Cheung, A. Y. and Sussex, I. M. (1992). *Fiddlehead - an arabidopsis mutant constitutively expressing an organ fusion program that involves interaction between epidermal cells* Developmental Biology **152**(2): 383-392.

Markham, J., Li, J., Cahoon, E. and Jaworski, J. (2006). *Separation and Identification of Major Plant Sphingolipid Classes from Leaves.* The Journal of biological chemistry **281**: 22684-22694.

Markham, J. E. (2013). *Detection and quantification of plant sphingolipids by LC-MS.* Methods in molecular biology (Clifton, N.J.) **1009**.

Markham, J. E. and Jaworski, J. G. (2007). *Rapid measurement of sphingolipids from Arabidopsis thaliana by reversed-phase high-performance liquid chromatography coupled to electrospray ionization tandem mass spectrometry.* Rapid Communications in Mass Spectrometry **21**(7): 1304-1314.

Markham, J. E., Molino, D., Gissot, L., Bellec, Y., Hematy, K., Marion, J., Belcram, K., Palauqui, J. C., Satiat-JeuneMaitre, B. and Faure, J. D. (2011). *Sphingolipids containing very-long-chain fatty acids define a secretory pathway for specific polar plasma membrane protein targeting in Arabidopsis.* Plant Cell **23**(6): 2362-2378.

McCallum, C. M., Comai, L., Greene, E. A. and Henikoff, S. (2000). *Targeted screening for induced mutations.* Nature Biotechnology **18**(4): 455-457.

Meinke, D. W., Cherry, J. M., Dean, C., Rounsley, S. D. and Koornneef, M. (1998). *Arabidopsis thaliana: a model plant for genome analysis.* Science **282**(5389): 662, 679-682.

Melser, S., Batailler, B., Peypelut, M., Poujol, C., Bellec, Y., Wattelet-Boyer, V., Maneta-Peyret, L., Faure, J. D. and Moreau, P. (2010). *Glucosylceramide Biosynthesis is Involved in Golgi Morphology and Protein Secretion in Plant Cells.* Traffic **11**(4): 479-490.

Men, S. Z., Boutte, Y., Ikeda, Y., Li, X. G., Palme, K., Stierhof, Y. D., Hartmann, M. A., Moritz, T. and Grebe, M. (2008). *Sterol-dependent endocytosis mediates post-cytokinetic acquisition of PIN2 auxin efflux carrier polarity.* Nature Cell Biology **10**(2): 237-U124.

Menne, H. (2014). *Classification of herbicides site of action 2014*, from <http://www.hracglobal.com/Education/ClassificationofHerbicideSiteofAction.aspx>.

References

Menon, A. K. and Stevens, V. L. (1992). *Phosphatidylethanolamine is the donor of the ethanolamine residue linking a glycosylphosphatidylinositol anchor to protein.* Journal of Biological Chemistry **267**(22): 15277-15280.

Michaelson, L. V. and Napier, J. A. (2010). *Sphingolipid Signaling in Plants.* Lipid Signaling in Plants. T. Munnik, Springer-Verlag Berlin: 307-321.

Mileykovskaya, E., Sun, Q., Margolin, W. and Dowhan, W. (1998). *Localization and function of early cell division proteins in filamentous Escherichia coli cells lacking phosphatidylethanolamine.* Journal of Bacteriology **180**(16): 4252-4257.

Millar, A. and Kunst, L. (1997). *Very-long-chain fatty acid biosynthesis is controlled through the expression and specificity of the condensing enzyme.* The Plant journal **12**(1): 121-131.

Millar, A. A., Clemens, S., Zachgo, S., Giblin, E. M., Taylor, D. C. and Kunst, L. (1999). *CUT1, an arabidopsis gene required for cuticular wax biosynthesis and pollen fertility, encodes a very-long-chain fatty acid condensing enzyme.* Plant Cell **11**(5): 825-838.

Mitchell, A. G. and Martin, C. E. (1997). *Fah1p, a Saccharomyces cerevisiae cytochrome b(5) fusion protein, and its Arabidopsis thaliana homolog that lacks the cytochrome b(5) domain both function in the alpha-hydroxylation of sphingolipid-associated very long chain fatty acids.* Journal of Biological Chemistry **272**(45): 28281-28288.

Mizoi, J., Nakamura, M. and Nishida, I. (2003). *A study of the physiological function of phosphatidylethanolamine in Arabidopsis.* Advanced Research on Plant Lipids. N. Murata, M. Yamada, I. Nishida et al., Springer Netherlands: 377-380.

Moller, B. and Weijers, D. (2009). *Auxin control of embryo patterning.* Cold Spring Harbor Perspectives in Biology **1**(5): a001545.

Moller, J. M. a. S. G. (2007). *Mutagenesis in Arabidopsis* Methods in Molecular Biology **362**.

Mortimer, J. C., Yu, X., Albrecht, S., Sicilia, F., Huichalaf, M., Ampuero, D., Michaelson, L. V., Murphy, A. M., Matsunaga, T., Kurz, S., Stephens, E., Baldwin, T. C., Ishii, T., Napier, J. A., Weber, A. P., Handford, M. G. and Dupree, P. (2013). *Abnormal glycosphingolipid mannosylation triggers salicylic acid-mediated responses in Arabidopsis.* Plant Cell **25**(5): 1881-1894.

Munro, S. (2003). *Lipid rafts: elusive or illusive?* Cell **115**(4): 377-388.

Murashige, T. and Skoog, F. (1962). *A revised medium for rapid growth and bio assays with tobacco tissue cultures.* Physiologia Plantarum **15**(3): 473-497.

References

Murray, M. G. and Thompson, W. F. (1980). *Rapid isolation of high molecular-weight plant DNA*. Nucleic Acids Research **8**(19): 4321-4325.

Nagano, M., Ihara-Ohori, Y., Imai, H., Inada, N., Fujimoto, M., Tsutsumi, N., Uchimiya, H. and Kawai-Yamada, M. (2009). *Functional association of cell death suppressor, Arabidopsis Bax inhibitor-1, with fatty acid 2-hydroxylation through cytochrome b(5)*. Plant Journal **58**(1): 122-134.

Nagano, M., Takahara, K., Fujimoto, M., Tsutsumi, N., Uchimiya, H. and Kawai-Yamada, M. (2012). *Arabidopsis sphingolipid fatty acid 2-Hydroxylases (AtFAH1 and AtFAH2) are functionally differentiated in fatty acid 2-hydroxylation and stress responses*. Plant Physiology **159**(3): 1138-1148.

Neff, M. M., Neff, J. D., Chory, J. and Pepper, A. E. (1998). *dCAPS, a simple technique for the genetic analysis of single nucleotide polymorphisms: experimental applications in Arabidopsis thaliana genetics*. Plant Journal **14**(3): 387-392.

Nobusawa, T., Okushima, Y., Nagata, N., Kojima, M., Sakakibara, H. and Umeda, M. (2013). *Synthesis of very-long-chain fatty acids in the epidermis controls plant organ growth by restricting cell proliferation*. Plos Biology **11**(4).

Oh, C. S., Toke, D. A., Mandala, S. and Martin, C. E. (1997). *ELO2 and ELO3, homologues of the Saccharomyces cerevisiae ELO1 gene, function in fatty acid elongation and are required for sphingolipid formation*. Journal of Biological Chemistry **272**(28): 17376-17384.

Ohlrogge, J. and Browse, J. (1995). *Lipid biosynthesis*. Plant Cell **7**(7): 957-970.

Okada, K., Komaki, M. K. and Shimura, Y. (1989). *Mutational analysis of pistil structure and development of Arabidopsis thaliana*. Cell Differentiation and Development **28**(1): 27-38.

Ossowski, S., Schneeberger, K., Clark, R. M., Lanz, C., Warthmann, N. and Weigel, D. (2008). *Sequencing of natural strains of Arabidopsis thaliana with short reads*. Genome Research **18**(12): 2024-2033.

Overath, P. and Stumpf, P. K. (1964). *Fat metabolism in higher plants .23. properties of soluble fatty acid synthetase from Avocado mesocarp*. Journal of Biological Chemistry **239**(12): 4103-&.

Paul, S., Gable, K., Beaudoin, F., Cahoon, E., Jaworski, J., Napier, J. A. and Dunn, T. M. (2006). *Members of the Arabidopsis FAE1-like3-ketoacyl-CoA synthase gene family substitute for the Elop proteins of Saccharomyces cerevisiae*. Journal of Biological Chemistry **281**(14): 9018-9029.

References

Perrot-Rechenmann, C. (2010). *Cellular responses to auxin: division versus expansion*. Cold Spring Harbor Perspectives in Biology **2**(5): a001446.

Pical, C., Westergren, T., Dove, S. K., Larsson, C. and Sommarin, M. (1999). *Salinity and hyperosmotic stress induce rapid increases in phosphatidylinositol 4,5-bisphosphate, diacylglycerol pyrophosphate, and phosphatidylcholine in Arabidopsis thaliana cells*. Journal of Biological Chemistry **274**(53): 38232-38240.

Pighin, J. A., Zheng, H. Q., Balakshin, L. J., Goodman, I. P., Western, T. L., Jetter, R., Kunst, L. and Samuels, A. L. (2004). *Plant cuticular lipid export requires an ABC transporter*. Science **306**(5696): 702-704.

Preuss D, L. B., Yen G, Davis RW. (1993). *A conditional sterile mutation eliminates surface components from Arabidopsis pollen and disrupts cell signaling during fertilization*. Gene Development **7**(6974-85).

Pruitt, R. E., Vielle-Calzada, J. P., Ploense, S. E., Grossniklaus, U. and Lolle, S. J. (2000). *FIDDLEHEAD, a gene required to suppress epidermal cell interactions in Arabidopsis, encodes a putative lipid biosynthetic enzyme*. Proceedings of the National Academy of Sciences of the United States of America **97**(3): 1311-1316.

Quist, T. M., Sokolchik, I., Shi, H., Joly, R. J., Bressan, R. A., Maggio, A., Narsimhan, M. and Li, X. (2009). *HOS3, an ELO-like gene, inhibits effects of ABA and implicates a S-1-P/ceramide control system for abiotic stress responses in Arabidopsis thaliana*. Molecular Plant **2**(1): 138-151.

Raffaele, S., Vailliau, F., Leger, A., Joubes, J., Miersch, O., Huard, C., Blee, E., Mongrand, B., Domergue, F. and Roby, D. (2008). *A MYB transcription factor regulates very-long-chain fatty acid biosynthesis for activation of the hypersensitive cell death response in Arabidopsis*. Plant Cell **20**(3): 752-767.

Revardel, E., Bonneau, M., Durrens, P. and Aigle, M. (1995). *Characterization of a new gene family developing pleiotropic phenotypes upon mutation in Saccharomyces cerevisiae*. Biochim Biophys Acta **1263**(3): 261-265.

Richards, E., Reichardt, M. and Rogers, S. (2001). *Preparation of genomic DNA from plant tissue*, John Wiley & Sons, Inc.

Roudier, F., Gissot, L., Beaudoin, F., Haslam, R., Michaelson, L., Marion, J., Molino, D., Lima, A., Bach, L., Morin, H., Tellier, F., Palauqui, J. C., Bellec, Y., Renne, C., Miquel, M., DaCosta, M., Vignard, J., Rochat, C., Markham, J. E., Moreau, P., Napier, J. and Faure, J. D. (2010). *Very-long-chain fatty acids are involved in polar auxin transport and developmental patterning in Arabidopsis*. Plant Cell **22**(2): 364-375.

References

Rowland, O. and Domergue, F. (2012). *Plant fatty acyl reductases: enzymes generating fatty alcohols for protective layers with potential for industrial applications*. Plant Science **193-194**: 28-38.

Rowland, O., Lee, R., Franke, R., Schreiber, L. and Kunst, L. (2007). *The CER3 wax biosynthetic gene from Arabidopsis thaliana is allelic to WAX2/YRE/FLP1*. FEBS Letters **581(18)**: 3538-3544.

Rowland, O., Zheng, H., Hepworth, S. R., Lam, P., Jetter, R. and Kunst, L. (2006). *CER4 encodes an alcohol-forming fatty acyl-coenzyme A reductase involved in cuticular wax production in Arabidopsis*. Plant physiology **142(3)**: 866-877.

Salas, J. J. and Ohlrogge, J. B. (2002). *Characterization of substrate specificity of plant FatA and FatB acyl-ACP thioesterases*. Archive of Biochemistry and Biophysics **403(1)**: 25-34.

Savaldi-Goldstein, S., Peto, C. and Chory, J. (2007). *The epidermis both drives and restricts plant shoot growth*. Nature **446(7132)**: 199-202.

Schneeberger, K., Ossowski, S., Lanz, C., Juul, T., Petersen, A. H., Nielsen, K. L., Jorgensen, J.-E., Weigel, D. and Andersen, S. U. (2009). *SHOREmap: simultaneous mapping and mutation identification by deep sequencing*. Nature Methods **6(8)**: 550-551.

Schrack, K., Mayer, U., Horrichs, A., Kuhnt, C., Bellini, C., Dangl, J., Schmidt, J. and Jurgens, G. (2000). *FACKEL is a sterol C-14 reductase required for organized cell division and expansion in Arabidopsis embryogenesis*. Genes Development **14(12)**: 1471-1484.

Schweizer, E. and Hofmann, J. (2004). *Microbial type I fatty acid synthases (FAS): major players in a network of cellular FAS systems*. Microbiology and Molecular Biology Review **68(3)**: 501-517.

Shi, L., Bielawski, J., Mu, J., Dong, H., Teng, C., Zhang, J., Yang, X., Tomishige, N., Hanada, K., Hannun, Y. A. and Zuo, J. (2007). *Involvement of sphingoid bases in mediating reactive oxygen intermediate production and programmed cell death in Arabidopsis*. Cell Research **17(12)**: 1030-1040.

Shockey, J. M., Fulda, M. S. and Browse, J. A. (2002). *Arabidopsis contains nine long-chain acyl-coenzyme A synthetase genes that participate in fatty acid and glycerolipid metabolism*. Plant Physiology **129(4)**: 1710-1722.

Sieber, P., Schorderet, M., Ryser, U., Buchala, A., Kolattukudy, P., Metraux, J. P. and Nawrath, C. (2000). *Transgenic Arabidopsis plants expressing a fungal cutinase show alterations in the structure and properties of the cuticle and postgenital organ fusions*. Plant Cell **12(5)**: 721-738.

References

Sikorska, E. and Kacperskapalacz, A. (1980). *Frost-induced phospholipid changes in cold-acclimated and non-acclimated rape leaves* Physiologia Plantarum **48**(2): 201-206.

Silve, S., Leplatois, P., Josse, A., Dupuy, P. H., Lanau, C., Kaghad, M., Dhers, C., Picard, C., Rahier, A., Taton, M., Le Fur, G., Caput, D., Ferrara, P. and Loison, G. (1996). *The immunosuppressant SR 31747 blocks cell proliferation by inhibiting a steroid isomerase in Saccharomyces cerevisiae.* Molecular and cellular biology **16**(6): 2719-2727.

Simoni, R. D., Criddle, R. S. and Stumpf, P. K. (1967). *Fat metabolism in higher plants. XXXI. Purification and properties of plant and bacterial acyl carrier proteins.* Journal of Biological Chemistry **242**(4): 573-581.

Simons, K. and Ikonen, E. (1997). *Functional rafts in cell membranes.* Nature **387**(6633): 569-572.

Simons, K. and Toomre, D. (2000). *Lipid rafts and signal transduction.* Nature reviews. Molecular cell biology **1**(1): 31-39.

Smith, M. A., Dauk, M., Ramadan, H., Yang, H., Seamons, L. E., Haslam, R. P., Beaudoin, F., Ramirez-Erosa, I. and Forseille, L. (2013). *Involvement of Arabidopsis Acyl-Coenzyme A Desaturase-Like2 (At2g31360) in the biosynthesis of the very-long-chain monounsaturated fatty acid components of membrane lipids.* Plant Physiology **161**(1): 81-96.

Spassieva, S. D., Markham, J. E. and Hille, J. (2002). *The plant disease resistance gene Asc-1 prevents disruption of sphingolipid metabolism during AAL-toxin-induced programmed cell death.* Plant Journal **32**(4): 561-572.

Sperling, P., Ternes, P., Moll, H., Franke, S., Zahringer, U. and Heinz, E. (2001). *Functional characterization of sphingolipid C4-hydroxylase genes from Arabidopsis thaliana.* FEBS Letters **494**(1-2): 90-94.

Sturbois-Balcerzak, B., Vincent, P., Maneta-Peyret, L., Duvert, M., Satiat-Jeunemaitre, B., Cassagne, C. and Moreau, P. (1999). *ATP-dependent formation of phosphatidylserine-rich vesicles from the endoplasmic reticulum of leek cells.* Plant Physiology **120**(1): 245-256.

TAIR TAIR. *The Arabidopsis Information Resource (TAIR),*.

Tamura, K., Mitsuhashi, N., Hara-Nishimura, I. and Imai, H. (2001). *Characterization of an arabidopsis cDNA encoding a subunit of serine palmitoyltransferase, the initial enzyme in sphingolipid biosynthesis.* Plant and Cell Physiology **42**(11): 1274-1281.

References

- Tanaka, T., Tanaka, H., Machida, C., Watanabe, M. and Machida, Y.** (2004). *A new method for rapid visualization of defects in leaf cuticle reveals five intrinsic patterns of surface defects in Arabidopsis.* Plant Journal **37**(1): 139-146.
- Titapiwatanakun, B., Blakeslee, J. J., Bandyopadhyay, A., Yang, H., Mravec, J., Sauer, M., Cheng, Y., Adamec, J., Nagashima, A., Geisler, M., Sakai, T., Friml, J., Peer, W. A. and Murphy, A. S.** (2009). *ABC19/PGP19 stabilises PIN1 in membrane microdomains in Arabidopsis.* Plant Journal **57**(1): 27-44.
- Todd, J., Post-Beittenmiller, D. and Jaworski, J. G.** (1999). *KCS1 encodes a fatty acid elongase 3-ketoacyl-CoA synthase affecting wax biosynthesis in Arabidopsis thaliana.* Plant Journal **17**(2): 119-130.
- Toke, D. A. and Martin, C. E.** (1996). *Isolation and characterization of a gene affecting fatty acid elongation in Saccharomyces cerevisiae.* Journal of Biological Chemistry **271**(31): 18413-18422.
- Trenkamp, M. a. T.** (2004). *Specific and differential inhibition of very long chain fatty acid elongases from Arabidopsis thaliana by different herbicides.* PNAS **101**(32).
- Uchida, N., Sakamoto, T., Tasaka, M. and Kurata, T.** (2014). *Identification of EMS-induced causal mutations in Arabidopsis thaliana by next-generation sequencing.* Methods in molecular biology **1062**: 259-270.
- Uemura, M., Joseph, R. A. and Steponkus, P. L.** (1995). *Cold-acclimation of Arabidopsis-thaliana - effect on plasma-membrane lipid-composition and freeze-induced lesions.* Plant Physiology **109**(1): 15-30.
- Uemura, M. and Steponkus, P. L.** (1994). *A contrast of the plasma-membrane lipid-composition of oat and rye leaves in relation to freezing tolerance.* Plant Physiology **104**(2): 479-496.
- van den Brink-van der Laan, E., Antoinette Killian, J. and de Kruijff, B.** (2004). *Nonbilayer lipids affect peripheral and integral membrane proteins via changes in the lateral pressure profile.* Biochimica et Biophysica Acta (BBA) - Biomembranes **1666**(1-2): 275-288.
- Vance, J. E. and Steenbergen, R.** (2005). *Metabolism and functions of phosphatidylserine.* Progress in lipid research **44**(4): 207-234.
- Vioque, J. and Kolattukudy, P. E.** (1997). *Resolution and purification of an aldehyde-generating and an alcohol-generating fatty acyl-CoA reductase from pea leaves (Pisum sativum L).* Archives of Biochemistry and Biophysics **340**(1): 64-72.

References

Voelker, T. (1996). *Plant acyl-ACP thioesterases: chain-length determining enzymes in plant fatty acid biosynthesis.* Genetic engineering **18**: 111-133.

Voisin, D., Nawrath, C., Kurdyukov, S., Franke, R. B., Reina-Pinto, J. J., Efremova, N., Will, I., Schreiber, L. and Yephremov, A. (2009). *Dissection of the complex phenotype in cuticular mutants of Arabidopsis reveals a role of SERRATE as a mediator.* Plos Genetics **5**(10).

Vriet, C., Russinova, E. and Reuzeau, C. (2012). *Boosting crop yields with plant steroids.* Plant Cell **24**(3): 842-857.

Wakashima, T., Abe, K. and Kihara, A. (2014). *Dual functions of the trans-2-enoyl-CoA reductase TER in the sphingosine 1-phosphate metabolic pathway and in fatty acid elongation.* Journal of Biological Chemistry **289**(36): 24736-24748.

Wang, W., Yang, X., Tangchaiburana, S., Ndeh, R., Markham, J. E., Tsegaye, Y., Dunn, T. M., Wang, G.-L., Bellizzi, M., Parsons, J. F., Morrissey, D., Bravo, J. E., Lynch, D. V. and Xiao, S. (2008). *An inositolphosphorylceramide synthase is involved in regulation of plant programmed cell death associated with defense in Arabidopsis.* Plant Cell **20**(11): 3163-3179.

Wang, W., Yang, X., Tangchaiburana, S., Ndeh, R., Markham, J. E., Tsegaye, Y., Dunn, T. M., Wang, G. L., Bellizzi, M., Parsons, J. F., Morrissey, D., Bravo, J. E., Lynch, D. V. and Xiao, S. (2008). *An inositolphosphorylceramide synthase is involved in regulation of plant programmed cell death associated with defense in Arabidopsis.* Plant Cell **20**(11): 3163-3179.

Wellesen, K., Durst, F., Pinot, F., Benveniste, I., Nettesheim, K., Wisman, E., Steiner-Lange, S., Saedler, H. and Yephremov, A. (2001). *Functional analysis of the LACERATA gene of Arabidopsis provides evidence for different roles of fatty acid omega - hydroxylation in development.* Proceedings of the National Academy of Sciences of the United States of America **98**(17): 9694-9699.

Welti, R., Li, W. Q., Li, M. Y., Sang, Y. M., Biesiada, H., Zhou, H. E., Rajashekar, C. B., Williams, T. D. and Wang, X. M. (2002). *Profiling membrane lipids in plant stress responses - Role of phospholipase D alpha in freezing-induced lipid changes in Arabidopsis.* Journal of Biological Chemistry **277**(35): 31994-32002.

Weng, H., Molina, I., Shockey, J. and Browse, J. (2010). *Organ fusion and defective cuticle function in a lacs1 lacs2 double mutant of Arabidopsis.* Planta **231**(5): 1089-1100.

Willemsen, V., Friml, J., Grebe, M., van den Toorn, A., Palme, K. and Scheres, B. (2003). *Cell polarity and PIN protein positioning in Arabidopsis require Sterol Methyl Transferase1 function.* Plant Cell **15**(3): 612-625.

References

Xia, Y., Gao, Q. M., Yu, K. S., Lapchyk, L., Navarre, D., Hildebrand, D., Kachroo, A. and Kachroo, P. (2009). *An intact cuticle in distal tissues is essential for the induction of systemic acquired resistance in plants.* Cell Host & Microbe **5**(2): 151-165.

Xue, H. W., Chen, X. and Me, Y. (2009). *Function and regulation of phospholipid signalling in plants.* Biochemical Journal **421**: 145-156.

Yang, H. B., Richter, G. L., Wang, X., Mlodzinska, E., Carraro, N., Ma, G. J., Jenness, M., Chao, D. Y., Peer, W. A. and Murphy, A. S. (2013). *Sterols and sphingolipids differentially function in trafficking of the Arabidopsis ABCB19 auxin transporter.* Plant Journal **74**(1): 37-47.

Li-Beisson, Y. B. S., Beisson, F., Andersson, M. X., Arondel, V., Bates, P. D., Baud, S., Bird, D., DeBono, A., Durrett, T. P., Franke, R. B., Graham, I. A., Katayama, K., Kelly, A. A., Larson, T., Markham, J. E., Miquel, M., Molina, I., Nishida, I., Rowland, O., Samuels, L., Schmid, K. M., Wada, H., Welti, R., Xu, C., Zallot, R., and Ohlrogge, J. (2013). *Acyl lipid metabolism* The Arabidopsis Book **11**. **11**.

Yoshida, S. and Uemura, M. (1986). *Lipid composition of plasma membranes and tonoplasts isolated from etiolated seedlings of Mung Bean (Vigna radiata L.).* Plant Physiol **82**(3): 807-812.

Zheng, H., Rowland, O. and Kunst, L. (2005). *Disruptions of the Arabidopsis Enoyl-CoA Reductase gene reveal an essential role for very-long-chain fatty acid synthesis in cell expansion during plant morphogenesis.* Plant Cell **16**: 1467-1481.

Zheng, Z., Xia, Q., Dauk, M., Shen, W., Selvaraj, G. and Zou, J. (2003). *Arabidopsis AtGPAT1, a member of the membrane-bound glycerol-3-phosphate acyltransferase gene family, is essential for tapetum differentiation and male fertility.* Plant Cell **15**(8): 1872-1887.

Appendix

Appendix I: Materials and methods

All tables below list the conditions of the mass spectrometry used to identify the species listed. Dwell is the time taken scanning for each MRM pair. DP is the declustering potential and CE the collision energy.

I.I Acyl-CoA analysis

Table I.I. A list of the acyl-CoA species and their MRM pairs.

Acyl CoA	Q1 Mass (Da)	Q3 Mass (Da)	Dwell(msec)	DP	CE
14:0 CoA	978.3	471.3	10	180	50
14:1 CoA	977.3	469.3	10	180	50
16:0 CoA	1006.4	499.4	10	180	50
16:0-OH CoA	1022.4	515.4	10	180	50
16:0KETO CoA	1020.4	513.4	10	180	50
16:1 CoA	1004.4	497.4	10	180	50
16:3 CoA	1000.4	493.4	10	180	50
18:0 CoA	1034.4	527.4	10	190	52
18:0-OH CoA	1050.4	543.4	10	190	52
18:0KETO CoA	1048.4	541.4	10	185	52
18:1KETO CoA	1046.4	539.4	10	185	52
18:1 CoA	1032.4	525.4	10	185	52
18:2 CoA	1030.4	523.4	10	180	52
18:3 CoA	1028.4	521.4	10	180	52
20:0 CoA	1062.4	555.4	10	190	52
20:0-OH CoA	1078.4	571.4	10	190	52
20:0KETO CoA	1076.4	569.4	10	190	52
20:1 CoA	1060.4	553.4	10	190	52
22:0 CoA	1090.4	583.4	10	190	53
22:0-OH CoA	1106.4	599.4	10	190	53
22:0KETO CoA	1104.4	597.4	10	190	53
22:1 CoA	1088.4	581.4	10	190	53
24:0 CoA	1118.5	611.5	10	210	57
24:1 CoA	1116.5	609.5	10	208	57
26:0 CoA	1146.4	639.5	10	220	58
26:1 CoA	1144.4	637.5	10	218	58
28:0 CoA	1174.4	667.5	10	220	58
28:1 CoA	1172.4	665.5	10	220	58
30:0 CoA	1202.4	695.5	10	220	58
30:1 CoA	1200.4	693.5	10	220	58

I.II Sphingolipid analysis

Table I.II A list of the ceramide species and their MRM pairs.

Cer	Q1 Mass (Da)	Q3 Mass (Da)	Dwell(msec)	DP	CE
d18:1/c12:0	482.5	264.3	19.39	60	35
t18:0/c16:0	556.5	300.3	19.39	100	35
t18:0/c18:0	584.6	300.3	19.39	100	35
t18:0/c20:0	612.6	300.3	19.39	100	37
t18:0/c20:1	610.6	300.3	19.39	100	37
t18:0/c22:0	640.6	300.3	19.39	100	43
t18:0/c22:1	638.6	300.3	19.39	100	43
t18:0/c24:0	668.7	300.3	19.39	100	43
t18:0/c24:1	666.7	300.3	19.39	100	43
t18:0/c26:0	696.7	300.3	19.39	100	43
t18:0/c26:1	694.7	300.3	19.39	100	43
t18:1/c16:0	554.5	298.3	19.39	100	38
t18:1/c18:0	582.6	298.3	19.39	100	38
t18:1/c20:0	610.6	298.3	19.39	100	40
t18:1/c20:1	608.6	298.3	19.39	100	40
t18:1/c22:0	638.6	298.3	19.39	100	42
t18:1/c22:1	636.6	298.3	19.39	100	42
t18:1/c24:0	666.7	298.3	19.39	100	42
t18:1/c24:1	664.7	298.3	19.39	100	44
t18:1/c26:0	694.7	298.3	19.39	100	44
t18:1/c26:1	692.7	298.3	19.39	100	44
d18:0/c16:0	540.5	266.3	19.39	40	42
d18:0/c18:0	568.6	266.3	19.39	40	43
d18:0/c20:0	596.6	266.3	19.39	42	43
d18:0/c20:1	594.6	266.3	19.39	40	48
d18:0/c22:0	624.6	266.3	19.39	39	48
d18:0/c22:1	622.6	266.3	19.39	40	48
d18:0/c24:0	652.7	266.3	19.39	39	44
d18:0/c24:1	650.7	266.3	19.39	37	43
d18:0/c26:0	680.7	266.3	19.39	43	48
d18:0/c26:1	678.7	266.3	19.39	46	48
d18:1/c16:0	538.5	264.3	19.39	40	39
d18:1/c18:0	566.6	264.3	19.39	38	39
d18:1/c20:0	594.6	264.3	19.39	44	39
d18:1/c20:1	592.6	264.3	19.39	42	42
d18:1/c22:0	622.6	264.3	19.39	44	46
d18:1/c22:1	620.6	264.3	19.39	39	44
d18:1/c24:0	650.7	264.3	19.39	38	49
d18:1/c24:1	648.7	264.3	19.39	42	43
d18:1/c26:0	678.7	264.3	19.39	38	46
d18:1/c26:1	676.7	264.3	19.39	46	48

Table I.III. A list of the GlcCer species and their MRM pairs.

GlcCer	Q1 Mass (Da)	Q3 Mass (Da)	Dwell(msec)	DP	CE
d18:1/c12:0	644.5	264.3	19.39	90	50
t18:0/h16:0	734.6	300.3	19.39	80	68
t18:0/h18:0	762.6	300.3	19.39	80	80
t18:0/h20:0	790.6	300.3	19.39	80	72
t18:0/h20:1	788.6	300.3	19.39	80	75
t18:0/h22:0	818.7	300.3	19.39	80	60
t18:0/h22:1	816.7	300.3	19.39	80	63
t18:0/h24:0	846.7	300.3	19.39	80	60
t18:0/h24:1	844.7	300.3	19.39	80	65
t18:0/h26:0	874.7	300.3	19.39	80	63
t18:0/h26:1	872.7	300.3	19.39	80	65
t18:1/h16:0	732.6	298.3	19.39	88	49
t18:1/h18:0	760.6	298.3	19.39	70	54
t18:1/h20:0	788.6	298.3	19.39	70	55
t18:1/h20:1	786.6	298.3	19.39	75	60
t18:1/h22:0	816.7	298.3	19.39	88	57
t18:1/h22:1	814.7	298.3	19.39	75	60
t18:1/h24:0	844.7	298.3	19.39	100	57
t18:1/h24:1	842.7	298.3	19.39	100	59
t18:1/h26:0	872.7	298.3	19.39	100	57
t18:1/h26:1	870.7	298.3	19.39	100	62
d18:0/h16:0	718.6	266.3	19.39	85	56
d18:0/h18:0	746.6	266.3	19.39	85	80
d18:0/h20:0	774.6	266.3	19.39	93	80
d18:0/h20:1	772.6	266.3	19.39	93	75
d18:0/h22:0	802.7	266.3	19.39	93	80
d18:0/h22:1	800.7	266.3	19.39	93	75
d18:0/h24:0	830.7	266.3	19.39	93	100
d18:0/h24:1	828.7	266.3	19.39	100	95
d18:0/h26:0	858.7	266.3	19.39	100	100
d18:0/h26:1	856.7	266.3	19.39	100	95
d18:1/h16:0	716.6	264.3	19.39	78	53
d18:1/h18:0	744.6	264.3	19.39	80	56
d18:1/h20:0	772.6	264.3	19.39	80	60
d18:1/h20:1	770.6	264.3	19.39	80	60
d18:1/h22:0	800.7	264.3	19.39	80	62
d18:1/h22:1	798.6	264.3	19.39	80	66
d18:1/h24:0	828.7	264.3	19.39	90	60
d18:1/h24:1	826.7	264.3	19.39	95	63
d18:1/h26:0	856.7	264.3	19.39	90	67
d18:1/h26:1	854.7	264.3	19.39	85	63

Table I.IV. A list of the HCEr species and their MRM pairs.

HCEr	Q1 Mass (Da)	Q3 Mass (Da)	Dwell(msec)	DP	CE
d18:1/c12:0	482.5	264.3	19.39	60	35
t18:0/h16:0	572.5	300.3	19.39	100	36
t18:0/h18:0	600.6	300.3	19.39	100	38
t18:0/h20:0	628.6	300.3	19.39	100	38
t18:0/h20:1	626.6	300.3	19.39	100	44
t18:0/h22:0	656.6	300.3	19.39	100	45
t18:0/h22:1	654.6	300.3	19.39	100	45
t18:0/h24:0	684.7	300.3	19.39	100	45
t18:0/h24:1	682.7	300.3	19.39	100	45
t18:0/h26:0	712.7	300.3	19.39	100	46
t18:0/h26:1	710.7	300.3	19.39	100	45
t18:1/h16:0	570.5	298.3	19.39	100	36
t18:1/h18:0	598.6	298.3	19.39	100	36
t18:1/h20:0	626.6	298.3	19.39	100	38
t18:1/h20:1	624.6	298.3	19.39	100	38
t18:1/h22:0	654.6	298.3	19.39	100	43
t18:1/h22:1	652.6	298.3	19.39	100	43
t18:1/h24:0	682.7	298.3	19.39	100	45
t18:1/h24:1	680.7	298.3	19.39	100	45
t18:1/h26:0	710.7	298.3	19.39	100	45
t18:1/h26:1	708.7	298.3	19.39	100	45
d18:0/h16:0	556.5	266.3	19.39	80	43
d18:0/h18:0	584.6	266.3	19.39	80	46
d18:0/h20:0	612.6	266.3	19.39	90	48
d18:0/h20:1	610.6	266.3	19.39	88	49
d18:0/h22:0	640.6	266.3	19.39	95	47
d18:0/h22:1	638.6	266.3	19.39	85	44
d18:0/h24:0	668.7	266.3	19.39	92	50
d18:0/h24:1	666.7	266.3	19.39	81	50
d18:0/h26:0	696.7	266.3	19.39	98	50
d18:0/h26:1	694.7	266.3	19.39	88	52
d18:1/h16:0	554.5	264.3	19.39	62	37
d18:1/h18:0	582.6	264.3	19.39	62	41
d18:1/h20:0	610.6	264.3	19.39	68	42
d18:1/h20:1	608.6	264.3	19.39	65	43
d18:1/h22:0	638.6	264.3	19.39	68	47
d18:1/h22:1	636.6	264.3	19.39	65	45
d18:1/h24:0	666.7	264.3	19.39	75	45
d18:1/h24:1	664.7	264.3	19.39	69	45
d18:1/h26:0	694.7	264.3	19.39	83	48
d18:1/h26:1	692.7	264.3	19.39	78	49

Table I.V. A list of the GIPC species and their MRM pairs.

GIPC	Q1 Mass (Da)	Q3 Mass (Da)	Dwell(msec)	CE	DP
GM1	1546.9	366.3	19.4	50	145
t18:0/h16:0	1152.6	554.5	19.4	60	145
t18:0/h18:0	1180.6	582.5	19.4	60	145
t18:0/h20:0	1208.7	610.6	19.4	60	145
t18:0/h20:1	1206.7	608.6	19.4	61	145
t18:0/h22:0	1236.7	638.6	19.4	62.5	145
t18:0/h22:1	1234.7	636.6	19.4	61	145
t18:0/h24:0	1264.7	666.6	19.4	62.5	145
t18:0/h24:1	1262.7	664.6	19.4	62	145
t18:0/h26:0	1292.8	694.7	19.4	63	145
t18:0/h26:1	1290.8	692.7	19.4	63	145
t18:1/h16:0	1150.6	552.5	19.4	56	145
t18:1/h18:0	1178.6	580.5	19.4	58	145
t18:1/h20:0	1206.7	608.6	19.4	61	145
t18:1/h20:1	1204.7	606.6	19.4	60	145
t18:1/h22:0	1234.7	636.6	19.4	61	145
t18:1/h22:1	1232.7	634.6	19.4	60	145
t18:1/h24:0	1262.7	664.6	19.4	62	145
t18:1/h24:1	1260.7	662.6	19.4	63	145
t18:1/h26:0	1290.8	692.7	19.4	63	145
t18:1/h26:1	1288.8	690.7	19.4	65	145
d18:0/h16:0	1136.6	538.5	19.4	57	145
d18:0/h18:0	1164.7	566.6	19.4	57	145
d18:0/h20:0	1192.7	594.6	19.4	57	145
d18:0/h20:1	1190.7	592.6	19.4	57	145
d18:0/h22:0	1220.7	622.6	19.4	58	145
d18:0/h22:1	1218.7	620.6	19.4	58	145
d18:0/h24:0	1248.7	650.6	19.4	61	145
d18:0/h24:1	1246.7	648.6	19.4	61	145
d18:0/h26:0	1276.8	678.7	19.4	63	145
d18:0/h26:1	1274.8	676.7	19.4	63	145
d18:1/h16:0	1134.6	536.5	19.4	57	145
d18:1/h18:0	1162.7	564.6	19.4	57	145
d18:1/h20:0	1190.7	592.6	19.4	57	145
d18:1/h20:1	1188.7	590.6	19.4	57	145
d18:1/h22:0	1218.7	620.6	19.4	58	145
d18:1/h22:1	1216.7	618.6	19.4	58	145
d18:1/h24:0	1246.7	648.6	19.4	61	145
d18:1/h24:1	1244.7	646.6	19.4	61	145
d18:1/h26:0	1274.8	676.7	19.4	63	145
d18:1/h26:1	1272.8	674.7	19.4	63	145

Table I.VI. A list of the LCB/LCBP species and their MRM pairs.

LCB(P)	Q1 Mass (Da)	Q3 Mass (Da)	Dwell(msec)	DP	CE
d17:1	286.3	268.3	19.4	55	19
t18:0	318.3	300.4	19.4	70	21
t18:1	316.3	298.4	19.4	60	18
d18:1	300.3	282.3	19.4	65	18
d18:0	302.3	284.3	19.4	75	21
d17:1-P	366.2	250.3	19.4	60	23
t18:0-P	398.3	300.3	19.4	65	22
t18:1-P	396.3	298.3	19.4	60	25
d18:0-P	382.3	266.3	19.4	65	19
d18:1-P	380.3	264.3	19.4	60	25

I.III Phospholipid analysis

Table I.VII. Range of masses that the different phospholipids are detected within, along with the time spent scanning.

PC - precursor ion				
Start (Da)	Stop (Da)	Time (sec)	CE	DP
660	970	2	50	100
lpc-precursor ion				
Start (Da)	Stop (Da)	Time (sec)	CE	DP
450	600	0.5	40	100
DGDG- neutral loss				
Start (Da)	Stop (Da)	Time (sec)	CE	DP
900	1000	1.5	24	90
MGDG - neutral loss				
Start (Da)	Stop (Da)	Time (sec)	CE	DP
740	840	1.5	21	90
PG - neutral loss				
Start (Da)	Stop (Da)	Time (sec)	CE	DP
670	920	2.5	30	70
LPG - precursor ion				
Start (Da)	Stop (Da)	Time (sec)	CE	DP
400	550	0.5	35	-100
PA - neutral loss				
Start (Da)	Stop (Da)	Time (sec)	CE	DP
600	850	2	38	75
PE - neutral loss				
Start (Da)	Stop (Da)	Time (sec)	CE	DP
620	900	1.75	28	90
PI - neutral loss				
Start (Da)	Stop (Da)	Time (sec)	CE	DP
800	950	1.5	32	90
PS - neutral loss				
Start (Da)	Stop (Da)	Time (sec)	CE	DP
650	920	3	30	100

Appendix II: Lipidomics of elongase mutants

II.I Acyl-CoA analysis- averages and standard errors

Table II.I. Average acyl-CoA results of the elongase mutants in the shoots. Based on 4 repeats. SE shows the standard error of the difference.

Sample	Wild type		<i>KCR RNAi</i>		<i>pas2-1</i>		<i>cer10-2</i>	
	AV	SE	AV	SE	AV	SE	AV	SE
14:0	3.78	0.70	3.95	0.25	3.94	0.13	3.75	0.40
16:0	25.73	2.79	30.29	1.99	24.03	1.40	31.94	1.18
16:0-OH	0.08	0.04	0.11	0.04	0.13	0.02	0.07	0.01
16:0-KETO	0.29	0.05	0.34	0.02	0.82	0.12	0.62	0.12
16:1	0.99	0.28	1.56	0.20	0.81	0.04	1.42	0.08
16:3	1.42	0.27	1.54	0.14	0.60	0.16	0.49	0.06
18:0	5.24	0.62	6.16	0.38	3.66	0.35	8.17	0.70
18:0-OH	0.05	0.01	0.07	0.01	4.82	0.42	0.29	0.07
18:0-KETO	0.13	0.02	0.33	0.16	0.10	0.01	0.41	0.26
18:1	2.09	0.40	2.22	0.41	4.99	0.34	4.60	0.85
18:2	9.14	0.49	10.93	0.33	6.14	0.75	9.64	0.55
18:3	16.47	1.49	22.00	1.15	10.97	0.61	13.02	2.19
20:0	4.29	0.64	4.88	0.31	3.25	0.40	4.62	0.18
20:0-OH	0.97	0.87	0.12	0.02	8.57	0.72	1.53	0.14
20:0-KETO	0.21	0.07	0.62	0.32	2.13	1.56	0.15	0.08
20:1	0.37	0.13	0.45	0.08	1.79	0.38	0.92	0.21
22:0	4.56	0.54	3.64	0.51	3.85	0.30	3.66	0.54
22:0-OH	0.12	0.01	0.13	0.04	6.57	0.50	2.18	0.30
22:0-KETO	0.38	0.04	0.78	0.32	0.20	0.04	0.23	0.04
22:1	0.21	0.07	0.15	0.03	0.22	0.05	0.58	0.08
24:0	6.67	0.93	2.73	0.56	3.38	0.43	3.88	0.47
24:1	1.31	0.33	0.83	0.19	0.30	0.08	0.94	0.22
26:0	5.82	0.51	2.46	0.45	1.92	0.29	2.98	0.54
26:1	0.28	0.10	0.18	0.04	0.37	0.06	0.22	0.08
28:0	7.40	1.18	2.14	0.45	2.24	0.22	2.33	0.60
28:1	0.40	0.08	0.30	0.07	0.39	0.09	0.25	0.09
30:0	1.18	0.06	0.69	0.12	1.57	0.57	0.67	0.19
30:1	0.42	0.06	0.40	0.10	1.35	0.32	0.42	0.14

Table II.II Average acyl CoA results of the elongase mutants in the roots. Based on 4 repeats. SE shows the standard error of the difference.

Sample	Wild type		<i>KCR RNAi</i>		<i>pas2-1</i>		<i>cer10-2</i>	
	AV	SE	AV	SE	AV	SE	AV	SE
14:0	8.28	1.62	8.00	0.83	5.83	0.56	8.44	2.58
16:0	26.20	3.07	24.87	2.76	21.78	1.18	33.36	5.58
16:0-OH	0.24	0.08	0.24	0.04	0.87	0.24	0.08	0.04
16:0-KETO	1.38	0.94	0.41	0.12	0.37	0.08	0.54	0.33
16:1	1.66	0.38	1.59	0.56	0.63	0.05	1.34	0.27
16:3	0.34	0.10	1.41	0.99	0.66	0.22	0.57	0.36
18:0	4.27	1.14	4.99	0.58	4.61	0.21	4.58	0.69
18:0-OH	0.16	0.12	0.25	0.05	12.31	0.57	0.11	0.05
18:0-KETO	0.14	0.05	2.12	0.55	0.41	0.06	0.17	0.19
18:1	3.12	0.73	4.11	0.97	5.35	0.32	2.04	0.62
18:2	11.41	1.27	9.26	0.53	5.02	0.41	13.11	2.96

Appendix

18:3	12.18	2.30	12.16	1.72	13.79	0.62	14.03	3.41
20:0	4.24	0.52	4.00	1.00	4.42	0.35	3.96	1.01
20:0-OH	0.22	0.11	1.59	0.38	13.81	0.78	0.26	0.17
20:0-KETO	0.53	0.06	15.19	3.41	0.60	0.11	0.41	0.18
20:1	0.29	0.09	0.15	0.07	0.34	0.06	0.32	0.14
22:0	9.14	1.41	3.32	0.68	2.06	0.28	6.13	2.87
22:0-OH	0.17	0.05	0.38	0.08	5.23	0.33	0.32	0.21
22:0-KETO	1.31	0.33	3.21	0.53	0.25	0.04	1.09	0.73
22:1	0.29	0.08	0.21	0.04	0.20	0.07	0.27	0.13
24:0	6.17	1.38	0.94	0.28	0.51	0.06	3.31	1.83
24:1	1.74	0.43	0.18	0.07	0.10	0.02	0.97	0.78
26:0	2.17	0.83	0.43	0.11	0.08	0.01	1.75	0.97
26:1	0.28	0.09	0.12	0.07	0.09	0.02	0.28	0.24
28:0	2.36	1.04	0.50	0.12	0.18	0.04	1.68	1.33
28:1	0.92	0.33	0.18	0.09	0.09	0.03	0.37	0.39
30:0	0.45	0.33	0.10	0.01	0.09	0.02	0.28	0.28
30:1	0.30	0.14	0.09	0.04	0.09	0.04	0.24	0.31

Table II.III. One way ANOVA output to determine significance between the elongase mutant and wild type plants in the acyl-CoAs in the shoots and in the roots (a) Acyl-CoA percentage values (b) Acyl-CoA intermediates (c) Acyl-CoA quantity values.

(a)

ANOVA table of the acyl CoA percentage of elongase mutants shoots					
Shoot	SED	LSD(5%)	d.f residual	Fstatistic	F test p. value
16:0	2.479	5.608	9	4.4	0.036
16 keto	0.141	0.319	9	6.63	0.012
16 OH	0.044		9	0.86	0.497
18:0	0.654	1.479	9	16.97	<0.001
18 keto	0.18		9	1.47	0.286
18 OH	0.305	0.69	9	118.42	<0.001
20:0	0.612		9	2.82	0.1
20 keto	1.064		9	1.48	0.283
20 OH	0.761	1.722	9	50.6	<0.001
22:0	0.659		9	0.42	0.746
22 keto	0.235		9	2.52	0.123
22 OH	0.463	1.047	9	86.22	<0.001
24:0	0.86	1.946	9	6.34	0.013
26:0	0.575	1.3	9	18.78	<0.001
28:0	0.753	1.703	9	26.78	<0.001
30:0	0.431		9	2.04	0.178
ANOVA table of the acyl CoA percentage of elongase mutants roots					
Root	SED	LSD 5%)	d.f residual	Fstatistic	F test p. value
16:0	3.565		9	3.78	0.053
16 keto	0.612		9	1.2	0.363
16 OH	0.172	0.39	9	8.29	0.006
18:0	0.921		9	0.2	0.891
18 keto	0.373	0.843	9	12.88	0.001
18 OH	0.432	0.976	9	395.19	<0.001
20:0	0.966		9	0.1	0.959
20 keto	2.426	5.488	9	18.31	<0.001
20 OH	0.652	1.476	9	204.33	<0.001
22:0	1.498	3.368	9	8.95	0.005
22 keto	0.349	0.789	9	25.59	<0.001

Appendix

22 OH	0.23	0.521	9	230.08	<0.001
24:0	0.973	2.202	9	14.3	<0.001
26:0	0.616	1.394	9	5.36	0.022
28:0	0.802		9	3.22	0.076

(b)

ANOVA table of the acyl CoA percentage of intermediates in the elongase mutant					
Shoots	SED	LSD (5%)	d.f residual	Fstatistic	F test p. value
Keto total	0.347		9	2.06	0.208
OH total	1.113	2.517	9	386.15	<0.001
≥ 20 +Intermediates	3.295	7.455	9	11.79	0.002
≥ 20 – Intermediates	3.157	7.141	9	7.05	0.01
≥ 22 +Intermediates	2.874	6.502	9	8.36	0.006
≥ 22 –Intermediates	2.715	6.142	9	11.17	0.002
≥ 24	2.182	4.963	9	16.03	<0.001
Roots	SED	LSD (5%)	d.f residual	Fstatistic	F test p. value
Keto total	2.96	6.71	9	19.64	<0.001
OH total	1.113	2.517	9	386.15	<0.001
≥ 20 +Intermediates	11.16		9	1.47	0.286
≥ 20 – Intermediates	3.93	8.9	9	11.1	0.002
≥ 22 +Intermediates	3.54	8.02	9	9.24	0.004
≥ 22 – Intermediates	3.46	7.82	9	14.42	<0.001
≥ 24	2.649	5.992	9	10.56	0.003

(c)

ANOVA table of the acyl CoA quantity in elongase mutants					
Shoots	SED	LSD (5%)	d.f residual	Fstatistic	F test p. value
Intermediate	4.015		6	2.51	0.155
Acyl CoA ≥ 24	10.314	25.236	6	50.8	<0.001
Total	97.993	239.779	6	7.53	0.019
Roots	SED	LSD (5%)	d.f residual	Fstatistic	F test p. value
Intermediate	14.973	36.637	6	7.39	0.019
Acyl CoA ≥ 24	5.89	14.411	6	5.81	0.033
Total	94.662		6	1.24	0.374

II.II Membrane glycerolipid analysis

Table II.IV. One way ANOVA output to determine significance between the elongase mutants and wild type plants in the membrane glycerolipids in the shoots and in the roots (a) proportion of each membrane glycerolipid class (b) chain lengths of each of the different phospholipid classes (c) the percentage of each chain length of PE and PS as a percentage of the total amount of PE or PS (d) the percentage of phospholipids containing VLCFAs.

(a)

ANOVA table of the total percentage of each phospholipid class in the elongase mutants									
Shoots	WT	<i>KCR RNAi</i>	pas2-1	cer10	SED	LSD (5%)	d.f residual	Fstatistic	F test p. value
PA	0.44	1.00	0.50	1.73	0.36	0.80	9	5.68	0.018
PC	23.59	22.81	24.47	22.62	1.63		9	0.53	0.67
PE	8.55	7.17	9.36	10.60	0.78	1.76	9	6.85	0.011
PG	13.06	9.35	7.94	10.64	2.23		9	1.91	0.199
PS	0.72	0.51	0.64	0.71	0.08		9	3.22	0.076
PI	3.19	2.41	2.68	2.89	0.21	0.49	9	4.75	0.03
Roots	WT	<i>KCR RNAi</i>	pas2-1	cer10	SED	LSD (5%)	d.f residual	Fstatistic	F test p. value
PA	2.17	3.47	3.15	3.55	0.64		6	1.95	0.223
PC	47.90	45.80	39.30	45.60	3.45		6	2.33	0.173
PE	35.78	36.90	40.28	36.16	2.42		6	1.43	0.323
PG	2.87	3.30	4.54	2.90	0.27	0.66	6	16.72	0.003
PS	0.86	0.79	0.80	0.79	0.17		6	0.09	0.964
PI	5.01	3.81	4.10	4.69	0.66		6	1.37	0.339

(b)

ANOVA table of different phospholipid chain lengths for elongase mutants									
Shoots	WT	<i>KCR RNAi</i>	pas2-1	cer10	SED	LSD (5%)	d.f residual	Fstatistic	F test p. value
PI ₃₂	0.04	0.28	0.00	0.00	0.00	0.00	9	200.71	<0.001
PI ₃₄	2.64	2.04	2.35	2.44	0.18		9	3.65	0.057
PI ₃₆	0.51	0.34	0.33	0.45	0.03	0.07	9	14.18	<0.001
PA ₃₄	0.22	0.35	0.24	0.56	0.11	0.26	9	3.89	0.05
PA ₃₆	0.22	0.64	0.26	1.16	0.23	0.52	9	7.23	0.009
PC ₃₄	9.39	9.13	10.05	9.29	0.69		9	0.7	0.578
PC ₃₆	14.20	13.69	14.42	13.14	1.03		9	0.61	0.623
PE ₃₄	3.05	2.69	3.50	4.04	0.35	0.79	9	5.6	0.019
PE ₃₆	5.17	4.24	5.72	6.41	0.45	1.03	9	8.12	0.006
PE _{38≥}	0.32	0.24	0.14	0.15	0.02	0.05	9	25.85	<0.001
PG ₃₂	1.23	0.59	0.95	0.98	0.23		9	2.55	0.121
PG ₃₄	11.83	8.76	6.99	9.66	2.04		9	1.96	0.191
PS ₃₄	0.23	0.18	0.25	0.29	0.02	0.05	9	9.05	0.004
PS ₃₆	0.12	0.09	0.12	0.16	0.00	0.04	9	5.41	0.021
PS _{38≥}	0.37	0.24	0.27	0.26	0.03	0.07	9	6.6	0.012
Roots	WT	<i>KCR RNAi</i>	pas2-1	cer10	SED	LSD (5%)	d.f residual	Fstatistic	F test p. value
PI ₃₄	4.50	3.27	3.54	4.21	0.56		6	2.11	0.201
PI ₃₆	0.51	0.54	0.56	0.48	0.11		6	0.25	0.861
PA ₃₄	1.07	1.34	1.26	1.44	0.25		6	0.8	0.538

Appendix

PA 36	1.10	2.13	1.89	2.11	0.42		6	2.66	0.142
PC 32	0.61	0.58	0.81	0.67	0.10		6	2.04	0.21
PC 34	21.39	19.38	17.80	22.89	2.03		6	2.43	0.164
PC 36	25.91	25.60	20.68	22.01	1.80		6	4.19	0.064
PE 34	21.29	20.93	21.31	20.64	1.65		6	0.08	0.971
PE 36	12.54	15.04	18.68	14.05	1.74	4.25	6	4.52	0.05
PE 38\geq	1.95	0.93	0.29	1.48	0.20	0.49	6	25	<0.001
PG 32	0.37	0.31	0.58	0.32	0.11		6	2.66	0.143
PG 34	2.33	2.18	3.59	2.42	0.12	0.28	6	62.86	<0.001
PG 36	0.17	0.81	0.37	0.17	0.20		6	4.53	0.055
PS 34	0.39	0.32	0.39	0.34	0.09		6	0.35	0.792
PS 36	0.12	0.27	0.18	0.13	0.03	0.01	6	13.23	0.005
PS 40	0.36	0.20	0.23	0.33	0.01		6	2.08	0.204

(c)

ANOVA table of the percentage of total PE and PE in elongase mutants					
Shoots	SED	LSD (5%)	d.f residual	Fstatistic	F test p. value
PE 34	1.554	3.515	9	0.81	0.522
PE 36	60.5	3.471	9	0.54	0.665
PE >38	0.1626	0.3677	9	112.49	<0.001
PS 34	1.762	3.986	9	11.48	0.002
PS 36	1.107	2.505	9	10.28	0.003
PS 38	1.12	2.534	9	5.74	0.018
PS 40	1.657	3.79	9	25.03	<0.001
Roots	SED	LSD (5%)	d.f residual	Fstatistic	F test p. value
PE 34	3.15		6	1.51	0.305
PE 36	3.14	7.69	6	4.47	0.05
PE >38	0.405	0.99	6	50.37	<0.001
PS 34	4.45	10.89	6	1.37	0.34
PS 36	5.06	12.38	6	8.44	0.014
PS 40>	3.82	9.34	6	10.04	0.009

(d)

ANOVA table of the total percentage of phospholipids containing VLCFAs in elongase mutants					
	SED	LSD (5%)	d.f residual	Fstatistic	F test p. value
VLCFA Shoots	0.1626	0.3677	9	112.49	<0.001
VLCFA Roots	0.2395	0.5859	6	21.11	0.001

II.III Sphingolipid analysis

Table II.V. One way ANOVA output to determine significance between the elongase mutant and wild type plants in the different sphingolipid classes in the shoots and in the roots (a) percentage of the total sphingolipids detected (b) quantity of sphingolipids.

(a)

ANOVA table of the percentage of sphingolipids in elongase mutants					
Shoots	SED	LSD (5%)	d.f residual	Fstatistic	F test p. value
VLCFA in sphingolipids (%)	4.17	10.19	6		
ceramides 16-18 (%)	2.89		6	1.89	0.232
ceramides VLCFA (%)	2.89		6	1.89	0.232
GIPC 16-18 (%)	1.83	4.50	6	13.58	0.004
GIPC VLCFA (%)	1.84	4.50	6	13.58	0.004
GlcCer 16-18 (%)	3.30	7.43	6	12.14	0.006
GlcCer VLCFA (%)	3.03	7.43	6	12.14	0.006
HCer 16-18 (%)	2.17	5.31	6	13.19	0.005
Hcer VLCFA (%)	2.17	5.3	6	13.19	0.005
Roots	SED	LSD (5%)	d.f residual	Fstatistic	F test p. value
VLCFA in sphingolipids (%)	6.05		6	3.73	0.08
GIPC 16-18 (%)	3.26	7.97	6	8.83	0.013
GIPC VLCFA (%)	3.26	7.97	6	8.83	0.013
GlcCer 16-18 (%)	4.01	9.81	6	11.16	0.007
GlcCer VLCFA (%)	4.01	9.81	6	11.16	0.007
HCer 16-18 (%)	2.96	7.24	6	27.36	0.001
Hcer VLCFA (%)	2.96	7.24	6	27.36	0.001

(b)

ANOVA table of the quantity of sphingolipids in elongase mutants					
Shoots	SED	LSD	d.f residual	Fstatistic	F test p. value
VLCFA in sphingolipids (quantity)	26.68	65.28	6	4.66	0.05
Total Sphingolipids (Quantity)	18.8	46	6	36.44	0.001
Total GIPC (Quantity)	11.81	28.91	6	109.3	0.001
Total GlcCer (Quantity)	15.74	38.51	6	9.22	0.012
Total ceramides (Quantity)	23.71		6	2.16	0.194
Total Hcer (Quantity)	11.45	28.02	6	21.75	0.001
ceramides 16-18 (quantity)	3.56	8.71	6	5.19	0.042
ceramides VLCFA (quantity)	20.71		6	1.87	0.235
GIPC 16-18 (Quantity)	6.04	14.77	6	5.08	0.044
GIPC VLCFA (Quantity)	9.2	22.52	6	192.45	0.001
GlcCer 16-18 (Quantity)	11.76	28.77	6	4.82	0.049
GlcCer VLCFA (Quantity)	7.36	18	6	21.06	0.001
HCer 16-18 (Quantity)	2.99	7.31	6	84.61	0.001
Hcer VLCFA (Quantity)	8.98	21.96	6	9.53	0.011
Total LCB (Quantity)	0.955	2.336	6	10.64	0.008
Roots	SED	LSD	d.f residual	Fstatistic	F test p. value
Total VLCFA in sphingolipids (%)	6.045		6	3.73	0.08
Total Sphingolipids (Quantity)	64.89		6	0.64	0.618
Total GIPC (Quantity)	39.6		6	2.46	0.161
Total GlcCer (Quantity)	22.94		6	1.82	0.243
Total ceramides (Quantity)	20.68	50.61	6	7.75	0.017

Appendix

Total Hcer (Quantity)	18.06		6	1.63	0.279
ceramides 16-18 (quantity)	6.1	14.93	6	22.02	0.001
ceramides VLCFA (quantity)	15.16		6	3.88	0.074
GIPC 16-18 (Quantity)	13.61		6	2.66	0.142
GIPC VLCFA (Quantity)	32.8	80.2	6	6.37	0.027
GlcCer 16-18 (Quantity)	9.77	23.91	6	6.02	0.031
GlcCer VLCFA (Quantity)	17.21	42.12	6	4.08	0.005
Hcer 16-18 (Quantity)	7.2	17.61	6	7.85	0.017
Hcer VLCFA (Quantity)	11.54		6	2	0.215
Total LCB (quantity)	2.461	6.023	6	5.81	0.033

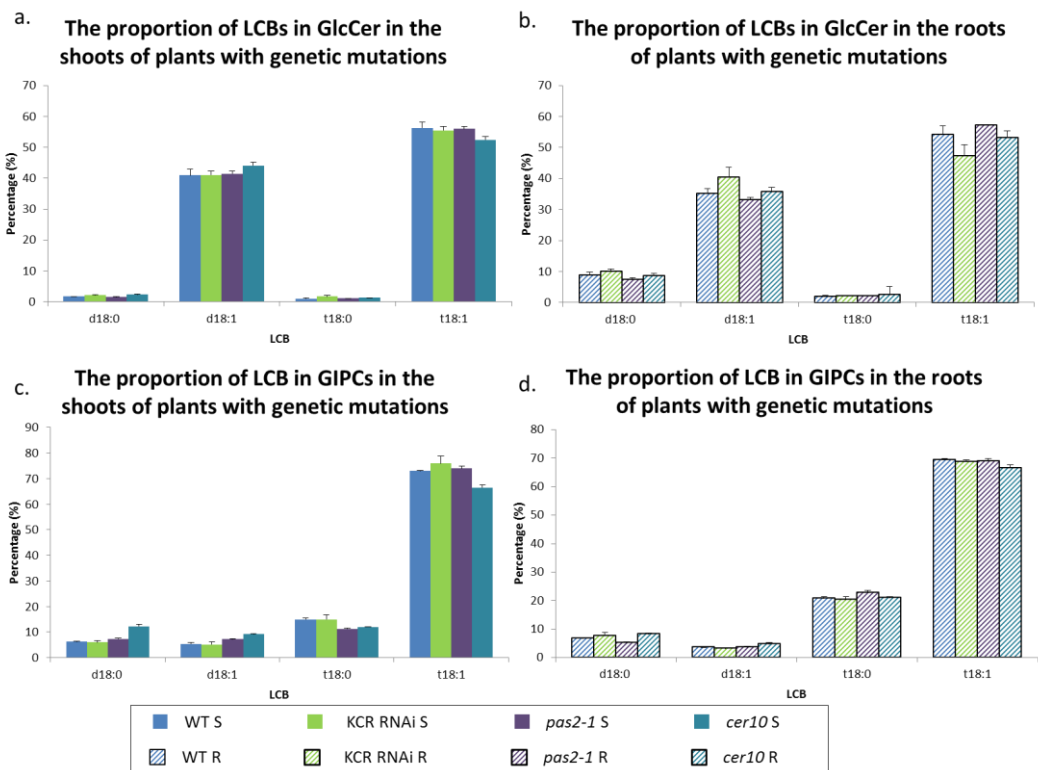


Figure II.I The proportion of different LCB species in elongase mutants compared to wild type plants. Values are based on the mean of 4 values +/- SE.

Appendix III: Lipidomics of herbicide treated plants

Table III.I. Average acyl-CoA results of the herbicide treated plants in the shoots and roots. Based on 4 repeats. SE shows the standard error of the difference.

Sample	Benfuresate shoot		Ethofumesate shoot		Flufenacet shoot	
	AV	SE	AV	SE	AV	SE
14:0	4.71	0.24	5.47	0.50	8.10	0.28
16:0	40.64	0.27	41.84	2.72	23.95	0.93
16:1	1.43	0.08	1.49	0.34	1.34	0.22
16:3	1.43	0.46	1.40	0.20	2.07	0.40
18:0	11.54	2.29	12.44	1.05	11.31	0.52
18:1	1.86	0.06	1.48	0.27	2.22	0.20
18:2	12.57	0.30	10.55	0.62	8.38	0.57
18:3	20.25	1.64	16.04	0.81	24.53	0.95
20:0	2.89	0.47	4.32	0.69	7.02	0.48
20:1	0.54	0.22	0.40	0.10	1.03	0.30
22:0	0.74	0.18	1.47	0.43	3.59	0.32
24:0	0.37	0.13	1.10	0.38	3.03	0.35
24:1	0.05	0.02	0.09	0.05	0.04	0.01
26:0	0.40	0.16	0.98	0.53	1.75	0.20
26:1	0.10	0.02	0.05	0.01	0.10	0.03
28:0	0.28	0.12	0.66	0.39	0.83	0.05
28:1	0.03	0.02	0.05	0.02	0.09	0.04
30:0	0.17	0.06	0.17	0.11	0.58	0.10
Sample	Benfuresate root		Ethofumesate root		Flufenacet root	
	AV	SE	AV	SE	AV	SE
14:0	10.79	1.88	10.80	2.11	14.60	1.49
16:0	31.45	2.31	29.09	2.67	30.74	4.29
16:1	2.09	0.78	1.17	0.50	1.56	0.30
16:3	0.45	0.13	0.32	0.16	0.69	0.17
18:0	3.38	0.23	3.73	0.52	8.69	0.76
18:1	1.60	0.30	2.19	0.50	2.39	0.53
18:2	16.63	0.95	14.47	1.01	14.41	2.37
18:3	14.44	1.22	13.07	2.91	16.53	3.85
20:0	3.24	0.62	4.56	0.51	2.24	0.79
20:1	0.18	0.05	0.45	0.19	0.29	0.11
22:0	7.16	1.33	10.04	2.00	2.32	1.39
24:0	3.33	1.00	5.73	1.42	0.44	0.10
24:1	1.02	0.24	1.05	0.49	0.15	0.06
26:0	1.44	0.49	1.21	0.49	0.68	0.16
26:1	0.26	0.09	0.27	0.10	2.90	1.24
28:0	1.56	0.56	1.13	0.50	0.43	0.21
28:1	0.66	0.24	0.48	0.31	0.24	0.14
30:0	0.32	0.11	0.24	0.06	0.69	0.34

Appendix

Table III.II. One way ANOVA output to determine significance between the herbicide treated plants and untreated plants in the percentage of acyl-CoA. (a) Shoots and the roots of all the acyl-CoA species analysed (b) the total percentage of VLC-acyl-CoAs.

(a)

ANOVA table of the percentage acyl CoA of herbicide treated plants					
Shoot	SED	LSD (5%)	d.f residual	Fstatistic	F test p. value
16:0	2.949	7.215	9	22.6	0.001
18:0	2.43	5.964	9	3.15	0.108
20:0	0.799	1.956	9	11.28	0.007
22:0	0.521	1.275	9	28.11	<0.001
24:0	0.697	1.705	9	36.56	<0.001
26:0	0.451	1.104	9	69.95	<0.001
28:0	0.871	2.131	9	34.15	<0.001
30:0	0.1199	0.2934	9	37.55	<0.001
root	SED	LSD (5%)	d.f residual	Fstatistic	F test p. value
16:0	4.375		9	0.28	0.839
18:0	1.044	2.361	9	9.86	0.003
20:0	0.923	2.088	9	3.57	0.06
22:0	1.596	3.61	9	8.2	0.006
24:0	1.159	2.621	9	11.07	0.002
26:0	0.746		9	1.58	0.262
28:0	0.87		9	1.81	0.215
30:0	0.351		9	0.68	0.585

(b)

ANOVA table of the percentage of acyl-CoAs containing VLCFAs					
	SED	LSD	d.f residual	Fstatistic	F test p. value
Shoot VLCFA	1.985	4.858	9	85.08	<0.001
Root VLCFA	4.728	10.695	9	5.96	0.016

Table III.III One way ANOVA output to determine significance between the herbicide treated plants and untreated plants in the membrane glycerolipids in the shoots and in the roots (a) proportion of each membrane glycerolipid class (c) the percentage of phospholipids containing VLCFAs (c) the percentage of each chain length of phospholipids.

(a)

ANOVA table of the total proportion of each phospholipid class in herbicide treated plants									
Shoots	WT	Fluf	Benf	Etho	SED	LSD (5%)	d.f residual	Fstatistic	F test p. value
PA	0.46	1.01	3.09	0.34	0.12	0.27	9	225.42	<0.001
PC	23.59	33.09	24.23	22.50	1.56	3.52	9	19.69	<0.001
PE	8.55	19.10	14.46	8.45	0.70	1.59	9	106.82	<0.001
PG	13.06	6.22	13.00	9.74	2.24	5.06	9	4.22	0.04
PS	0.72	1.54	0.95	0.83	0.11	0.24	9	24.01	<0.001
PI	3.19	4.06	4.47	2.90	0.28	0.63	9	13.88	0.001
Roots	WT	Fluf	Benf	Etho	SED	LSD (5%)	d.f residual	Fstatistic	F test p. value
PA	2.17	1.89	8.06	1.55	0.70	1.72	6	38.99	<0.001
PC	49.90	44.90	35.90	52.50	3.52	8.61	6	8.72	0.013
PE	35.78	39.76	39.53	33.34	2.13		6	4.24	0.063
PG	2.87	2.57	3.15	2.71	0.23		6	1.87	0.236
PS	0.86	1.58	1.57	0.94	0.18	0.45	6	8.89	0.013

Appendix

PI	5.01	5.05	7.88	5.83	0.80	1.95	6	5.72	0.034
DGDG	1.17	1.22	1.30	1.14	0.08		6	1.45	0.318
LPC	0.61	0.73	0.51	0.54	0.19		6	0.51	0.692
MGDG	3.32	3.92	3.83	3.14	0.27		6	3.92	0.073

(b)

ANOVA table of phospholipids containing VLCFA in herbicide treated plants									
Shoots	WT	Fluf	Benf	Etho	SED	LSD(5%)	d.f residual	Fstatistic	F test p. value
Sum \geq 38 PE+PS	0.69	0.72	0.32	0.40	0.051	0.116	9	31.05	<0.001
All VLCFA	0.69	0.73	2.78	0.40	0.219	0.496	9	50	<0.001
Roots	WT	Fluf	Benf	Etho	SED	LSD(5%)	d.f residual	Fstatistic	F test p. value
All VLCFA	2.31	0.62	2.08	1.78	0.236	0.577	9	20.1	0.002

(c)

ANOVA table of different phospholipid chain lengths for herbicide treated plants									
Shoots	WT	Fluf	Benf	Etho	SED	LSD(5%)	d.f residual	Fstatistic	F test p. value
PI32	0.04	0.00	0.00	0.00	0.001	0.003	9	395.58	<0.001
PI 34	2.64	3.38	3.78	2.51	0.241	0.544	9	12.55	0.001
PI 36	0.51	0.68	0.69	0.38	0.044	0.100	9	22.2	<0.001
PA 34	0.22	0.41	0.98	0.17	0.062	0.141	9	70.5	<0.001
PA 36	0.22	0.58	1.99	0.17	0.133	0.331	9	82.02	<0.001
PA 38	0.00	0.01	0.04	0.00	0.002	0.004	9	196	<0.001
PC 34	9.39	11.47	9.30	8.62	0.650	1.470	9	7.15	0.009
PC 36	14.20	21.63	13.46	13.88	0.958	2.166	9	33.22	<0.001
PC \geq 38	0.00	0.00	1.47	0.00	0.160	0.362	9	42.14	<0.001
PE 34	3.05	6.82	5.72	3.34	0.326	0.738	9	63.09	<0.001
PE 36	5.17	12.13	8.49	4.98	0.503	1.138	9	89.72	<0.001
PE 38 \geq	0.32	0.15	0.25	0.12	0.017	0.038	9	58.8	<0.001
PG 32	1.23	0.70	1.55	0.81	0.215	0.487	9	6.69	0.011
PG 34	11.83	5.52	10.49	8.93	2.062		9	3.48	0.064
PG 38	0.00	0.00	0.00	0.95	0.047	0.107	9	202.39	<0.001
PS 34	0.23	0.58	0.53	0.36	0.047	0.107	9	23.36	<0.001
PS 36	0.12	0.40	0.36	0.20	0.029	0.065	9	39.94	<0.001
PS 38 \geq	0.37	0.57	0.28	0.07	0.453	0.102	9	41.68	<0.001
Roots	WT	Fluf	Benf	Etho	SED	LSD(5%)	d.f residual	Fstatistic	F test p. value
PI 34	4.50	4.33	7.11	5.23	0.71	1.73	6	6.48	0.026
PI 36	0.51	0.71	0.77	0.59	0.11		6	2.54	0.152
PA 34	1.07	0.95	3.05	0.77	0.27	0.66	6	31.88	<0.001
PA 36	1.10	0.95	5.01	0.79	0.44	1.00	6	42.74	<0.001

Appendix

PC 32	2.61	2.86	2.47	2.65	0.06	0.14	6	16.25	0.003
PC 34	21.39	17.67	16.46	22.44	2.15		6	3.58	0.086
PC 36	25.91	24.32	16.92	27.44	2.21	5.40	6	8.91	0.013
PE 34	21.29	21.45	23.24	18.47	1.41		6	3.92	0.073
PE 36	12.54	17.73	14.74	13.48	1.07	2.62	6	8.9	0.013
PE 38 \geq	1.95	0.57	1.55	1.40	0.20	0.49	6	16.86	0.003
PG 32	0.37	0.34	0.32	0.25	0.03		6	4.14	0.066
PG 34	2.33	2.07	2.67	2.33	0.24		6	2.11	0.2
PG 36	0.17	0.17	0.16	0.13	0.01	0.03	6	5.47	0.037
PS 34	0.39	1.01	0.73	0.40	0.13	0.31	6	11.05	0.007
PS 36	0.11	0.52	0.30	0.16	0.04	0.11	6	34.15	<0.001
PS 40	0.36	0.05	0.54	0.38	0.05	0.13	6	28.83	<0.001

Table III.IV. One way ANOVA output to determine significance between herbicide treated plants and untreated plants in the different sphingolipid classes in the shoots and in the roots (a) percentage of the total sphingolipids detected (b) quantity of sphingolipids.

(a)

ANOVA table of the percentage of sphingolipids in herbicide treated plants					
Variable	SED	LSD (5%)	d.f residual	Fstatistic	F test p. value
VLCFA 22 \geq sphingolipids (%)	5.36	13.13	6	27.14	<0.001
VLCFA 24 \geq sphingolipids (%)	3.84	9.40	6	51.83	
ceramides 16-18 (%)	7.15	17.53	6	14.58	0.004
ceramides \geq 22 (%)	6.96	17.04	6	18.38	0.002
ceramides \geq 24 (%)	6.33	15.50	6	20.35	0.002
GIPC 16-18 (%)	6.72	16.45	6	13.82	0.004
GIPC \geq 22 (%)	6.29	15.39	6	23.63	0.001
GIPC \geq 24 (%)	3.08	7.53	6	114	<0.001
GlcCer 16-18 (%)	9.98		6	4.19	0.064
GlcCer \geq 22 (%)	10.97		6	4.01	0.07
GlcCer \geq 24 (%)	9.60	21.51	6	4.36	0.05
HCer 16-18 (%)	3.63	8.89	6	37.16	<0.001
Hcer \geq 22 (%)	3.39	8.31	6	49.68	<0.001
Hcer \geq 24 (%)	3.09	7.58	6	48.48	<0.001

(b)

ANOVA table of the quantity of sphingolipids in herbicide treated plants					
Variable	SED	LSD (5%)	d.f residual	Fstatistic	F test p. value
VLCFA 22 \geq sphingolipids (quantity)	26.44	64.69	6	99.67	<0.001
VLCFA 24 \geq sphingolipids (quantity)	22.93	56.1	6	93.84	<0.001
Total Sphingolipids (Quantity)	85.25		6	1.13	0.409
Total GIPC (Quantity)	52.9		6	2.69	0.139
Total GlcCer (Quantity)	30.31		6	1.96	0.222
Total ceramides (Quantity)	18.37	44.96	6	14.03	0.004
Total Hcer (Quantity)	10.73		6	0.23	0.874
ceramides 16-18 (quantity)	16.17	39.56	6	5.69	0.035
ceramides \geq 22 (Quantity)	11.95	29.25	6	21.98	0.001
ceramides \geq 24 (Quantity)	14.69	35.95	6	5.19	0.042

Appendix

GIPC 16-18 (Quantity)	40.1		6	3.51	0.089
GIPC ≥ 22 (Quantity)	25.56	62.53	6	43.95	<0.001
GIPC ≥ 24 (Quantity)	18.37	44.94	6	81.26	<0.001
GlcCer 16-18 (%)	35.1		6	0.93	0.482
GlcCer ≥ 22 (%)	14.41	35.25	6	18.3	0.002
GlcCer ≥ 24 (%)	12.64	30.93	6	18.33	0.002
HcCer 16-18 (Quantity)	11.5		6	4.11	0.067
HcCer ≥ 22 (Quantity)	8.64	21.13	6	5.86	0.032
HcCer ≥ 24 (Quantity)	7.69	18.81	6	5.34	0.039

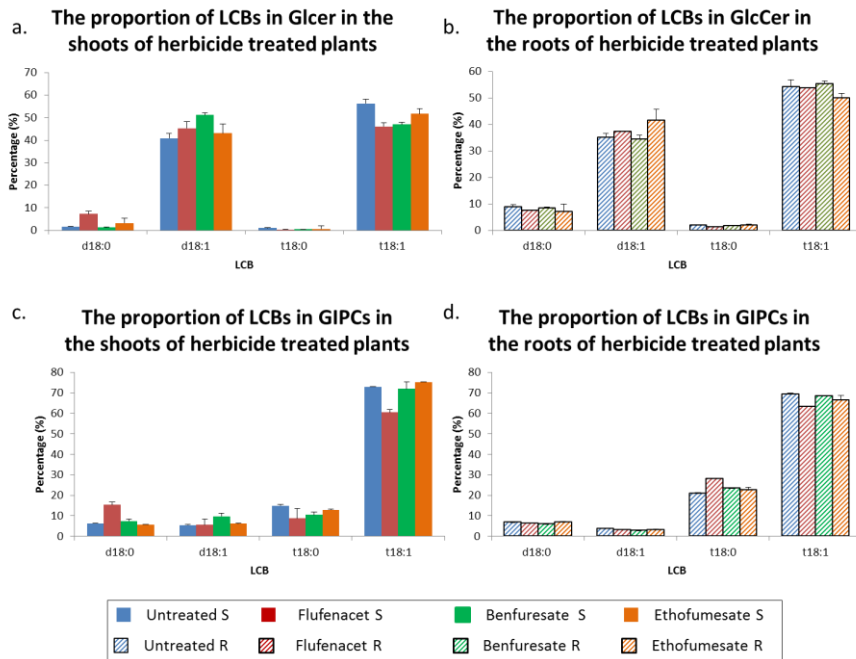


Figure III.I The proportion of different LCB species in herbicide treated plants compared to untreated plants. Values are based on the mean of 4 values +/- SE.

Appendix IV: Characterisation of suppressor mutants

Table IV.I. One way ANOVA results to determine significance between phenotypic traits between the suppressor mutants and *cer10-1* and *ler* plants.

ANOVA table of phenotypes of suppressor mutants					
Phenotype	SED	LSD (5%)	d.f residual	F statistic	F test p. value
Area	1.307	2.956	9	88.56	<0.001
Height	1.189	2.69	9	24.52	<0.001
Area no <i>ler</i>	0.454	1.112	6	125.14	<0.001
Height 80 vs <i>Ler</i>	1.094		3	5.02	0.111

Table IV.II. One way ANOVA results to determine significance between acyl-CoAs.

ANOVA table of the percentage of acyl-CoAs in the suppressor mutants									
Shoots	<i>ler</i>	<i>cer10-1</i>	sup 36	sup 80	SED	LSD (5%)	d.f residual	F statistic	F test p. value
22 ≥	33.49	25.22	25.2	33.99	3.53	7.988	9	3.9	0.049
24 ≥	29.8	22.1	22.5	30.4	3.27	7.41	9	3.8	0.05
18:0	4.54	4.56	4.6	3.85	0.39		9	1.65	0.245
20:0	3.58	3.32	2.52	3.21	0.43		9	2.16	0.162
22:0	3.7	3.11	2.73	3.59	0.46		9	1.89	0.201
24:0	6.26	3.82	5.35	4.28	0.71	1.609	9	4.75	0.03
26:0	6.41	4.49	3.72	5.85	0.64	1.467	9	7.26	0.009
28:0	6.87	5.74	4.47	8.27	1.53		9	2.23	0.154
30:0	7.01	4.56	7.14	8.34	1.16	2.624	9	3.73	0.05
Roots	<i>ler</i>	<i>cer10-1</i>	sup 36	sup 80	SED	LSD (5%)	d.f residual	F statistic	F test p. value
22 ≥	22.67	17.23	19.88	18.3	2.34		9	2.04	0.179
24 ≥	10.63	8.64	11.13	8.45	1.44		9	1.8	0.217
18:0	3.606	5.027	3.886	4.446	0.79		9	1.24	0.351
20:0	5.17	4.18	4.09	4.08	0.73		9	1.05	0.419
22:0	11.84	8.07	8.5	9.52	0.99	2.258	9	5.69	0.018
24:0	6.37	3.78	5.24	4.19	0.91		9	3.22	0.075
26:0	1.03	1.08	1.4	0.87	0.37	0.836	9	0.72	0.563
28:0	0.656	0.646	0.80	0.558	0.25		9	0.33	0.805
30:0	0.42	0.45	1.55	0.75	0.37		9	3.96	0.047

Table IV.III. Average acyl-CoA results of the elongase mutants in the shoots. Based on 4 repeats +/- SE.

Acyl CoA proportions								
Shoots	<i>Ler</i>		<i>cer10-1</i>		Sup 36		Sup 80	
	AV	SE	AV	SE	AV	SE	AV	SE
14:0	3.74	0.06	4.85	0.22	4.11	0.17	3.93	0.13
16:0	26.47	1.21	26.50	1.79	26.41	0.84	22.51	0.75
16:1	1.05	0.09	0.84	0.03	0.80	0.06	0.64	0.15
16:3	1.22	0.11	2.31	0.35	2.27	0.20	1.90	0.16
18:0	4.54	0.29	4.56	0.29	4.60	0.15	3.85	0.31
18:1	1.84	0.17	1.32	0.11	1.65	0.09	1.01	0.14
18:2	7.41	0.35	9.12	0.51	8.45	0.20	9.12	0.83
18:3	15.29	0.78	18.53	0.60	21.74	0.98	16.13	1.23

Appendix

20:0	3.58	0.60	3.32	0.27	2.52	0.08	3.21	0.16
20:1	0.66	0.14	0.74	0.08	0.40	0.07	0.72	0.15
22:0	3.70	0.18	3.11	0.37	2.73	0.15	3.59	0.27
24:0	6.26	0.68	3.82	0.36	5.35	0.27	4.28	0.48
24:1	0.59	0.04	0.72	0.10	0.33	0.03	0.37	0.07
26:0	6.41	0.78	4.49	0.36	3.72	0.23	5.85	0.29
26:1	0.25	0.02	0.19	0.05	0.17	0.03	0.20	0.02
28:0	6.87	0.43	5.74	0.71	4.47	0.18	8.27	1.69
28:1	0.70	0.06	1.29	0.21	0.38	0.03	0.96	0.11
30:0	7.01	1.36	4.56	0.32	7.14	0.41	8.34	0.26
32:0	1.68	0.60	1.32	0.25	0.92	0.10	2.13	0.33
Sample	Ler		cer10-1		Sup 36		Sup 80	
Roots	AV	SE	AV	SE	AV	SE	AV	SE
14:0	12.67	2.90	11.01	1.48	10.24	1.13	10.99	1.52
16:0	35.02	6.21	38.38	2.97	34.27	0.92	37.46	0.72
16:1	1.14	0.10	1.45	0.31	1.31	0.42	1.91	0.07
16:3	0.40	0.04	0.63	0.13	0.51	0.10	0.56	0.12
18:0	3.57	0.47	4.19	0.99	3.99	0.38	4.67	0.53
18:1	1.28	0.10	2.88	0.31	2.98	0.23	2.30	0.73
18:2	9.21	0.49	10.55	0.38	10.32	0.95	9.23	0.09
18:3	10.11	0.76	10.04	0.57	11.90	1.11	9.32	0.60
20:0	5.42	0.72	3.32	0.45	4.37	0.05	3.96	0.62
20:1	0.38	0.04	0.65	0.06	0.38	0.17	0.47	0.01
22:0	11.00	1.76	7.50	0.17	8.94	0.51	9.93	0.17
22:1	0.30	0.10	0.49	0.08	0.34	0.18	0.44	0.10
24:0	6.18	1.53	4.55	1.26	5.17	0.90	4.48	0.65
24:1	0.80	0.16	1.36	0.07	1.13	0.23	1.20	0.20
26:0	0.82	0.31	0.88	0.25	1.49	0.13	0.85	0.15
26:1	0.25	0.09	0.46	0.13	0.57	0.04	0.26	0.10
28:0	0.34	0.15	0.44	0.14	0.58	0.15	0.52	0.15
28:1	0.70	0.17	0.61	0.11	0.51	0.10	0.74	0.09
30:0	0.39	0.06	0.61	0.16	1.01	0.06	0.71	0.13

Table IV.IV. One way ANOVA to show the proportion of each of the wax components in suppressor stems compared to *cer10-1*.

ANOVA table of quantity of wax in the stem					
Stem	SED	LSD (5%)	d.f residual	F statistic	F test p. value
Total wax	7.63	21.17	4	13.76	0.016
Total ALK	4.35	12.09	4	9.8	0.029
Total ALC I	1.89		4	3.9	0.115
C29 ketone	0.75	2.09	4	11.78	0.021
C29 ALC II	1.75	4.85	4	67.78	<0.001
C27 ALK	0.26		4	0.92	0.468
C28 ALK	0.15		4	3.81	0.119
C29 ALK	3.75	10.41	4	10.6	0.025
C30 ALK	0.09		4	3.91	0.115
C26 ALC I	0.16	0.445	4	7.78	0.042
C28 ACL I	0.59		4	1.96	0.255
C29 ALC I	0.15	0.40	4	8.7	0.035
C30 ALC I	0.97		4	3.92	0.114

Table IV.V. One way ANOVA to show the quantity of alkanes in the flower wax in the suppressor mutants compared to *cer10-1*.

ANOVA table of quantity of alkanes in flower waxes								
Flower (quant)	cer10-1	sup 36	sup 80	SED	LSD (5%)	d.f residual	Fstatistic	F test p. value
C25 ALK	0.80	1.55	1.06	0.20	0.57	4	6.85	0.05
C26 ALK	0.17	0.52	0.48	0.16		4	2.75	0.18
C27 ALK	2.79	4.51	3.65	0.38	1.05	4	10.31	0.03
C27 iso ALK	0.59	1.10	0.82	0.10	0.28	4	12.43	0.02
C28 ALK	0.84	0.87	0.96	0.05		4	3.53	0.13
C29 ALK	54.50	64.30	63.60	2.89	8.03	4	7.23	0.05
C29 iso ALK	6.41	8.81	10.19	2.03		4	1.78	0.28
C30 ALK	1.39	1.32	1.73	0.09	0.25	4	11.54	0.02
C30 iso ALK	1.19	0.35	1.45	0.15	0.43	4	27.75	0.01
C31 iso ALK	4.18	6.80	5.21	0.61	1.69	4	9.45	0.03
C31 ALK	3.45	4.12	4.06	0.50	1.30	4		0.13
C31 iso ALK	4.18	6.80	5.21	0.61	1.69	4	9.45	0.03
Total ALK	76.10	94.60	93.30	6.14		4	5.68	0.07

Table IV.VI. One way ANOVA to show the proportion of alkanes in the flower wax in the suppressor mutants compared to Ler and *cer10-1*.

ANOVA table of the proportion of alkanes in flower waxes									
Flower (mol %)	Ler	cer10-1	sup 36	sup 80	SED	LSD (5%)	d.f residual	F statistic	F test p. value
c25 ALK	1.79	1.44	2.23	1.52	0.38		4	1.78	0.251
C26 ALK	0.46	0.31	0.37	0.61	0.37		4	0.26	0.852
C27 ALK	5.39	4.26	5.54	4.52	0.52		4	3	0.117
C27 iso ALK	0.88	0.90	1.36	1.10	0.21		4	2.35	0.172
C28 ALK	1.18	1.20	0.99	1.10	0.06	0.16	4	4.39	0.05
C29 ALK	72.67	71.72	68.20	68.31	1.83		4	3.19	0.105
C29 iso ALK	7.32	8.44	9.41	10.91	1.71		4	1.59	0.287
C30 ALK	1.37	1.71	1.30	1.74	0.10	0.30	4	6.76	0.024
C30 iso ALK	2.63	1.47	0.34	1.45	0.11	0.28	4	133.51	<0.001
C31 iso ALK	4.03	4.81	6.23	4.88	0.42	1.04	4	9.28	0.011
C31 ALK	2.27	3.74	4.03	3.94	0.30	0.68	4	17.55	0.002
C31 iso ALK	4.03	4.81	6.23	4.88	0.42	1.04	4	9.28	0.011

Appendix V: Identification of the position of the suppressor mutant

Table V.I. The 25 INDEL primers used to find the location of the suppressor mutant.

Primer name	Primer condition	Size Col alleles bp	Size Ler alleles bp	Primer sequences
T23J18	49 °C	182	150	F=GATATTTGTTTTGCTAACAC R=TAATAAAGTTCCAGCTTTGA
T22J18	52.5 °C	171	156	F=CACTGCAACAAAGTGGAAT R= ATCCGTTCAATATCCACAA
F28H19	52.5 °C	148	102	F=TGCGGGAGTGTGATAGAATA R= TCCTCGAAAGATTCAATTGAT
F19K23	55 °C	200	<200	F=GAATTCTGTAACATCCCATTTCC R= GGTCTAATTGCCGTTGTTGC
T17F3	51.5 °C	130	114	F= GGACCGACGGTTACGAGAGT R= TAACGGGCCGTTGCAAGA
T23K3	50 °C	133	118	F=CGTGTTTACCGGGTCGGA R=AAAACCCTTGAAGAATACG
T12H3	52 °C	99	89	F=TAGTCTGAGCTTACCAATA R=TTACCCTCGACTCGTAAC
F3P11	50 °C	210	150	F=ATGTATTTGTTGCAAAAATAA R=TGCACAGAAGAAAAACTA
T20P8	50 °C	124	112	F=TCCGATTTCGATTAACCTC R=TTATTTCTATTTCAAGACT
T16B24	50 °C	143	129	F=ATGAACGGAGTAGCTATC R=CGCGTAGAACATAATCTGTA
F20H23	49.3 °C	186	168	F=CAATGGGAAGAAGGTGTGAG R=CGCATTTCATAAGTTTGTT
MGL6	50 °C	218	165	F=ACCTGTTCAGTCTATGTTAC R=GGGAATTATTAACATTATCA
K1G2	50 °C	171	157	F=ATGAGCTTTAGGAGTGTGTA R=AATTTTGTCCCAAAAAGAATA
T32N15	50 °C	143	124	F=CAAAAGAAATGCAACGAGAC R=TTTGATCATGAATGGTAGTG
T26I12	50 °C	181	165	F=GAGCAACATTAAGGATAGAA R=ATCTCATACTCATAATATGTAG
T4I9	49.3 °C	145	101	F=TTATAGCAAACGTACAAGTC R=CTGCATACACGTCGTCTC
F17A8	49.3 °C	137	117	F=CTGGACCCTAGTGGATGT R=GACGGTTCTCCATTAATTAT
FCA8	49.3 °C	151	126	F=TTCGGAGAAAAGAAACGACAT R=ATGGAACTATTCAGGCATTA
T15N24	50 °C	99	91	F=CAAAAGAAATGCAACGAGAC R= TTGATCATGAATGGTAGTG
T4L20	52 °C	128	118	F=ACCCTAAAACAATGTCTCTT R=TGCTAACATGGAAATTTGTC
MBK20	51 °C	220	146	F=CTCTGTTGGGGCAAAACC R=GATGCTGGAGAGTAGCTTAG
MYJ24	50 °C	112	100	F=TTTCATGAGAGCGGCATTTC R=GCAAAATGTTTGGACAATTA
T26D22	50 °C	181	138	F=CACAGGCCATTGGATGTA R=TGTTAGAACCACCATTG
K6M13	50 °C	141	108	F=CCTGTTCCAATGAATATG R=TGTAGCTGCTGAGTTGTC
MQB2	50 °C	135	115	F=AAAAGGCGACTACTAGCA R=GCCATTTATTTGGTCAAC

Appendix

Table V.II. The result of the initial 25 primer pass for suppressor 36, the results of the chi-squared test are also shown. n= the number of samples tested, χ^2 = the chi-squared result. Markers that showed a significant result, at the 5% level, are highlighted in red.

Marker	Chromosome	Arm	Ler	Col	Hetero	n	x2	p-value
T23J18	1	Top	0	0	0	0	NA	
T22J18	1	Top	1	2	3	6	0.33333	>0.05
F28H19	1	Bottom	1	1	4	6	0.66667	>0.05
F19K23	1	Bottom	1	2	3	6	0.33333	>0.05
T17F3	1	Bottom	0	2	4	6	2	>0.05
T23K3	2	Top	6	0	1	7	13.8571	<0.01
T12H3	2	Top	5	0	2	7	8.42857	<0.05
F3P11	2	Bottom	0	1	3	4	1.5	>0.05
T20P8	2	Bottom	3	0	4	7	2.71429	>0.05
T16B24	2	Bottom	2	1	4	7	0.42857	>0.05
F20H23	3	Top	0	0	0	0	NA	>0.05
MGL6	3	Top	2	1	1	4	1.5	>0.05
K1G2	3	Top	3	1	1	5	3.4	>0.05
T32N15	3	Bottom	1	1	3	5	0.2	>0.05
T26I12	3	Bottom	0	0	7	7	7	>0.05
T4I9	4	Top	2	1	2	5	0.74	>0.05
F17A8	4	Bottom	1	2	2	5	0.85	>0.05
FCA8	4	Bottom	1	2	3	6	0.81	>0.05
T15N24	4	Bottom	2	1	4	7	0.61	>0.05
T4L20	4	Bottom	3	1	4	8	0.41	>0.05
MBK20	5	Top	2	0	3	5	2.42857	>0.05
MYJ24	5	Top	4	0	3	7	4.71429	>0.05
T26D22	5	Bottom	1	0	2	3	1	>0.05
K6M13	5	Bottom	1	0	3	4	1.5	>0.05
MQB2	5	Bottom	2	0	4	6	2	>0.05

Table V.III. Additional primers used to fine map the position of the mutation in suppressor 36.

Primer name	Position	Primer condition	Size Col alleles bp	Size Ler alleles bp	Primer sequences
F23H14	Chr2, 83080	50 °C	104	95	F=GCACTACTTCGACAAATGA R=CAACATCTGGGTAGTAATC
T12H1	Chr2, 5388871	50 °C	126	113	F=TCGATTTTGTCTTACTATCT R=AATTAAGGAATCAATTACAC
T17A11	Chr2, 109556	50 °C	149	113	F=GAAGATACTTCCCAGACA R=CCAACCACGCATTAACTA
F10A8	Chr2, 305391	50 °C	100	91	F=TTACCAACCAATAATAATC R=CCATTCCACCCATACAC
T16F16	Chr2, 552610	50 °C	121	109	F=GATGCAATCCTCCGGTAA R=GAGGCAAAGCCGAAAAG
T8O11	Chr2, 451104	50 °C	122	111	F=TAATTGAAGATTAGACACAG R=TTTACCCGAATCCGACCC
F5O4	Chr2, 595718	50 °C	165	110	F=CACCAGCATTGCCAGAGT R=TCGGCAAGCTGAAGATCG

Appendix

Table V.IV. The result of the initial 25 primer pass for suppressor 80, the results of the chi-squared test are also shown. n= the number of samples tested, χ^2 =the chi-squared result. Markers that shown a significant result, at the 5% level, are highlighted in red.

Marker	Chromosome	Arm	Ler	Col	Hetero	n	x2	p-value
T23J18	1	Top	0	0	0	0	NA	NA
T22J18	1	Top	1	0	7	8	4.75	>0.05
F28H19	1	Bottom	1	3	5	9	1.00	>0.05
F19K23	1	Bottom	4	2	3	9	1.89	>0.05
T17F3	1	Bottom	3	2	4	9	0.33	>0.05
T23K3	2	Top	3	4	3	10	1.80	>0.05
T12H3	2	Top	4	7	0	11	12.64	<0.05
F3P11	2	Bottom	2	2	4	8	0.00	NA
T20P8	2	Bottom	3	1	5	9	1.00	>0.05
T16B24	2	Bottom	7	0	4	11	9.73	<0.05
F20H23	3	Top	0	0	0	0	NA	>0.05
MGL6	3	Top	3	1	6	10	11.20	>0.05
K1G2	3	Top	4	2	2	8	11.00	>0.05
T32N15	3	Bottom	0	2	6	8	11.00	>0.05
T26I12	3	Bottom	2	0	3	5	6.80	>0.05
T4I9	4	Top	5	1	5	11	3.00	>0.05
F17A8	4	Bottom	2	2	7	11	0.82	>0.05
FCA8	4	Bottom	2	5	2	9	4.78	>0.05
T15N24	4	Bottom	3	5	2	10	4.40	>0.05
T4L20	4	Bottom	2	4	4	10	1.20	>0.05
MBK20	5	Top	1	3	5	9	1.00	>0.05
MYJ24	5	Top	0	0	0	0	14.14	NA
T26D22	5	Bottom	1	1	2	4	0.00	>0.05
K6M13	5	Bottom	0	3	4	7	2.71	>0.05
MQB2	5	Bottom	1	0	5	6	3.00	>0.05

Table V.V. Additional primers used to fine map the position of the mutation in suppressor 80.

Marker	Position	Primer condition	Size Col alleles bp	Size Ler alleles bp	Primer sequences
F13A10	Chr2, 19096370	50 °C	94	102	F=TACGAGATTCTGTTTTTTTG R=AGTCTGTCGGTGCATTTA
T3G21	Chr2, 16862898,	50 °C	99	91	F=TTTCTTTAACCGAATCTAGC R=CACAGTTTTGACGTTTCAAT
F13H10	Chr2, 17235779	50 °C	157	137	F=TGTGTGAATCGTGATTGA R=CACCACCATGTAAAACCTTAG
F16M14	Chr2, 15988203	50 °C	116	106	F=CGCCGTGAAATTTAAAATG R=GCTTAATCTCTGCTTATTTG
F19I3	Chr2, 14714870	50 °C	167	131	F=TTGTCTTAAGGGTAGTTATG R=AGGGACTTGACGAAAGAG
T6A23	Chr2, 16203906	50 °C	116	106	F=GTAGTAACGCTTTAGGCATA R=TCACGTACTTGAGAAATACA
F13M22	Chr2, 15829129	50 °C	147	135	F=GGCTCCTCCGAGCAATTA R=CGCCCCGCTCCCATTA

Table V.VI. Homozygous SNP identified in suppressor 36 within the candidate window.

Position on chromosome	Ref allele	Alternate allele	%reads showing alternate allele	Position in gene	Gene name
2193791	C	T	80	intergenic	
2489826	C	A	82	intergenic	
2496890	A	G	81	intergenic	
2542293	G	A	80	intergenic	
2544172	G	A	80	intergenic	
2565278	A	C	83	intergenic	
2577188	A	G	91	intergenic	
2623760	A	G	82	intronic/noncoding	AT2G06570
2623848	G	T	82	intronic/noncoding	AT2G06570
2643111	C	T	85	intergenic	
2670571	C	T	85	intergenic	
2680413	C	A	84	intergenic	
2716566	C	A	81	intergenic	
2903643	C	T	92	intergenic	
2904767	G	T	90	intergenic	
2906456	G	T	90	intergenic	
3021506	C	T	81	intergenic	
3043489	C	T	80	intergenic	
3086769	C	T	85	intergenic	
3089290	G	T	85	intergenic	
3098044	C	T	84	intergenic	
3098247	G	T	90	intergenic	
3141770	G	T	80	intergenic	
3210839	A	G	81	intergenic	
3210845	A	G	84	intergenic	
3217243	T	C	93	intergenic	
3217355	C	T	93	intergenic	
3229863	A	G	81	intergenic	
3238381	T	C	83	intergenic	
3507157	T	C	98	intergenic	
3536059	A	G	81	intergenic	
3582659	G	A	96	intergenic	
3592435	A	C	82	intergenic	
3592441	T	C	81	intergenic	
3604505	A	C	82	intergenic	
3604891	T	C	82	intergenic	
3610848	A	C	93	intergenic	
3611336	T	C	89	intergenic	
3614023	T	G	90	intergenic	
3614703	T	G	90	intergenic	
3617716	G	T	94	CDS	AT2G07981
3620208	G	A	81	CDS	AT2G08986
3627968	A	G	88	intergenic	
3634161	A	C	93	intergenic	
3634649	T	C	89	intergenic	
3658508	G	A	83	intergenic	
3694801	C	A	88	intergenic	
3695643	C	T	87	intergenic	
3696901	C	T	87	intergenic	
3698971	G	A	88	intergenic	
3718821	C	T	80	intergenic	

Appendix

3770637	T	C	81	intergenic	
3865117	C	A	87	intergenic	
3865130	T	G	88	intergenic	
3866239	C	A	83	intergenic	
3867922	T	C	89	intergenic	
3867943	T	C	88	intergenic	
3867979	A	G	86	intergenic	
3882647	T	C	88	intergenic	

Table V.VII. Homozygous SNP identified in suppressor 80 within the candidate window.

Position	Ref allele	Alternate allele	%reads showing alternate allele	Position in gene	Gene name
2009260	T	C	97	intergenic	
2047878	T	C	80	intergenic	
2060305	C	A	96	intergenic	
2060336	A	G	99	intergenic	
2479378	A	G	100	intergenic	
2479737	G	A	87	intergenic	
2480890	A	G	100	intergenic	
2481249	G	A	87	intergenic	
2643029	G	A	100	intergenic	
2643055	T	C	100	intergenic	
2670489	G	A	100	intergenic	
2670515	T	C	100	intergenic	
3187415	T	C	93	intergenic	
3240642	A	C	100	intergenic	
3251022	G	T	82	CDS	AT2G07777.1
3290052	T	G	100	splice_site_change	AT2G07681.1
3331890	A	C	81	intergenic	
3331900	A	C	82	intergenic	
3385678	A	C	84	CDS	AT2G07706.1
3385688	C	T	84	CDS	AT2G07706.1
3385694	G	A	83	CDS	AT2G07706.1
3496314	G	T	82	intergenic	
3496319	G	T	82	intergenic	
3591500	C	T	81	intergenic	
3609104	A	C	85	intergenic	
3610097	Y	C	86	intergenic	
3610168	K	T	86	intergenic	
3612119	T	G	97	intergenic	
3613871	T	G	97	intergenic	
3615628	T	C	80	intronic/noncoding	AT2G07981.1
3623164	C	A	88	intronic/noncoding	AT2G08986.1
3630571	T	G	80	intergenic	
3632553	A	C	85	intergenic	
3633099	T	G	80	intergenic	

Appendix VI: General Discussion

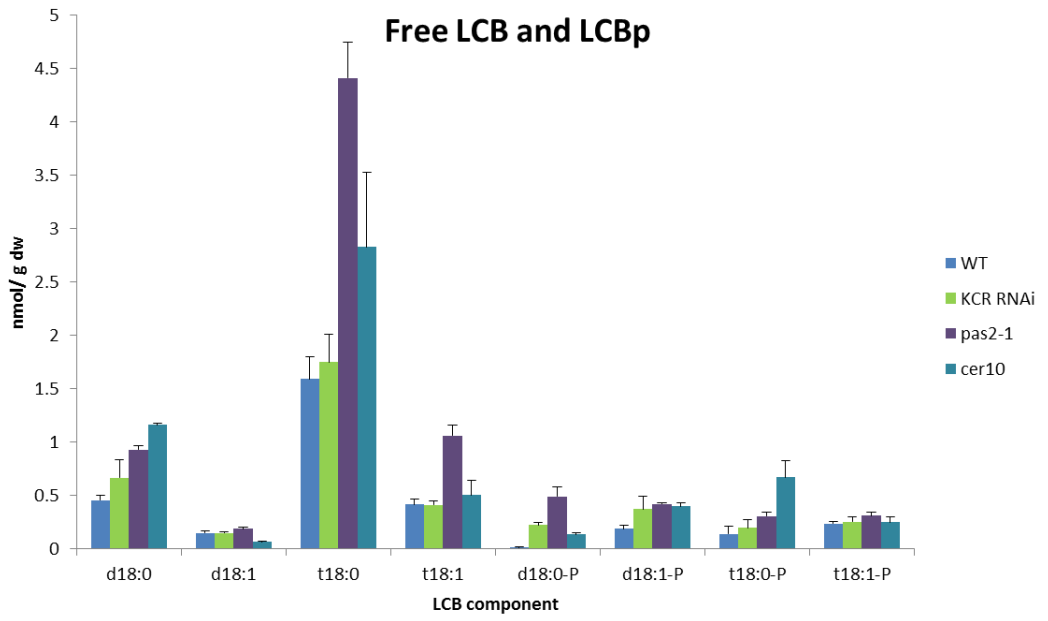


Figure VII. The amount of free LCB and LCBp in the shoots of elongase mutants based on an average of 3 values +/- the SE.